

**MAGNETIC SUSCEPTIBILITY SCALING OF ROCKS USING GEOSTATISTICAL
ANALYSIS: AN APPROACH TO GEOLOGIC AND GEOPHYSICAL MODEL
INTEGRATION**

by

NICOLÁS PIZARRO

B.Sc. University of Chile, 2000

**A THESIS SUBMITTED IN PARTIAL FULFILLMENT OF THE REQUIREMENTS
FOR THE DEGREE OF**

MASTER OF SCIENCE

in

THE FACULTY OF GRADUATE STUDIES

(Geological Sciences)

**THE UNIVERSITY OF BRITISH COLUMBIA
(Vancouver)**

September 2008

© Nicolás Pizarro, 2008

Abstract

Rock physical properties are usually associated with important geologic features within mineral deposits and can be used to define the location, depth and size of the deposit, type of ore, or physical property contrast between the host and country rock. Geophysical surveys are sensitive to physical properties and therefore are widely used in mining exploration, especially in concealed terrains. The surveys can be performed at multiple scales, resulting in corresponding physical property datasets at different scales. Survey scale can vary from core or hand sample, involving few cubic centimeters, to regional-scale surveys providing information about physical property contrasts between distinct regional geological features. The understanding of the relationship between the physical property distributions with the sample volume (e.g. district, deposit, and drill-hole scale) is required where point scale physical property measurements are going to be consistent with measurements at larger volumetric scales during the integration of data for geophysical modeling

The approach used to address the problem of understanding the scaling relations of physical properties, was achieved by considering them as second order stationary regionalized variables and then applying the random function formalism, provided by geostatistics theory. Geostatistics provide the required framework to characterize, quantify, model and link the spatial variability of the random variable at the different volumetric scales. The aim of this study is to apply geostatistics to effectively integrate data collected at several scales and bring knowledge to the understanding of the scaling relations of magnetic susceptibility. For this purpose, measurements of magnetic susceptibility available from Flin Flon copper-zinc district in Canada will be used. The data available at point scale were collected with hand portable magnetic susceptibility meter. The larger volumetric scale dataset were acquired using frequency domain electromagnetic instruments capable of measuring larger sample volumes, and then used to obtain magnetic susceptibility models using geophysical inversion algorithms. Once different scale models of magnetic susceptibility were available, quantification of the scaling relation using geostatistics, specifically variogram models and dispersion variance were determined.

The understanding provided by the scaling analysis of the Flin-Flon magnetic data is applied to data from the Rio Blanco copper district in central Chile. Magnetic susceptibility measurements collected with a hand magnetic susceptibility meter on drill-core is integrated in larger scale volumes used for geophysical inversion modeling of regional scale airborne magnetic field measurements to recover magnetic susceptibility models.

The methodology resulting from this application of geostatistics is used to address the problem of integrating multiple scales of physical property data in an effective way. The resulting physical property models capture the small-scale magnetic susceptibility variability observed and can guide larger-scale variability within geophysical inversion models. Establishing reliable statistical correlations between physical properties and rock units controlling ore within deposits are crucial steps leading predictive mine exploration tools. Any numerical modeling approach to establish these correlations should consider in some way the scaling nature of both physical property and ore content.

Table of Contents

Abstract.....	ii
Table of Contents.....	iii
List of Tables.....	vii
List of Figures.....	viii
Acknowledgements.....	xii
Dedication.....	xiii
Chapter 1. Introduction.....	1
1.1 Motivation of the research project.....	1
1.2 Purpose and scope.....	2
1.3 Thesis structure.....	3
Chapter 2. Background information.....	5
2.1 Introduction.....	5
2.2 Magnetic susceptibility of rocks and minerals.....	5
2.2.1 Magnetism in rocks and magnetic material classification.....	5
2.2.2 Magnetic minerals.....	8
2.2.3 Magnetic properties of rocks and scaling.....	9
2.2.4 Geophysical surveys and physical properties.....	10
2.3 Geologic framework.....	11
2.3.1 Introduction.....	11
2.3.2 Volcanogenic massive sulfide deposits.....	12
2.3.3 Magnetic properties of volcanogenic massive sulfide deposits.....	13
2.3.4 Porphyry copper deposits.....	14
2.3.5 Magnetic Properties within porphyry copper deposits.....	15
2.4 Geostatistic theory review and its application to volumetric scaling.....	16
2.4.1 Basic geostatistics concepts.....	16
2.4.2 Regionalized variables and random functions.....	17

2.4.3 Spatial variability and the variogram.....	18
2.4.4 Variogram Models.....	20
2.4.4.1 Nugget effect model.....	20
2.4.4.2 Spherical model.....	21
2.4.4.3 Exponential model.....	21
2.4.4.4 Gaussian model.....	22
2.4.5. Scaling laws using geostatistical tools.....	22
2.5 Geophysical Inversion theory.....	23
2.5.1 Introduction.....	23
2.5.2 Forward modeling.....	24
2.5.3 Inverse problem.....	25
Chapter 3. Scaling of magnetic susceptibility using synthetic models.....	36
3.1 Introduction.....	36
3.2 Model parameters.....	38
3.3 Synthetic models.....	38
3.3.1 Geologic and physical property setting.....	38
3.3.2 Cell size setting.....	40
3.3.3 Populating the rock type and physical property models.....	41
3.4 Statistics of synthetic magnetic susceptibility models.....	42
3.5 Experimental variograms of magnetic susceptibility models.....	43
3.5.1 Experimental variograms of global magnetic susceptibility models.....	44
3.5.2. Experimental variograms of local magnetic susceptibility models.....	45
3.6 Spatial continuity of magnetic susceptibility models.....	47
3.6.1 Adding spatial continuity to the physical property models.....	47
3.6.2 Quantifying spatial continuity of the physical property using experimental variograms.....	48
3.6.3 Modeling the pattern of spatial variability of an isotropic smoothed physical property model.....	49
3.7 Scaling the variogram model using geostatistical tools.....	52
3.7.1. Scaling variograms of synthetic magnetic susceptibility models.....	55
3.8 Conclusions.....	56

Chapter 4. Scaling magnetic susceptibility measurements from field data.....	83
4.1 Introduction.....	83
4.2 Site geology.	84
4.2.1 Mafic Volcanics site	84
4.2.2 Boundary Intrusive site	85
4.2.3 Quartz Porphyry site	86
4.2.4 Granite site.....	86
4.2.5 Sedimentary rock site.....	86
4.3 Survey geometric design.....	87
4.4 Point scale data set.....	88
4.4.1 Mafic Volcanics grids.....	88
4.4.2 Mafic Boundary Intrusive grids.....	90
4.4.3 Quartz Porphyry grids.....	91
4.4.4 Sedimentary Rocks grid.....	93
4.4.5 Granite grid.....	94
4.5 Spatial variability of magnetic susceptibility at the point scale.....	94
4.5.1 Isotropic point-scale magnetic susceptibility experimental variograms.....	95
4.5.2 Directional experimental variograms of magnetic susceptibility at the point scale	96
.....	96
4.5.2.1 Mafic Volcanics.....	97
4.5.2.2 Mafic Boundary intrusive.....	98
4.5.2.3 Quartz Porphyry.....	99
4.5.2.4 Sedimentary Rocks.....	100
4.5.2.5 Granite Site.....	100
4.6 Modeling of point scale magnetic susceptibility spatial variability.....	101
4.7 EM-31 survey dataset	103
4.7.1 EM-31 results.....	103
4.7.2 Comparing KT-9 magnetic susceptibility with EM-31 physical property distributions.....	106
4.8 Scaling magnetic susceptibility variogram models.....	108
4.9 Conclusions.....	109

Chapter 5. Magnetic modeling at Rio Blanco	149
5.1 Introduction.....	149
5.2 Available information.	150
5.3 Geology.....	150
5.3.1 Regional and district context.	150
5.3.2 Rock types.....	151
5.3.3 Tridimensional model of rock types.	152
5.4 Magnetic susceptibility distribution within the rock units.....	153
5.5 Magnetic susceptibility variograms.	154
5.5.1 Variogram modeling.	155
5.6 Magnetic susceptibility model.	156
5.7 Integrating magnetic data and models.	156
5.8 Conclusions.....	157
Chapter 6. Conclusions.....	174
6.1 Summary of work completed.....	174
6.2 Recommendation for further work.....	175
References.....	177
Appendix.....	181
A.1 Petrography study at Flin-Flon.	181
A.2 Geophysical and magnetic susceptibility data from Flin-Flon.	182

List of Tables

Table 2.1.	Types of magnetization and associated magnetic susceptibility ranges.....	35
Table 2.2.	Magnetic susceptibility for minerals observed within hydrothermal ore deposits.....	35
Table 3.1.	Rock types magnetic susceptibility statistical parameters, used to constrain synthetic models.....	77
Table 3.2.	Statistics summary for global and local models of magnetic susceptibility	78
Table 3.3.	Variance reduction factors	79
Table 3.4.	Magnetic susceptibility average, variance and range resulting from smoothing procedure.....	79
Table 3.5.	Basic statistics summary isotropic smoothed models.....	79
Table 3.6.	Range and variance parameters values used in variogram modeling.	80
Table 3.7.	Variogram modeling cross validation results	81
Table 3.8.	Error estimation basic statistics.	82
Table 4.1.	Point scale magnetic susceptibility statistics summary for the 10 m grids. Minimum, maximum and mean values in SI units scaled by a factor of 10^{-3}	146
Table 4.2.	Nugget effect, relative nugget effect calculated as a variance percent, and range distance in meters from isotropic experimental variograms at each grid. nc=no calculated. .	147
Table 4.3.	Variogram parameters calculated from directional variograms of magnetic susceptibility.....	147
Table 4.4.	Parameters for quantitative assessment of variogram cross validations.....	148
Table 4.5.	Statistics summary of magnetic susceptibility distribution recovered from geophysical inversion of EM-31 data. Minimum, maximum and mean values in SI units scaled by a factor of 10^{-3}	148
Table 5.1.	Rock codes, average and standard deviation of magnetic susceptibility measurements available from drill-hole cores from Rio Blanco Deposit.....	173
Table 5.2.	Variogram model parameters.....	173

List of Figures

Figure 2.1.	Different types of ferrimagnetic materials.....	27
Figure 2.2.	Magnetic susceptibility versus the volumetric percent of magnetite and pyrrhotite.....	28
Figure 2.3.	Magnetic susceptibility of rocks and magnetic minerals.....	29
Figure 2.4.	Schematic vertical section across a VMS deposit. A) Mineral assemblages within magmatic-hydrothermal and hydrothermal alteration zones.	30
Figure 2.5.	Schematic vertical section across a Porphyry copper deposit model	31
Figure 2.6.	Variogram parameters.....	32
Figure 2.7.	Example of a tolerance region used in experimental variogram calculations. The sample point located at origin will be paired with all the points within the tolerance region.....	32
Figure 2.8.	Variogram models of common use in geostatistics.	33
Figure 2.9.	Geostatistical scaling law for two variograms models at different volumetric scales v and V	34
Figure 3.1.	Three dimensional view of the synthetic rock model.	57
Figure 3.2.	Comparison between estimated scales associated with different geophysical surveys and the volumetric scales proposed for synthetic models..	58
Figure 3.3.	Basic synthetic model of magnetic susceptibility.....	59
Figure 3.4.	Magnetic susceptibility model scaled to a cell size of 10 m.....	60
Figure 3.5.	Magnetic susceptibility model scaled to a cell size of 25 m.....	61
Figure 3.6.	Magnetic susceptibility model scaled to a cell size of 50 m.....	62
Figure 3.7.	Magnetic susceptibility variance versus cell volume for global and local synthetic models.....	63
Figure 3.8.	Global experimental variogram for magnetic susceptibility models oriented parallel to X axis at the four cell size scalesable.	64
Figure 3.9.	Experimental variograms of global magnetic susceptibility model.....	65
Figure 3.10.	Experimental variograms of magnetic susceptibility model for rock type 1... ..	66
Figure 3.11.	Experimental variograms of magnetic susceptibility model for rock type 2... ..	67

Figure 3.12.	Experimental variograms of magnetic susceptibility model for rock type 3...	68
Figure 3.13.	Smoothed magnetic susceptibility models for rock type 3..	69
Figure 3.14.	Isotropic smoothed magnetic susceptibility models calculated within rock type 3.....	70
Figure 3.15.	Isotropic experimental (black dots) and fitted theoretical variograms	71
Figure 3.16.	Estimate value vs. True value quartile plots.	72
Figure 3.17.	Error estimation histograms for spherical, exponential and gaussian variogram models.....	73
Figure 3.18.	Error estimation standardized variograms for spherical, exponential and Gaussian variogram models.....	74
Figure 3.19.	Up-scaled variogram models for the rock type 3 model.....	75
Figure 3.20.	Decrease in variance with volume plotted in logarithmic scale.	76
Figure 4.1.	Geologic sketch of the Mafic Volcanic site.....	111
Figure 4.2.	Geologic sketch of Mafic Boundary Intrusive site.	112
Figure 4.3.	Geologic sketch of Quartz Porphyry site.....	113
Figure 4.4.	Geologic sketch of Granite site.....	114
Figure 4.5.	Geologic sketch of Sedimentary rock site.	115
Figure 4.6.	Geometric arrays used in the geophysical surveys.	116
Figure 4.7.	Mafic Volcanic site 10 m grids.....	117
Figure 4.8.	Local average magnetic susceptibility as a function of position at Mafic Volcanics.....	118
Figure 4.9.	Mafic Boundary Intrusive 10 m grids.....	119
Figure 4.10.	Local average magnetic susceptibility as a function of position at Mafic Boundary Intrusive.....	120
Figure 4.11.	Quartz Porphyry 10 m grids.....	121
Figure 4.12.	Local average of magnetic susceptibility at Quartz Porphyry grids.....	122
Figure 4.13.	Sedimentary Rocks and Granite 10 m grids.....	123
Figure 4.14.	Average magnetic susceptibility as a function of position in station and line at Sedimentary Rock grid and Granite grid.....	124
Figure 4.15.	Isotropic Magnetic Susceptibility Experimental Variograms calculated using the point scale measurements collected at 10 m grids.	125

Figure 4.16. Relation between the directional experimental variograms and the grid coordinate system.....	126
Figure 4.17. Directional point scale magnetic susceptibility experimental variograms at Mafic olcanics.....	126
Figure 4.18. Directional point scale magnetic susceptibility experimental variograms at Mafic Boundary Intrusive.....	127
Figure 4.19. Directional point scale magnetic susceptibility experimental variograms at Quartz Porphyry.....	128
Figure 4.20. Directional point scale magnetic susceptibility experimental variograms at Sedimentary Rocks and Granite.....	129
Figure 4.21. Isotropic variogram models	130
Figure 4.22. Variogram modeling cross validation.....	131
Figure 4.23. Histograms of the standardized estimation errors plotted for the analyzed grids.....	132
Figure 4.24. Standardized estimation error vs. estimated value.....	133
Figure 4.25. Geometric sample array for the EM-31 survey.....	134
Figure 4.26. Magnetic susceptibility distribution recovered from inversion of EM-31 data at the Mafic Volcanic 1B.....	135
Figure 4.27. Magnetic susceptibility distribution recovered from the geophysical inversion of EM-31 data at the Mafic Boundary Intrusive North Grid.....	136
Figure 4.28. Magnetic susceptibility distribution recovered from the geophysical inversion of EM-31 data at the Mafic Boundary Intrusive South Grid.....	137
Figure 4.29. Magnetic susceptibility distribution recovered from the geophysical inversion of EM-31 data at the Quartz Porphyry West Grid.....	138
Figure 4.30. Magnetic susceptibility distribution recovered from geophysical inversion of EM-31 data at the Quartz Porphyry East Grid.....	139
Figure 4.31. Magnetic susceptibility distribution recovered from the geophysical inversion of EM-31 data at the Sedimentary Rock site.....	140
Figure 4.32. Quartile-quartile scatter plots in log-scale of magnetic susceptibility at the point scale (KT-9) vs. magnetic susceptibility recovered from the geophysical inversions of the EM-31.....	141

Figure 4.33. Average magnetic susceptibility at the hand sample scale (k_{KT9}) vs. average magnetic susceptibility at the scale of the EM-31 (k_{EM31}) data.	142
Figure 4.34. Isotropic experimental variogram of magnetic susceptibility at KT-9 and EM-31 scales.....	143
Figure 4.35. Modeled curve of magnetic susceptibility variance as a function of the sampled volume at the Boundary Intrusive South grid.....	144
Figure 4.36. Scaling of experimental and modeled isotropic variograms of magnetic susceptibility for the Mafic Boundary Intrusive South grid.	145
Figure 5.1. Tectonic setting of the Miocene-Pliocene porphyry copper deposits located in central Chile.....	159
Figure 5.2. Magnetic data at the Rio Blanco District.....	160
Figure 5.3. Geologic Map of the Rio Blanco District.....	161
Figure 5.4. Vertical cross sections through the Rio Blanco porphyry copper deposit.....	162
Figure 5.5. Three dimension rock model of the Rio Blanco deposit.....	163
Figure 5.6. Magnetic susceptibility histograms for the rock types studied.....	164
Figure 5.7. Magnetic susceptibility ranges for core measurements from rock units within Rio Blanco Deposit.....	165
Figure 5.8. Magnetic susceptibility experimental variograms at Rio Blanco.	166
Figure 5.9. Variogram models for the plutonic rocks.....	167
Figure 5.10. Variogram models for the breccia rock types.....	168
Figure 5.11. Variogram models for the Dacitic Porphyry and Felsic Volcanics.	169
Figure 5.12. Rock type model and magnetic susceptibility model.....	170
Figure 5.13. Histograms for the magnetic susceptibility distribution for each of the rock types modeled using the geostatistical analysis.....	171
Figure 5.14. Comparison of magnetic data and airborne magnetic anomaly over the district.	172

Acknowledgements

I would like to thank my supervisor Richard Tosdal for his support, suggestions and proof editing of my Spanish writing style. Special thanks to Nigel Phillips and Peter Lelièvre for helping me learn how to use UBC-GIF geophysical inversion codes. Also Nigel Phillips helped with Matlab codes used at different stages through the thesis.

I must thank Patricio Cuadra, Michel Galeb and Luis Serrano from Codelco Division Andina for authorizing the use in this project of the magnetic susceptibility data from core measurements. Also Francisco Camus and Gonzalo Yáñez from Codelco-Exploraciones are thanked for authorizing and providing the airborne magnetic data. A special thanks to Carlos Soto who kindly help me in the coordinate system translations.

I also would like to thank Nick Williams and Diane Mitchinson. They made valuable suggestions when I presented the methodology used during the research.

This project was funded by the Mineral Deposit Research Unit–Geophysical Inversion Facility collaborative project, which is sponsored by a consortium of ten companies with funds matched by the NSERC Collaborative Research and Development program. The companies involved are Anglo American, Anglo Gold Ashanti, Barrick, BHP Billiton, CVRD Inco, Geoinformatics Exploration, Kennecott Exploration, Teck Cominco and Xstrata. The data from Rio Blanco Deposit in Chile is provided by Codelco.

Dedication

I dedicate this thesis to my wife Daniela and my children Diego and Martina

Chapter 1. Introduction

1.1 Motivation of the research project.

Mining and exploration projects are potential sources of vast amounts of both geologic and geophysical information. Geophysical data are obtained through different survey methods which are widely used as mineral exploration tools. The importance of geophysical surveys in the exploration industry dates back to the beginning of modern metal search. Today application of geophysics is of greater importance, as the number of outcropping ore deposits diminishes with time, especially in extensively explored areas, such as the north of Chile, some portions of Australia and Canada. Among the variety of geophysical survey methods, magnetic and gravity are the most commonly applied in the exploration of ore deposits.

Geophysical data are rarely collected at a single scale, for either technical or economic reasons. Integrated interpretation of multi-scale data has the potential of producing quantitative physical property models which can be used to enhance geologic and geophysical modeling. Also collection of rock magnetic susceptibility measurements is an increasing practice among economic geologists during district geologic mapping or drill-hole core logging. This procedure results in establishing statistical distributions of the physical property which can be available also at different scales depending on the sample volume. These physical property distributions can be used to characterize the magnetic character of rocks within an ore deposit as well as constrain and guide geophysical interpretation and processing of magnetic data.

Despite the increased use of geophysical inversions, a mathematical algorithm used to interpret and model gravity, magnetic and electromagnetic data, little attention has been paid to the relation between physical properties, such as density, magnetic susceptibility or electrical conductivity of rocks and the sampling scale of the measurements. Magnetic surveys usually are performed at large scales, involving rock volumes in the order of tens to hundreds of cubic meters. In contrast, drill-core and well log measurements involve rock

volumes of a few cubic meters or less. Integration of geophysical data collected at different scales requires therefore the understanding of the scaling relation between large and small scale data sets.

The scaling property of magnetic and gravity potential of crustal rocks has been widely recognized (Pilkinton, Gregostski and Todoeschuck, 1994, Maus and Dimri, 1994; Pilkington and Todoeschuck, 1995). A large amount of evidence provided from these authors pointed out that power law is appropriate for modeling the spatial variation of many geophysical parameters. This study aims to contribute to the understanding of the scaling relationship of rock magnetic data. Here, the approach used includes the collection of magnetic measurements of rocks at several volumetric scales in order to determine if a scale dependency is observed. The collected data are processed using geophysical inversion algorithms to calculate physical property models at the specific sampling scales. The calculated models are used to investigate the scaling relation of magnetic data.

Magnetic susceptibility models, in general, correspond to spatial distributions of the physical property which map how it varies in a 1-D, 2-D or 3-D space. These models can be considered as random functions. As a consequence, scaling geostatistics tools can be applied to integrate physical property models available at different volumetric scales. This thesis applies the geostatistics methodology to effectively integrate the magnetic susceptibility measurements collected at several scales. As a result, scaled physical property models can be obtained and can be incorporated into the geophysical inversion algorithm

1.2 Purpose and scope.

This thesis characterizes the relation between magnetic susceptibility measurements of rocks and the sampled rock volume. This broad objective attempts to address the question of how to incorporate magnetic susceptibility measurements collected at the point scale (e.g. drill-hole core measurements) into larger scale models (10 to 100 cubic meters), such as those physical property models, derived from geophysical inversions. This 'scale' issue is not only restricted

to the geophysics. It is recognized in almost all other earth science disciplines as data linked to the sample volume. Therefore, much physical property data are scale dependant and the resultant models built from them create an image or map revealing features at the data scale.

The thesis presents a methodology to be used in scaling issues associated with numerical models, interpretation and integration of magnetic susceptibility of rocks within ore deposits. The approach is to characterize, model and scale the spatial variability from point scale magnetic susceptibility measurements available from field surveys. The resulting geostatistical model should be suitable to be integrated into larger scale models of this physical property. To perform the task of understanding and scaling the magnetic susceptibility spatial variability, a set of tools provided by geostatistics theory are used. The integration of the point scale spatial variability features of magnetic susceptibility is tested by comparing the results obtained from the geostatistic modeling of magnetic susceptibility with larger scale models derived from geophysical inversions of magnetic and electromagnetic data.

1.3 Thesis structure.

The thesis begins with an introductory chapter where the problem, objectives and scope of the project are stated. The second chapter corresponds to a review of the physical properties of rocks within ore deposits, basic concepts of geostatistics and geophysical inversion theories. The third chapter includes a synthetic modeling where geostatistical scaling techniques will be tested in ideally constrained situations.

Once an understanding of the use of geostatistics scaling tools is attained, this knowledge is applied to the field data collected at Flin-Flon district in chapter four. In chapter four, point scale magnetic susceptibility measurements collected with a hand portable magnetic susceptibility meter (KT-9) are analyzed and modeled using geostatistics. Also larger scale physical property models recovered from geophysical inversion of electromagnetic data collected using EM-31 instrument are analyzed and also modeled using geostatistics. At both

scales, data are compared and a scaling relation is obtained. Geostatistics scaling tools are also tested and applied to both data sets.

Using the knowledge acquired from the Flin-Flon field data, where different scales will be used to obtain a scaling relation for magnetic susceptibility, a second approach will be attempted and presented in chapter five. Available magnetic information from Rio Blanco deposit in central Chile collected at two extreme volumetric scales provides the opportunity to test the methodology. Regional- and district-scale airborne magnetic field surveys with flight lines separated 150 m and 50 m, respectively, and core magnetic susceptibility measurements from drill-holes within the ore deposit, provide an exceptional opportunity to test the magnetic susceptibility scaling relation, integrate different types of magnetic data, as well as to understand the magnetic behavior of a giant porphyry copper system.

Finally chapter six includes a synopsis of the completed work, future work recommendation, discussion and conclusions obtained as a result of this research project.

Chapter 2. Background information

2.1 Introduction

This thesis describes the scaling relation of magnetic susceptibility of rocks within hydrothermal ore deposits and provides a methodology to integrate magnetic field and susceptibility measurements collected at different scales. An important starting point is an understanding of the topics involved. This chapter reviews the background information related to magnetic properties of rocks and minerals by describing basic notions of magnetism and magnetic materials, elementary concepts related to geophysical surveys, the geological models of the ore deposits being studied and basics on geophysical inversions and geostatistical theory.

2.2 Magnetic susceptibility of rocks and minerals.

2.2.1 Magnetism in rocks and magnetic material classification.

Rocks magnetism is complicated, as several factors control the magnetic properties of rocks and minerals. Once rock or mineral is formed, superimposed geologic processes, such as metamorphism, rock deformation and hydrothermal alteration can modify the original magnetic signature. Thus, a summary of the basic definitions and important aspects of magnetic properties of rocks and minerals is required to help clarify the following thesis.

Magnetic susceptibility, the relevant variable in magnetic surveys, is a measure of the ability of a particular material to become magnetized under the presence of a magnetic field (Telford et al., 1976). All materials, under the presence of a weak external magnetic field (H), acquire induced magnetization (M_I) according to a linear relation:

$$M_i = \kappa \times H \quad (2.1)$$

The proportionality constant κ in equation 2.1, is called the volume magnetic susceptibility and is measured in the international system of units (SI). Although it is defined by the above simple mathematical relation, magnetic susceptibility of rocks is in fact, a complex product of the atomic and macroscopic properties of magnetic materials (Blakely, 1995). In the presence of a strong magnetic field; materials become magnetized following complex relations (Telford et al., 1976). A second type of magnetization, the permanent or ‘remnant’ magnetization is only found in ferromagnetic minerals (see below). Furthermore, multiple remnant magnetizations may characterize the magnetic history of the rocks. In sum the total magnetization of a material is the vector addition of the induced and remnant magnetization. For the purpose of this research no remnant magnetization is considered, as the geophysical inversion code used to process the magnetic data requires this assumption. Furthermore no measurements of this component of the magnetization in the data used herein are available.

Rock materials may be 1) Diamagnetic, 2) Paramagnetic and 3) Ferromagnetic, the latter being subdivided in ferromagnetic, ferrimagnetic and anti-ferrimagnetic (Table 2.1) (Clark, 1997). In diamagnetism, an inherent property of all materials, a small induced magnetization is oriented in an opposite direction to the applied field, resulting in low negative magnetic susceptibility, in the range of -6×10^{-5} to -1×10^{-5} SI units (Clark, 1997). Paramagnetic materials are characterized by a net magnetization oriented in the direction of the applied field, due to partial alignment of the magnetic dipoles. As a result, paramagnetic materials display a large range of positive magnetic susceptibility between 10^{-5} and 10^{-2} SI units. Both materials are poor contributors to the geomagnetic field (Blakely, 1995). The third type of material is the most important for magnetic prospecting, as 1) such material can be spatially related to an ore body in some deposit types and 2) they can have magnetic susceptibility several orders of magnitude larger than paramagnetic materials. Both ferromagnetic and ferrimagnetic materials derive their high magnetic response from spontaneous magnetization, a complex microscopic property caused by exchange energy resulting from quantum mechanical effects (Blakely, 1995). Ferromagnetic materials have the highest positive magnetic susceptibility, in the range of 10^{-4} to 10^0 SI units, as the magnetic moments are

aligned parallel resulting in large magnetization (Fig.2.1). In ferrimagnetic materials, some of the magnetic moments are aligned parallel to the applied field whereas other is aligned in the opposite direction (anti-parallel) resulting in a slightly smaller magnetic susceptibility compared to the ferromagnetic. In anti-ferromagnetic materials, magnetic moments are aligned anti-parallel, thereby cancelling one another (Blakely 1995) resulting in lower ranges of susceptibility values, between 10^{-5} and 10^{-2} SI units (Table 2.1). Finally, the magnetic susceptibility of a geological sample must be understood as a composite average of the diamagnetic, paramagnetic and ferromagnetic components that are present within the sample volume (Gubbins and Herrero-Bervera, 2007).

It is widely accepted (Telford et al., 1976, Clark, 1997) that for rocks with small amount of magnetic mineral (for example, <10%), magnetic susceptibility is directly related with the volumetric percent of magnetic minerals. In contrast, for larger magnetic mineral amounts, magnetic susceptibility can depart from linearity (Fig. 2.2). Magnetic susceptibility is grain size dependant as grain size exerts important control on the magnetic domain structure at the microscopic scale (Clark 1997, Hunt et al., 1995). Susceptibility can differ with crystallographic directions, depending on the crystal symmetry of the mineral, being isotropic for cubic crystals and anisotropic for lower symmetries (Clark, 1997). At the volumetric scales studied here, the induced magnetization is considered parallel to the direction of the applied field, and therefore magnetic susceptibility is an isotropic quantity. As a general rule, mafic rocks are expected to display higher magnetic susceptibility than felsic rocks, as there is an overall trend of increasing magnetite content with mafic content. For example, andesite has similar or slightly lower susceptibility than basalt on average, due to their lower magnetite content (Blakely, 1995). However, comparing rock types and magnetic susceptibility (Fig. 2.3), it is evident that for most rock types the range of susceptibilities is quite large, precluding the use of magnetic susceptibility as diagnostic of rock type (Clark 1997). Nonetheless, some rock types can have characteristic of paramagnetic and ferromagnetic populations, leading to a bimodal distribution of magnetic susceptibility. Finally, regardless of rock types, the variation in magnetic susceptibility can be large at almost all scales, from regional to the outcrop scale.

2.2.2 Magnetic minerals.

Magnetic minerals in nature are restricted in number and can be grouped in major mineral groups, the iron-titanium oxides and the iron sulfide mineral group (Clark, 1997). Magnetite (Fe_3O_4) is the most important and common magnetic mineral of both groups and has the greatest magnetic susceptibility. Magnetite is an end member phase of the titano-magnetite solid solution series with ulvöspinel (Fe_2TiO_3). Magnetic susceptibility of these minerals is inversely related to Ti composition, which replaces Fe, and is directly related to grain size (Clark, 1997). Magnetic susceptibility ranges from 0.1 to 120 SI in the case of magnetite and from 0.1 to 0.3 SI for a phase of Ti rich composition (68% ulvöspinel).

The most important magnetic mineral within the iron sulfide group is monoclinic pyrrhotite, with a composition of Fe_7S_8 . Magnetic susceptibility of monoclinic pyrrhotite varies significantly with the grain size, as decreasing the size from 1 to 0.01 mm results in a reduction of two orders of magnitude in susceptibility units, from 1.3 to 0.05 SI (Clark, 1997).

An important property of the ferromagnetic minerals is the Curie point temperature at which these minerals lose their spontaneous magnetization or ferromagnetic character. Only the paramagnetic behavior remains at higher temperatures. For magnetite and monoclinic pyrrhotite, the Curie temperature is 578°C and 320°C, respectively (Clark, 1997).

Most hydrothermal ore deposits display zones where specific hydrothermal alteration assemblages and ore minerals prevail. Therefore, it can be expected that the bulk (or average) magnetic susceptibility within each zone will be a composite of the susceptibility of the minerals present. For most cases, this average is mainly controlled by the quantity of magnetite and/or pyrrhotite. Reliable interpretation of magnetic surveys in magnetite- and/or pyrrhotite-rich environments must also consider several factors, including type of magnetism, anisotropy, ratio of remnant to induced magnetization and self-demagnetization (Clark et al 1995). Moreover, in monoclinic pyrrhotite and magnetite rich ores, a dependency between magnetic susceptibility and frequency can be observed. Electromagnetic surveys in high magnetic susceptibility and low conductivity sites can result in negative in-phase component

of the secondary field (Beard and Nyquist, 1998, Huang and Fraser, 2001, Farquharson et al., 2003). To solve this, some corrections are proposed (Huang and Fraser, 2001) and also low frequency surveys (1 KHz or less) are recommended (Clark et al., 1995).

2.2.3 Magnetic properties of rocks and scaling.

In order to characterize the scale dependency of magnetic susceptibility, two scales have to be considered. The first is the macroscopic scale, at which magnetic susceptibility is controlled almost entirely by the amount and distribution of magnetic minerals. The second corresponds to the microscopic scale for which the physical property depends mainly on the grain size, composition and temperature, as these parameters can control the quantity and type of magnetic domains-zones with a uniform magnetization direction within a grain or within magnetic grains (Gubbins and Herrero-Bervera, 2007). The latter physical properties present a scaling behavior at the macroscopic level (Leonardi and Kämpel, 1996, Pilkington and Todoeschuck, 1995) that can be represented through a simple mathematical relation:

$$P \propto f^{\beta} \quad (2.2)$$

Where P is the power spectra, f is the spatial frequency and β is the spectral exponent or scaling exponent, reflecting the degree of correlation between successive points.

The spectral analysis performed by Leonardi and Kämpel (1996) using more than 26,000 magnetic susceptibility borehole measurements from the KTB project in Germany, confirmed the scaling behavior of magnetic susceptibility of crustal rocks. The results obtained indicate a negative value for the spectral exponent in the range between -1.4 and -0.3, implying a positive correlation between successive data in the range of meters to hundred of meters. Pilkington and Todoeschuck (1995), using similar spectral analysis over large magnetic susceptibility dataset from Sierra Nevada (USA) and Flin-Flon (Canada), also confirm the scaling nature of the physical property. Their results indicated a spectral exponent equal to -4.

The large variation in the spectral exponent implies that the scaling is not constant and the use of a fixed value of b should be avoided. Zhou and Thybo (1998) concluded that magnetic scaling factor may change with the source burial depth and proposed that magnetic sources located within the uppermost 1 km of the crust can have a scaling exponent value of -2.3 whereas deeper magnetic sources can have a value of -1.

2.2.4 Geophysical surveys and physical properties

Geophysical surveys are sensitive to Earth's physical properties and therefore can be used to map variations in these properties at and beneath the surface. They are used commonly to detect directly or indirectly some ores, geologic and/or structural features, and are routinely used in mining exploration programs. Geophysical information used in this thesis was collected using magnetic and electromagnetic surveys. The first can be used to map magnetic susceptibility variations whereas the second is used to obtain information about electrical conductivity and magnetic susceptibility of the ground.

In this thesis the EM-31 frequency domain electromagnetic (FEM) instrument is used. This instrument is based on the principle of electromagnetic induction. The induction process in a FEM survey is produced by a transmitter coil which emits a sinusoidal time-varying electrical current at a specific frequency which produces a primary magnetic field. This primary magnetic field induces electrical currents, referred to as eddy currents, in the ground where it is conductive. Eddy currents in turn generate a secondary magnetic field which is characterized by the same frequency, different phase and lower amplitude than the primary magnetic field. At a receiver coil, separated from the transmitter, a resultant magnetic field is recorded corresponding to a superposition of the primary and the secondary magnetic fields. The total field is a complex quantity consisting of a real part and an imaginary part. The real part has the same phase as the primary field and is referred to as the in-phase component. The imaginary part shows a 90-degree phase difference from the primary magnetic field and is referred to as the out of phase or quadrature component. The units of both components are expressed in parts per million or percent of the primary magnetic field, which is measured in

ampere·meter⁻¹ in SI units. The resultant magnetic field depends on the operating frequency, the electrical and magnetic properties of the conductor and host material, the shape and size of the conductor, and the geometric configuration of the transmitter receiver pair. The surveys design used during data collection for this thesis involves the horizontal coplanar loop configuration which results in vertical magnetic dipoles as a model for the electromagnetic source (Lange and Seidel, 2007).

Magnetic methods are based on the fact that Earth possesses a magnetic field which induces magnetization according to equation 2.1. Therefore magnetic surveys are sensitive to rocks magnetic susceptibility changes and are suitable to detect spatial variations of the earth's magnetic field.

2.3 Geologic framework

2.3.1 Introduction

Scaling of magnetic susceptibility is investigated herein in two different ore deposits. These are volcanogenic massive sulfide (VMS) and porphyry copper (PCDs) deposits. The study uses Flin-Flon VMS district in Canada and Rio Blanco porphyry copper in central Chile. Before discussing the scaling parameters, it is important to establish the geologic context for both ore deposits models. These models provide the framework to distinguish rock types, hydrothermal alteration and mineralogy zones forming the deposits and how these zones are spatially distributed. These conceptual models help to predict and establish zones of contrast in the physical property values (low-high) are useful way to define the expected value ranges for the magnetic susceptibility at different locations within the deposit, and therefore are required for the interpretation of magnetic susceptibility measurements.

2.3.2 Volcanogenic massive sulfide deposits.

Volcanogenic massive sulfide (VMS) deposits are found in several geological environments (Franklin et al., 2005). The Flin Flon (Manitoba) VMS deposit are located within bimodal mafic volcanic rocks. In general, VMS deposits are “strata-bound accumulations of sulfide mineral that precipitated at or near the sea floor in spatial, temporal, and genetic association with contemporaneous volcanism” (Franklin et al, 2005). The litho-tectonic type used to classify Flin-Flon deposit corresponds to a bimodal-mafic formed in an oceanic supra-subduction rifted arc (Fig. 2.4A). The dominant rock types commonly found in this setting are pillowed and massive basaltic flows with up to 25% of the total volcanic strata column constituted by felsic volcanic flows. A small proportion of volcanoclastic and sedimentary rocks are also present. Sub-volcanic intrusions at depth are considered the heat source of the convective hydrothermal system responsible for the formation of the VMS deposit, and may also be a source of metals. The upper crustal mafic intrusive complexes develop hydrothermal systems operating at a temperature range between 400°C and 300°C within the zone of brittle fracture permeability (Franklin et al., 2005).

Magmatic-hydrothermal and hydrothermal alteration zones characterize VMS deposits. The magmatic-hydrothermal alteration zone is formed by a mineral assemblage of quartz, albite, epidote, amphibole and magnetite. A peripheral zone of hydrothermally altered rocks extended up to hundreds of kilometers along the strike. These zones are located between the sea-floor and the associated intrusive complexes located at depth (Fig. 2.4A) and are divided into five alteration assemblages including the diagenetic-zeolite zone, carbonate zone, spilitic-greenschist zone, silica rich zone, epidote-quartz altered rocks. This alteration scheme can be largely modified during the evolution of the hydrothermal system. The ore bodies are bulbous shape with horizontal length variable between 80 and 2,000 m and vertical extension from 20 to 500 m. There is an inner or core zone rich in pyrrhotite, chalcopyrite and subordinate pyrite, enclosed by a zone with pyrite, sphalerite, galena and less chalcopyrite, which in turn is surrounded by an external zone with sphalerite, galena, pyrite and barite (Fig. 2.4B) (Lydon, 1988). A common feature to VMS districts is that ore bodies tend to be associated with a favorable horizon, commonly spatially related to felsic volcanic rocks intercalated to

thick basaltic sequences (Syme and Bailes, 1993). Typically the ore bodies are concordant lens of massive sulfides deposited above a discordant stockwork zone enclosed by a pipe of hydrothermal strongly altered rocks (Lydon, 1988). Most VMS deposits are preferentially aligned, located near submarine volcanic centers and syn-volcanic faults (Franklin et al., 2005).

2.3.3 Magnetic properties of volcanogenic massive sulfide deposits.

VMS deposits in general are characterized by a positive magnetic signature due to: 1) the associated sub-volcanic intrusions are derived from magmas with primary composition in the magnetite series and 2) hydrothermal activity resulting in ore and alteration mineral assemblages characterized by high content of iron-rich oxides and sulfides, formed during high temperature stages of the system (Franklin et al., 2005).

VMS deposits consist of formed by up to 50-60% of sulfides. Pyrrhotite is common, and the most important magnetic mineral of the ore in VMS deposits, and controls the magnetic susceptibility. In addition, a high content of magnetite can be associated with either the ore bodies or the far field hydrothermal alteration aureoles. Consequently VMS deposits are characterized by high magnetic susceptibility. For example, at San Nicolas VMS deposit, located in central Mexico, the ore body has a high average magnetic susceptibility (23×10^{-3} SI units) but also has a high contrast with the magnetic susceptibility of the host rocks within the deposit, which can be as high as one order of magnitude (Phillips, 1996 and Phillips et al., 2001). The contrast makes magnetic prospecting methods a suitable exploration tool.

The association of VMS ore bodies with felsic volcanic strata, hosted in mafic volcanic sequences provides an additional opportunity to detect high magnetic susceptibility contrast between rock units and therefore assist targeting VMS style mineralization.

2.3.4 Porphyry copper deposits.

Porphyry copper deposits (PCDs) form as the result of late-magmatic to hydrothermal activity related to crystallizing magma bodies emplaced at shallow crustal levels along convergent magmatic arcs (Hedenquist and Lowerstern, 1994). Magmas related to porphyry copper deposits are oxidized, may have elevated Fe content and are characterized by magnetite as the major iron-oxide mineral. The PCD related intrusive rocks, are commonly calc-alkaline metaluminous magmas with high to moderate K_2O , (Cooke et al., 2005) and compositions from diorite to granite (Camus, 2003). A porphyry copper deposit consists of stockwork, disseminated and breccia-hosted styles of copper mineralization together with K-silica alteration assemblages generally restricted to the intrusions and their immediate wall rocks (Cox, 1986). The deposits are characterized by high tonnage and low-grades of copper, but nonetheless they are the dominant source of the world's copper production and commonly carry molybdenum, silver and gold as byproducts.

Formation of porphyry copper deposit involves the exsolution of metals and sulfur-rich fluids from magmas, followed by ore deposition in response to temperature decrease, pressure changes, wall-rock reaction and fluid mixing (Richards, 2003). The typical mineralogical zones (Fig. 2.5) observed within PDCs include a core of high temperature minerals, including K-feldspar, biotite, anhydrite and magnetite with an associated ore constituted by iron-copper sulfides, mainly chalcopyrite and bornite. This potassic core gradually grade towards the periphery to an external shell where a propylitic assemblage, dominated by chlorite, epidote and calcite with pyrite as the stable sulfide phase, is present. These zones are interpreted to have formed simultaneously, reflecting different fluid source and chemical composition. The potassic alteration zone can be partially overprinted by lower temperature phyllic or quartz-sericitic assemblage, characterized by the replacement of the feldspar and biotite by fine muscovite-sericite and quartz as hydrothermal minerals and chalcopyrite and pyrite as the non-silicate phases. In the upper levels top of these deposits, acid-stable mineral assemblages in advanced argillic zone are characterized by the presence of complex associations of dickite, pyrophykite, kaolinite, illite and chlorite with the sulfides composed by pyrite, marcasite, enargite and copper sulphosalts.

Sulfide minerals and hydrothermal alteration zones within these deposits are centered on a cylinder or cone shape intrusive-stock or porphyry- and therefore display a concentric zonation pattern around the intrusive body. The dimensions of each zone are variable, however the horizontal extension of the propylitic envelopment, which generally define the external limit of PCDs, vary in surface from 0.5-2 km² and can have vertical extensions of 1 up to 3 km, as in some of the Andean PCDs (Camus, 2003). Minerals typically founded in the different hydrothermal alteration assemblages of a porphyry copper deposit are included in Table 2.2 with the expected range in magnetic susceptibility.

2.3.5 Magnetic Properties within porphyry copper deposits.

Magnetic response will vary from one deposit to another, depending on the characteristics of the wall rocks, the degree of exposure to weathering and supergene alteration. For example, in the Stinkingwater district in Wyoming (USA), Gettings (2005) reports a high magnetic variability detected on the different altered rock types. Nonetheless, there is a distinct trend from higher susceptibility within the potassic assemblages to medium susceptibility values in the propylitic zone and the lowest magnetic susceptibility values within the phyllic zone. Similarly, Berger *et al* (2003) reports magnetic susceptibility recovered from geophysical inversion of aeromagnetic data in the vicinity of Red Mountain in Arizona (Corn 1975, Quinland, 1986) demonstrated that the phyllic zone has lower susceptibility than the propylitic and potassic zones and that the difference might be as great as a one order of magnitude. However a magnetic susceptibility difference between the potassic and propylitic zones in this case was not detected. These observations are in agreement with the arguments presented by Clark (1997) who proposed that both phyllic and propylitic alteration associated with porphyry intrusions will destroy magnetite; whereas the potassic alteration zone associated with oxidized felsic intrusions are magnetite rich.

2.4 Geostatistic theory review and its application to volumetric scaling.

2.4.1 Basic geostatistics concepts.

Geostatistics concepts were developed in the 1950's by D.G Kriege, a South African mining engineer, and H.S. Sichel, a statistician. Later in 1962 Georges Matheron (1962) coined the term geostatistics and defined it as “the application of the formalism of random functions to the characterization and estimation of natural phenomena” (Journel and Huijbrechts, 1978). It is a branch of applied statistics focused in the geologic context, spatial relation and the volumetric support of the data. Natural phenomena are considered to have an ‘organization’ or ‘structure’ in the space. This can be characterized by the distribution of one or more variables called Regionalized Variables” (ReV). The definition of a regionalized variable, as a variable distributed in space, is purely descriptive and from mathematical point of view is simply a function which takes a value at every point within a spatial field or temporal ‘domain’. The main difference between the classic statistics and the geostatistics analysis is the probabilistic interpretation of the regionalized variable, which considers it as a Random Variable (RV) and the available measured data set (Rev) as a particular realization or event of the RV. Assuming homogeneity and stationary hypothesis for the RV, some degree of statistical inference is required in order to apply the geostatistical tools.

Examples of regionalized variables of mining interest are metal grades, density, grain size, and metallurgic recovery, which all characterize some aspect of the mineralization phenomenon. In the case of geophysics, physical properties of earth material such as density, electrical conductivity and magnetic susceptibility may also be considered as regionalized variables, as they take a value at particular spatial locations.

2.4.2 Regionalized variables and random functions

The following review summarizes some of the formal definitions related to the mathematics involved in the use of geostatistics. Conceptual details and further theory background are provided in the seminal works of Matheron (1971) and Journé and Huijbregts (1978) on which this review is based.

Regionalized variables are mathematical functions taking values at every point within a domain (D) or field which in earth sciences usually are one, two or three dimensional spaces. Therefore the location of each sampled point can be uniquely characterized by the spatial coordinates. Regionalized variables possess two apparently contradictory characteristics; a local random erratic aspect (random variable), and a general (or average) structured aspect which requires a certain functional representation.

A Random Variable is a variable which takes a certain number of numerical values according to a particular probability distribution. For example, magnetization of an infinitely extended horizontal slab would constitute a random function if the magnetization at any location could be described by a Gaussian probability distribution. The regionalized variable can be considered as a realization of the set of random variables $\{Z(x), x \in D\}$; this is called a Random Function (RF).

The probabilistic interpretation of a regionalized variable as a particular realization of a random function requires a partial or total knowledge of the probability law of the random function, which in practice is not possible. To solve this issue, certain assumptions involving various degrees of spatial homogeneity are required. These assumptions are included under the hypothesis of stationarity. A random function is strictly stationary where the spatial law is invariant by translation. This means that two $Z(x)$ and $Z(x+h)$ random variables evaluated at the locations x and $x+h$ have the same distribution law independent of the translation vector h .

2.4.3 Spatial variability and the variogram.

Consider two realization of a random function $Z(x)$ and $Z(x+h)$ at two locations, separated by a particular distance, h . For small separations, the values of the function might be similar, but as the separation distance increases, they will likely become different. A measure of the variability between the values is provided by a function, called the variogram which is defined, as the mathematical expectation of the squared difference between the numerical values at each of the two locations x and $x+h$.

$$2 * \gamma(x, h) = E\{[Z(x) - Z(x + h)]^2\} \quad (2.3)$$

The semi-variogram is the half of the variogram and in this thesis is referred to simply as the variogram. It increases in value as the samples become more dissimilar with the distance (Gringarten and Deutsh, 2001). Second order stationarity hypothesis establishes that the mean of the random variable has to exist and must be constant within the domain. Furthermore the variance of the variable has to exist and must depend only on the separation between the values but not on the location. The meaning of the stationarity hypotheses is that the regionalized variable $z(x)$ varies around the same constant value within a domain (constant mean) and the variations have the same dispersion over the entire domain because the variance depends only on the separation.

Under the stationary hypothesis, statistical inference allows estimation of the variogram from the available data (sample) using the experimental variogram. This estimator is the arithmetic mean of the squared differences between two experimental measures at any pair of points separated by the distance h :

$$\gamma(h) = \frac{1}{2 \times N(h)} \times \sum_{i=1}^{N(h)} [z(x_i) - z(x_i + h)]^2 \quad (2.4)$$

Where $N(h)$ is the quantity of pairs of data separated at the distance h .

The definition of the variogram in equation 2.3 entails the following properties:

$$\gamma(0) = 0 \quad (2.5)$$

$$\gamma(h) = \gamma(-h) \geq 0 \quad (2.6)$$

The first of these two properties defines that at the origin or ‘zero’ separation distance the variogram should have a null value. A variogram whose value at the origin is different from zero is said to be discontinuous at the origin. This discontinuity is known as the ‘nugget’ effect. The nugget represents spatial variability at distances smaller than the sample spacing or the random component of the spatial variability. The second property (equation 2.6) implies that the variogram is an even function and also a positive function.

As h increases, in general, the mean quadratic deviation between the two variables $z(x)$ and $z(x+h)$ tends to increase and so $\gamma(h)$ increases from the initial zero value. Eventually, the variogram stops increasing value and levels off beyond a particular distance. This value is called the ‘range’. Close to the range, the variogram becomes more or less stable around a limit value $\gamma(\infty)$ called the ‘sill’ value, which, under certain conditions, is equal to the *a priori* variance of the random function (Fig. 2.6). The range represents the greatest distance within which there is a spatial correlation. For separation distances that exceed the range, the random variables, $Z(x)$ and $Z(x+h)$ are no longer correlated.

Computing variograms from sample data requires setting the separation distance vector parameters. They include the successive spacing distance or ‘lag distance’, the tolerance distance used to compute each lag. The spatial orientation of the lag which is referred to as the lag azimuth and the angular tolerance associated to the lag azimuth. These parameters require the definition of an area, referred as the tolerance region, within which the samples will be paired for the variogram calculation (Fig. 2.7). The selection of these parameters depends on the sampling pattern of the available data. For regular sampling grids, the lag distances will be equal to the sample spacing. Irregular sampling grids require trial and error to set the lag distances that yield the best variogram in terms of the degree of smoothing (noise reduction).

2.4.4 Variogram Models.

Any geostatistical study, including estimation, simulation or a simple spatial variability description require the construction of a legitimate model to characterize the spatial structure of the regionalized variable (Journel and Huigbrejts, 1978). Legitimate variogram models are those that satisfy a property called conditional negative definite; a variogram $\gamma(h)$ is conditional negative definite if:

$$\forall k \in \mathbb{R}, \forall \lambda_1, \dots, \lambda_k \in \mathbb{R} \setminus \sum_{i=1}^k \lambda_i = 0, \forall x_1, \dots, x_k \in \mathbb{R}^n \quad (2.7)$$

$$\sum_{i=1}^k \sum_{j=1}^k \lambda_i \lambda_j \gamma(x_i - x_j) \leq 0$$

Equation 2.7 constrains the infinite possible functions to those that warrant the intrinsic hypothesis for the random process under study (Journel and Huigbrejts, 1978).

Four isotropic variogram models most commonly used in geostatistical modeling are presented below. The models use h to represent the separation or lag distance, a to represent the range distance, and c to represent the sill value.

2.4.4.1 Nugget effect model.

This model reflects a lack of spatial structure or no spatial correlation. In practice, it is due to measurement errors or to the existence of a micro-structure not detectable at the survey scale (Emery, 2000). In physics and geophysics, this is the case of ‘white noise’ signal (Fig 2.8A).

$$\gamma(h) = \begin{cases} 0 & \text{if } h = 0 \\ c & \text{if } h > 0 \end{cases} \quad (2.8)$$

2.4.4.2 Spherical model.

The spherical model is the most common in geostatistical modeling (Fig 2.8B). The equation that defines this model is:

$$\gamma(h) = \begin{cases} \frac{3}{2} \left(\frac{h}{a}\right) - \frac{1}{2} \left(\frac{h}{a}\right)^3 & \text{if } h \leq a \\ c & h > a \end{cases} \quad (2.9)$$

The model has linear behavior at separation distances close to the origin. A tangent to the model at the origin cuts the sill at a distance equal to two thirds of the range distance (Fig. 2.8B)

2.4.4.3 Exponential model

The Exponential model is defined as:

$$\gamma(h) = c \left(1 - \exp\left(-\frac{3h}{a}\right)\right) \quad (2.10)$$

It has a linear behavior for small separation distances and reaches the sill asymptotically at a practical range a' , which is the separation distance at which the variogram value is 95% of the sill value c (Isaaks and Srivastava, 1989). This practical range a' , when compared to the effective range- a for a spherical model which reaches the sill value c , is three times larger (Fig. 2.8C).

2.4.4.4 Gaussian model.

The Gaussian model is used for extremely continuous phenomena, as it has a parabolic behavior at the origin (Journal and Huijbregts, 1978). The analytic expression is given by:

$$\gamma(h) = c \left(1 - \exp\left(-\frac{3h^2}{a^2}\right)\right) \quad (2.11)$$

The sill value c , for this model is reached asymptotically, and the practical range a' is larger than the effective range of a spherical model, with $a' \sim 1.73a$ (Fig. 2.8D)

2.4.5. Scaling laws using geostatistical tools

Evidence from geophysical field data suggests that physical properties of rocks exhibit scaling behavior. Therefore physical property depends on the scale at which they are measured and it can expect changes in the distribution with variation in the volumetric scale. Geostatistics provides tools to quantify the histogram and variogram change with the volumetric scale (Frykman and Deutsch, 2002).

Consider a stationarity variable from which two sets of measurements are available at two arbitrary volumetric scales v and V , with the size of v being smaller than the size of V . Geostatistical scaling laws establish that the spatial variability quantified by the variogram at the larger volumetric scale V , denoted by $\gamma_v(h)$ is equal to the point scale variogram, denoted by $\gamma(h)$ minus the average variogram within the volume V , denoted by $\bar{\gamma}(V,V)$. The average variogram value is constant for separation distances larger than the size of the volume V (Fig. 2.9). The term $\bar{\gamma}(V,V)$ quantifies the magnitude of the change in spatial variability with the size of the volume.

Assuming that the mean and variance of any set of measured data does not depend on the particular sampling locations and only depends on the separation distance between the measurements (stationarity), intuitively it is expected that with an increase of the size of the sampling volume, the spatial variability should decrease because extreme values will be averaged within the larger volumes.

Using the relation:

$$\gamma_v(h) = \gamma(h) - \bar{\gamma}(V, V) \quad (2.7)$$

from Journel and Huijbregts (1978), it is possible to calculate variance as function of the size of the sampling volume (Frykman and Deutsch, 2002), when point scale and larger scale measurements are available.

2.5 Geophysical Inversion theory.

2.5.1 Introduction

Geophysical inverse theory has foundations in linear algebra and optimization of several variable functions. It has been applied to geophysics as an aid to solve large sets of engineering, geotechnical and mining exploration problems, all related to the subsurface distribution (model) of one or more physical properties, using (Parker, 1994) surface geophysical data such as gravity, magnetic or electromagnetic surveys. Where limited knowledge of the subsurface is required, geophysical data can be directly interpreted. Otherwise, geophysical data are processed to obtain quantitative subsurface information. Conceptually, a physical property model requires a decision of how the Earth is going to be represented. If the relevant physical property is expected or assumed to vary in all three

spatial directions, then the 3-D space being investigated is divided into equal volume cells, each of which has a constant physical property value.

The procedure considers the surface measured data (d) as a function of one or more subsurface physical property distribution, usually referred as the model (m). This is written as:

$$d=F(m) \tag{2.9}$$

In this equation, F is a function usually named the forward operator. Geophysical inversion solves this relation for ‘m’ by finding the inverse function of F, denoted by F^{-1} . This can be written as:

$$m=F^{-1}(d) \tag{2.10}$$

Geophysical data are finite in number and inaccurate. Together along with the fact that the number of cells within the model is normally greater than the quantity of collected data means that the problem is under-determined and equation 2.10 has a non-unique solution. To solve for non-uniqueness, some information regarding the expected solution must be known prior solving an inverse problem.

2.5.2 Forward modeling.

Before any inversion procedure, the forward problem has to be solved. Most forward problems in geophysics are solved numerically and discretization is required. According to the space dimension of the studied problem, the Earth is divided in different ways. Cubic cells are used in a 3-D case, rectangular cells in a 2-D case and layered model is suitable in the 1-D case. Within each cell of the Earth model, the physical property is considered constant (Oldenburg and Li, 2005). The forward model is performed by estimating an initial “guess” for the earth model. Available prior information is used to constrain the first model. Using the initial model, predictions of what measurements or data, referred to as the predicted data,

would be collected if a survey is carried out over the initial Earth model. Mathematically, the forward modeling problem is solved by finding a solution to the linear system of equations, in matrix notation:

$$\bar{\mathbf{d}} = \mathbf{G} \times \bar{\mathbf{m}} \quad (2.11)$$

Where, $\bar{\mathbf{d}}$ and $\bar{\mathbf{m}}$ are vectors of N (number of data) and M (number of model cells) components, respectively. \mathbf{G} is a matrix of $N \times M$ elements, accounting for the physics of the problem, boundary conditions and geometric array of the survey (Oldenburg and Li, 2005).

2.5.3 Inverse problem.

In the inverse problem, the goal is to calculate a model \mathbf{m} that satisfies equation 2.11, considering that a limited and noisy set of data is available. As mentioned previously, the problem is under-determined and therefore an infinite number of models can solve the system of equations. Selecting one model from the infinite possible solutions requires definition of a model norm that provides a way to measure the ‘length’ or size of each model to sort them using some criteria. One approach is, for example, sorting in decreasing order and then selecting the smallest norm model.

Geophysical data are always inaccurate, but in practice the errors are unknown and must be estimated. For the purpose of geophysical inversion, the data errors are assumed to be independent and follow a Gaussian distribution with zero mean and the standard deviation for each error datum is known. A function is designed to measure how well the predicted data fit or match the observations:

$$\phi_d = \sum_{i=1}^N \left(\frac{d_i^{\text{obs}} - d_i^{\text{pre}}}{\epsilon_i} \right)^2 \quad (2.12)$$

Where N is the number of observations, d_i^{obs} is the i^{th} observed datum, d_i^{pre} is the i^{th} predicted datum from the forward modeling and ε_i is the standard deviation of the associated error to the i^{th} datum (Phillips, 1996; Oldenburg and Li, 2005).

The inverse problem is posed as the following optimization problem:

Minimize:

$$\phi(m) = \phi_d + \beta \times \phi_m \quad (2.13)$$

Where ϕ_m is the model norm function, which is defined to penalize discrepancies between the constructed model and a reference model and to keep the model as flat as possible in all particular spatial directions (Oldenburg and Li, 2005). The following equation represents a model function for a tridimensional physical property model:

$$\phi_m = \alpha_s \int_V (m - m_{\text{ref}})^2 dz + \alpha_x \int_V \left(\frac{\partial m}{\partial x}\right)^2 dz + \alpha_y \int_V \left(\frac{\partial m}{\partial y}\right)^2 dz + \alpha_z \int_V \left(\frac{\partial m}{\partial z}\right)^2 dz \quad (2.14)$$

The alpha coefficients in equation 2.14 control how small and flat the model solution is permitted. The smaller the coefficients the higher the particular component is allowed. For example, suppose an extreme case in which alpha in the x direction in the model is fixed to zero, this would mean that in that particular direction, large fluctuations in the physical property are allowed, so zero flatness is introduced in that direction.

The coefficient beta is a positive constant parameter that accounts for the balance between best fit of the data for the simplest and flattest model solution. For small beta values, (near zero), the recovered model would fit the data exactly but some noise related features would be added to the model solution. Conversely, if beta is large, some of the structural information that is in the data is not being introduced into the models as the misfit is large and only the large scale features are incorporated (Oldenburg and Li, 2005).

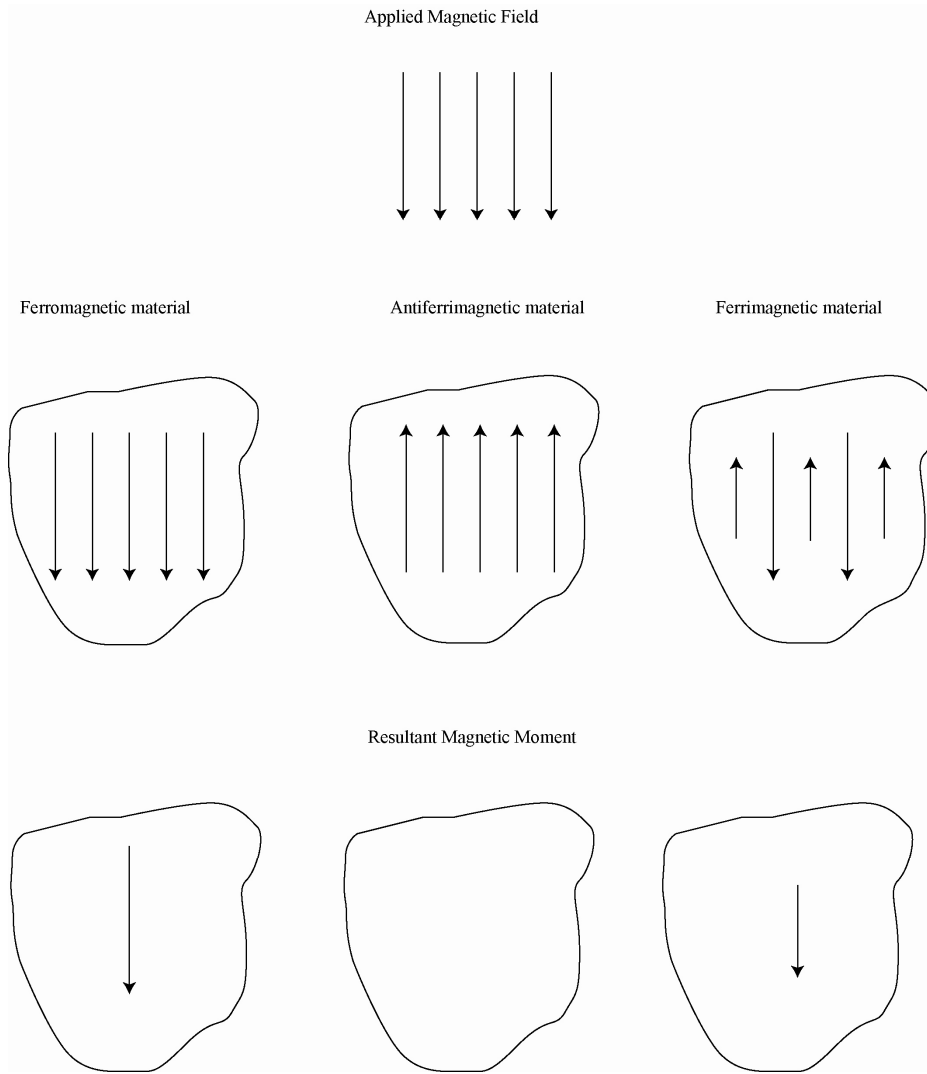


Figure 2.1. Different types of ferrimagnetic materials. Top panel shows direction of the applied magnetic field, middle panel display the three types of magnetic materials, from left to right: in ferromagnetic materials magnetic dipoles orientation are parallel to the applied field, in antiferromagnetic the magnetic dipoles are 'anti-parallel and in ferrimagnetic material some dipoles are oriented parallel and some are oriented anti-parallel. Bottom panel indicates the resultant magnetic moments, largest value for ferromagnetic, zero for antiferromagnetic and a mid-value for ferrimagnetic material (Modified from Gubbins and Herrero-Bervera, 2007)

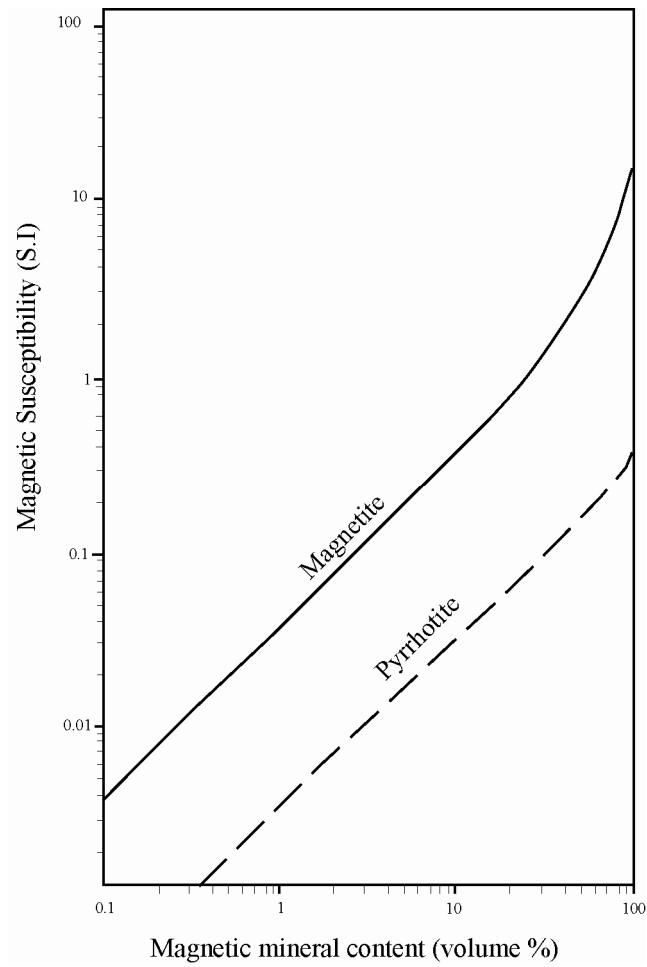


Figure 2.2. Magnetic susceptibility versus the volumetric percent of magnetite (solid) and pyrrhotite (dashed). A linear relation is observed for volumetric mineral content lower than 10% for magnetite and practically for the entire range of pyrrhotite content (Modified from Clark, 1997).

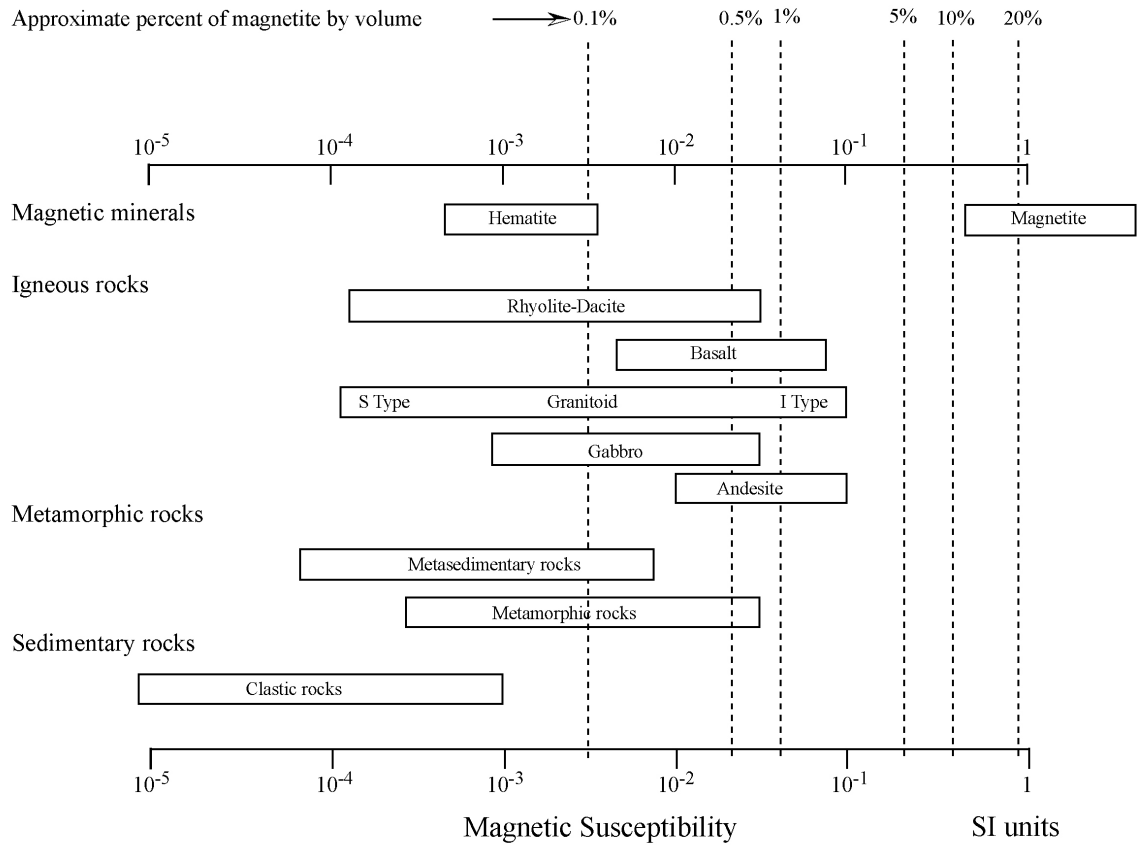


Figure 2.3. Magnetic susceptibility of rocks and magnetic minerals. (Modified from Clark, 1997).

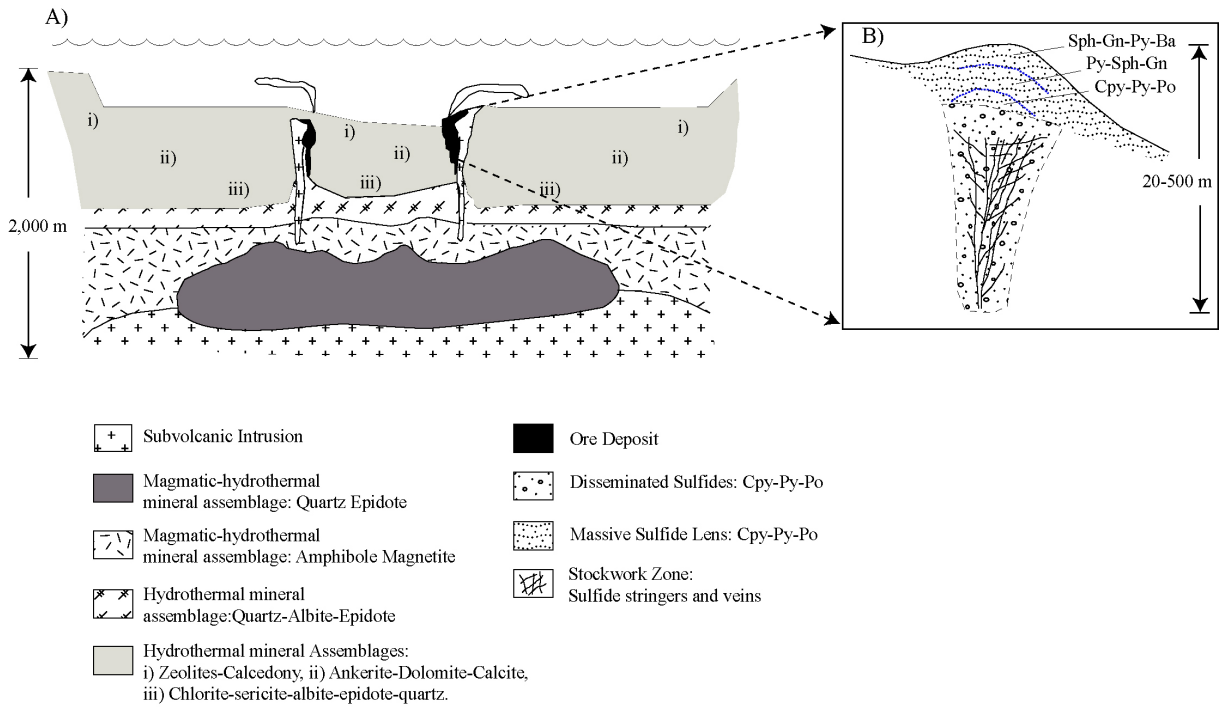


Figure 2.4. Schematic vertical section across a VMS deposit. A) Mineral assemblages within magmatic-hydrothermal and hydrothermal alteration zones (modified from Franklin et al., 2005). B) VMS ore body mineralogical zones. Abbreviations: Cpy=Chalcopyrite, Py=Pyrite, Po=Pyrrhotite, Sph=Sphalerite, Gn=Galena, Ba=Barite (Modified from Lydon, 1988).

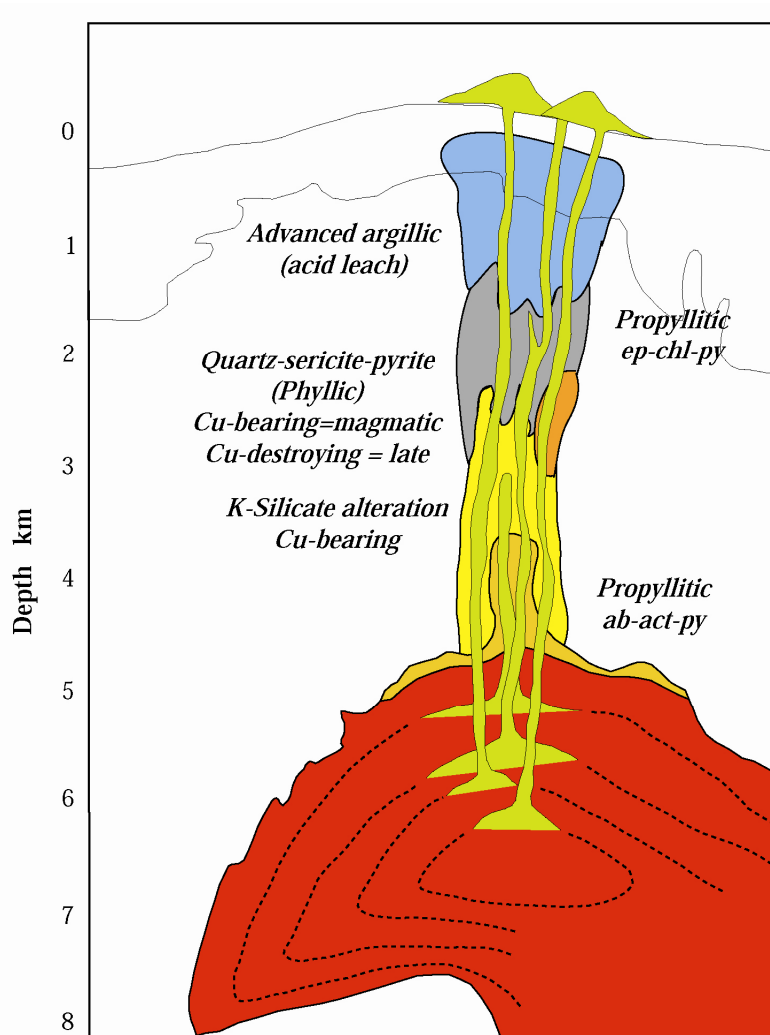


Figure 2.5. Schematic vertical section across a Porphyry copper deposit model, showing the distribution of hydrothermal alteration zones (modified from Dilles and Eunadi, 1992).

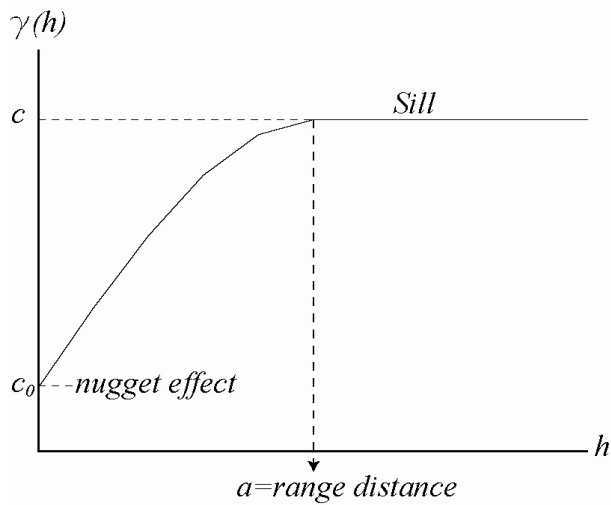


Figure 2.6. Variogram parameters. Nugget effect c_0 is the variogram value at the 'origin' or zero distance. The range distance 'a' is the distance at which the sill (c) value is reached.

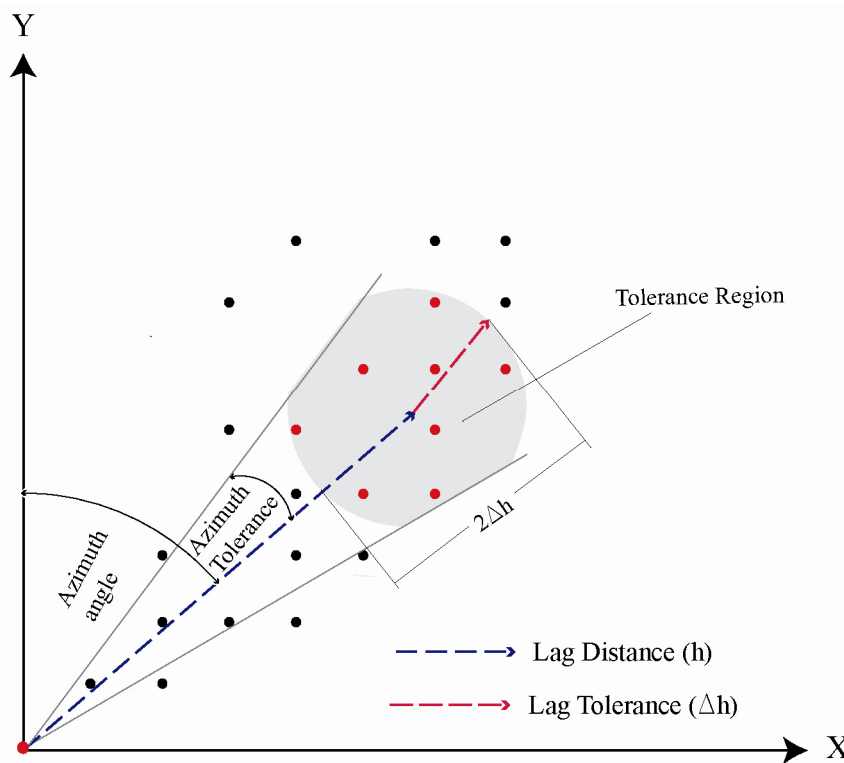
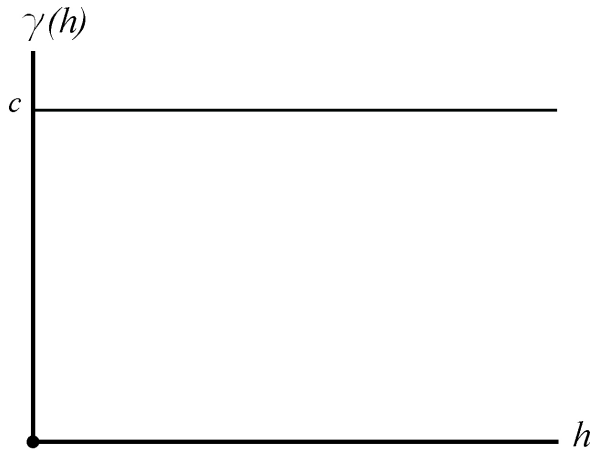
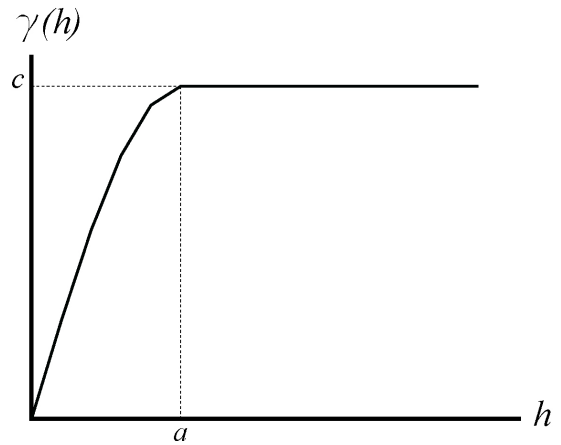


Figure 2.7. Example of a tolerance region used in experimental variogram calculations. The sample point located at origin will be paired with all the points within the tolerance region (gray shaded area).

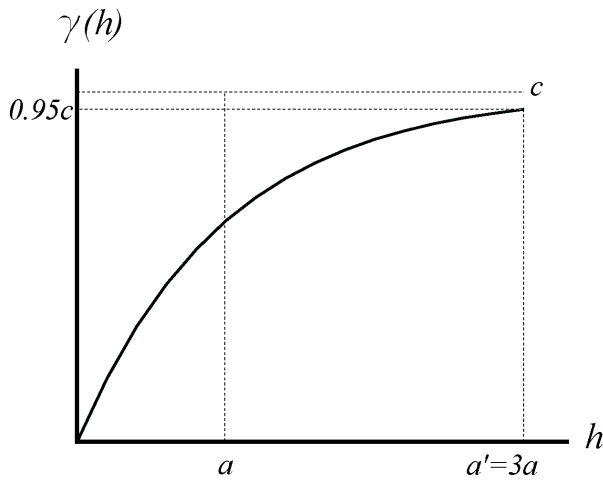
A) Nugget Effect



B) Spherical



C) Exponential



D) Gaussian

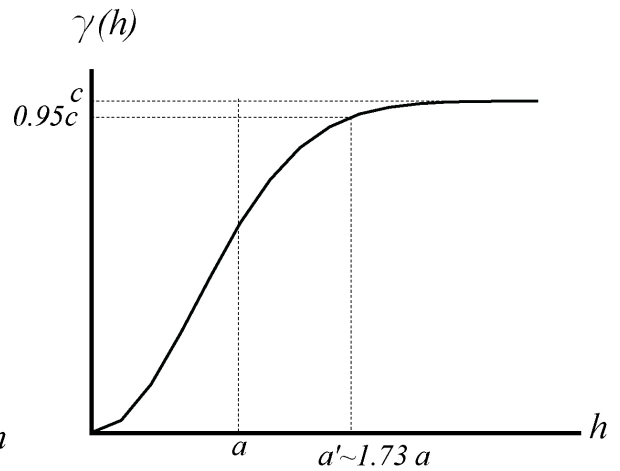


Figure 2.8. Variogram models of common use in geostatistics. A) Nugget effect, B) Spherical, C) Exponential and D) Gaussian. Sill and range parameters are illustrated, showing the relation between the range distance a of a spherical model and the range a' of exponential and gaussian models which reach their sills asymptotically (modified from Journé and Huijbregts, 1978).

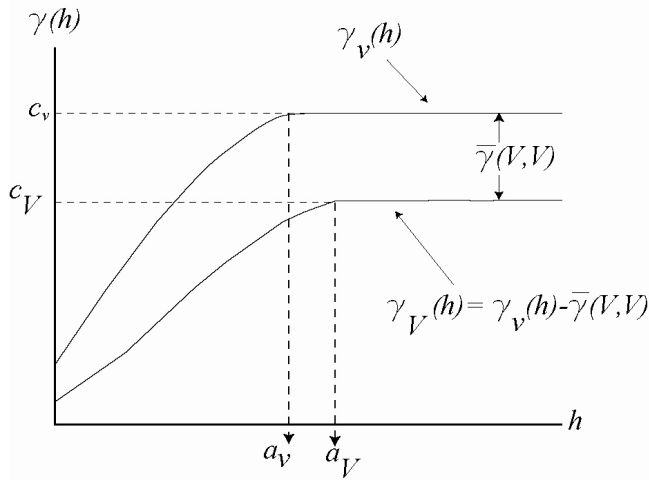


Figure 2.9. Geostatistical scaling law for two variograms models at different volumetric scales v and V . Smaller scale variogram $\gamma_v(h)$ spreads out from larger scale variogram $\gamma_V(h)$ with the separation distance h . For distances greater than the range of the larger scale data, the magnitude of the spread is constant and equals to the average variogram value, thereby providing a tool to scale variogram models (modified from Journel and Huigbrejts, 1978).

Table 2.1. Types of magnetization and associated magnetic susceptibility ranges. (based on Clark 1997)

Type of Material	Magnetization	Magnetic susceptibility (SI)
Diamagnetic	Low negative	$-5.9 - 1.1 \times 10^{-5}$
Paramagnetic	Low positive	$10^{-5} - 10^{-2}$
Antiferromagnetic	Low positive	$10^{-5} - 10^{-2}$
Ferrimagnetic	High Positive	$10^{-4} - 1$

Table 2.2. Magnetic susceptibility for minerals observed within hydrothermal ore deposits. (based on Clark 1997).

Mineral	Type of magnetism	Magnetic susceptibility (SI)
Pyrrhotite (monocline)*	Ferromagnetic	0.1 - 0.4
Magnetite*	Ferromagnetic	1.3 - 12.5
Chalcopyrite	Paramagnetic	$30 - 40 \times 10^{-5}$
Pyrite	Paramagnetic	4.3×10^{-5}
Bornite	Paramagnetic	$30 - 40 \times 10^{-5}$
Biotite	Paramagnetic	$90 - 330 \times 10^{-5}$
Muscovite	Paramagnetic	$4 - 75 \times 10^{-5}$
Epidote	Paramagnetic	100×10^{-5}
Amphibole	Paramagnetic	$50 - 340 \times 10^{-5}$
K-Feldspar	Diamagnetic	-1.4×10^{-5}
Quartz	Diamagnetic	-1.5×10^{-5}
Calcite	Diamagnetic	-1.3×10^{-5}
Gypsum	Diamagnetic	-2.9×10^{-5}
Anhydrite	Diamagnetic	-5.9×10^{-5}
Dolomite	Paramagnetic	1.2×10^{-5}

*Single domain

Chapter 3. Scaling of magnetic susceptibility using synthetic models.

3.1 Introduction

Synthetic geologic models are tools used to build idealized representations of a particular geologic setting. They also are useful to explore physical property (e.g. magnetism, density, conductivity, and resistivity) links to geologic features within the geologic setting of interest. Rock physical property contrasts generally are related to important geologic features that can be associated with mineral deposits. These properties can be used to define the type of ore, location, depth and size of the deposit, depending on the physical property contrast between the deposit and the host, or country rock. Geophysical surveys are sensitive to changes in physical properties and therefore are widely used in mineral exploration, especially in the search for concealed deposits. Physical property models capturing the small-scale spatial behavior of magnetic susceptibility make possible their integration into larger-scale distributions obtained with geophysical inversions. Establishing reliable statistical correlations between physical properties and rocks are crucial for building up predictive mine exploration tools. Numerical modeling approaches attempting to establish these correlations should take into account the scaling nature of both physical property and ore content.

This chapter addresses the issue of physical property scaling using synthetic magnetic susceptibility models. The models are constructed with cubic cells of different sizes in order to reproduce different scales. For this application of the synthetic tool, a three dimensional domain is considered. Geologic information for the synthetic exercise is established using models of rock type and magnetic susceptibility. The physical property models are constructed to test volumetric scaling relations of magnetic susceptibility using geostatistics tools. These models provide the opportunity to understand how the statistical distribution of the physical property is affected by the volume changes associated with measurements.

The synthetic model exercise attempts to reproduce the volume scale change from core, hand samples or well-log magnetic susceptibility measurement volumes to that of a larger scale geophysical survey and geophysical inversion. The volumetric scale change is reproduced synthetically by modifying the size of the unit cell of a basic physical property model. Specifically, the cell size is increased systematically from a small to large cell size, in order to reproduce differences in the sample volumes applicable to exploration geophysical data. A rough estimate of the volumetric scale change can be achieved considering that the volume involved through point scale measurements of magnetic susceptibility, such as hand sample or drill-hole core scale samples, commonly involve few cubic centimeters whereas the volume associated with ground or regional magnetic or electromagnetic survey measurements involve larger volumes, likely in the range of 10^3 to 10^6 m³. Hence, the scale ‘jump’ might involve several orders of magnitude; thus, a suitable procedure to address the scaling issue is required to enhance the utility of small scale measurements in regional surveys.

The basic magnetic susceptibility model utilized herein is progressively scaled to larger cell size models using two methods. First, a simple arithmetic average of physical property values of cells at the small-scale model is calculated to fill the larger scale model cells. Second, moving average windows provide smoothed physical property models at the large volumetric scales. The synthetic scaling analysis of all rock types in the synthetic model is referred to as a global model, whereas in the cases where single rock types are considered individually, a local model results.

Once several scale models are calculated, statistical and geostatistical analyses evaluate the resulting models. Histograms describe how the physical property distributions change scales. Experimental semi-variograms characterize and quantify the spatial variability of the magnetic susceptibility distributions at the different scales. The advantage of geostatistics to the scaling problem is the available tools (e.g., variance dispersion and averaged variogram) which predict how the statistical distribution, variance and the pattern of spatial variability change with a change in the volume associated with the data. The result permits point source data to be scaled, leading to the calculation of larger scale physical property models. The

scaled models must honor the small scale features of the measurements and therefore can be integrated into the geophysical inversion procedure or other numerical model technique.

3.2 Model parameters

Evaluating the scaling of magnetic susceptibility requires the construction of synthetic magnetic susceptibility models. A simple geologic setting is appropriate to reproduce the scale changes in the physical property distribution. Model parameters should include rock type, physical property value and a cell size. The first two parameters are related because physical properties are linked to rock units. The third is variable and can be changed to reflect the desired scale of investigation.

3.3 Synthetic models

Scaling of synthetic models requires knowledge of the geology, physical property values and cell size. This section provides the details on how each model parameter is established for the synthetic analysis discussed herein.

3.3.1 Geologic and physical property setting

Geologic features include the number of rock types, the characteristics of the contacts between the geologic units and the shape and size of the rock bodies. Magnetic susceptibility values to be applied to each synthetic rock unit are selected from physical property measurements collected from drilled rocks within a porphyry copper deposit. The

measurements, available at the scale of drill-hole cores, are used as reference values to populate the basic magnetic susceptibility model at the smallest cell size scale.

Three rock types define the geologic setting for the synthetic exercise. Simple geometric shapes for the rocks are utilized. The rock bodies have tabular shapes with sharp planar geologic contacts. Contacts are oriented parallel to the Y axis of the model (Fig. 3.1). Dimensions on the three orthogonal X, Y, Z axes of the model correspond to 450 m in the X direction, and 300 m in each the Y and Z directions. In this geometric configuration of a geologic setting, the size of each rock unit is completely defined by the thickness measured along the X axis, with values of 100 m for rock type 1, 200 m for rock type 2 and 150 m for rock type 3 (Fig. 3.1). The identical geologic configuration is used for all the cell size models in the synthetic models presented herein.

For the magnetic susceptibility model population, measurements collected from core samples from drilled rocks at Rio Blanco porphyry copper deposit in the Andes of central Chile are used as reference values to constraint the statistical distributions of the basic model. Specifically, the average and standard deviation from the available measurements are used as target values for the synthetic physical property distributions. Histograms of the available measurements of magnetic susceptibility, plotted in logarithmic scale, showed a similar shape to those of logarithmic normal distributions. Such a distribution is likely associated with the dominance of positive values, the high quantity of low values and the high variance of the physical property distributions (Limpert, et al., 2001) that commonly characterize magnetic susceptibility data sets. These distributions also apply to the concentration of gold and other metallic elements on the crust (Krige, 1966). Based on these constraints, a Matlab code designed to randomly select magnetic susceptibility (k) values conditioned to follow a log-normal distribution particular mean and standard deviation is applied to the model. These values populate the model cells. The resulting physical property models follow log-normal distributions. The constraints on physical property used are shown in Table 3.1, where the mean and standard deviation for each unit is presented. Furthermore, a high magnetic susceptibility contrast is imposed between rock type 1 and rock types 2 and 3. The contrast between rock units 2 and 3 is constrained to describe a smoother transition on the physical property values.

3.3.2 Cell size setting.

Field magnetic and electromagnetic surveys provide measures of geophysical variable within volumes, through areas or along lengths. Accurate measurements of the sampled volume are not generally available because of the uncertainty in the parameters (electrical conductivity of the material, signal frequency and the degree of heterogeneity of the subsurface geology) affecting the signal propagation within the observed portion of the Earth. To obtain an accurate quantification of the actual volume associated with magnetic susceptibility measurements, a calibration of the magnetic measurements must be performed (Gattacceca et al, 2004). These analyses are complex and beyond of the scope of this thesis.

Arrays of magnetic susceptibility measurements are geophysical surveys that can involve multiple scales and can be performed using different instruments and techniques. Magnetic susceptibility data for this study were collected using a KT-9 instrument, a hand portable magnetic susceptibility meter, which acquires measurements involving sample volumes of a few cubic centimeters. Therefore the data collected using this instrument correspond to the smallest volumetric scale measurements, and are a data-type commonly collected during exploration. Larger scale magnetic susceptibility measurements can be derived from electromagnetic surveys performed using frequency domain instruments (e.g., EM-31). The sample volume depends on the separation between the transmitter and the receiver and how deep the electromagnetic signal penetrates the subsurface. To estimate the volume associated with the measurements, it is assumed that the electromagnetic signal penetrates a constant depth equal to the separation between the transmitter and the receiver of the instrument. This depth is commonly referred to as the coil separation, and provides the basis for calculating the associated volume.

In the synthetic models herein, the volume of the cubic cells of the models is set to be representative of the volume sampled during the field data collection using different survey tools. Therefore the smallest volume cell model should represent the smallest scale data set and higher volume cells should correspond to larger scale physical property measurements.

Estimated volumes for the different surveys and the cell volumes (Fig. 3.2) indicate that the change in volumetric scale can be from 4 to 10 orders of magnitudes, considering the jump from the smallest volumetric scale data set with the KT-9 (10^{-4} m^3) to the largest volumetric scale obtained, for example, with the MAXMIN instrument with a coil separation of 100 m (10^6 m^3).

Synthetic models of cubic cells with sizes of 5, 10, 25 and 50 m are then constructed using the UBC-GIF mesh-tools software. The change in 3 orders of magnitude in volumetric scale from cell size equal to 5 m ($1.25 \times 10^3 \text{ m}^3$) to the volume of $1 \times 10^6 \text{ m}^3$ associated with a cell size (or a coil separation) of 50 m reproduces the actual change in volumetric scale from the EM-31 to MAXMIN surveys (Fig. 3.2). The change in scale from KT-9 to the EM-31 is also equivalent to the jump between the synthetic models of 5 m to the model of 50 m cell size (Figure 3.2). The volume comparison between the estimated sampled volumes and those of the synthetic models has shown that starting with a basic model with 5 m cell size and then scaling it up to 50 m can reproduce the change in the volumetric scale estimated for the field measurements collected during the study.

3.3.3 Populating the rock type and physical property models.

Once the geologic features and the physical property are established, the three-dimensional domain is divided into cubic cells of 5 m size, representing the smallest cell size scale for the synthetic models. Each cell is filled with a unique rock type code and a constant magnetic susceptibility value. In essence, each cell of this basic model is characterized by the three following parameters, a numeric code to describe the rock type, the magnetic susceptibility value and the cell size.

The basic magnetic susceptibility model at 5 m cell size is progressively scaled to 10, 25 and 50 meter cell sizes by arithmetically averaging values from the basic model contained within the larger cells of the 10, 25 and 50 meters cell models (Figs. 3.4 A, 3.5 A, 3.6 A).

3.4 Statistics of synthetic magnetic susceptibility models.

Calculating averages of the physical property over successively larger cells sizes produces changes the basic statistics (Table 3.2). For example, increasing the cell size of the model from 5 to 50 meters is accompanied by a reduction of the spread between the maximum and minimum values of the physical property distribution. In the global model, the maximum magnetic susceptibility value decreases from 837.5 in the basic model (5 m cell size) to 27.8 for the 50-meter cell size model (Table 3.2). The decrease in the maximum value reflects the averaging of extreme magnetic susceptibility values in the 5 meter cell size where they are surrounded by smaller values in the nearly 5 m cells, all combined within the 50 m cell size. Conversely, the minimum value is averaged with larger magnetic susceptibility values, which produces an increase from 0.005 in the smallest scale model to 1.7 in the 50 m cell size model. Furthermore, the magnetic susceptibility variance values of the global model also diminished, from the small-scale model to the larger scales model, from a variance of 640.06 for the 5 m cell size model to a value of 85.64 in the largest scale model (Table 3.2).

The decrease in the magnetic susceptibility variance value with the increase in cell volume for the local models follows a linear inverse relation in a logarithmic plot, indicating a power law relationship (Fig. 3.7). The effect of increasing cell volume in the reduction of the magnetic susceptibility variance is greater for the local models than the global model over the selected cell size scales. The deviation of the global model from the local models derives from a faster reduction in the magnetic susceptibility variance over the scale changes investigated (Fig. 3.7). In the case of the local magnetic susceptibility models, averaging the physical property produces a reduction in the difference between the maximum and the minimum magnetic susceptibility for the three up-scaled models (Table 3.2). This also reduces the difference

between the magnetic susceptibility value of every particular cell values for the 10, 25 and 50 m model and the average of the physical property mean for the entire rock unit. The effect is a rapid decrease of the physical property variance for the different cell sizes scales. The reduction in variance with the cell volume following an inversely proportional relation is a consequence of the uncorrelated (random) nature of the physical property distribution within the local models (Isaaks and Srivastava, 1989).

When calculating the variance for global magnetic susceptibility models at the three up-scaled models, cell values from the three different physical property distributions associated with the 3 rock types contribute to the variance computation. The physical property contrast between the three rock types attenuates the smoothing effect achieved by the averaging, which is reflected in the lower variance reduction.

The calculated variance for each model can be used to obtain a factor, f , referred to as the variance reduction factor (Isaaks and Srivastava, 1989). This factor represents the rate at which the variance is reduced when passing from a particular scale to another. If the original scale data has a variance s^2 , then the scaled model will have a variance equivalent to fs^2 . In the synthetic examples, investigated herein, both variances are available. It is therefore possible to calculate the reduction factor associated with each scale change. Table 3.3 presents the variance reduction factor associated with the scale change involved in the synthetic model. For the global synthetic model, the variance reduction factor drops from 0.24 to 0.13 as the cell size is increased from 5 to 50 meters. In contrast, the local model involves a stronger variance reduction as the factor fall from 0.13 to 0.001 over the same scale change.

3.5 Experimental variograms of magnetic susceptibility models

The magnetic susceptibility models created at the different cell size scales are used to calculate experimental variograms, including global variograms where the three rock types are analyzed together and local variograms where the three rock types are considered

individually. To perform the calculations, the orientation of the separation distance vector, which is referred to as the direction of the variogram, is set to be parallel to the X, Y and Z axis of the grids to describe the spatial variability in the 3-D space. The details of variogram calculation, interpretation and modeling are discussed in detail previously (see section 2.4.3 in chapter 2) and therefore will not be repeated below.

3.5.1 Experimental variograms of global magnetic susceptibility models.

Different shape and variogram values are noted in the global variograms at all scales where comparing the X-axis oriented variograms to those oriented parallel to the Y and Z axes, (Figs. 3.8 and 3.9). All scale variograms demonstrate the presence of anisotropy in the X direction, consistent with the synthetic models. For the smallest scale magnetic susceptibility model (cell size 5 m), the X oriented variogram (Fig. 3.8A) begins at a value for the average squared difference or variogram value of 550, gradually increases to a value around 720 at a separation distance of 100 m, before the variogram levels off at this value up to a separation distance of 150 m. At greater distances, the variogram decreases to a value of 620 at a separation distance of 250 m. As the variogram is a measurement of the spatial variability, it increases as the cell values become more dissimilar (Gringarten and Deutsch, 2001). In the synthetic model considered herein, at 100 m from the origin of the X axis, the rock type abruptly changes from rock type 1 to rock type 3 (Fig. 3.2). Here, the physical property distribution also changes significantly from a magnetic susceptibility mean within rock type 1 of 1.9 to an average of 25.6 within rock type 3. The next transition in the model occurs at 250 m from the X axis origin where rock type 3, which has a thickness of 150 m, changes into rock type 2. The physical property also changes slightly to a mean value of 22.5, which is detected by the drop in the variogram values for separation distances greater than 250 m.

The variogram behavior observed at the four scales in the global magnetic susceptibility models reflects an anisotropic nature of the synthetic physical property model. The shape of the experimental variogram depends on the orientation of the separation distance vector. At all

the scales, the experimental variogram of the global magnetic susceptibility models oriented in the X direction rapidly increases value within the first 100 m, before leveling off or increasing at a lower rate. Considering that the physical property values are randomly populated and no correlation between cells should be expected, the observed variogram behavior (Fig. 3.8) is related to the link between geology and physical property. Conversely, the Y and Z oriented experimental variograms have a value independent of the separation distance. These variograms reflect a pure nugget effect, or lack of spatial correlation for the analyzed variable (Fig 3.9). This is consistent with the geologic model as no change is established in the synthetic model for those directions

3.5.2. Experimental variograms of local magnetic susceptibility models.

Local magnetic susceptibility models at the four analyzed scales are used to calculate experimental variograms. Calculation of the synthetic magnetic susceptibility variograms tested how statistical parameters change where the cell size increases from 5 to 50 m. The results are equivalent for the three rock type units. They provide important information for the variogram interpretation, and are characterized by the following four features:

- i) Nugget effect with amplitudes close and in some cases replicating the respective magnetic susceptibility variance values calculated for each model. Barring edge effects, the variogram sills should all be close to the variances for the local data sets.
- ii) The X-oriented variograms are characterized by the largest fluctuations around the variance values (red curves on figures 3.10 through 3.12). This variance fluctuation is related to the geometric constraints of the geologic model where the thickness of the rock bodies is smaller in the X direction (see above) and consequently a fewer numbers of cells in this particular direction are involved in the variogram calculation. As the cell values are randomly populated, the value of the difference between nearby cells may be large. As a result, the average square difference of the physical property cell values will be also large.

- iii) As the separation distances become greater than one half of rock units size, the oscillations of the variogram values around the variance are larger. The quantity of pairs of cells separated more than one half of the rock unit size decrease largely in the three spatial directions. This is usually accompanied by more erratic variogram values (Gringarten and Deutsch, 2001; Isaaks and Shrivistava, 1989 and Journel and Huijbregts, 1978). This feature is so commonplace in dealing with assay values that the standard procedure is to entirely omit any $\gamma(h)$ values for sample separations greater than half the field width.
- iv) As the scale of the cell size is increased from 5 to 50 m (Figs 3.10 through 3.12), a systematic reduction of the variogram values is achieved, as is detected by the variance values calculated (Table 3.2). This is the smoothing effect of averaging over increasingly large volumes

The observed behavior in the experimental variograms for the local magnetic susceptibility models includes two important properties of the synthetic variable: (1) the independence of the variogram value with distance, commonly known as the pure nugget effects (Journel and Huijbregts, 1978), and (2) the independence of the variogram with the orientation of the separation distance vector or isotropy for the Y and Z orientations. Both features are a result of the random method used to populate the models cells with magnetic susceptibility values. Using this method, no spatial correlation is present and therefore, the average squared difference between the numbers of cells values separated by any particular distance should coincide with the variance of the physical property distribution for the rock type under consideration. The random nature of the magnetic susceptibility cell population is then confirmed by the coincidence between the experimental variogram values for the local models and the variance values calculated directly from the models. The second feature is related to the fact that for the X, Y, and Z oriented variograms, small changes in variogram values are detected. The small differences are mainly attributable to fluctuations in the quantity of pairs involved in the experimental variogram calculations.

3.6 Spatial continuity of magnetic susceptibility models.

As shown previously, histograms and experimental variograms of magnetic susceptibility synthetic models are affected by a change in the volumetric scale. These models tested the inverse scaling relation between cell volume and variance of magnetic susceptibility for randomly populated physical property models. The question that arises is whether there is a scaling relation in the cases where the physical property displays a degree of spatial correlation in a particular spatial direction. To address the question, a degree of correlation has to be added into the synthetic magnetic susceptibility models.

This section has three closely related objectives. These are: (1) Adding spatial continuity to physical property models using three dimensional average moving windows; (2) Quantifying the spatial continuity with the experimental variogram; and (3) Modeling the spatial variability by fitting theoretical variograms to the experimental ones.

3.6.1 Adding spatial continuity to the physical property models.

To add spatial continuity into magnetic susceptibility models, a smoothing procedure used average moving windows in three directions. The procedure also incorporates preferential smoothing of the magnetic susceptibility models. The intention is that larger weighting factors applied in a particular direction will increase the smoothness. The results are smoother transitions in the physical property values between high and low values zones increasing the degree of spatial correlation of the physical property within the rock units. These models create anisotropic magnetic susceptibility distributions suitable to represent relations between physical property and geologic features as commonly observed in geophysical surveys.

To describe the process and test the first results, a simple smoothed model is created within rock type 3 using three smoothing factors (3, 7, and 21) only in the X direction. The other two

orthogonal directions (Y and Z) lack smoothing. The effect of the physical property smoothing process can be detected with the achieved spatial variability pattern (Fig. 3.13).

3.6.2 Quantifying spatial continuity of the physical property using experimental variograms.

The spatial continuity of the physical property becomes larger as evidenced by the higher observed range distances. As the smoothing factor changes from 3 to 21, the range distances increase their values from 15 to 100 m. In contrast, the experimental variograms oriented in the Y and Z directions display a pure nugget effect as they oscillate around the variance values for all the separation distances (Fig. 3.13).

The resulting magnetic susceptibility average, variance and variogram range for each of the smoothing procedures are indicative of the degree of spatial continuity. Lower variances of the physical property are achieved by the more-smoothed models. These are associated with the increase in the range distance observed for X-oriented variograms (Table 3.4). With the application of smoothing, the dissimilarity between the cell values becomes lower, which is translated into lower variance values.

Smoothing results in an increased spatial correlation pattern for the different cell size scales magnetic susceptibility models. This is detected and quantified using the experimental variograms (Fig. 3.13). Utilizing the same smoothing factors of 3, 7 and 21 in the three spatial directions, smoothed isotropic models of magnetic susceptibility are constructed within rock type 3 (Fig. 3.14). The basic statistics of each calculated model is shown in Table 3.5. Smoothing procedures with factors of 3, 7 and 21 produce small changes in the magnetic susceptibility mean of the models, but a greater change in the variance values of the physical property, ranging from 480.46 to 22.02.

3.6.3 Modeling the pattern of spatial variability of an isotropic smoothed physical property model.

The spatial variability pattern of the pertinent physical property is quantified with experimental variograms which can be modeled by theoretical variograms. These theoretical variograms provide the analytical representation of the observed spatial variability. In these models, mathematical functions that best explain the observed experimental patterns are fitted to the experimental variograms. Reasons for applying variogram modeling to physical property data include:

- i) The variogram function must be known at all distances and spatial directions within the studied area for interpolation or simulation purposes (Gringengarten and Deutsch, 2001). This is a crucial parameter because the experimental variogram usually is incomplete and therefore provides only partial information about the spatial variability. It is only applicable within the sampled site.
- ii) There is a need to introduce geologic and sampling information regarding anisotropy, trends, data clustering and errors. The variogram can thus be a reliable representation of the geologic variability (Frykman and Deutsch, 2002).
- iii) Geostatistics scaling tools use the analytical function provided by the variogram model instead of the experimental variogram.

The variogram model provides useful information about the degree of continuity of the variable under investigation, any anisotropy, a value for the variance, and the range distance at which the variance value is reached. Another important aspect provided by the variogram model is the possibility to construct linear models of regionalization, which are represented by the sum of basic variogram models. Such models may explain complex patterns of spatial variability resulting from the superposition of independent components acting simultaneously, but at a different scale. The linear models of regionalization are also referred as the nested variogram models or nested structures (Journal and Huijbregts, 1978; Emery, 2000). The importance of variogram modeling in the scaling issue is described in the variogram scaling section (see below).

Once a variogram model is obtained, it must be cross validated by extracting a value from the data set at a particular location and then estimating that value with kriging using the remaining information. At completion over the whole data set, several criteria are used (Deutsch and Journel, 1998) to assess the goodness of the fit:

- i) The correlation factor between the estimated and true values should be close to 1.
- iv) The distribution of the estimation errors (estimated-true) should be symmetric and centered on a zero mean with minimum spread.
- v) The plot of the error versus the estimated value should display a symmetric scatter and centered on the zero error line.
- vi) The experimental variogram of the error values should display a pure nugget effect, indicating the absence of a spatial correlation.

The pattern of spatial variability achieved in the isotropic smoothed models with the smoothing factors of 3, 7 and 21 is modeled by fitting analytical functions, also referred as variogram models, to the resulting experimental variograms (Fig. 3.15). For this example, the spherical, exponential and Gaussian functions are used. These functions usually explain many of the spatial variability patterns observed in most of the ore estimation problems (Isaaks and Srivastava, 1989). The parameters used to fit the experimental variograms are selected considering the range distances (Figures 3.13 and 3.14) and the variance values calculated for the physical property models (Table 3.6). The experimental variograms are fit by the variogram models (Figs 3.15) for separation distances equal or strictly lesser than the range distances in the experimental models (Fig 3.13 and 3.14). In this case, the range distances are a threshold value, because only within this distance can the spatial variability be explained by a variogram model. For cell values separated by more than the threshold, no correlation between cell values is expected.

For the purpose of completing the variogram models, a cross validation procedure is performed for 9 variogram models. The different criteria are useful to constrain which variogram model best explains the observed (experimental) spatial variability pattern. Results

regarding the quality of the geostatistical modeling are presented in Table 3.7. The correlation factor between the estimated versus the true value, the average of the error and the variance of the error for each variogram model for the different smoothing factors are described herein. For the smoothing factor value equal to 3, the best correlation factor is achieved by the Gaussian variogram model. In the case of the smoothing factor equal to 7, the best correlation factor corresponds to the spherical model. Finally for the highest smoothing factor, the largest correlation factor is achieved using the Gaussian variogram model.

The high correlation factor between the estimate and the true values achieved is shown (Fig. 3.16) by the linear relations between the estimate and the true quartile values. The quartile-quartile plot is a useful tool to describe the linear relation as well as where the estimation is over or under the true values. For the smoothing factor of 3, the best fit is achieved by the Gaussian model whereas both the spherical and exponential models yield an underestimation of the true values. For the smoothing factor of 7 and 21, the quartile plot shows the good linear adjustment and no major differences can be observed except for the tails of the distributions.

Basic statistics and frequency histogram of the error estimation are presented respectively in Table 3.8 and Figure 3.17. The unbiased property of the kriging interpolation method results in a mean value of the estimation error that is approximately zero in all cases. The standard deviation of the error estimation is then used to determine which variogram model provides a better model of the pattern of spatial variability. Considering an increasing order of smoothing factors, the lowest standard deviation for each case is achieved by the Gaussian, spherical and Gaussian variogram models respectively (Table 3.8).

The experimental variogram of the estimation error can be used as a measure of the quality of the variogram model. A good spatial variability model (variogram model) should show a pure nugget effect for the associated estimation error. Figure 3.18 show standardized¹ experimental

¹A standardized variogram is calculated by dividing the variogram value at each lag distance by the variance value of the data used. This results in a sill value equal to 1.

variograms of the estimation error for each different model. In the case of the smoothing factor of 3, the estimation error variograms oscillate around a variance value of one (standardized variograms) indicating that the error estimation presents a zoned (periodic) pattern of spatial correlation. This correlation is associated with the size and location of the higher magnetic susceptibility zones within the magnetic susceptibility model (Fig. 3.14B). For the smoothing factor of 7, the error estimation variograms behave very similarly for the three variogram models. Spatial correlation of the estimation errors is detected by the increase of variogram values with separation distance until 30 to 35 m where the sill is reached. Finally, for the smoothing factor of 21, the spherical and exponential variogram models show the presence of correlated estimation errors whereas the error estimation associated with the Gaussian variogram model is similar to a pure nugget effect (Fig. 3.19).

The resulting variogram models are then suitable to be scaled, using the geostatistics scaling tools. However, before examining these models, scaling tools need to be briefly described. Along with the scaled variogram models at 10, 25 and 50 m cell size, it is important to compare the variance value decrease with the different averaging methods.

3.7 Scaling the variogram model using geostatistical tools.

Through variogram modeling, mathematical functions can be used to fit the experimental variograms. The modeled variogram captures and reproduces the pattern of spatial variability of the physical property at 5 m cell size scale. To represent the physical property at larger cell sizes, scaling of the variogram model is required. In this section, the spherical variogram model that fits the magnetic susceptibility model at the 5 m cell size is calculated with a smoothing factor of 7. This model will be scaled to 10, 25 and 50 m cell sizes using the scaling relations for second order stationarity random variables reviewed by Frykman and Deutsch (2002).

Before applying the scaling procedure, a brief review of important assumptions and definitions linked to the scaling relations are required. Detailed explanations are beyond the scope of this exercise, but excellent reviews are available from Journel and Huijbregts (1978). The first important definition is the notion of dispersion variance, denoted by $D^2(v/V)$. Consider two volumetric domains V and v for which a mean value of a variable (physical property, ore grade, pollutant concentration) is known. The dispersion variance is defined as the expectation (probabilistic case) or the average (deterministic case) of the square difference of the error where the mean value of the variable within the volume V is estimated using the values available at the volume, v (Matheron 1971, Journel and Huijbregts 1978). To illustrate this analogy in a mining environment, the dispersion variance corresponds to the average of the error that is made when a mean ore grade of a mine production block of volume V is estimated using ore grades available from drill-hole core or blast-hole assays, which reflect much smaller volumes. Rigorous mathematical demonstration presented by Matheron (1971) demonstrates that average variogram values at two arbitrary volumes and dispersion variance are related by:

$$D^2(v/V) = \bar{\gamma}(V, V) - \bar{\gamma}(v, v) \quad (3.1)$$

Where $\bar{\gamma}(V, V)$ and $\bar{\gamma}(v, v)$ are the average variogram values over all the possible separation vectors contained within the respective volumes V and v . This apparently simple relation describes the essence of the scaling issue. It shows that the dispersion variance corresponds to the drop in variance associated with a change in the volumetric scale. Again, by analogy to the mine case, the dispersion of the grades of mining production blocks (large volume) is less than the dispersion of the grades from drill-hole cores assays (small volume).

As the volume or cell size scale increases, the range of the variogram also increase. The magnitude of the increment is related to the difference in the cell size between both scales by:

$$a_V = a_v + (|V| - |v|) \quad (3.2)$$

Where a_V and a_v denote the ranges at larger and smaller volumetric scales respectively, $|V|$ and $|v|$ correspond to the cell sizes at the two considered scales.

From the geostatistics point of view, any regionalized variable can be described by two components that contribute to the spatial variability: a random component quantified by the nugget effect and a structured or spatially correlated component modeled by the function used to fit the spatial variability pattern of the variogram. When the volumetric scale increases, both components decrease to account for the variance reduction. Previously, it has been shown that the random component decreases in an inverse relation with the volume (Fig. 3.7).

Frykman and Deutsh (2002), present the following relation to quantify the reduced variance value at the larger volumetric scale V from the smaller volumetric scale v :

$$C_V = C_v \times \frac{(1 - \bar{\gamma}(V, V))}{(1 - \bar{\gamma}(v, v))} \quad (3.3)$$

Where C_V and C_v correspond to the variance at the two scales considered V and v . The terms $\bar{\gamma}(V, V)$ and $\bar{\gamma}(v, v)$ are the average variogram values calculated within the respective volumes and are related to the dispersion variance value (Frykman and Deutsh, 2002; Isaaks and Srivastava, 1989), as is shown in equation 3.1.

3.7.1. Scaling variograms of synthetic magnetic susceptibility models

In the synthetic example, the scaling of the variogram model is performed using a visual basic program developed by Oz et al (2002). The code allows the input of the variogram model parameters and the data as well as target scales. The code performs the calculations to obtain the parameters of the scaled variogram model by applying the formulas presented above and numerically calculating the average variogram values at the respective scales.

The spherical model calculated previously in section 3.6.3 is used here to test the scaling relations. This variogram model is used to fit the magnetic susceptibility variogram for the physical property model within rock type 3 with a smoothing factor of 7. The scaled up variogram models (Fig. 3.19) show that as the scale increase from 5 to 50 m, the respective variograms reach their sill or variance values at systematically lower values, as is expected. Figure 3.19 shows the scaled variogram models obtained using the geostatistical tools implemented in the scaling code (Oz et al, 2002) and the experimental variograms calculated from physical property models using block kriging to interpolate the physical property data. This interpolation method used the spherical variogram model at 5 m. The degree of adjustment between the experimental and modeled variograms is suitable within the range at each of the scales. The level of fit achieved in each case explains the differences in the magnetic susceptibility variance value obtained with the three different methods, arithmetic average, weighting average with the block kriging and the dispersion variance by the variogram scaling. The three methods establish a drop in the variance value. At smaller scales, the three methods predict some values whereas at larger scales, some differences should be expected (Fig. 3.20).

3.8 Conclusions

Physical property synthetic models have been used to test how the statistical distribution and the spatial variability pattern of magnetic susceptibility models change when the cell size of the models is increased. The approach described represents a methodology to integrate physical property measurements available at different sample volumetric scales. The approach depends on the development of a series of steps, each one providing some insights on the key aspects regarding the scaling issue.

Reproducing the sampled volume shift between the different field methods is achieved by setting a basic 5m cell size model and then increasing the cell size successively to 10m, 25m and 50m. Comparing the estimations of the sampled volumes and the volumes of cells of the synthetic models has shown that starting with the basic model at 5 m cell size and then scaling up to 50 m reproduced, with an acceptable level of matching, the change in volumetric scale estimated for the different field survey methods used during this study.

Testing scaling relations of magnetic susceptibility models requires that both random and smoothed models at several scales are examined. The results of the tests indicate that where randomly populated physical property models are simply scaled up by arithmetic averaging, the variance of the magnetic susceptibility of the scaled models and the volume/cell size of the models follow a linear inverse relation. How the variance is reduced depends on the rate of volume change. Similarly, for the smoothed physical property models, the scaling relation between the variance of the magnetic susceptibility and the cell volume follows an inverse relation, but is not linear.

Geostatistical scaling relations applied to synthetic physical property models have resulted in the estimation of larger scaled magnetic susceptibility models from a basic small scale model. This process has been shown to be valid, for this simple synthetic example, and constitutes a framework to be applied to the magnetic measurements available from Flin Flon in northern Canada and Rio Blanco in central Chile.

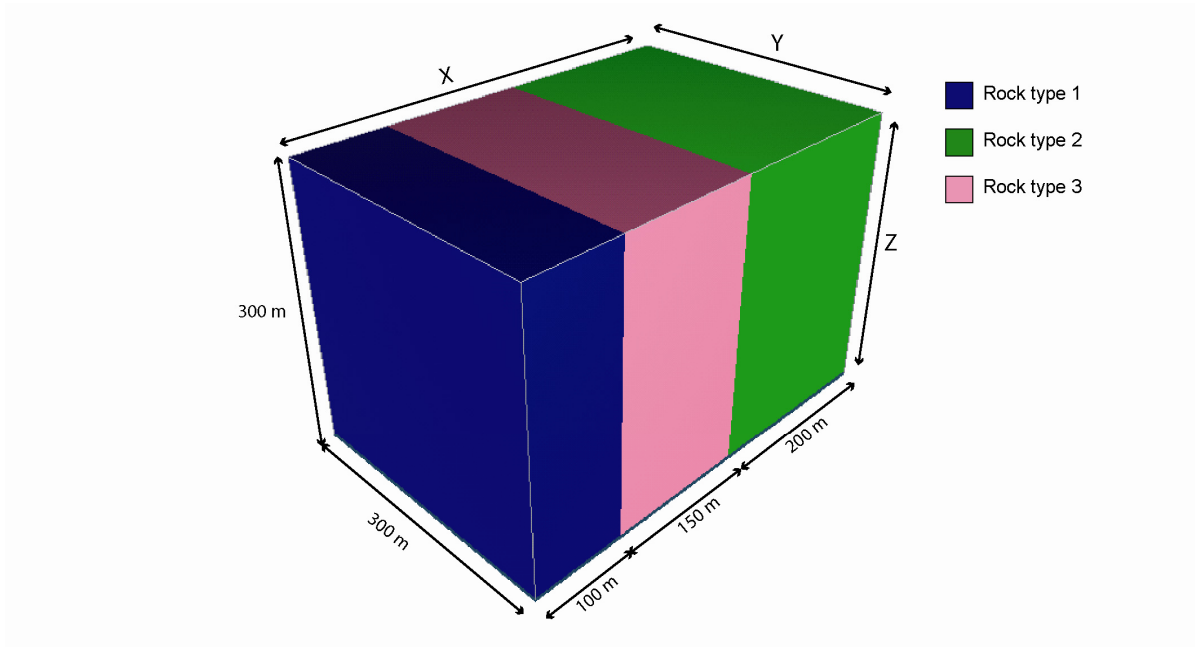


Figure 3.1. Three dimensional view of the synthetic rock model. Three rock types with tabular shapes, sharp and vertical geological contacts are oriented parallel to the Y axis of the model. The dimensions along the orthogonal X, Y and Z axis of the model are indicated along with the thickness of each rock type in the X direction.

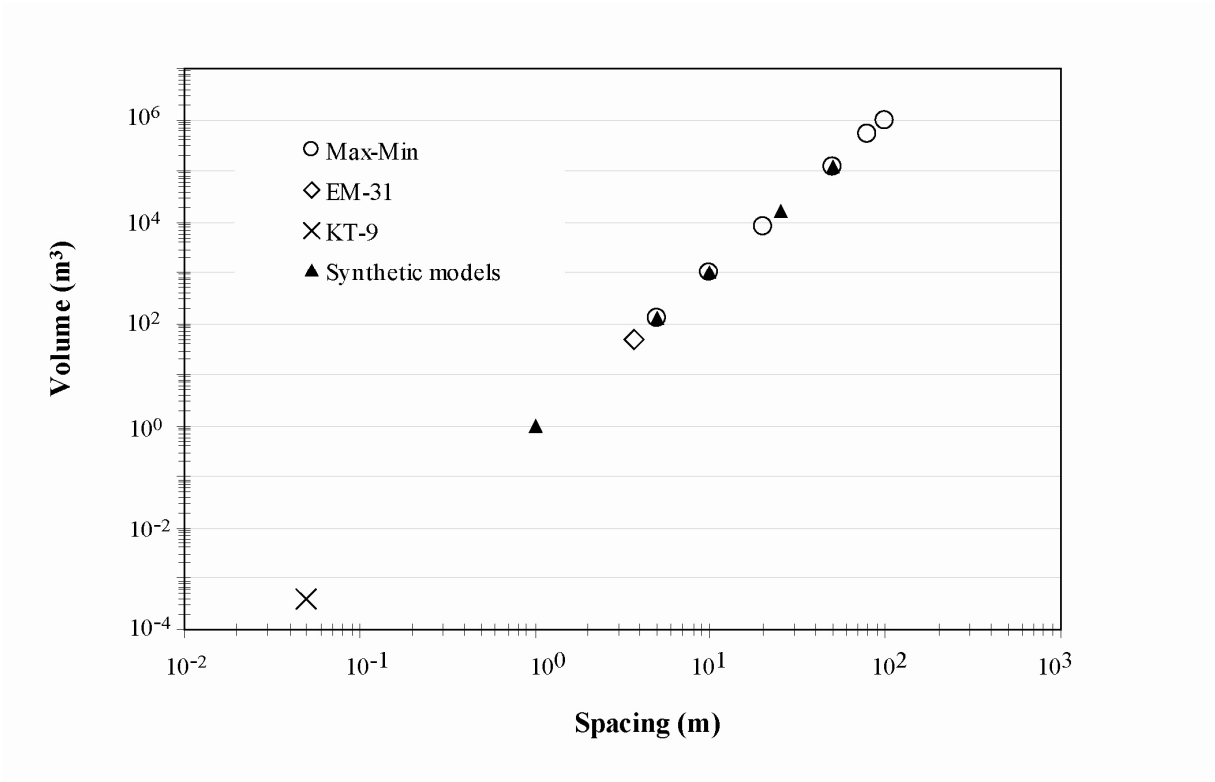


Figure 3.2. Comparison between estimated scales associated with different geophysical surveys and the volumetric scales proposed for synthetic models. Volume varies 10^{-4} m^3 for the smallest scale field method (KT-9) to larger scale methods (EM-31 and Max-Min) involving 4 to 9 orders of magnitude. The synthetic models were built to reproduce an equivalent amount of change in volume by increasing cell size (spacing) from 5 m to 50 m.

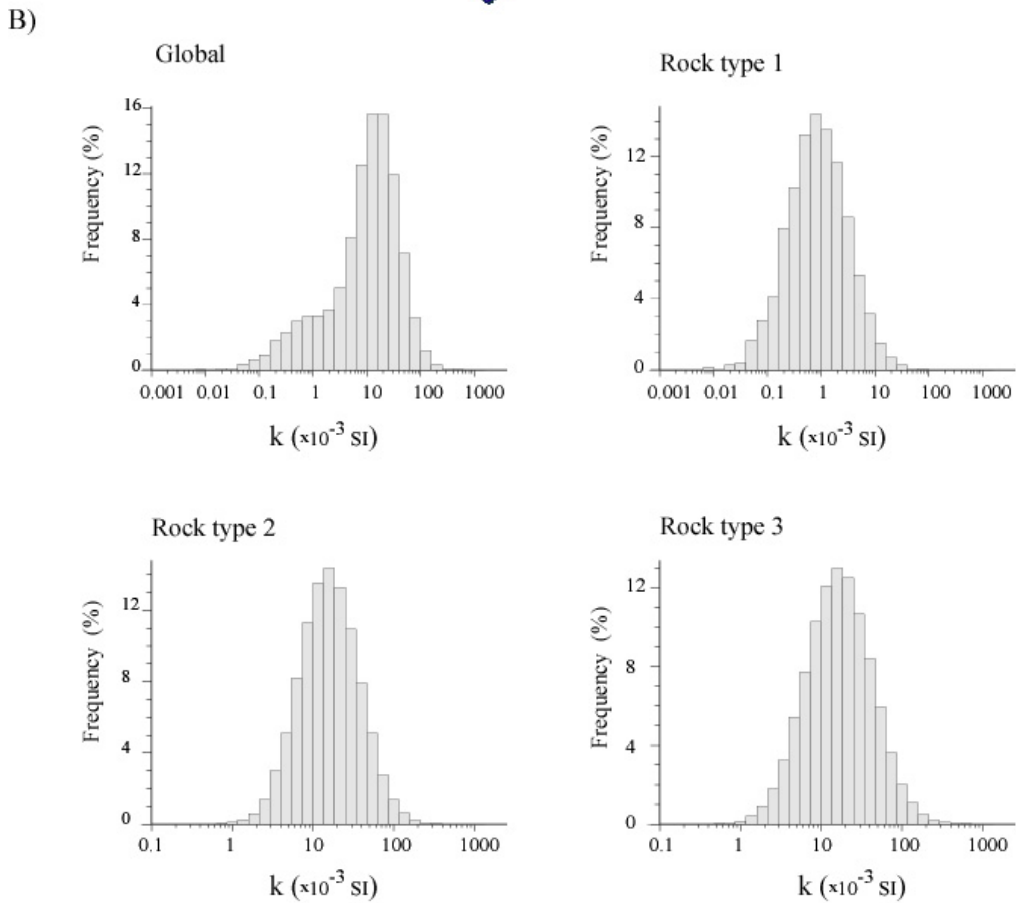
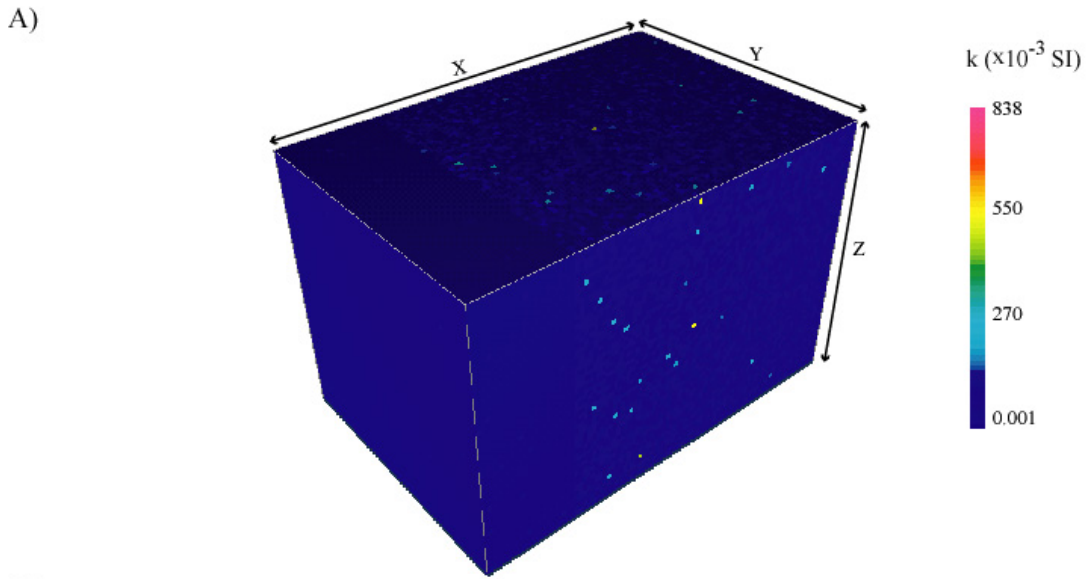


Figure 3.3. Basic synthetic model of magnetic susceptibility (k). A) 3-D perspective view. B) Frequency histograms of the global and local models. Histogram for local models display a log-normal shape, but the global model has a long tail for the low values displaying an asymmetric shape. Summary of the statistics are presented on table 3.3.

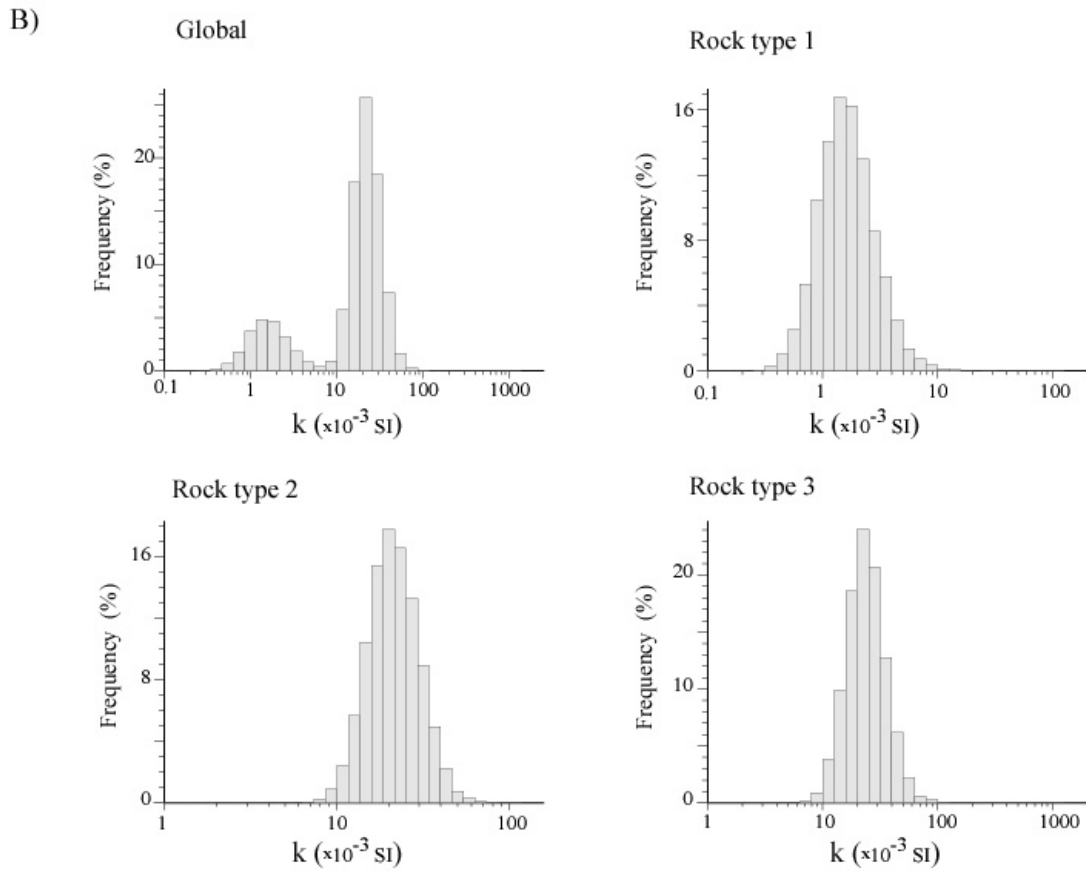
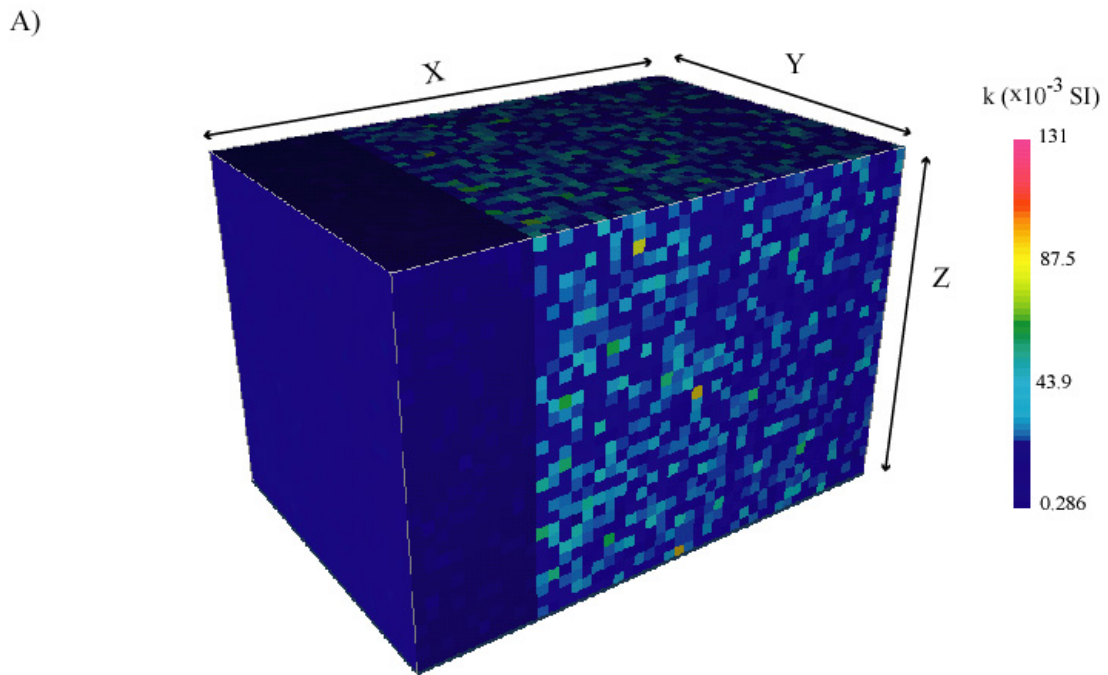


Figure 3.4. Magnetic susceptibility model scaled to a cell size of 10 m. A) 3-D perspective view. B) Frequency histograms of the global and local magnetic susceptibility models. Note the global model displays bimodal distribution and local models show log-normal distributions. Summary statistics for each histogram are presented in Table 3.3.

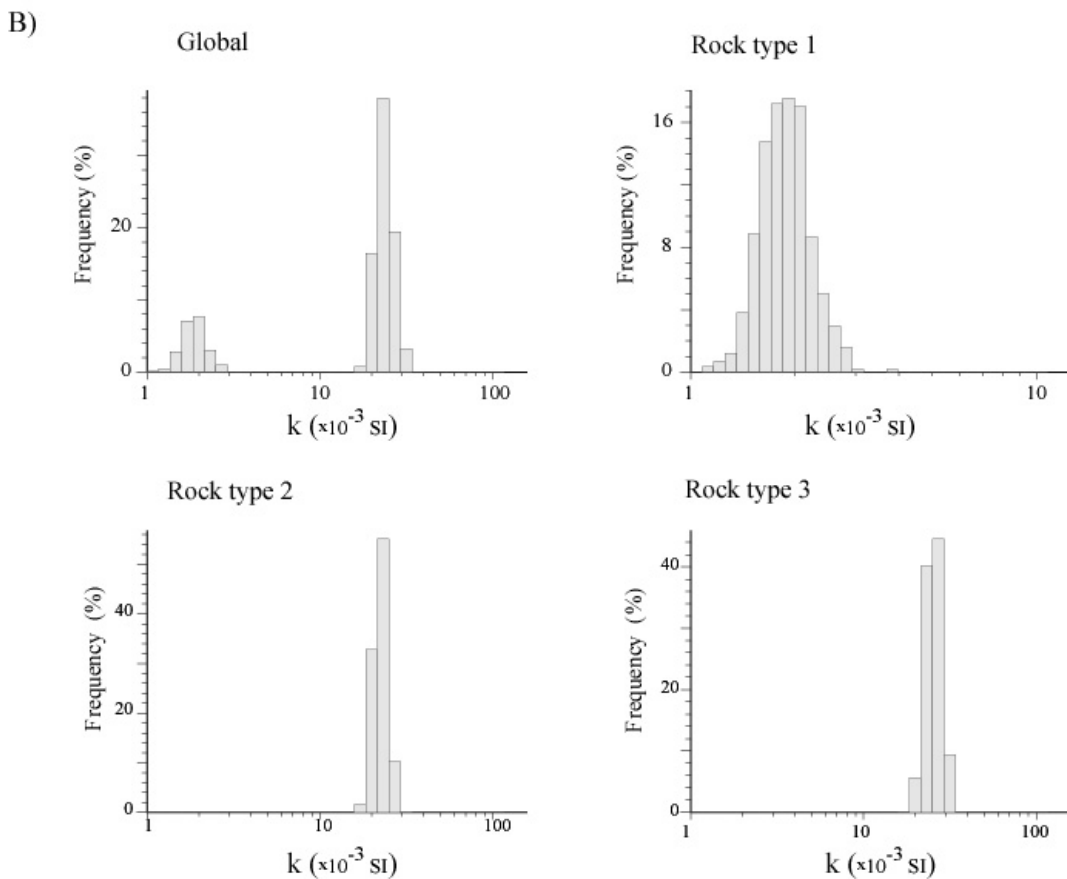
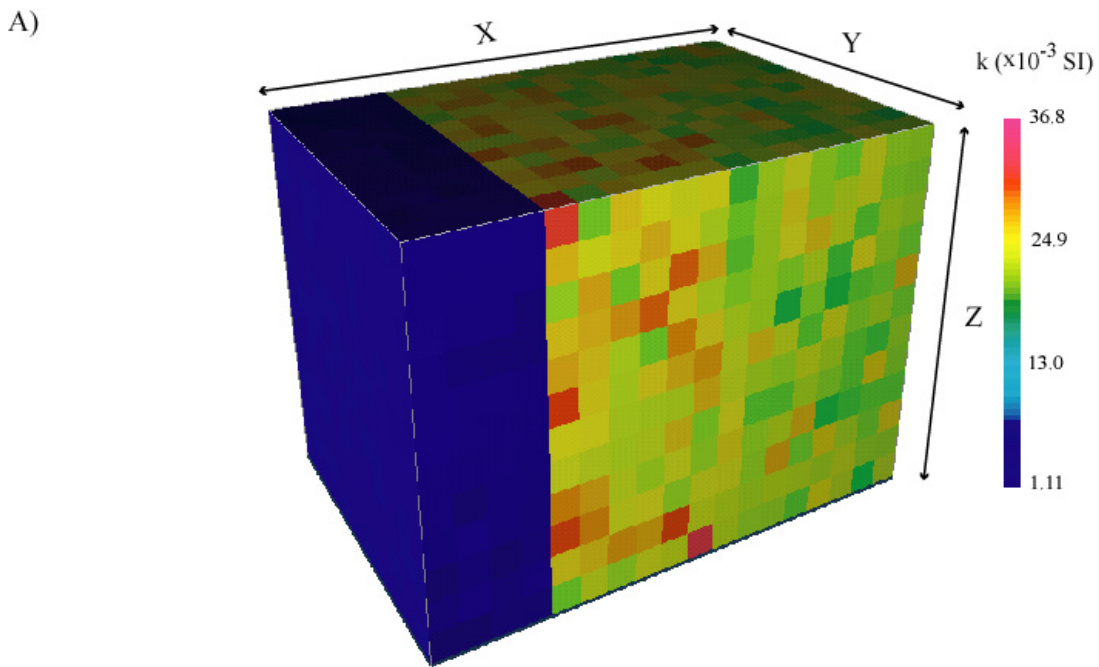
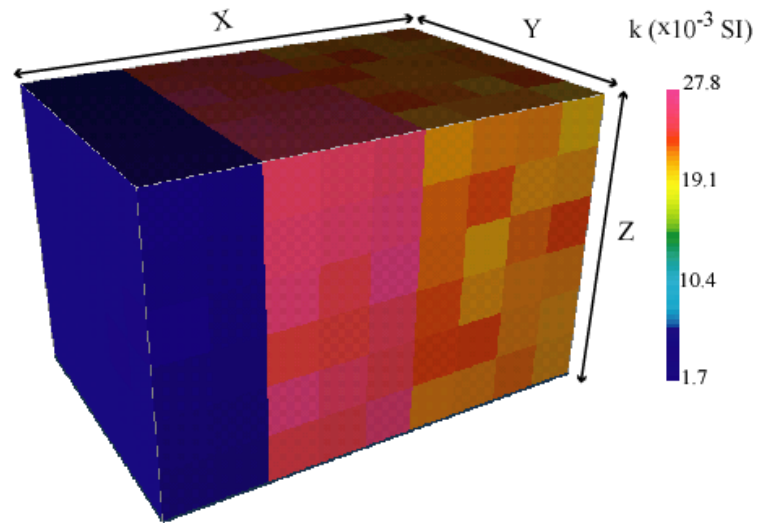


Figure 3.5. Magnetic susceptibility model scaled to a cell size of 25 m. A) 3-D perspective view. B) Frequency histograms of global and local physical property models.

A)



B)

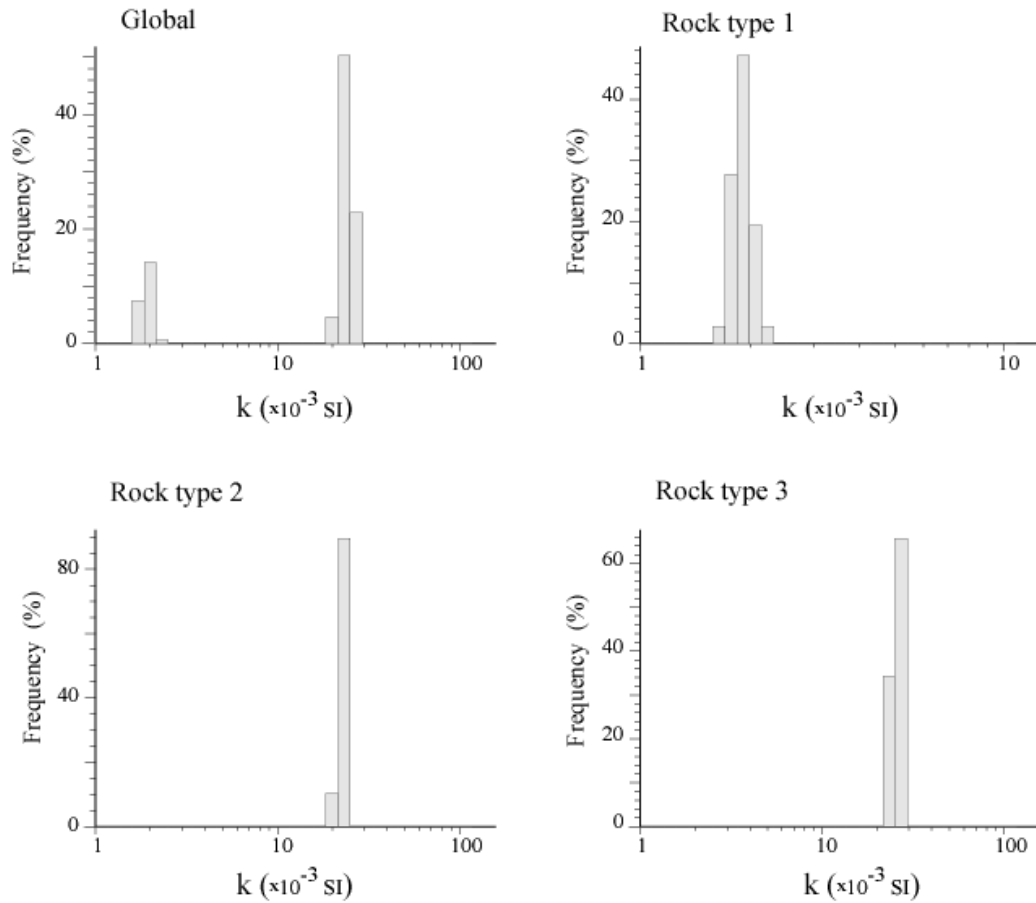


Figure 3.6. Magnetic susceptibility model scaled to a cell size of 50 m A) 3-D perspective view B) Histograms for global and local magnetic susceptibility models.

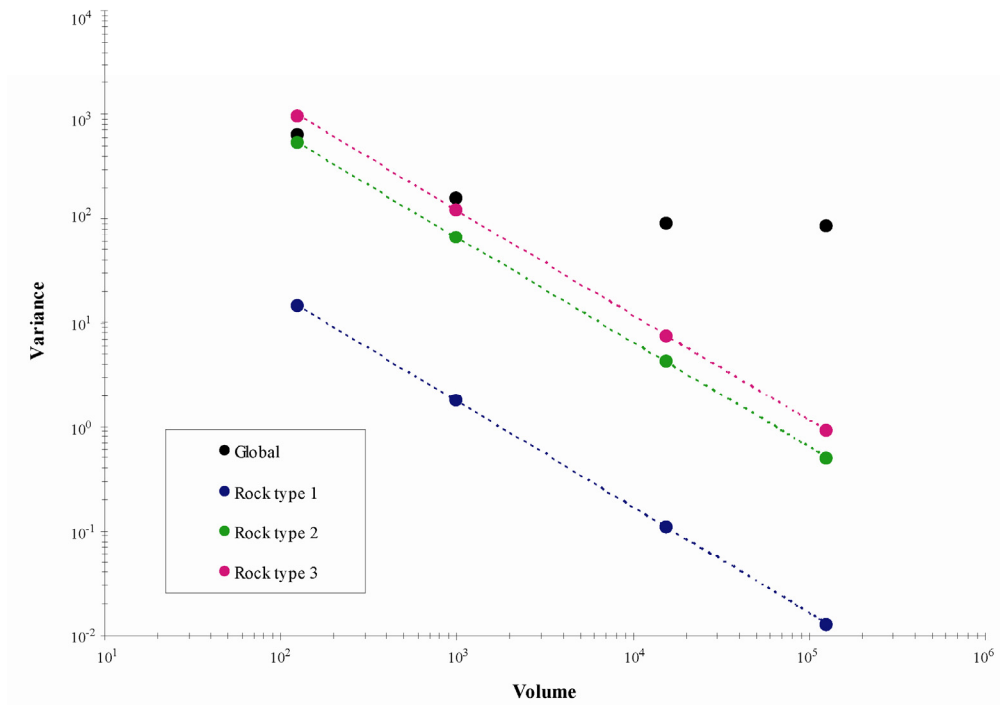


Figure 3.7. Magnetic susceptibility variance versus cell volume for global and local synthetic models. The three local models display an inverse linear relation between variance and cell volume, indicating a power law relation. Global model depart from the linearity and for the larger cell volumes the global magnetic susceptibility variance levels off.

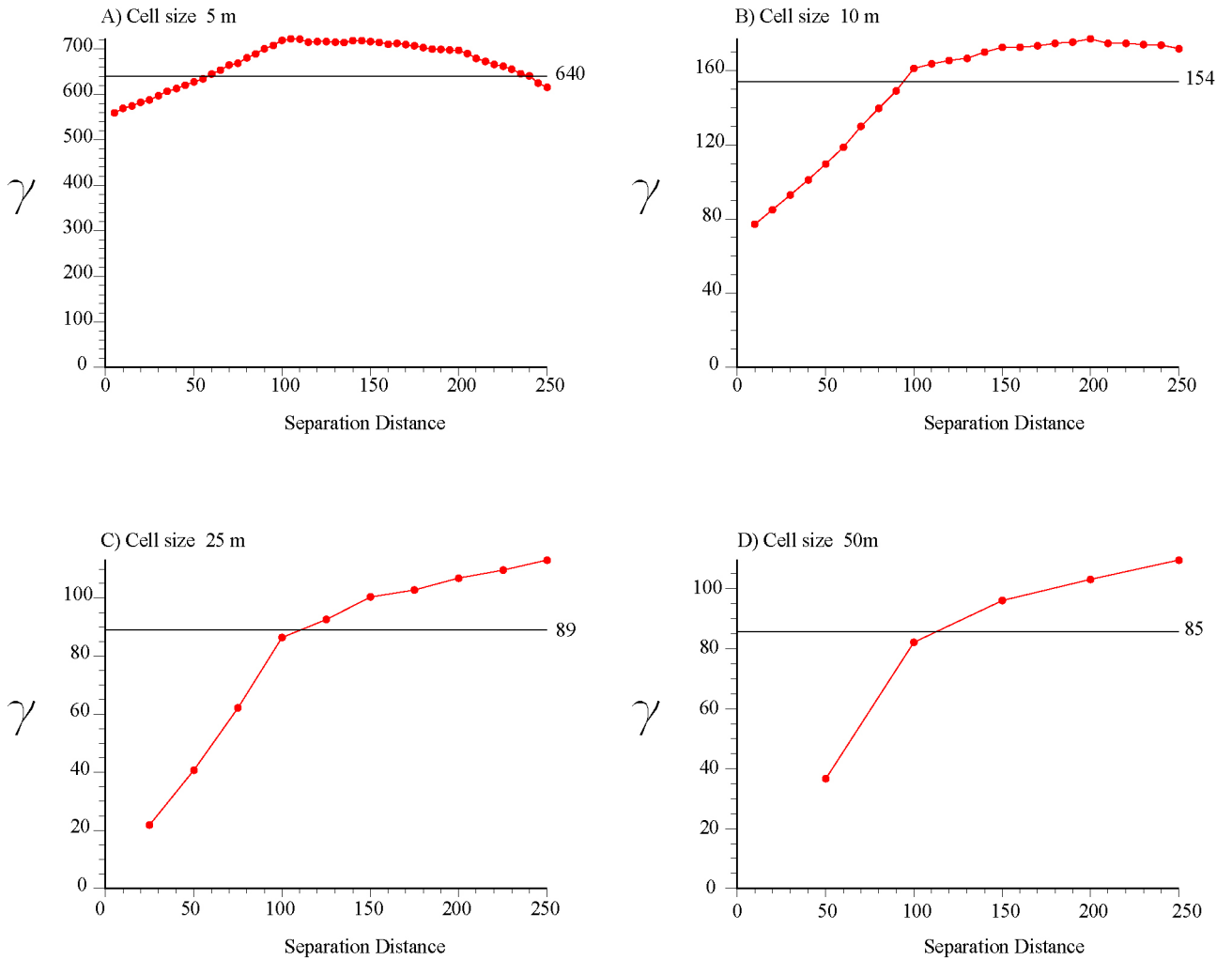


Figure 3.8. Global experimental variogram for magnetic susceptibility models oriented parallel to X axis at the four cell size scales A) 5m; B) 10m; C) 25 m and D) 50 m. Solid black line plotted at the magnetic susceptibility variance value calculated for each model (Table 3.3).

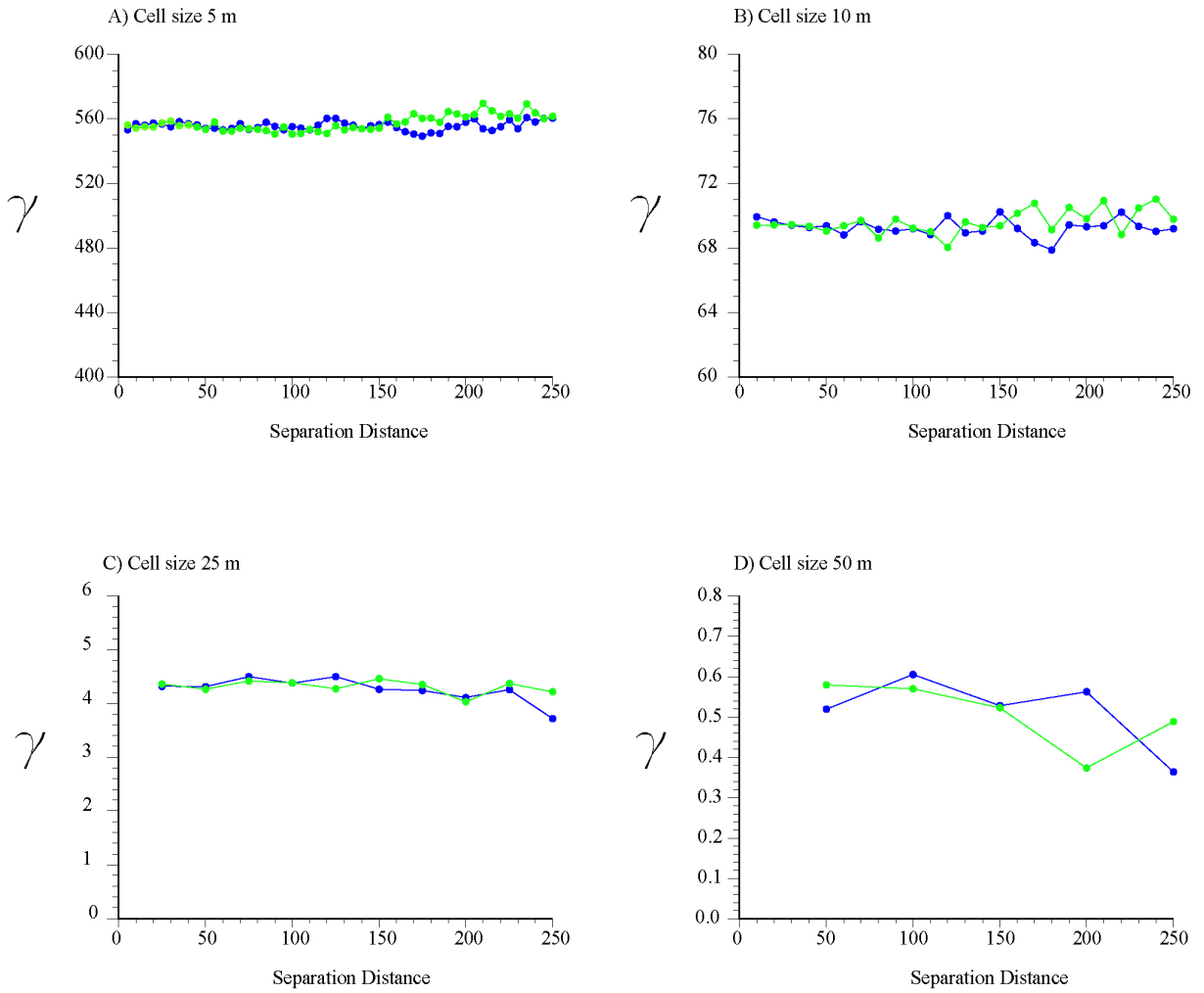


Figure 3.9. Experimental variograms of global magnetic susceptibility model, oriented parallel to the Y (blue) and the Z (green) grid axis calculated for: A) 5m; B) 10m; C) 25 m and D) 50 m.

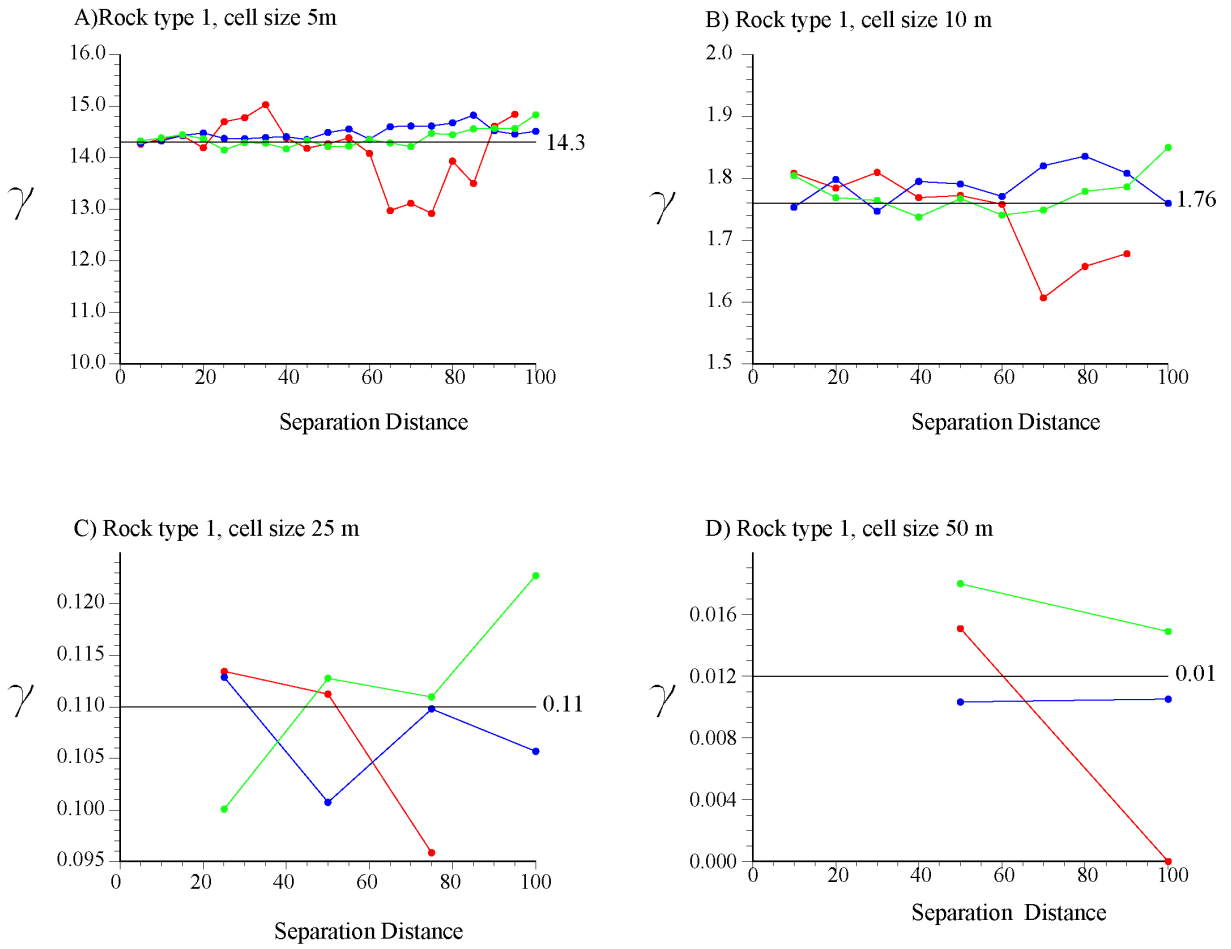


Figure 3.10. Experimental variograms of magnetic susceptibility model for rock type 1. Calculated at the 4 scales; A) 5m; B) 10m; C) 25 m and D) 50 m. Separation distance vector oriented parallel to X (red), Y (blue) and the Z (green) grid axis. Solid black line plotted at the respective variance value from table 3.3.

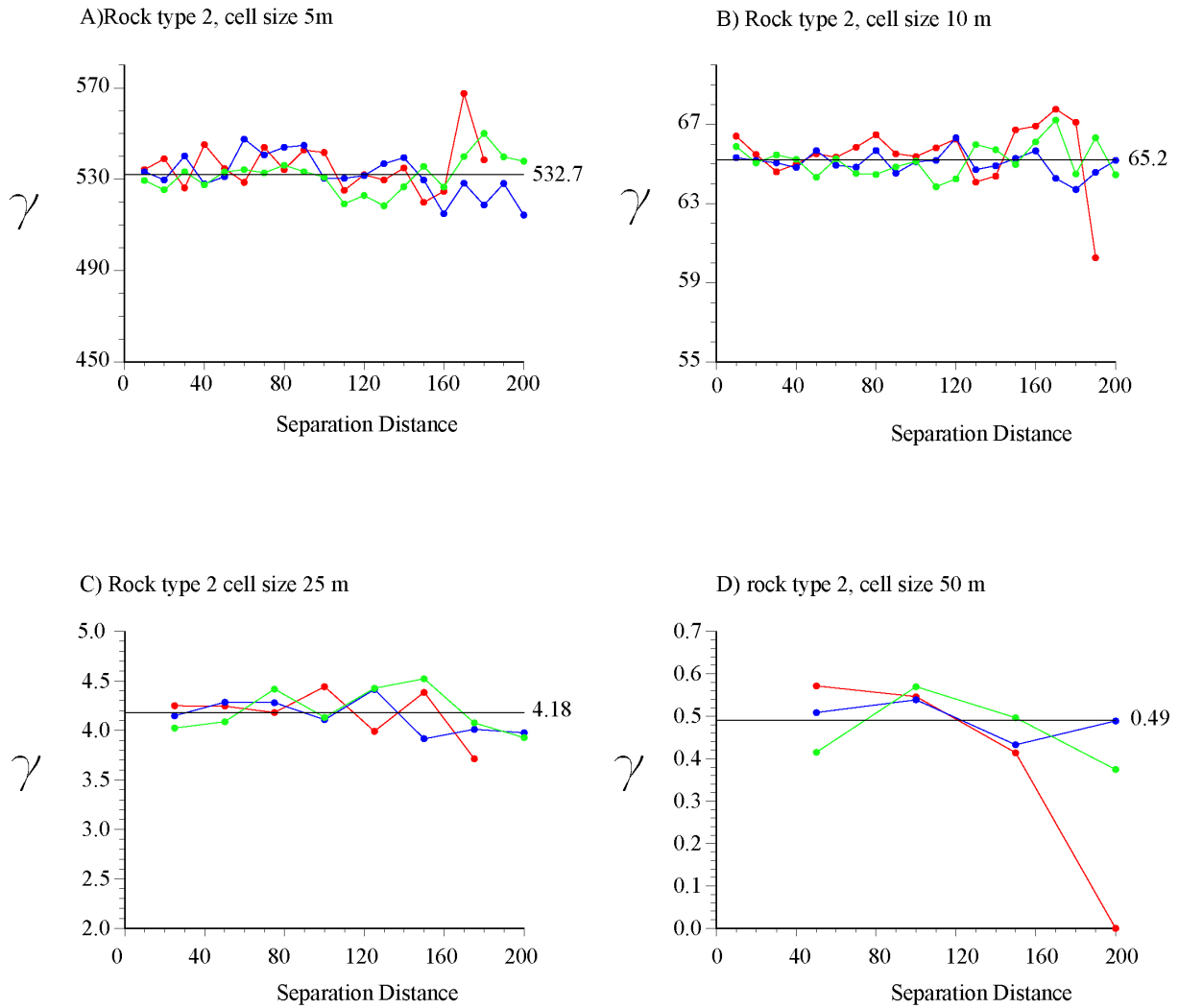


Figure 3.11. Experimental variograms of magnetic susceptibility model for rock type 2. Calculated at the 4 scales; A) 5m; B) 10m; C) 25 m and D) 50 m. Separation distance vector oriented in X (red), Y (blue) and the Z (green) directions. Solid black line at the respective variance value from table 3.3.

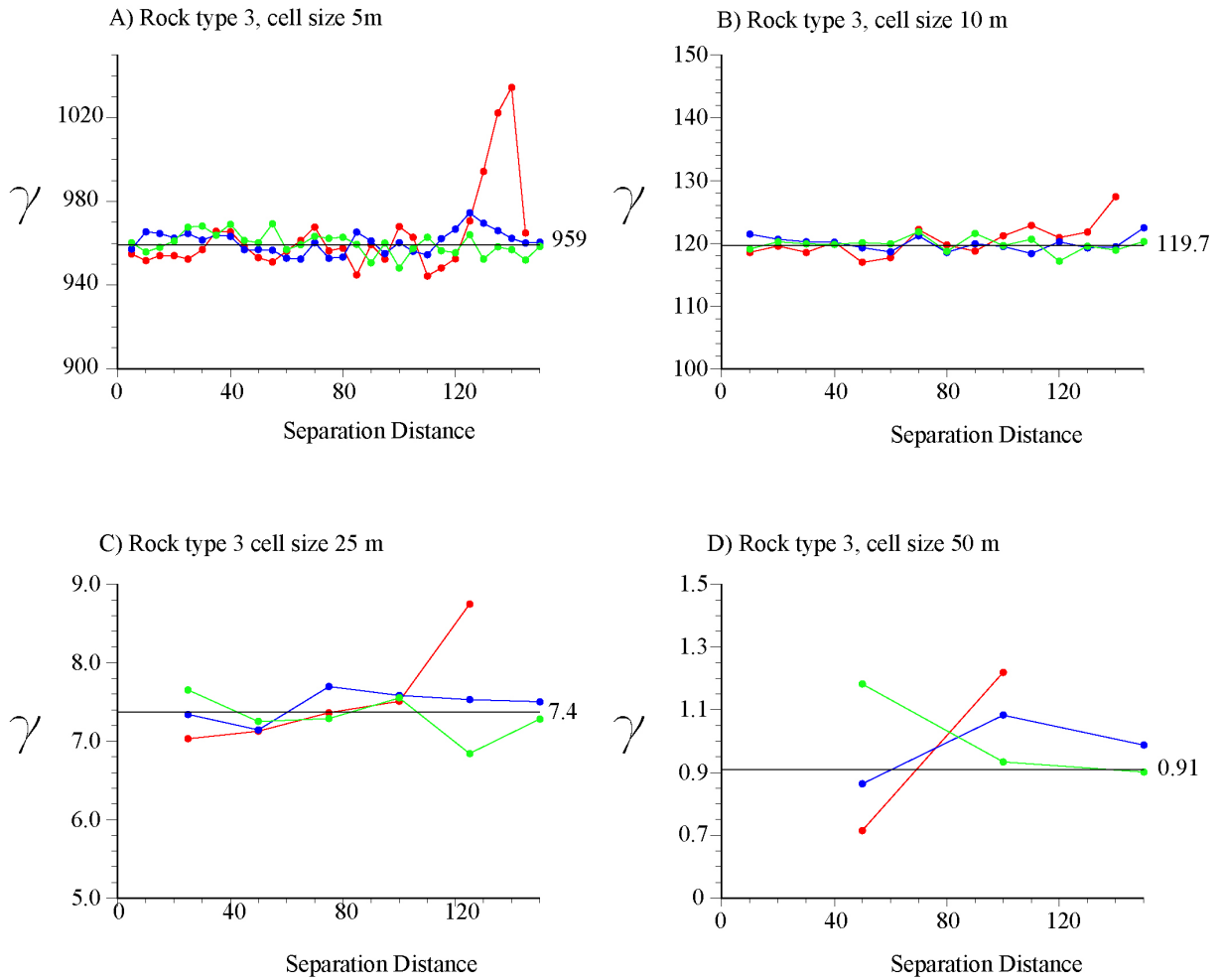
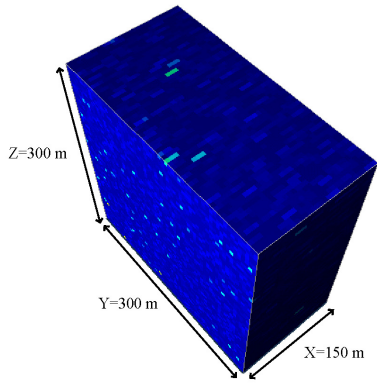
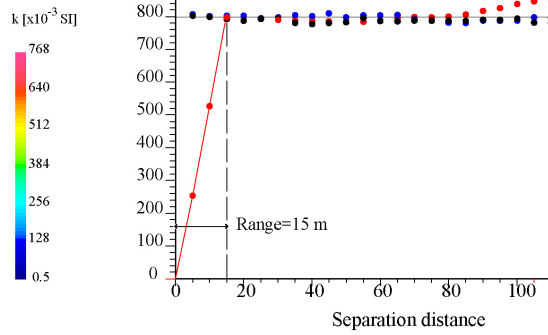


Figure 3.12. Experimental variograms of magnetic susceptibility model for rock type 3. Calculated at the 4 scales; A) 5m; B) 10m; C) 25 m and D) 50 m. Separation distance vector oriented in X (red), Y (blue) and the Z (green) directions. Solid black line at the respective physical property variance value from table 3.3.

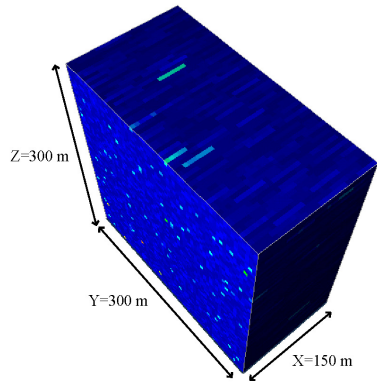
A) Rock type 3 - Smoothing factor=3



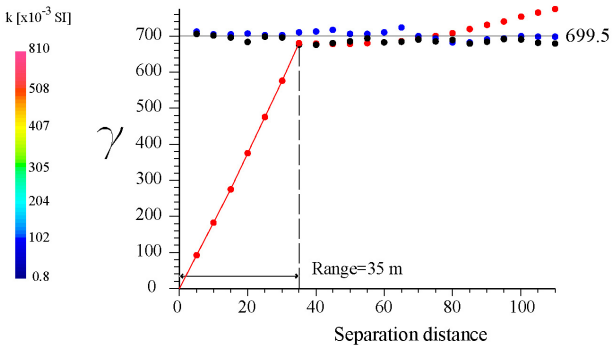
Smoothing factor=3



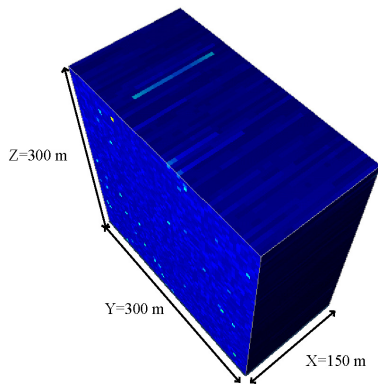
B) Rock type 3 - Smoothing factor=7



Smoothing factor=7



C) Rock type 3 - Smoothing factor=21



Smoothing factor=21

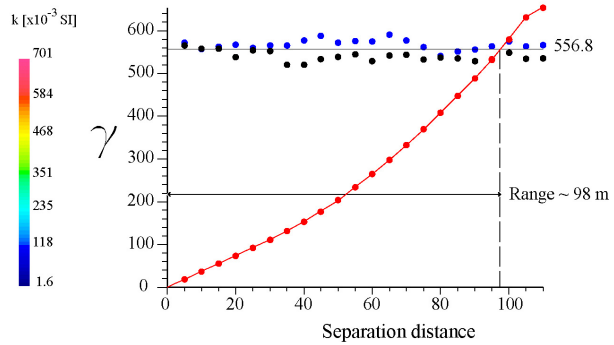


Figure 3.13. Smoothed magnetic susceptibility models for rock type 3. Perspective (left) view and experimental variograms (right). A) Smoothing factor = 3; B) Smoothing factor = 7; C) Smoothing factor = 21. The experimental variograms oriented in Y (blue dots) and Z (black dots) show a pure nugget effect with an amplitude equivalent to the variance value (from table 3.5). The X (red line and dots) oriented experimental variograms reach the variance values at range distances 15, 35 and 98 m for the smoothing factor of 3, 7 and 21, respectively.

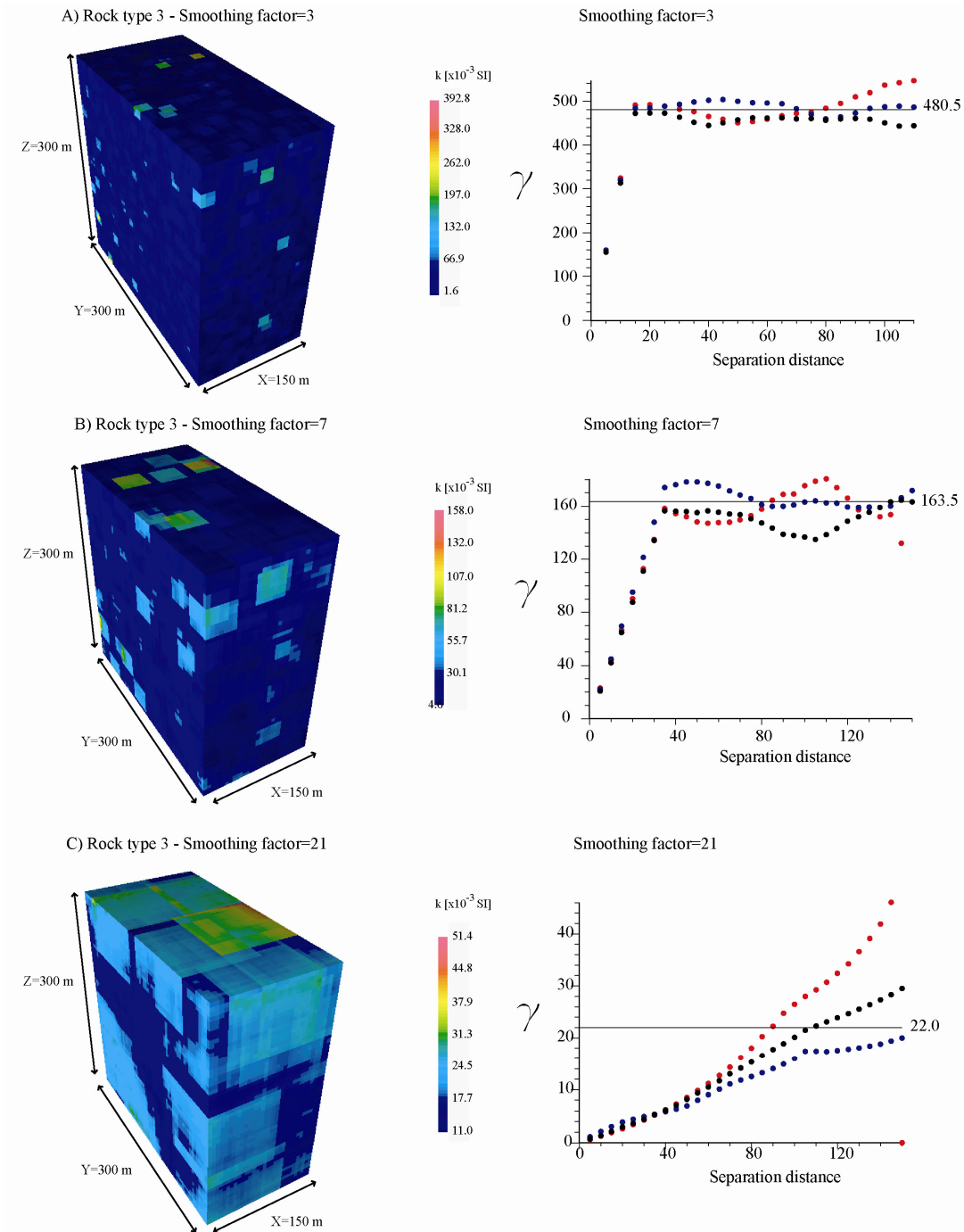


Figure 3.14. Isotropic smoothed magnetic susceptibility models calculated within rock type 3; perspective view (left) and experimental variograms (right). A) Smoothing factor = 3; B) Smoothing factor = 7; C) Smoothing factor = 21. The experimental variograms in A) and B) models display an isotropic behavior and reach the sill at the expected range distance 15 and 35 m respectively, after which they oscillate around the variance value with a period approximately equal to the size of magnetic susceptibility zones greater than 30.1. The model at a smoothing factor of 2,1 behaves isotropic until a distance of 50 m, then an isotropic tendency is observed, the Y oriented experimental variogram (blue) does not reach the sill suggesting a zonal anisotropy.

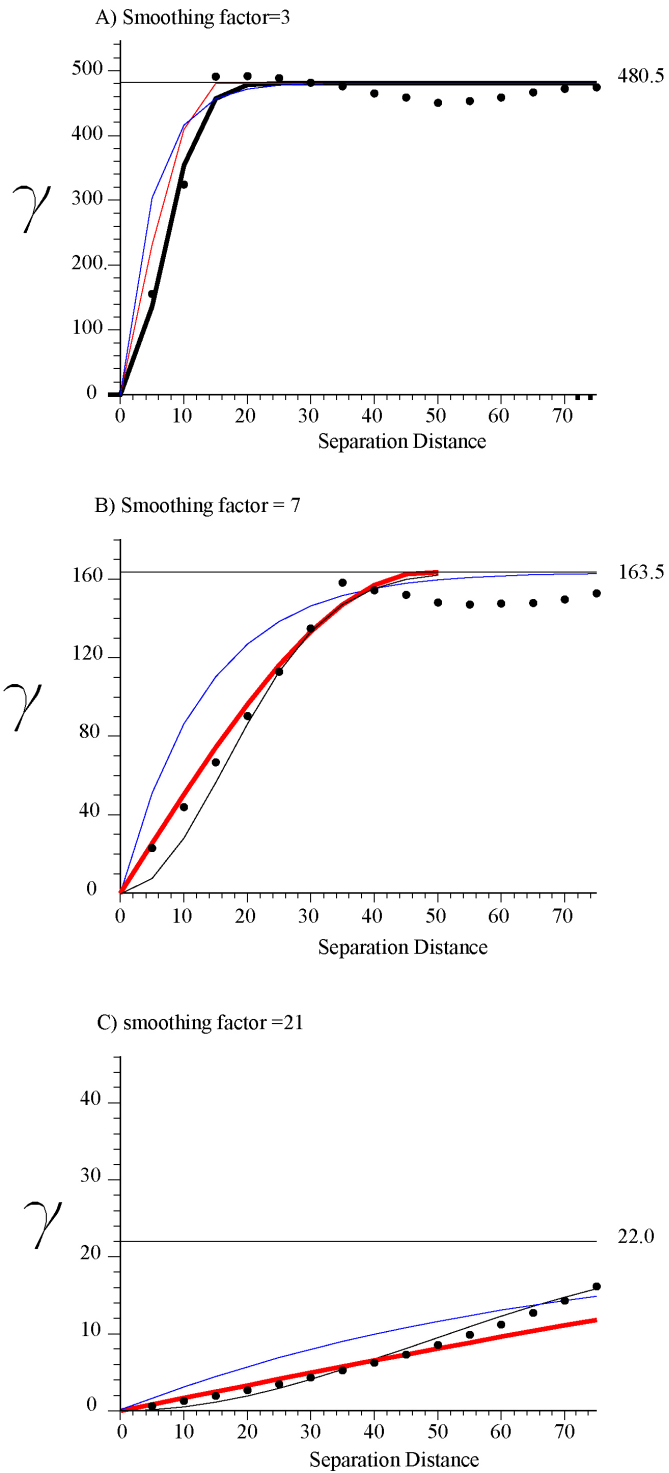


Figure 3.15. Isotropic experimental (black dots) and fitted theoretical variograms (colored solid lines). A) Smoothing factor = 3, B) Smoothing factor = 7, C) Smoothing factor = 21. The colored lines are different variogram models: blue = exponential model, red = spherical model and black = Gaussian model. In each diagram the coarser line indicates which model display a better fit to the experimental variogram. Black horizontal lined located at the variance value for each model (Table 3.6).

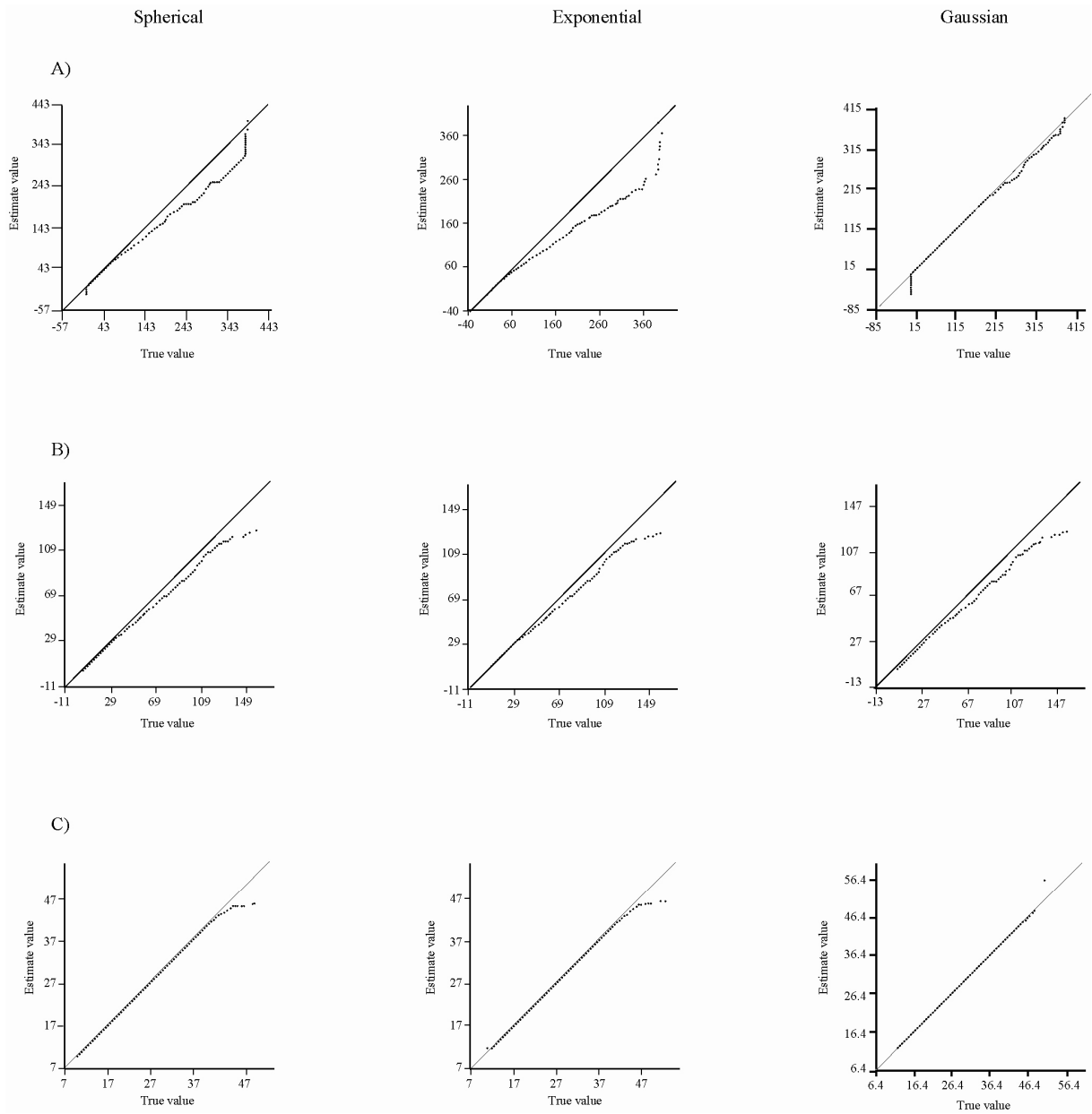


Figure 3.16. Estimate value versus True value quartile plots, resulting for the cross validation procedure using the spherical (left), exponential (middle) and Gaussian (right) variogram models. A) Smoothing factor = 3, B) Smoothing factor= 7 and C) Smoothing factor = 21.

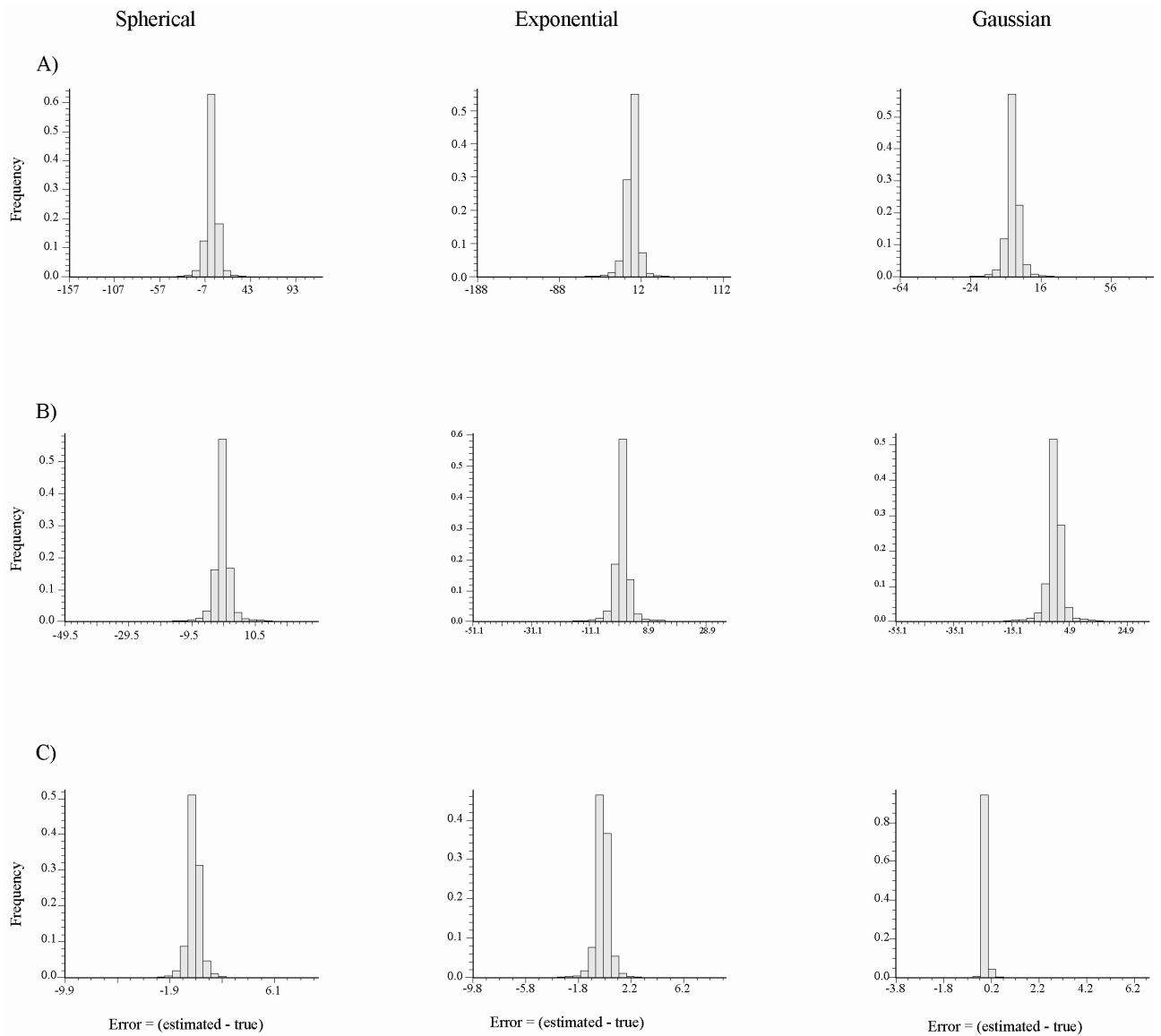


Figure 3.17. Error estimation histograms for spherical, exponential and gaussian variogram models. Error estimation calculated using the cross validation procedure explained in text. A) smoothing factor = 3, B) smoothing factor = 7 and C) smoothing factor = 21

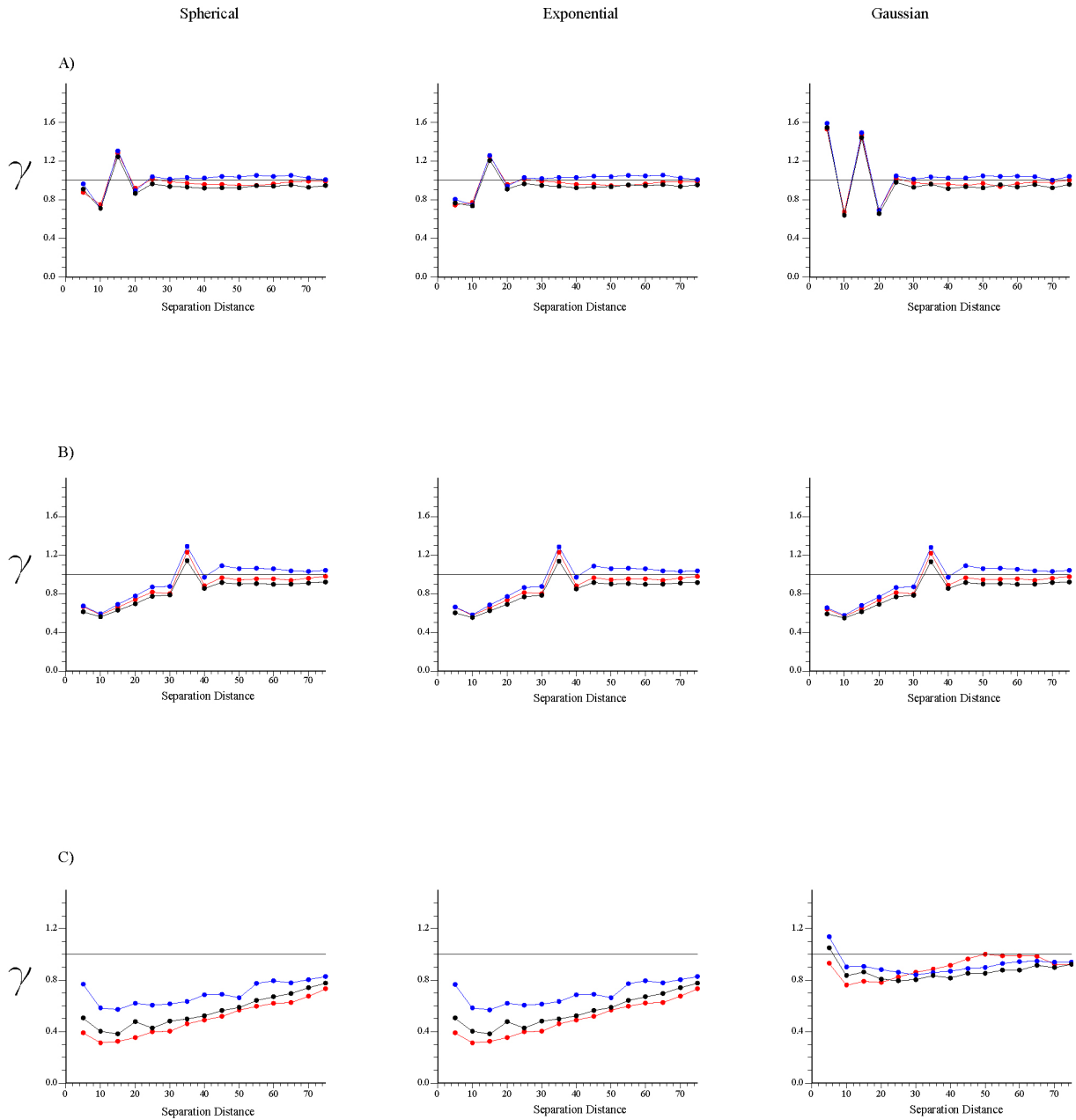


Figure 3.18. Error estimation standardized variograms for spherical, exponential and Gaussian variogram models used in the cross validation procedure as was explained in text. A) smoothing factor = 3, B) smoothing factor = 7 and C) smoothing factor = 21. Colors indicate spatial orientation; red=X, blue=Y and black =Z.

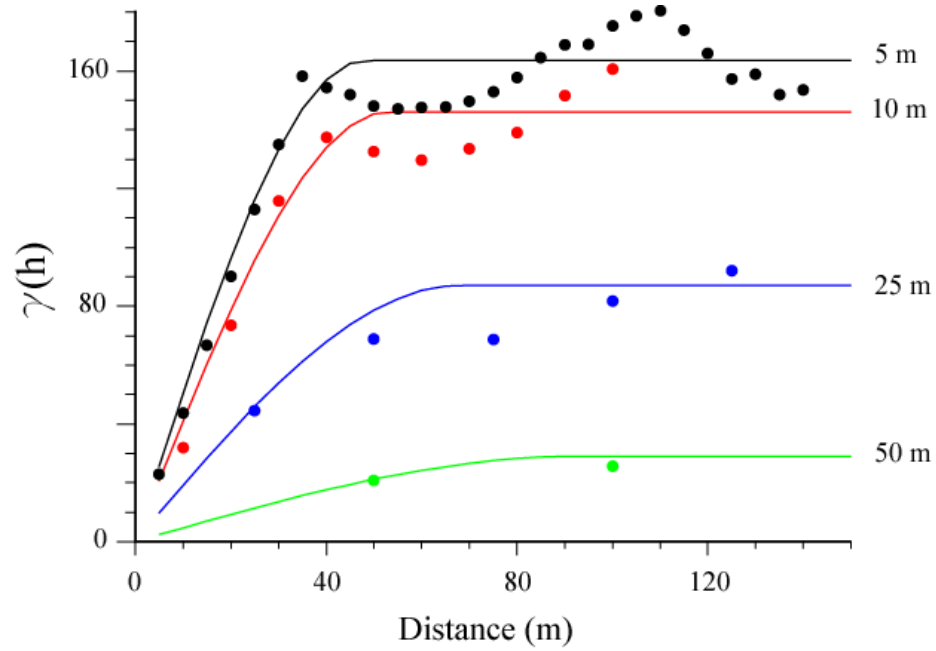


Figure 3.19. Up-scaled variogram models (solid color lines) from 5 m to 50 m cell size scale and experimental variograms (dots) calculated to magnetic susceptibility models using block kriging at the respective block size within rock type 3 model.

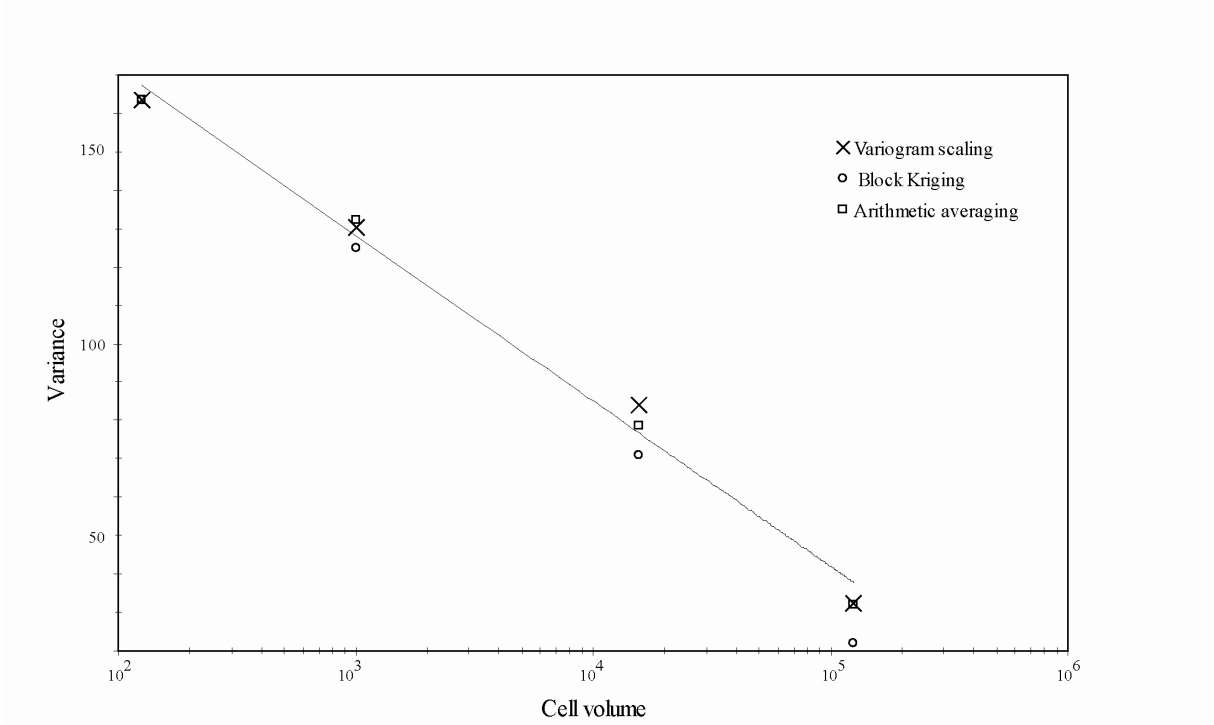


Figure 3.20. Decrease in variance with volume plotted in logarithmic scale. Three values of the variance of the physical property models were calculated. Dispersion variance calculated from variogram scaling (crosses), block model variance calculated from block kriging (open circles) and variance from arithmetic averaging, the physical property within blocks (open squares). Differences between the two first are explained by the quality of the match between the models and the experimental variograms.

Table 3.1. Rock types magnetic susceptibility statistical parameters, used to constrain synthetic models.

Rock Type	Magnetic Susceptibility Average	Magnetic Susceptibility Standard deviation
1	1.9	3.8
2	22.5	23.2
3	25.6	30.4

Table 3.2. Basic statistics summary for global and local models of magnetic susceptibility

Global	5m	10m	25m	50m
Cell number	324,000	40,500	2,592	324
Mean	18.94	18.95	18.95	18.95
Variance	640.06	154.11	89.22	85.64
Maximum	837.51	131.12	36.80	27.76
Upper quartile	24.00	26.05	24.83	24.92
Median	11.67	19.29	22.59	22.72
Lower quartile	4.19	11.82	19.53	21.40
Minimum	0.005	0.29	1.11	1.70
Rock Type 1	5m	10m	25m	50m
Cell number	72,000	9,000	576	72
Mean	1.90	1.90	1.90	1.90
Variance	14.27	1.76	0.11	0.01
Maximum	217.97	29.63	3.91	2.21
Upper quartile	2.01	2.29	2.09	1.98
Median	0.85	1.57	1.87	1.89
Lower quartile	0.36	1.10	1.68	1.83
Minimum	0.00	0.29	1.11	1.70
Rock Type 2	5m	10m	25m	50m
Cell number	144,000	18,000	1152	144
Mean	22.47	22.48	22.48	22.48
Variance	522.71	65.23	4.18	0.496
Maximum	565.34	102.39	30.25	24.38
Upper quartile	27.79	26.60	23.77	23.00
Median	15.66	21.04	22.44	22.50
Lower quartile	8.84	16.82	20.94	21.90
Minimum	0.48	5.02	17.23	20.67
Rock Type 3	5m	10m	25m	50m
Cell number	108,000	13,500	864	108
Mean	25.59	25.60	25.60	25.60
Variance	959.36	119.65	7.37	0.91
Maximum	837.51	131.12	36.80	27.76
Upper quartile	30.93	30.45	27.37	26.25
Median	16.45	23.34	25.42	25.60
Lower quartile	8.72	18.29	23.64	24.95
Minimum	0.15	5.76	18.42	23.27

Table 3.3. Variance reduction factors

Factor	Global Model	Local Model
f_{5-10}	0.24	0.123
f_{5-25}	0.14	0.008
f_{5-50}	0.13	0.001

Table 3.4. Magnetic susceptibility average, variance and range resulting from smoothing procedure.

Smoothing factor	Magnetic Susceptibility Average	Magnetic susceptibility Variance	Range (m)
3	25.42	798.46	15
7	25.67	699.54	35
21	24.97	556.76	95-100

Table 3.5. Basic statistics summary isotropic smoothed models

Smoothing factor	Cells #	Mean	Variance	Minimum	Maximum	Quartile 25%	Quartile 50%	Quartile 75%
3	108,000	24.76	480.46	1.69	392.79	12.95	19.08	29.28
7	108,000	23.34	163.49	4.59	157.83	15.86	20.22	26.27
21	108,000	20.38	22.02	11.00	51.35	17.16	19.51	22.31

Table 3.6. Range and variance parameters values used in variogram modeling.

Smoothing factor = 3

Variogram Model	Range	Variance
Spherical	15	480.5
Exponential	15	480.5
Gaussian	15	480.5

Smoothing factor = 7

Variogram Model type	Range	Variance
Spherical	48	163.5
Exponential	40	163.5
Gaussian	35	163.5

Smoothing factor = 21

Variogram Model type	Range	Variance
Spherical	200	22.0
Exponential	200	22.0
Gaussian	115	22.0

Table 3.7. Variogram modeling cross validation results

Smoothing Factor = 3			
Variogram Model	True vs. Estimate Correlation factor	Error average	Error standard deviation
Spherical	0.9349	-0.00019	8.10054
Exponential	0.9184	0.00059	9.53691
Gaussian	0.9779	-0.00511	4.62134
Smoothing Factor = 7			
Variogram Model	True vs. Estimate Correlation factor	Error average	Error standard deviation
Spherical	0.9790	-0.0063	2.7988
Exponential	0.9772	-0.0036	2.9083
Gaussian	0.9737	-0.0122	3.1059
Smoothing Factor = 21			
Variogram Model	True vs. Estimate Correlation factor	Error average	Error standard deviation
Spherical	0.99375	0.00145	0.5344
Exponential	0.99375	0.00128	0.5345
Gaussian	0.99983	0.00025	0.0860

Table 3.8. Error estimation basic statistics.

Smoothing factor=3	Spherical	Exponential	Gaussian
Number of data	108,000	108,000	108,000
Mean	0.00	0.00	-0.01
Standard deviation	8.10	9.54	4.62
Maximum	96.94	92.54	66.97
Upper quartile	3.15	3.88	1.71
Median	0.21	0.65	-0.02
Lower quartile	-2.77	-2.93	-1.72
Minimum	-156.26	-188.28	-64.02

Smoothing factor=7	Spherical	Exponential	Gaussian
Number of data	108,000	108,000	108,000
Mean	0.01	0.00	-0.01
Standard deviation	2.80	2.91	3.11
Maximum	23.06	27.96	24.75
Upper quartile	1.08	1.13	1.20
Median	0.10	0.11	0.12
Lower quartile	-0.94	-0.97	-1.04
Minimum	-49.55	-51.10	-55.09

Smoothing factor=21	Spherical	Exponential	Gaussian
Number of data	108,000	108,000	108,000
Mean	0.02	0.00	0.00
Standard deviation	0.53	0.53	0.09
Maximum	7.74	7.64	5.88
Upper quartile	0.23	0.23	0.01
Median	0.18	0.02	0.00
Lower quartile	-0.21	-0.21	-0.01
Minimum	-9.86	-9.84	-3.79

Chapter 4. Scaling magnetic susceptibility measurements from field data

4.1 Introduction

This chapter addresses scaling of magnetic susceptibility of rocks where the sample volume is changed from the point scale of the measurements performed with a susceptibility meter to those recovered from the inversions of the electromagnetic data collected using the EM-31 instrument. The data available for this purpose include geophysical information gathered at five geologically distinct sites at Flin-Flon District in northern Canada. As a complement of the geophysical surveys, geologic information is collected including maps and descriptions of the sampled rocks. The geophysical surveys included direct magnetic susceptibility measurements, collected with a hand magnetic susceptibility meter and electromagnetic measurements performed in the frequency domain. In the first case, the data were collected using a portable magnetic susceptibility meter, the KT-9 instrument. For the electromagnetic survey, the EM-31 instrument is used. The uses of the different instruments allow sampling different rock volumes in order to test the scaling property of magnetic susceptibility of the studied rocks.

The scale of each survey, for the purpose of this study, depends on the separation between the transmitter and the receiver, referred to as the coil separation. The measurements collected using the hand magnetic susceptibility meter are considered as point scale measurements and provide the smallest volumetric scale data set used in this study. The coil separation used in the electromagnetic experiments is fixed to 3.66 m.

The chapter begins with a description of the geologic features that characterize the five sites studied which will be followed by a description of the geometry of geophysical surveys to illustrate how the data were collected and which were the volumetric scales involved. Then, information of the detailed geology and point scale magnetic susceptibility measurements, gathered in the 10 m grids is described.

4.2 Site geology.

Geologic maps of the five sites and geophysical survey at Flin-Flon district provide the surface constraints on the physical property distribution. The sites are known as Mafic Volcanics (MV), Quartz Porphyry (QP), Mafic Boundary Intrusive (BI), Granite (GR) and Sedimentary rock (SED). They were selected to be as geologically homogeneous as possible, in order to prevent merging magnetic susceptibility measurements from more than rock type. Geologic contacts, faults and hydrothermal alteration zones boundaries control physical property features at the regional scale features, and can juxtapose rocks with high physical property contrast. Typical small-scale controls on the magnetic properties include the type and quantity of magnetic minerals and the grain size. Rock samples, representative of the different rock units, are macroscopically described to classify the rock type, characterize the hydrothermal alteration, and determine the presence of magnetic minerals. Geologic hand samples are also collected for magnetic susceptibility measurements as well as petrography descriptions.

4.2.1 Mafic Volcanics site

Geologic mapping at the Mafic Volcanic site includes an area of 150x150 m² approximately (Fig. 4.1). The rocks within the site are grouped in 7 units, corresponding to 6 mafic volcanic rocks and intrusive units and 1 felsic intrusive rock unit. The mafic rock units are separated according to their textural characteristics, whereas the felsic unit is defined based on the mineralogy. The rock units outcrop as small bodies (< 25 m²) surrounded by Quaternary overburden. Observed geologic contacts are mainly oriented in a N30W strike, with measured dips of 55 to 65 degrees to the NE and SW. The mafic rock units thus appear as stripes of variable horizontal thickness in the surface map. The mafic rock units correspond to basaltic flows characterized by textural variations. The most commonly observed texture corresponds to pillowed flows of the Pillowed Mafic Unit. This unit dominates the western margin and the central zone of the site. Usually these rocks have abundant amygdules, but brecciated in the

southeastern outcrops. In the northeast area, a 35 m thick strip, measured perpendicular to the observed structural trend (N30W), of massive and banded basaltic flows, locally pillowed, forms the Massive Mafic Unit. Coarse amygduled bearing basaltic flows form small outcrops located at the south-east quadrant of the grid. They are grouped in the Coarse Amygdule Mafic Unit. A sub-elliptical outcrop with long axis oriented parallel to the N30W trend and an outcrop length of 30 m approximate, located close to the center of the grid is formed by banded amygduled basaltic flows, in the Banded Mafic Unit.

Mafic rock units are intruded by banded tabular sills of the same composition. The intrusive bodies have horizontal thickness between 0.5 to 4 m, spatially oriented in the N30W trend with a dip of 60 SW. These intrusive rocks are grouped as the Mafic Dyke Unit and characterized by the presence of amygdules, porphyritic and flow banded textures. The Felsic Dyke Unit outcrops as a small body in the north east quadrant of the site. It corresponds to an intrusive rock, rich in feldspar crystals and with a porphyritic texture.

4.2.2 Boundary Intrusive site

At this site, three mafic rock units are encountered (Fig. 4.2). The western border of the site is dominated by a mafic volcanic unit, characterized by a black to dark green rock with aphanitic to porphyritic texture. Hand samples are strongly chloritized and have disseminated and clots of magnetite commonly with hematite, pyrrhotite and chalcopyrite. At the center of the site is a mafic unit with coarse amygdules, whereas the eastern margin of the site is dominated by the gabbroic Boundary Mafic intrusive. Mafic minerals are strongly chloritized. The contact between units trends northerly.

4.2.3 Quartz Porphyry site

Outcropping rocks were grouped in a mafic volcanic unit and a quartz porphyry unit, which dominates the exposed outcrops (Fig. 4.3). The quartz porphyry is characterized by phenocrysts of quartz and feldspar in fine-grained quartzofeldspathic groundmass with chloritized micas with fine disseminated magnetite. The contact between the mafic volcanic unit and the quartz porphyry are sharp and oriented N20-30W.

4.2.4 Granite site

Two rock units are encountered. The most common is granite which is intruded by basaltic dykes. The dikes are tabular bodies with horizontal thickness between 1 to 5 meters, and located in the southern sector half of the site (Fig 4.4). The dikes are vertical with an azimuth near N45-60 W. In the east and north sector of the site, quartz veins outcrop. The veins are vertical and strike N20-30W. Petrography description of one sample indicates that mafic minerals are altered to chlorite and hematite fills fractures.

4.2.5 Sedimentary rock site

This site is underlain by a schist unit which preserves the texture of the sedimentary protolith (Fig. 4.5). Macroscopically the rock is a black to dark gray with a fine fragmental texture, and a fine grained matrix composed of a fine aggregate of quartz, feldspar and biotite. The matrix is altered to chlorite and has disseminated fine magnetite crystals as the single grains.

4.3 Survey geometric design.

Magnetic surveys performed at several scales provide the field data used to explore the scaling relation of magnetic properties of the rocks within the sites at Flin-Flon. The smallest scale data corresponds to the magnetic susceptibility measurements collected using the KT-9 instrument, a hand portable magnetic susceptibility meter. A Larger scale survey is performed using the EM-31 frequency domain instrument. The data collected with the latter instrument require a geophysical inversion process to recover magnetic susceptibility distributions. This procedure includes one dimension half space forward modeling and geophysical inversions performed using available UBC-GIF codes.

To accomplish the goal of understanding the scaling nature of magnetic susceptibility, the field surveys were designed to involve several rock volumes. The collection of field data follows a sequence involving each of the geophysical surveys and is illustrated in figure 4.6. At each site, the first step includes the measurement of magnetic susceptibility using the hand magnetic susceptibility meter over a squared grid with a length of 10 meters. The grid was divided into 11 lines regularly spaced 1 meter apart, defining 121 intersection nodes. At each node, magnetic susceptibility measurements were recorded on the KT-9 instrument to generate the smallest scale data. The volume involved in each small scale measurements should be on the order of magnitude of few cubic centimeters, and are referred as the point scale data set.

The EM-31 electromagnetic instrument was used as a large scale magnetic susceptibility meter over each grid. For this geophysical method, the sampled zone was divided by perpendicular lines located at 0, 2, 5, 8, and 10 m away from the origin of the 10 m squared grid. At each intersection point between these lines, the electromagnetic survey was performed and a larger scale data set recorded. The depth of investigation reached by the EM-31 instrument determines the sample volume involved and hence the rock volume associated to the physical property values obtained with the geophysical inversions. For the EM-31 experiment, the depth of investigation is considered to be less than five meters constraining the sample volume to be in the order of 10 cubic meters.

4.4 Point scale data set.

Direct magnetic susceptibility measurements collected at several 10 m grids within the studied sites at Flin Flon District provide the point scale physical property data set. Measurements using the KT-9 hand portable magnetic susceptibility meter acquire data involving few cubic centimeters. At each site, 10 m square grids are defined by a local coordinate system in metric units, composed of 2 perpendicular axes, known as Line and Station axes. During the survey, measurements were collected at the intersections (nodes) between the grid axes. Wherever possible, additional measurements were collected 20 cm from each intersection node in the direction of each cardinal point to increase the number of measurements and have a data set at 20 cm of sample separation.

The magnetic susceptibility results at each of the grids are presented using location maps to display the spatial distribution, along with summary statistics (Table 4.1) and profiles of the average magnetic susceptibility calculated plotted as a function of the location.

On the location maps, the value measured at each sampled location, is represented by a circle in a colored magnetic susceptibility scale in SI units, multiplied by a factor of 10^{-3} . The color scale varies from blue for low magnetic susceptibility values to red representing high magnetic susceptibility values. Statistical distributions of the data measured at each grid are presented using frequency histograms plotted at a logarithmic scale, along with the basic statistics of the dataset. Location maps and histograms are calculated and plotted using WinGslib© software.

4.4.1 Mafic Volcanics grids

Direct magnetic susceptibility measurements are collected at 2 grids on this site, referred to as the Mafic Volcanic 1A (MV-1A) and the Mafic Volcanic 1B (MV-1B). The location of each, in the site's geologic context is showed in figure 4.1. MV-1A is oriented with the line axis

parallel to the direction of the geographic north of the site but the line axis of the MV-1B grid is rotated about 20 degrees to the west respect to the site's geographic north. The point scale magnetic susceptibility dataset at the Mafic Volcanic site consists in 362 measurements at MV-1A grid and 415 measurements at the MV-1B grid (Fig. 4.7).

Rock units (Figs.4.7A and 4.7D) at each grid correspond to the basaltic pillowed flow. Some of these rocks are weathered, which can strongly modify magnetic properties. Within MV-1A grid, the oxidized rocks form a triangular zone defined by the vertices located at the origin (0,0), (0,6) and (5,0). Most outcrops of the MV-1B grid are oxidized rocks. In fact, the area delimited by stations 2 to 8 and lines 0 to 5 display the effect of weathering.

At the MV-1A grid, the spatial distribution of the measurements (Fig 4.7B) is characterized by a dominance of magnetic susceptibilities less than 3 for most of the nodes. Three nodes located at station coordinate equal to 1 and line coordinates equal to 8, 9 and 10, have the highest measured values, in the range 9 to 15. The impact of these high values is illustrated on figure 4.8A, the peaks on the physical property values produce an average around the zone between 3 and 4 units larger than the global magnetic susceptibility average. Medium to high magnetic susceptibility values are irregularly distributed over the grid area. They are indicated by the peaks in the average magnetic susceptibility in the station and line profiles (Fig 4.8). The highest magnetic susceptibility zone is located in overburden, which may be the result of the accumulation of detritus with high iron content.

The MV-1B grid shows a similar spatial distribution of magnetic susceptibility compared to MV-1A. Most of the 100 m² grid has magnetic susceptibility value less than 2, as illustrated by an upper quartile value of 1.5 (Fig. 4.7F). A zone located in the upper-left corner of the grid has the highest susceptibility values, ranging from 4 to 12 (Fig. 4.7E). Isolated spots are irregularly distributed over the grid with magnetic susceptibility values between 2 and 6.

Frequency histograms plotted at logarithmic scale for both grids (Fig.4.7C) display similar shape, centered around the mean values of 1.42 and 1.49 for MV-1A and MV-1B,

respectively. Also the extreme and the quartiles values are similar indicating a homogeneous statistical distribution of the surface physical property on both grids.

The profiles of average susceptibility versus position in Line and Station (Fig 4.8B) show an overall fluctuating behavior for the local magnetic susceptibility average around the global mean of the physical property.

4.4.2 Mafic Boundary Intrusive grids

Two grids complete the point scale magnetic susceptibility survey at this site. They are the Mafic Boundary Intrusive North (BI- North) grid with 376 measurements and the Mafic Boundary Intrusive (BI- South) grid which contains 419 data. Both are located at the center of the site, separated by 25 m in a north to south direction (Fig. 4.2). The line axis of BI-North grid is rotated about 10 degrees with respect to the geographic north of the site, whereas the line axis of the BI-South grid is oriented parallel.

Geologic sketches (Fig. 4.9A and Fig 4.9D) performed at both grids indicate that 2 rocks units are common to grids. The Mafic Boundary Intrusive unit, composed by small tabular shaped bodies of gabbros and massive basaltic flows unit dominate outcrops at BI-North. At BI-North grid, brecciated basaltic flows and quartz-epidote altered rocks are also present. Similarly, at the BI-South grid, a basaltic amygdule-rich flow is differentiated from a massive flow. The amygdule-rich rock dominates this grid.

Spatial distributions of magnetic susceptibility measurements collected at each grid are shown in figures 4.9B-C and figures 4.9E-F, respectively. At Mafic Boundary Intrusive North grid, the highest magnetic susceptibility values are located within the northern third portion of the grid. There, most of the values are in the range between 30 and 90. To the south, a decreasing magnetic susceptibility trend is observed as most values in the southern part of the grid are less than 20. These two zones of such different magnetic susceptibility values explain the

bimodal distribution observed on the frequency histogram (Fig. 4.9C and Fig. 4.9F), and also explain the large standard deviation value (18.69).

The analysis of the local magnetic susceptibility average profile (Fig 4.10A) reveals a trend in the average susceptibility with the line coordinates in the north grid. The first 4 meters of the local magnetic susceptibility average curve is almost entirely less than the global magnetic susceptibility. For line coordinates greater than 4, the local average tends to be higher than the global mean. The same analysis of the local average susceptibility as a function of the station coordinate in turn indicates that between station coordinates 2.2 and 4.2, the local average susceptibility is higher than the global mean. Outside those station coordinate intervals, the local susceptibility average fluctuates around the global physical property mean.

At Boundary Intrusive South (BI-South) grid; the measurements are characterized by low magnetic susceptibility values between 0.48 and 1.15. This small range of variation is also accompanied by a homogenous spatial distribution across the grid (Fig 4.10B).

The magnetic susceptibility statistical distribution of the measurements collected at both grids indicates that different populations are encountered. The magnetic susceptibility range between 20 and 90 observed at BI-North is not present at BI-South, indicating that despite the presence of an apparently homogeneous rock type, the magnetic susceptibility distribution can be quite different.

4.4.3 Quartz Porphyry grids

Magnetic susceptibility measurements were collected at two grids on the Quartz Porphyry site; named Quartz Porphyry West (QP-West) and Quartz Porphyry East (QP-East) grids (Figs. 4.3, 4.11A and 4.11D). Line axes of both grids are nearly oriented parallel to geographic north. The grids are separated by 150 m, measured in the east-west direction.

Rocks at the two grids are the Quartz Porphyry unit and the Mafic Dyke unit. Quartz porphyry dominates both grids. Macroscopically, it is characterized by quartz and feldspar phenocrysts in a dark to gray, finely foliated groundmass with disseminated magnetite. At both grids, it appears as stripes with a N45W orientation, trending diagonally across the squared grid. The horizontal thickness varies from 0.5 to 2.5 m, with an average of 1 m for the QP-West grid and 2 m in the case of the QP-East grid.

Spatial distribution of the 303 point scale magnetic susceptibility values at QP-West grid (Fig. 4.11B) and the 314 magnetic susceptibility measurements within QP-East is displayed on figure 4.11E. Small cluster of magnetic susceptibility between 10 and 25 are located near the upper left corner of the QP-West grid (Fig 4.11B) around the nodes (7,0), (4,6) and (1,4) in the station-line coordinate system. Zones of magnetic susceptibility between 5 and 10 dominate the rest of the grid and define 2 sub-elliptical zones at the central area left border of the grid. They are separated by the magnetic susceptibility background value of 5. At QP-East, a near N45W oriented zone of magnetic susceptibility between 10 and 25 is located in the lower half of the grid. It has an envelope of magnetic susceptibilities between 5 and 10 which in turn, is immersed in the dominating magnetic susceptibility background below 5 (Fig 4.11E).

In the profiles of local average magnetic susceptibility with position (Fig 4.12A) for the QP-West Grid, the main feature is a fluctuation of the local average around the global magnetic susceptibility mean. However considering the line profile, the observed trend is a consistent increase in the local susceptibility average with line coordinate. In fact, the local average remains below the global average until the line coordinate 3.8, then fluctuate around the mean to the line coordinate 8, to finally end with local average values over the global mean. At QP-East (Fig 4.12B), there is a clear trend of decreasing local susceptibility average with line coordinate. The line profile starts above the global mean up to the 3.8 line coordinate and then stays below the global mean almost to the end of the profile, except for the line coordinates 6, 7.8 and 9.8 where it slightly exceeds the global mean. The station profile fluctuates constantly around the global mean with changes in location.

The statistical distributions described using the frequency histograms (Figs. 4.11C and 4.11F) display a large range of variation, involving two orders of magnitude in the magnetic susceptibility scale. This large spread is responsible for the high standard deviation 5.32 and 5.12, observed for QP-West and QP-East, respectively.

4.4.4 Sedimentary Rocks grid.

At this grid, 324 measurements of magnetic susceptibility with the KT-9 instrument were collected over a single rock type, known as sedimentary rock unit (Fig. 4.13A). This rock unit is weathered, as detected in the area limited by lines 5 to 8 and stations 5 to 6. Two shear zones of 0.5 m of horizontal width and with a near eastern orientation located in the southern half of the grid complete the geologic features.

The spatial distribution of the magnetic susceptibility values (Figure 4.13B) reveals a central strip of low (<10) magnetic susceptibility. This zone is oriented in an almost E-W direction, has a thickness between 1.5-2.5 m. It separates two higher magnetic susceptibility zones (>10) located to the north and south of this low magnetic susceptibility feature. Both zones of higher magnetic susceptibility contain small clusters of susceptibility in the range between 20 and 25.

The frequency histogram for the 324 measurements collected within this grid is characterized by a symmetric shape, centered on a mean value of 10.87 in a logarithmic scales histogram (Fig 4.13C).

4.4.5 Granite grid.

At this grid, granite constitutes the only rock type encountered (Fig. 4.13D). Only a quartz vein cuts the granite. The vein has a strike N20-30E and extends from the (0,0) node to the (4,9) node, with an horizontal thickness of 0.2 to 0.5 m.

The magnetic susceptibility measurements collected within the 10 m grid have a homogenous spatial distribution (Fig 4.13E). Most of the values are in the range 0.2-0.3 with scattered nodes displaying measurements out of this interval. Local average magnetic susceptibility plotted as a function of line and station coordinates (Fig. 4.14B) show this quantity fluctuates around the global physical property mean. The small amplitude of the oscillations reflects the homogeneous statistical distribution.

4.5 Spatial variability of magnetic susceptibility at the point scale.

This section analyzes the spatial variability of magnetic susceptibility data collected at a point volumetric scale, using the KT-9 meter at the 10 m grids. The goal is to qualitatively and quantitatively characterize the pattern of the physical property spatial variability observed within each grid, using experimental variograms. This geostatistics tool summarizes how the physical property variability changes with the separation of the samples. Calculating variograms allows the determination of some of the features that characterize the spatial variability of the magnetic susceptibility. These include the nugget effect, the sill (variance) and the range distance. The parameters characterize the spatial variability of the sample data set and therefore are relevant for fitting a model to the experimental variogram. The obtained variogram model should honor the data to be scaled using the geostatistical tools as described in chapter 2. As a result, a larger scale data set can be calculated and then compared to the physical property models resulting from geophysical inversions of larger scale data sets, such as EM-31.

Within each of the measured grids, experimental variograms of the magnetic susceptibility measurements collected at the point scale are calculated and interpreted to describe the spatial variability at this scale. The calculations are performed using WinGSLIB©, which is a flexible FORTRAN based code.

A variogram is isotropic if it behaves similarly in all the spatial directions of the separation distance vector. Conversely, if the variogram changes the shape or value with orientation, there is anisotropy for the analyzed variable. The magnetic susceptibility distributions within the grids are characterized by the maps described and presented in previous sections. In general, magnetic susceptibility is not characterized by spatial orientations that control the physical property distribution, excepting at the Mafic Boundary Intrusive North Grid. The most common observed features are zones where the susceptibility values appear to be related, which might produce an erratic or noisy experimental variogram behavior, thereby hindering interpretation and modeling.

4.5.1 Isotropic point-scale magnetic susceptibility experimental variograms.

As a starting point of the spatial continuity analysis, isotropic experimental variograms are calculated for the magnetic susceptibility measurements collected at several 10 m grids. This step is useful for establishing some parameters important in the variogram calculations. The nugget effect or short distance spatial variability can be calculated from isotropic variograms. The main factors controlling the genesis of a nugget effect are sampling errors, small scale variability and a random nature of the variable analyzed. These factors may cause a variogram to take values different than zero at the origin, which should be the case by definition (Equation 2.5). Extremely close sample values having quite different physical property values might result in a not null variogram value.

To proceed with the calculations of the isotropic variograms, some parameters are required to define the tolerance region for searching the pairs of data involved in the computations. They include the separation distance and associated tolerance, the band width and the azimuth. The separation distance, h , also referred as the lag spacing, lag increment or simply the lag

distance. In this case, the lag is set equal to 1 m as it is the separation distance available from the data set. The lag distance tolerance is set to 0.4 m to incorporate the information provided by the additional measurements 20 cm away from the sampling nodes. These constraints produce a smoother variogram curve suitable to be interpreted. The band width is set to 1 meter to constrain the data to be used in the calculations.

The nugget effect (C_0) is calculated from the isotropic experimental variograms by extending the straight line that connects the two first points of the experimental variogram to intersect the variogram axis (Figure 4.15). Table 4.2 displays the nugget effect values obtained with this procedure and the relative nugget effect, the latter being calculated as a percent of the variance of the data set. The results indicate that the relative nugget effect varies from 16 to 52 percent indicating that an important (as high as 50%) portion of magnetic susceptibility spatial variability within the point scale measurements is associated with the nugget effect. This can be related to either sampling errors or to a spatial variability feature undetectable with a grid geometric array characterized by a minimum of 20 cm of sample separation.

The resulting isotropic variograms reveal scarce information about the spatial variability of magnetic susceptibility, as they do not clearly reach the sill/variance. The variograms at MV-1B, BI-North and QP-East detect the presence of trends in the magnetic susceptibility as they steadily increase their values with the separation distance (Fig. 4.15). For MV-1A, BI-South, QP-West, QP-East and Granite grids a sill value is detected and therefore associated range distance can be calculated (Fig. 4.15 and Table 4.2).

4.5.2 Directional experimental variograms of magnetic susceptibility at the point scale.

Directional variogram are used to determine whether the magnetic susceptibility spatial variability is isotropic or not. If anisotropy is detected, then major and minor axes of spatial continuity can be determined. The maximum spatial continuity axis coincides with the direction at which the largest range distance is encountered (Isaacs and Srivastava, 1989).

For computing each directional variogram, a separation distance vector is oriented in four spatial directions; denoted by D1 to D4 corresponding to azimuth angles of 0, 45, 90 and 135 degrees respectively. The angles are measured clockwise respect of the Line axis of each of the grids. The selected orientations are intended to ‘sweep’ the complete 2-D space to capture the magnetic susceptibility spatial variability within each of the grids. Setting an azimuth tolerance angle of 22.5 degrees to each direction ensures this purpose (Figure 4.16). In order to increase the numbers of pairs involved in computing the variogram values at each of the lag distances, tolerances in the lag separation distances are set to 0.4 m, similar to the isotropic case. This procedure is recommended for a robust and more suitable experimental variograms, as an aid to interpreting and geostatistical modeling (Deutsch and Journel, 1998).

4.5.2.1 Mafic Volcanics

The directional variograms at MV-1A grid display different shape and values. With the different spatial orientation of the separation distance vector (Fig. 4.17A and Fig. 4.17B). Within separation distances of 2 m the directional variograms are quite similar for D2, D3 and D4 directions. They rapidly reach a sill/variance value of 3.65 at a separation distance between 0.9 and 1 m, and then drop below the sill. Therefore in these three spatial directions, magnetic susceptibility is expected to be correlated within a range of 1 m. The directional variogram oriented parallel to the line axis (D1) indicates a larger range of correlation for the physical property. It grows gradually from separations smaller than 1 m and rises smoothly to reach the sill/variance value at a range distance of 3 m, indicating spatial continuity to that distance in this particular orientation (Fig. 4.17A). A nugget effect of 1.2, obtained by averaging the individual nugget values of each directional variograms and also in the isotropic case, will be used in the spatial variability modeling for this grid. Both range distances observed at D1 and the other three directional variograms will be compared to determine which one provides the best modeling results (Table 4.3).

D2, D3 and D4 directional variograms at MV-1B (Fig. 4.17C and Fig. 4.17D) share similar behavior for separation distances smaller than 1m. These curves quickly reach the magnetic

susceptibility variance value of 1.8 (Table 4.1) calculated for the grid. After this value, they drop below the grid's magnetic susceptibility variance. D1 directional variogram at MV-1B starts as a pure nugget effect for the first 2 m separations. After this value, it constantly increases, and crosses over the variance at 5 m and keeps increasing value with separation distance, revealing a trend in magnetic susceptibility in that spatial orientation.

4.5.2.2 Mafic Boundary intrusive

Directional magnetic susceptibility variograms calculated for the Mafic Boundary Intrusive North (BI-North) grid (Fig. 4.18A and Fig. 4.18B) display a similar behavior in the 4 spatial orientations analyzed for separation distances smaller than 3 m. Within this small separation, the variability increases steadily, indicating some degree of magnetic susceptibility spatial correlation. For larger separations, however the four directional variogram behave differently. D1 and D4 variograms indicate a trend in magnetic susceptibility, because their variogram values rise continuously over the magnetic susceptibility variance value of 349 calculated for this grid (Table 4.1) for separations beyond their respective ranges distances, in both cases near 5.2 m (Table 4.3). In turn, both D2 and D3 oriented variograms show a slower rate of increasing variability and they do not reach the variance value at separation distances less than 5 m. Modeling the spatial variability for this grid within the first 3 m would consider an isotropic model, as no major changes in the shape and variogram values are observed within this separation distance.

Directional variograms of magnetic susceptibility at the BI-South grid (Fig. 4.18C and Fig. 4.18D) at the four analyzed orientations rise quickly within the first 1m of separation distances and then drop their values abruptly for D2 and D4 orientations and at a slower rate for the D1 and D3 cases. Within this short separation distances, D2 and D4 reaches the variance value of 3.65 whereas the D1 and D3 oriented variograms reach it at separation distances of 5.6 and 4.3 m respectively. This reveals that larger spatial continuity of magnetic susceptibility is achieved for D1 and D3 orientations.

4.5.2.3 Quartz Porphyry

The directional magnetic susceptibility variograms at the Quartz Porphyry West (QP-West) grid are characterized by a nearly isotropic behavior for the first 4 m at the 4 analyzed orientations, as no important changes in shape or variogram value are detected (Fig. 4.19A and Fig. 4.19B). The directional variograms display a fast increase of the variogram value for the first two lags. Starting at nugget values between 6 and 16, the variogram values rapidly increase their values with distance, almost reaching the variance value within the first meter. The variograms then tend to level off and oscillate around variogram values between 26 and 28. Range distances can be calculated for directions D2, D3 and D4, corresponding to 2.5, 1.8 and 3 m respectively (Table 4.3). For the D1 case, the range separation is 6 meters. Spatial variability modeling for this grid will test which is the suitable range distance and how an isotropic model of variogram explains the observed pattern of spatial magnetic susceptibility distribution (see below).

At the QP-East grid, directional magnetic susceptibility variograms (Fig 4.19C-D) are characterized by similar spatial variability pattern for D1 and D3 orientation, at least within the first 4 meters. At larger distances, the D1 oriented variogram displays a trend in magnetic susceptibility, whereas D3 drops in value with increasing separation distances. The range is achieved at 3 and 4 m for D1 and D3, respectively. The D2 oriented variogram is similar to D1 and D3, but it reaches the sill at a range of 2 m and the sill value is slightly higher than the magnetic susceptibility variance for this grid (Table 4.1). When modeling the magnetic susceptibility spatial variability, an isotropic variogram will test with the nugget, sill and ranges parameters observed from this analysis (Table 4.3).

4.5.2.4 Sedimentary Rocks

For this grid, a similar behavior for the D1, D2 and D4 directional variograms is detected (Fig. 4.20A and Fig. 4.20B) which entails a similar pattern of spatial variability in three of the four analyzed orientations. The three curves have same shape, but differ in the variogram values. Within the first 2 lags, D1 and D2 reach the magnetic susceptibility variance value at this grid (Table 4.1) while D4 reach the variance for a separation distance of 2.5 m approximately (Fig. 4.2B). After reaching the variance, the three variograms display a feature usually referred as a 'hole effect'. This is characterized by a wave like shape with an approximate period of 2.5 m and a amplitude near 10 variance units. This variogram behavior is associated with a cyclic pattern of spatial variability. The repetition of zones of medium (10-20) and low (5-10) magnetic observed within this grid when moving from low to high line coordinates can explain the observed variogram cyclic behavior (Fig.4.10E). The D3 directional variogram (Fig 4.20A) grows at lower rate compared to the other three; it display a sill leveled at a variogram value equals to 14. This sill values is 4 units lower than the variance value and is reached at a range distance of 2 m.

4.5.2.5 Granite Site

The directional variograms oriented at D1, D2 and D4 for this site are characterized by similar behavior, indicating a common pattern of spatial variability for these 3 orientations (Fig. 4.20C and Fig. 4.20D). At small separations these three directional variograms have a nugget value near 0.001 (Table 4.3). They increase the variability up to separations of 2 m, where they level off, defining a sill value of 0.0028. This sill value is smaller than the 0.0033 variance value for this grid (Table 4.1). Therefore, 85% of the total variability of the physical property is accounted by the information captured by these 2 variograms. Comparing the D3 directional variogram to the other three detects major differences. First D1 starts at a high variogram value, defining a nugget of 0.0026 for the small separations. For larger separations the variogram fluctuates, but a systematic increase of the variogram values is achieved. The

variogram cut the variance value at 4 m and keeps growing beyond this distance without defining any sill.

4.6 Modeling of point scale magnetic susceptibility spatial variability.

In this section variogram modeling of magnetic susceptibility is performed. This procedure consists on fitting a mathematical function to the experimental variogram calculated from the sampled data. The variogram models used here, correspond to those implemented within the GSLIB© software. They include the Spherical, Exponential, Gaussian and Power models which are the classical negative definite functions² used in geostatistical modeling (Journel and Huijbregts, 1978). The variogram models are parameterized functions that require the input of values estimated for the nugget effect, the sill and the range distance in order to calculate an output model. After the parameters are estimated from the experimental variograms, the procedure calculates an output variogram model and graphically evaluates the degree of fitting between the model and the experimental variogram. The visual assessment is accompanied by cross-validation (see chapter 2) which allows quantifying the quality of the variogram model fitted. Ideally, the correlation factor between the true (measured) magnetic susceptibility values and the estimated (calculated) values should be 1.

Experimental variograms contain reliable information for lag distances smaller than half of the size of the sampled region, providing that the number of pairs is not too small (Journel and Huijbregts, 1978). Therefore, here, the modeling is constrained to lag separations less or equal to five meters, as the sampled grids are 10 m length. All the cases are treated as isotropic variograms, as no principal axis of anisotropy are detected with the directional variograms or in the magnetic susceptibility spatial distributions. The type of models and the parameters used for fitting them are presented on Table 4.4. The resulting output variogram models along with their respective experimental variograms are plotted on figure 4.21. Cross validation of

² A function $g(h)$ is said to be negative-definite function if for any integer $k > 0$, any set x_1, \dots, x_k of points of the n -dimensional space and any system of coefficients $\lambda_1, \dots, \lambda_k$ of real numbers, the equation

$$\sum_i \sum_j \lambda_i \lambda_j g(x_i - x_j) \leq 0 \text{ is always satisfied.}$$

each model is performed and true-estimated pairs of magnetic susceptibility are obtained. The scatter plots of true versus estimated magnetic susceptibility are characterized by point clouds with large spread which is reflected by poor correlations (Fig. 4.22). The correlation factor between the true magnetic susceptibility and the estimated magnetic susceptibility is calculated. In the example under study, the values fluctuate between 0.56 and 0.73. The fact that these results are significantly less than the ideal value of 1 indicates limitations of the fitted variogram modeling. This limitation is related to the fact that the experimental variograms obtained are erratic and do not display well defined structures (sill/range) to be modeled.

In order to further evaluate the quality of the variogram models fitted to the experimental variograms calculated for each grid, graphical tests are performed using histograms of the standardized estimation error³ and scatter plots of the standardized estimation errors versus the estimated values. The histograms of the standardized estimation errors are centered on the zero value for all of the analyzed grids indicating that the estimation is globally unbiased (Fig 4.23). However, the scatter plot of the standardized estimation errors versus the estimated values are characterized, for most of the analyzed grids, by not being centered around the zero error line, indicating the presence of conditional biased estimations (Fig. 4.24) (Emery, 2000, Deutsch and Journel, 1998). Moreover, in most of the grids, the scatter plots have unequal spread evidenced by triangular shape of the point clouds, revealing a proportional effect or that the variance has a non constant value (heterocedasticity) (Emery, 2000, Deutsch and Journel, 1998). The only exceptions correspond to the Sedimentary Rock and Granite grids which display symmetric point clouds around the zero error line (Figs 4.23G and Fig 4.23H).

Finally, two quantitative parameters are used for the assessment of the cross validation results. The first one is the percent of estimated values for which the standardized error is out of the interval defined by a lower limit of -2.5 and an upper threshold of 2.5. Reasonable percent values (<5%) are obtained at all grids except for the Quartz Porphyry West Grid (Table 4.4). The second parameter used is the mean of the quadratic standardized errors which should be close to 1, and it represents how well the variogram model estimates the amplitude of the

³ The standardized estimation error is the estimation error divided by the kriging standard deviation calculated for each estimated value.

associated error (Emery, 2000). The average quadratic error values are close enough to 1 for 5 of the measured grids, indicating that the variogram models reproduced correctly the amplitude of the estimation error. On the other hand, at the Mafic Volcanic 1A, Quartz Porphyry West and Granite grids the values indicated the variogram models are not reliable, as the average quadratic error are deviated more than 5% from the target value of 1 (Table 4.4).

4.7 EM-31 survey dataset

Magnetic susceptibility models recovered from geophysical inversions of electromagnetic data collected using the frequency domain EM-31 instrument provide a larger scale of magnetic susceptibility data compared to the KT-9 measurements. The EM-31 survey is performed over the same 10 m grids used for the point scale magnetic susceptibility measurements. The data collection includes measurements over perpendicular lines oriented in the same way as the KT-9 grids. They are located at coordinates 0, 2, 5, 8 10 in the station-line geographic system (Figure 4.25), generating 25 nodes. At each intersection node, the instrument is oriented parallel to the line and station axes and measurements of in-phase and out of phase components of the secondary electromagnetic field are collected in the vertical dipole mode (see section 2.2.4). As a result, 4 measurements are recorded at each node. This survey involves larger rock volume where compared to the point scale magnetic susceptibility survey.

4.7.1 EM-31 results

Geophysical inversion performed to the electromagnetic data collected within the 8 grids results in larger scale magnetic susceptibility distributions. To calculate the distributions a 'look-up' table containing the electromagnetic (EM) data forward modeled considering a half space, one dimension layered earth with large range of magnetic susceptibility and electrical

conductivity as an input model. This procedure is performed using “EM1DFM” code designed at the UBC-GIF facility. The algorithm searches within the look up table for those EM data that best fit the EM observations, outputting the corresponding magnetic susceptibility and electrical conductivity pair.

The results of the recovered magnetic susceptibility distributions at Mafic Volcanics 1B, Mafic Boundary Intrusive North, Mafic Boundary Intrusive South, Quartz Porphyry West, Quartz Porphyry East and Sedimentary Rock grids are plotted in Figures 4.26 to 4.31. Negative ‘In-phase’ component of the secondary electromagnetic signal measured for each site did not allow completion of the inversions at the two remaining grids (Mafic Volcanic 1A and Granite). All the values are reported in SI units of magnetic susceptibility scaled by a factor of 10^{-3} .

The magnetic susceptibility spatial distribution plot at the Mafic Volcanic 1B grid, (Fig 4.26A) shows that the sampling is located almost exclusively along the central line of the grid where the values are between 1.18 and 3.42. The statistical distribution of the recovered magnetic susceptibility is characterized by an approximate log-normal distribution (Fig 4.26B).

The recovered magnetic susceptibility distribution at the Mafic Boundary intrusive North grid is characterized by a minimum value of 0.64 to a maximum value of 67.68 (Fig 4.27B). This large range in the physical property accounts for the large variance value of 382.9. The high variability is related to the presence of several magnetic susceptibility populations. The recovered physical property range includes all the spectrum of possible magnetic susceptibilities, from diamagnetic for the lowest ($10^{-6} - 10^{-5}$ SI), paramagnetic for the population in the range 10^{-4} to 10^{-3} SI to the lower part of the ferromagnetic materials for the values in the range of 10^{-2} SI units. The values are spatially zoned, with the high value population located at the upper right corner of the grid and the low values ($<20 \times 10^{-3}$ SI) on the opposite corner (Fig 4.27A). This contrast in the physical property is associated with materials of differing magnetic minerals content. Magnetic susceptibility spatial variability for the short separation distance (<2 m) is characterized by a small nugget effect ($C_0=20$) due to

the fact that nearby locations tend to have similar physical property values. For separations between 2 and 4 m, a smooth increase in the variability is achieved (Fig 4.27C). For separations between 4 and 5, the variability is approximately steady at a variogram value of 280, which is interpreted as a sill value (variance value at the scale of the EM-31 survey). The behavior beyond 5 m is characterized by an increase in the variability which is expected as the values from the high and the low magnetic susceptibility zones contribute to the variogram for the larger lag distances.

The recovered magnetic susceptibility distribution at the Mafic Boundary Intrusive South is characterized by a range of values, varying between 0.59 and 5.32 scaled by a factor of 10^{-3} in SI units (Fig 4.28B). This one order of magnitude in variability, from 10^{-4} to 10^{-3} SI units, is compatible with a single population of magnetic susceptibility values with paramagnetic characteristics. Magnetic susceptibility spatial variability is described by the experimental variogram at the scale of the EM-31 survey which is characterized by a large increase for the first two lag distance less than 2m. Between separation distances between 2 and 5 m, variability stays constant around a variogram value of 0.6 which is considered a sill value for this data set (Fig 4.28C).

The magnetic susceptibility distribution recovered at Quartz porphyry West grid is characterized by a range of values between 0.001 and 19.52. The minimum value is achieved at a single location in the grid, location (0,0) at the physical property spatial distribution map (Fig 4.29A). Excluding this value, the physical property range fluctuates between 0.78 and 19.52. This range is compatible with the presence of two magnetic susceptibility populations, a paramagnetic and a ferromagnetic. Most of the grid is dominated by the low or susceptibility population (paramagnetic), below 14 ($\times 10^{-3}$ SI). In contrast the ferromagnetic population of values is restricted to the upper left corner of the grid (Fig. 4.29A). The isotropic experimental variogram is characterized by a high variogram value at the first lag (~ 1 m) accounting for half of the variance value (Fig 4.29C). Thus, over this separation, the physical property can be quite different. For the next lags, the variogram k steadily increases, cutting the variance value at 6 m without reaching a sill value, likely indicating a trend in the data.

For the Quartz porphyry East grid, only at 9 locations magnetic susceptibility values are recovered from the inversion of the EM-31 data (Fig 4.30A). The values range (0.73 – 8.4 $\times 10^{-3}$ SI) indicates a population of paramagnetic material. The small quantity of physical property values does not allow the calculation of a reliable experimental variogram as few pair of sampled locations would be involved in the calculations.

At the Sedimentary Rocks grid, the recovered magnetic susceptibility dataset from the EM-31 data is characterized by a range of physical property values between 0.74 and 23.11 ($\times 10^{-3}$ SI). The range of values can be considered as a single statistical population with one paramagnetic material. The maximum value (23.11) could be related to a more ferromagnetic population, but this value is spatially constrained to a unique location in the grid (Fig. 4.31A). The spatial variability characterized by the isotropic experimental variogram indicates that the physical property at nearby locations can be quite different implying a low spatial correlation at the short distances (<1 m). Up to a separation of 3 m, the variogram increases value and cuts the variance value but no sill value can be observed.

4.7.2 Comparing KT-9 magnetic susceptibility with EM-31 physical property distributions.

In this section, a comparison between the results obtained in the previous sections is presented. The objective is to probe whether, or not, magnetic susceptibility is sensitive to variations in the volumetric scale by comparing the statistical distribution and the spatial variability pattern of the magnetic susceptibility at the point scale and at the volumetric scale of the EM-31 survey.

Available magnetic susceptibility data set at the two scales have a different quantity of sampled locations, which inhibits a strict one to one comparison between them. However, quartile-quartile plots can be used to investigate the relation between both variables. The quartiles of the two magnetic susceptibility distributions (KT-9 versus EM-31) are plotted in a logarithmic scaled diagram (Fig. 4.32). At all of the grids, a linear behavior is observed, but

departing from the bisector line, indicating that both variables have same shape (log-normal) but their mean and variance are different (Table 4.4). They moreover do not follow exactly the same distribution, as their quartiles are quite different. The changes in the slope of the q-q regression line in most of the diagrams accounts for the departure from the bisector line. This slope changes are associated with the presence of more than one magnetic susceptibility population. One important aspect derived from this observation is that although both methods differ in the resulting physical property distribution, they produce similar results in terms of the shape of the distribution but having different statistical parameters. These indicate that where the sampling volume changes, the statistical parameters (mean, variance, range, quartiles) of the physical property distributions also change. This conclusion is considered as a probe of the scaling nature of the physical property. For example, at Mafic Boundary North (Fig 4.32C), the change in slope is quite evident and therefore a change in the two physical property populations occurred from KT-9 to the EM-31 data.

Continuing with the comparison, the average magnetic susceptibility within each grid at each scale is calculated (Table 4.4). The results indicate that the mean values are different in all of the cases. A scatter plot of the magnetic susceptibility average at the point scale versus the magnetic susceptibility average at the scale of the EM-31 survey is used to obtain insight about the relation between the physical property averages at the two scales (Figure 4.33). This diagram suggests a linear relation between the logarithms of the averaged magnetic susceptibility, implying a power law relation between them. The next equation can be proposed as an empiric relation between the magnetic susceptibility measurements at the point scale and the magnetic susceptibility at larger scales:

$$\kappa_{KT9} = A * \kappa_{EM31}^{\beta} \quad [4.1]$$

Where κ_{KT9} , κ_{EM31} = average magnetic susceptibility at the point scale measurements and at the scale of the EM-31 survey and A, b= constants

Comparisons of the spatial variability at the two analyzed scales are achieved by plotting the experimental variograms obtained from the available magnetic susceptibility data sets at both scales. For all of the field sites investigated where the separation distance is smaller than 3 m, the variability at the point-scale is larger than the variability at the higher scale, as the point scale variograms are larger than their counterparts at the higher scale in all of the sites (Fig. 4.34). This indicates that the spatial variability is attenuated by the physical property averaging (smoothing) associated with the increase in the sampled volume. This can be expected where using the EM-31 instrument as a large scale magnetic susceptibility meter. The largest and more consistent (maintained for all the lag separations) variogram spread is achieved at the Mafic Boundary Intrusive grid with a difference of 2.82 variance units between both curves (Figure 4.34). The differences between both variograms tend to be reduced for lag separations higher than 3 m, due to either data trends or variogram value fluctuations.

4.8 Scaling magnetic susceptibility variogram models

Modeled variograms at the scale of the KT-9 magnetic susceptibility survey at the different grids are used as input to a FORTRAN code implemented by Oz et al (2002) for scaling variograms. The program is based on the geostatistics scaling laws (Oz et al, 2002) and can be used for analyzing scaling relations between different types of data. The scaling laws require the following assumptions according to Frykman et al. (2002):

- 1) The variogram model type does not change with the scale.
- 2) The averaging is achieved with non-overlapping volumes.
- 3) Physical property scales in a linear fashion or scales linearly after a power law transformation.

Applying the methodology for several target scales allows the establishment of the relationship of the dispersion variance with the measured volume associated with the physical property. This curve can be used to solve the uncertainty in the volume under investigation

with the EM-31 instrument. The available experimental variograms at the point scale (KT-9 measurements) and at a larger volumetric scale (EM-31 magnetic susceptibility) provide the opportunity to test this volume/variance relationship and understand the physical property scaling.

The grid selected for testing the variogram scaling method is the Mafic Boundary Intrusive South, because of the single one well defined sill/variance at both scales. Starting with a volume of five cubic centimeters as the scale of the point magnetic susceptibility measurements and the variogram model fitted to the data at the point scale for this grid and using the variogram scaling code, a curve of the variance versus the sampled volume is calculated. As the experimental variance for the EM-31 value is 0.83, the volume associated is 0.85 m³ (Fig 4.35). This result is validated using the scaled variogram model and cross validation with the experimental values at the EM-31 scale. The results indicate that the scaled variogram model fits adequately the experimental magnetic susceptibility variogram (Fig. 4.36A). The correlation factor (Fig. 4.36B) between the estimated and 'true' magnetic susceptibility value is 0.79 which suggest that the scaled variogram model reproduce in an acceptable way the experimental spatial variability at the larger scale.

4.9 Conclusions

Point scale magnetic susceptibility measurements for the 8 analyzed grids display a wide range of values, spanning the complete spectrum for diamagnetic, paramagnetic and ferromagnetic materials. The statistical distributions of the physical property are skewed to the low values classes which is compatible with a log-normal distribution. At each grid the variability is a function of the quantity of magnetic susceptibility populations present within the grids.

Spatial variability of magnetic susceptibility can be described by experimental variograms although the random or noisy characteristics of the available physical property data hindered their interpretation and modeling.

Comparison between physical property datasets available at two volumetric scales proved a dependency of magnetic susceptibility with the size and hence the scale of the sampling support. The relation between point scale magnetic susceptibility measurements and the recovered distribution of the physical property at larger volumetric supports seem to follow a power law, with an exponent (scaling factor) less than 1.

Variogram scaling of magnetic susceptibility can results in a suitable methodology to integrate different scale physical property distribution when a reliable model is fitted to the experimental variogram.

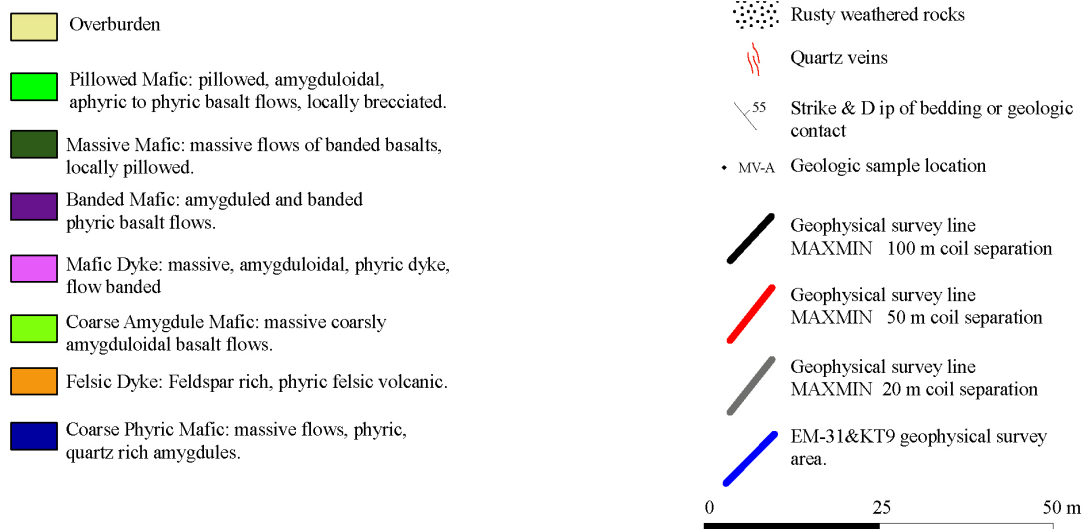
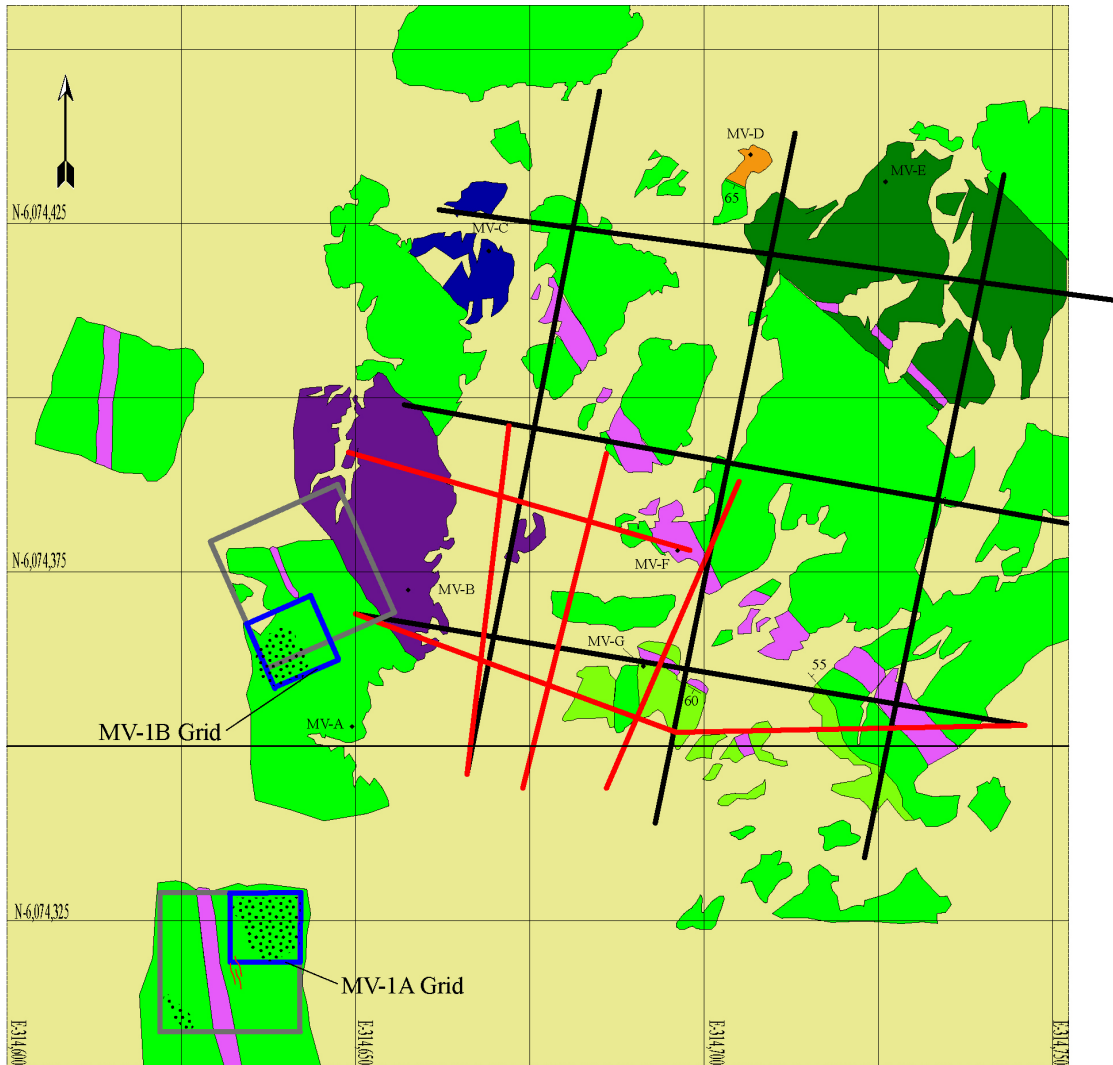


Figure 4.1. Geologic sketch of the Mafic Volcanic site.

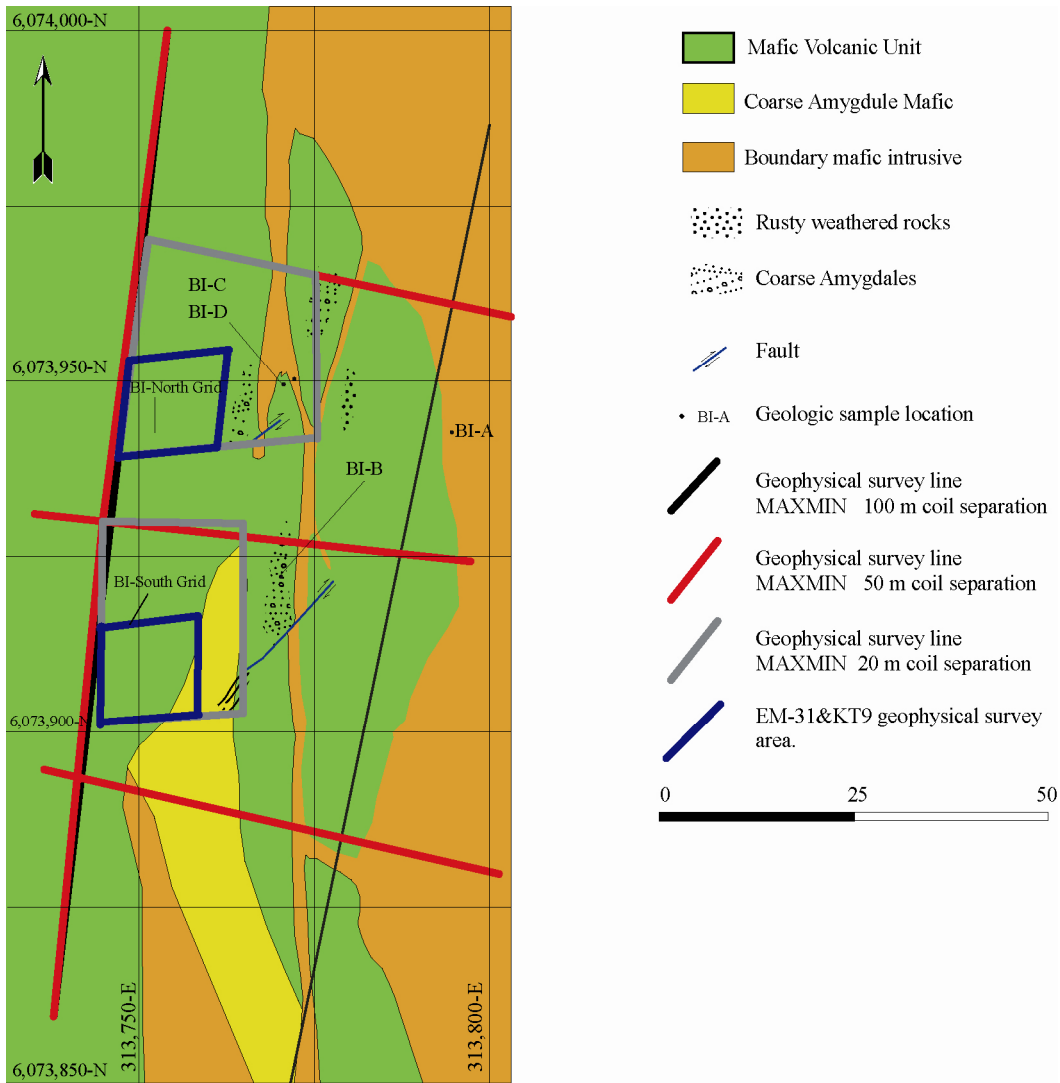


Figure 4.2. Geologic sketch of Mafic Boundary Intrusive site.

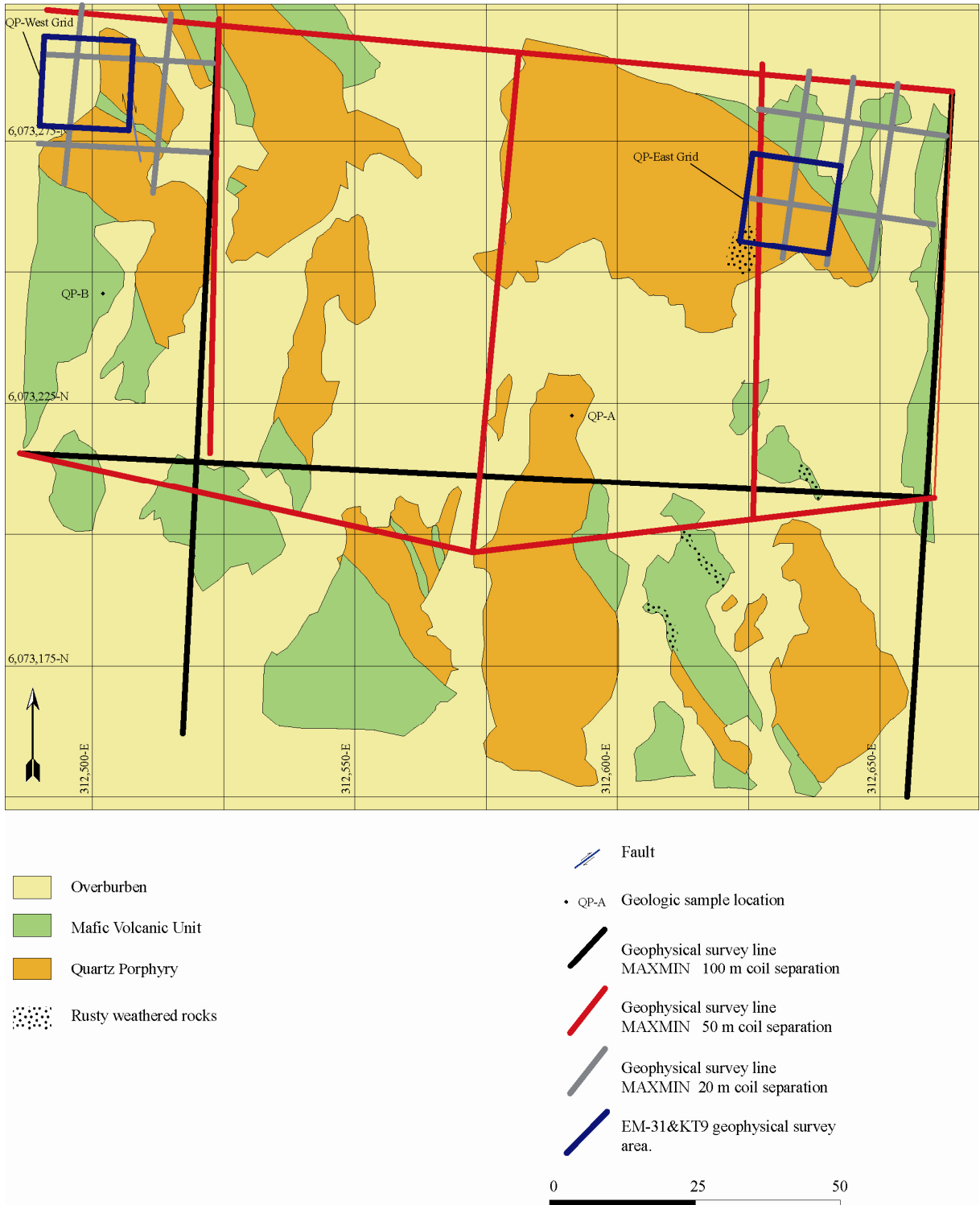


Figure 4.3. Geologic sketch of Quartz Porphyry site.

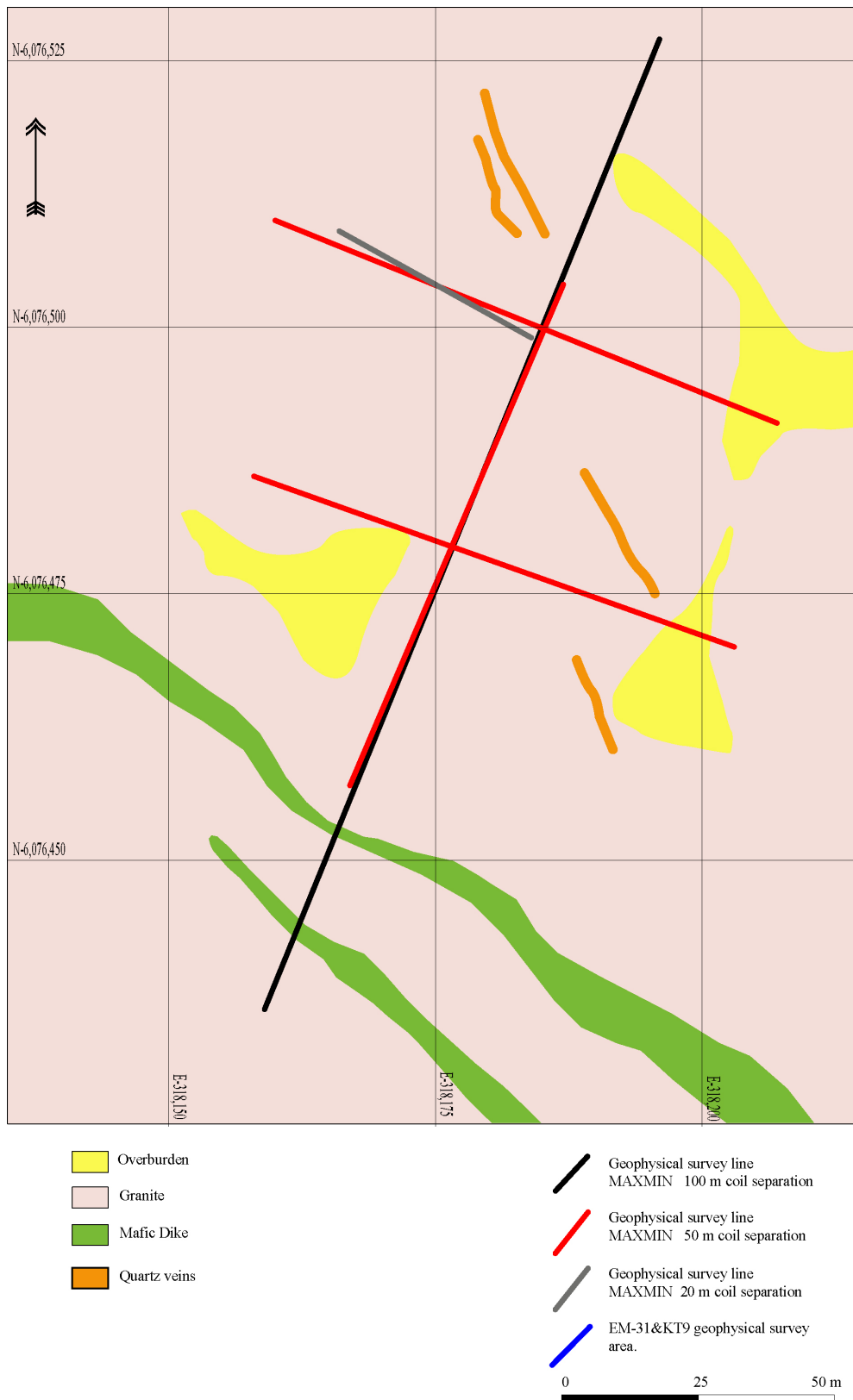


Figure 4.4. Geologic sketch of Granite site

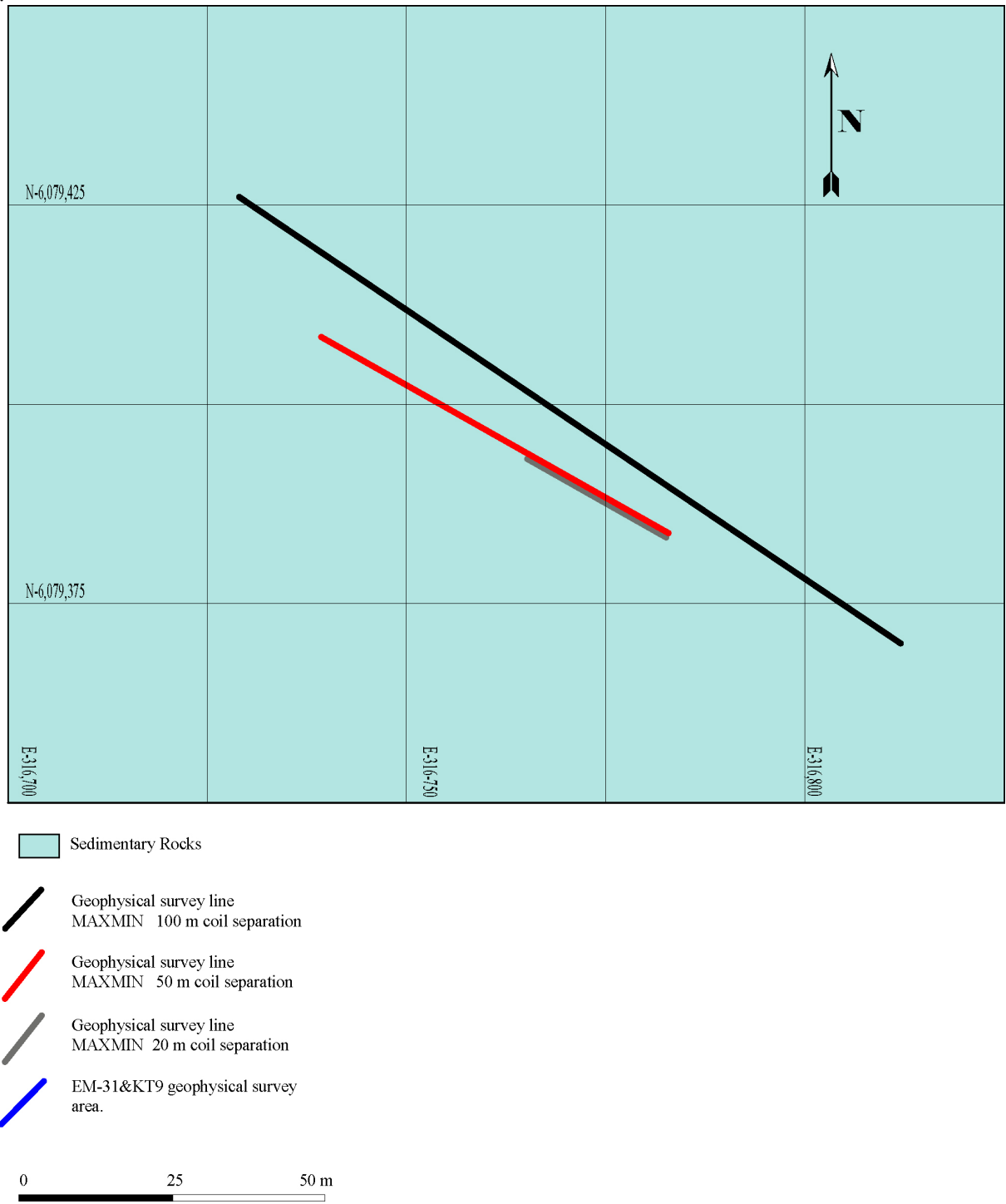


Figure 4.5. Geologic sketch of Sedimentary rock site.

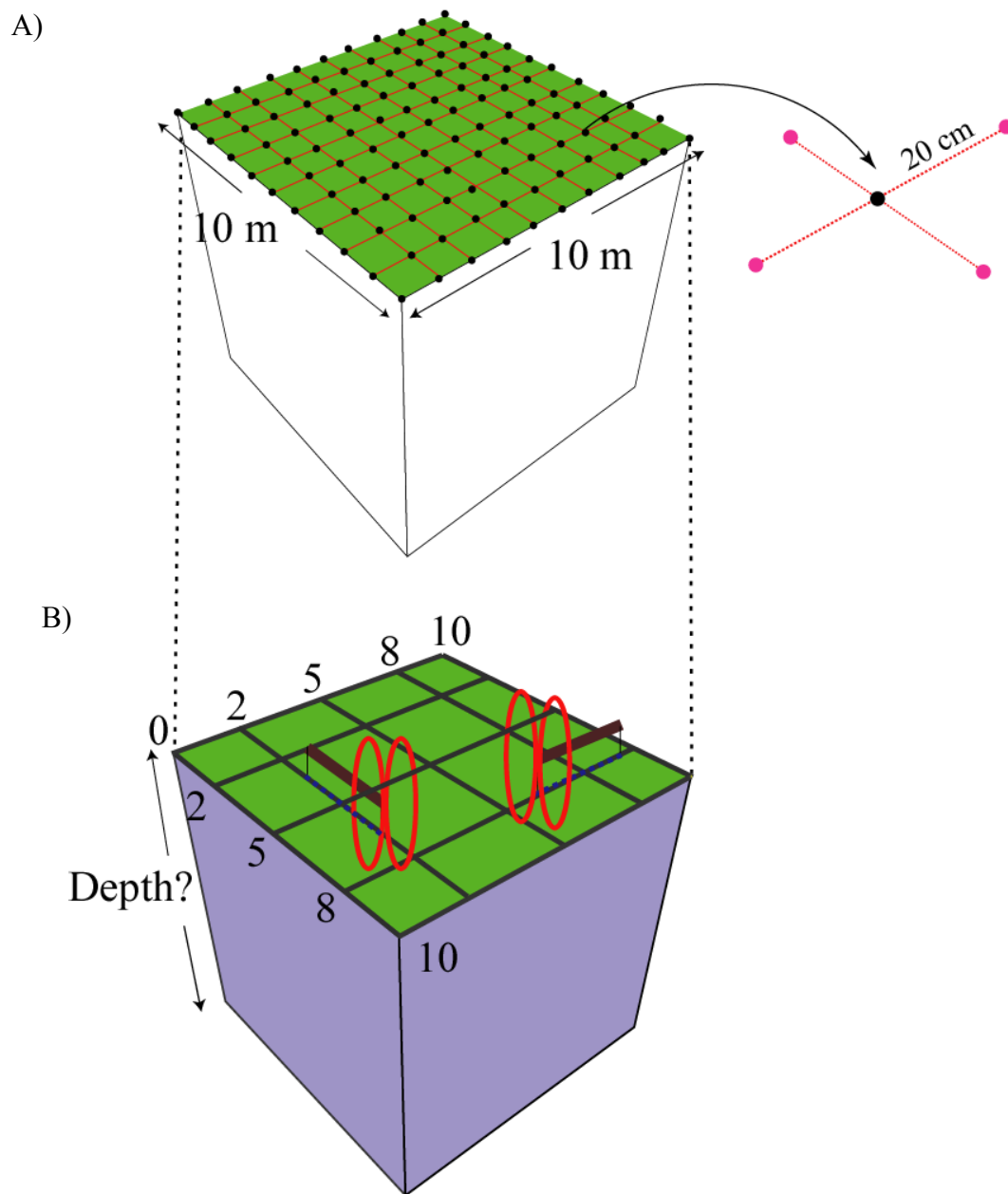


Figure 4.6. Geometric arrays used in the geophysical surveys designed to involve different sampling volumes. A) Point scale measurements with KT-9 hand portable magnetic susceptibility meter, B) EM-31 fixed inter-coil spacing of 3.66 meters can yield depth of exploration of about 6 meters allowing sampling larger rock volumes.

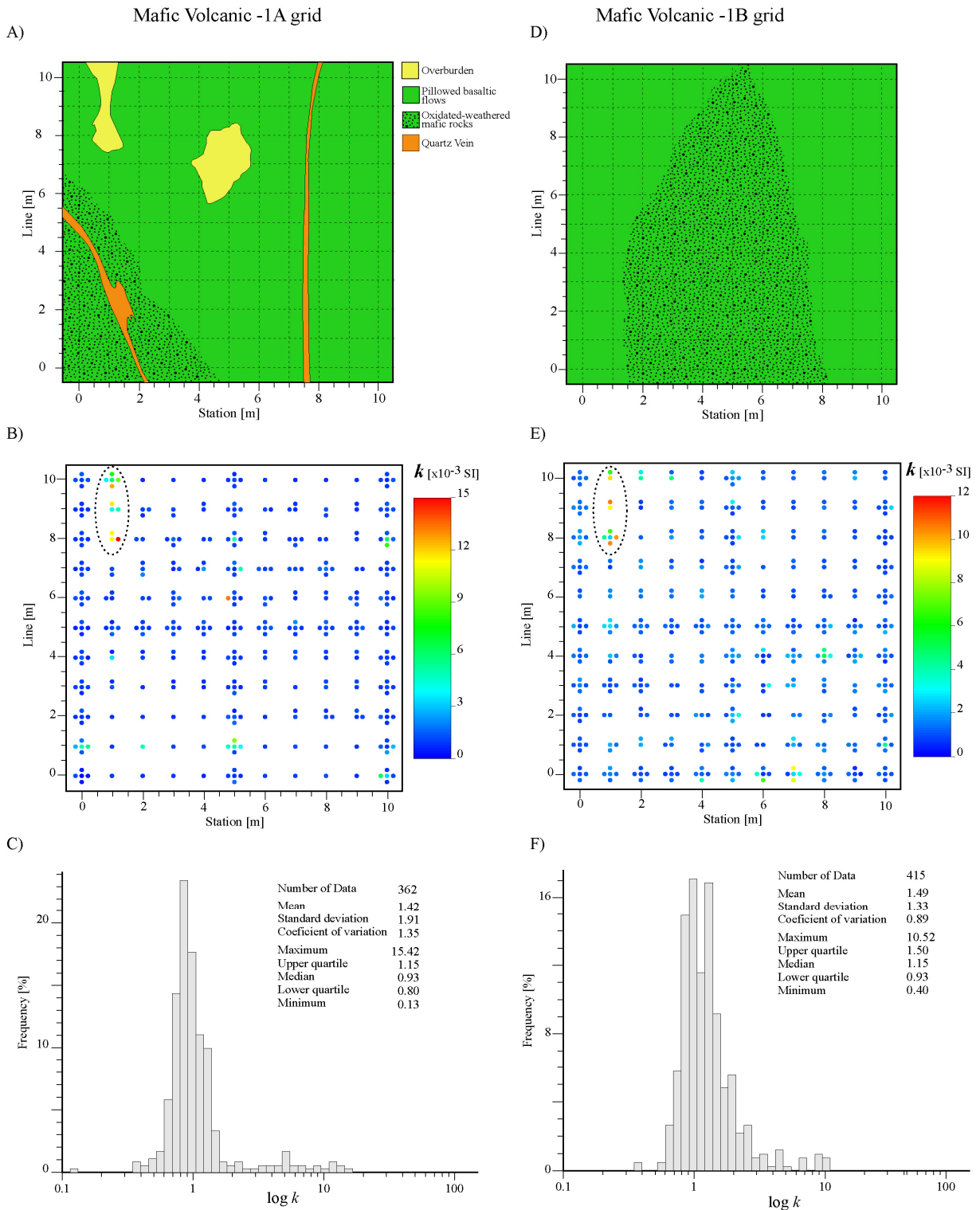
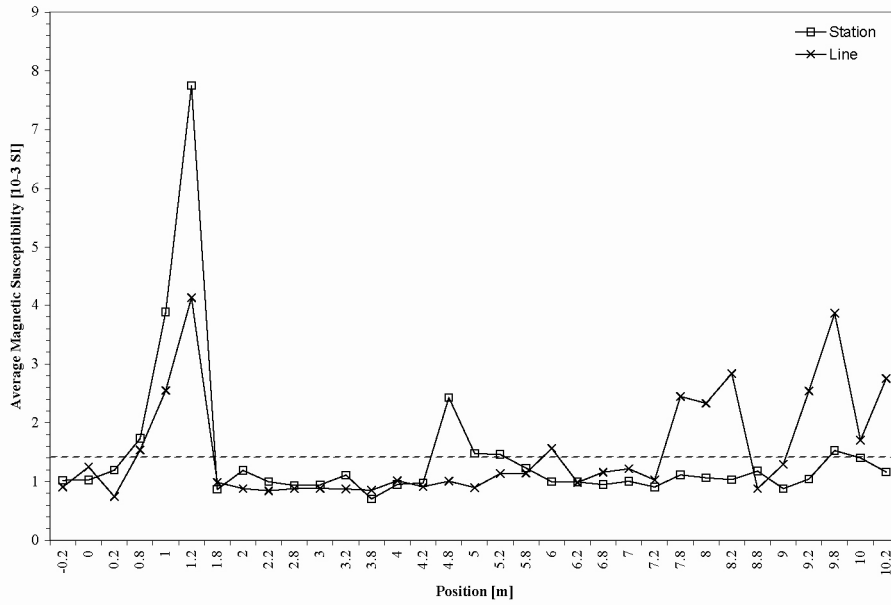


Figure 4.7. Mafic Volcanic site 10 m grids, MV-1A (left) and MV-1B (right). A), D) Geologic sketch, B), E) Spatial distribution of the point scale magnetic susceptibility data set and C), F) Frequency histogram and statistical distribution of the collected measurements.

A) Mafic Volcanic 1A



B) Mafic Volcanic 1B

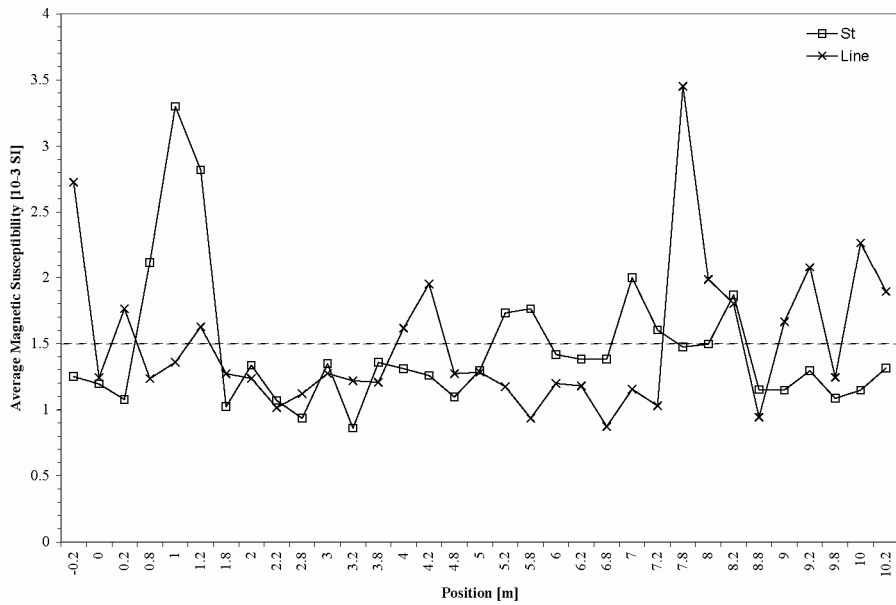


Figure 4.8. Local average magnetic susceptibility as a function of position in station and line axis. A) Mafic Volcanic 1A grid and B) Mafic Volcanic 1B grid. Dashed horizontal lines plot the global magnetic susceptibility mean for each grid.

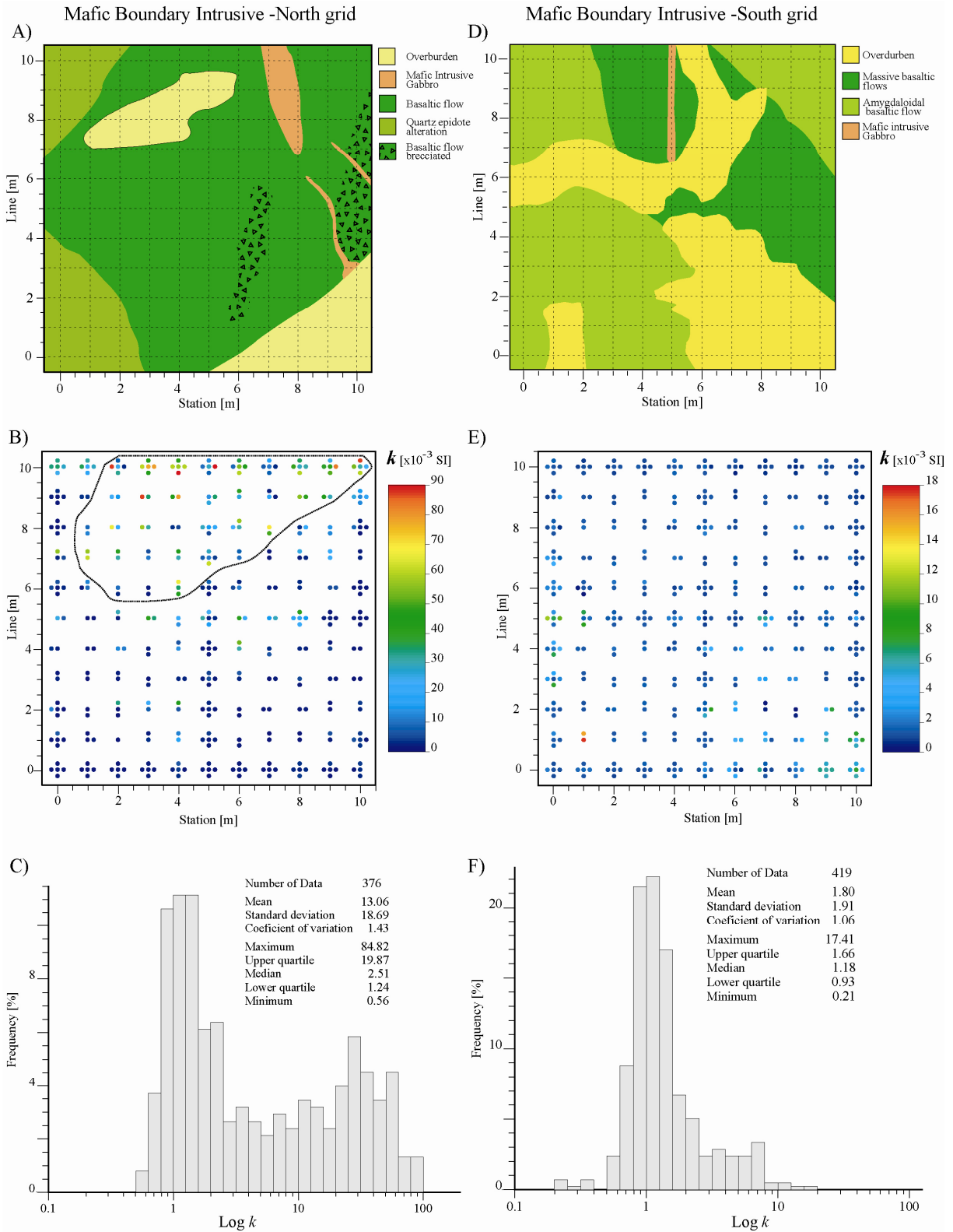
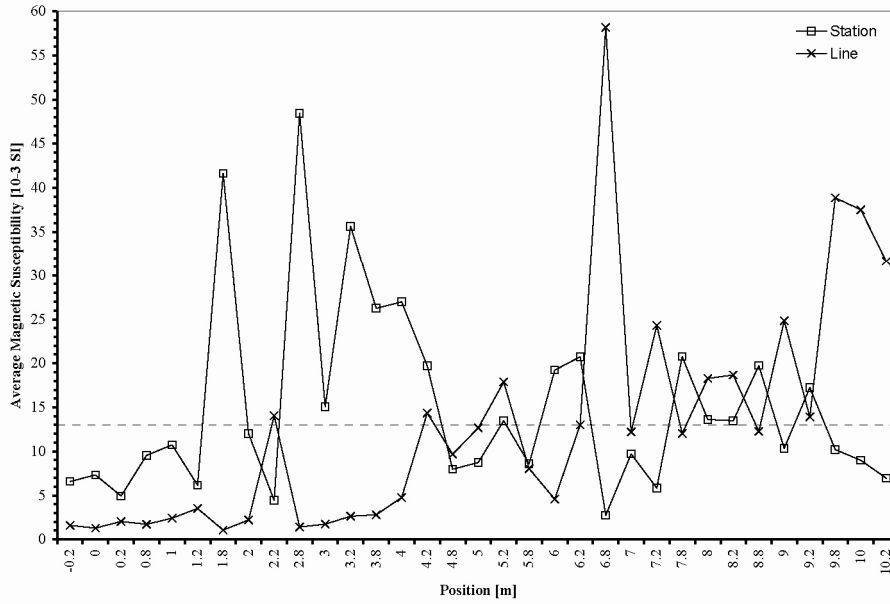


Figure 4.9. Mafic Boundary Intrusive 10 m grids, North (left), South (right). A), D) Geologic sketch, B), E) spatial distribution of the point scale magnetic susceptibility data set and C), F) frequency histogram and statistical distribution of the collected measurements.

A) Mafic Boundary Intrusive North



B) Mafic Boundary Intrusive South

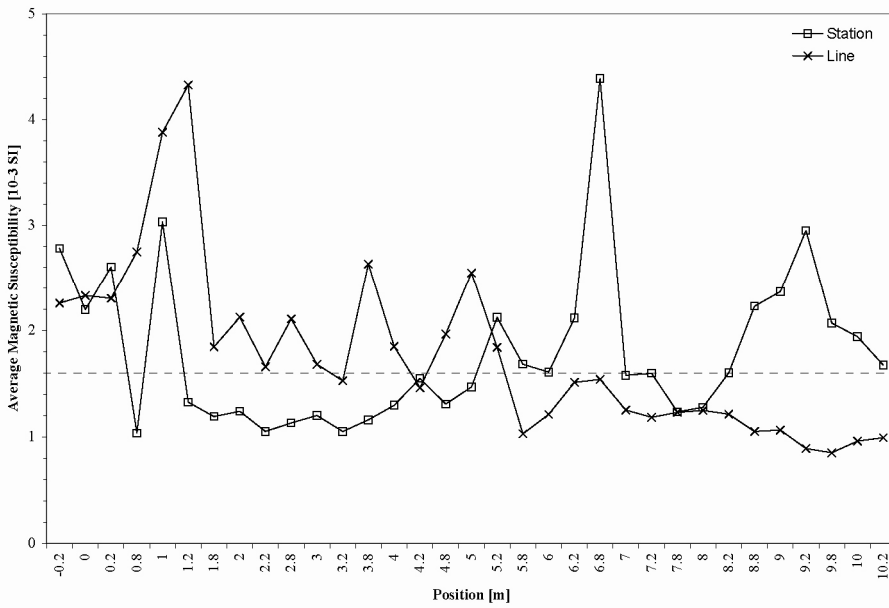


Figure 4.10. Local average magnetic susceptibility as a function of position in Station and Line axis. A) Mafic Boundary Intrusive North grid and B) Mafic Boundary Intrusive South grid. Dashed horizontal lines plot the global magnetic susceptibility average for each grid.

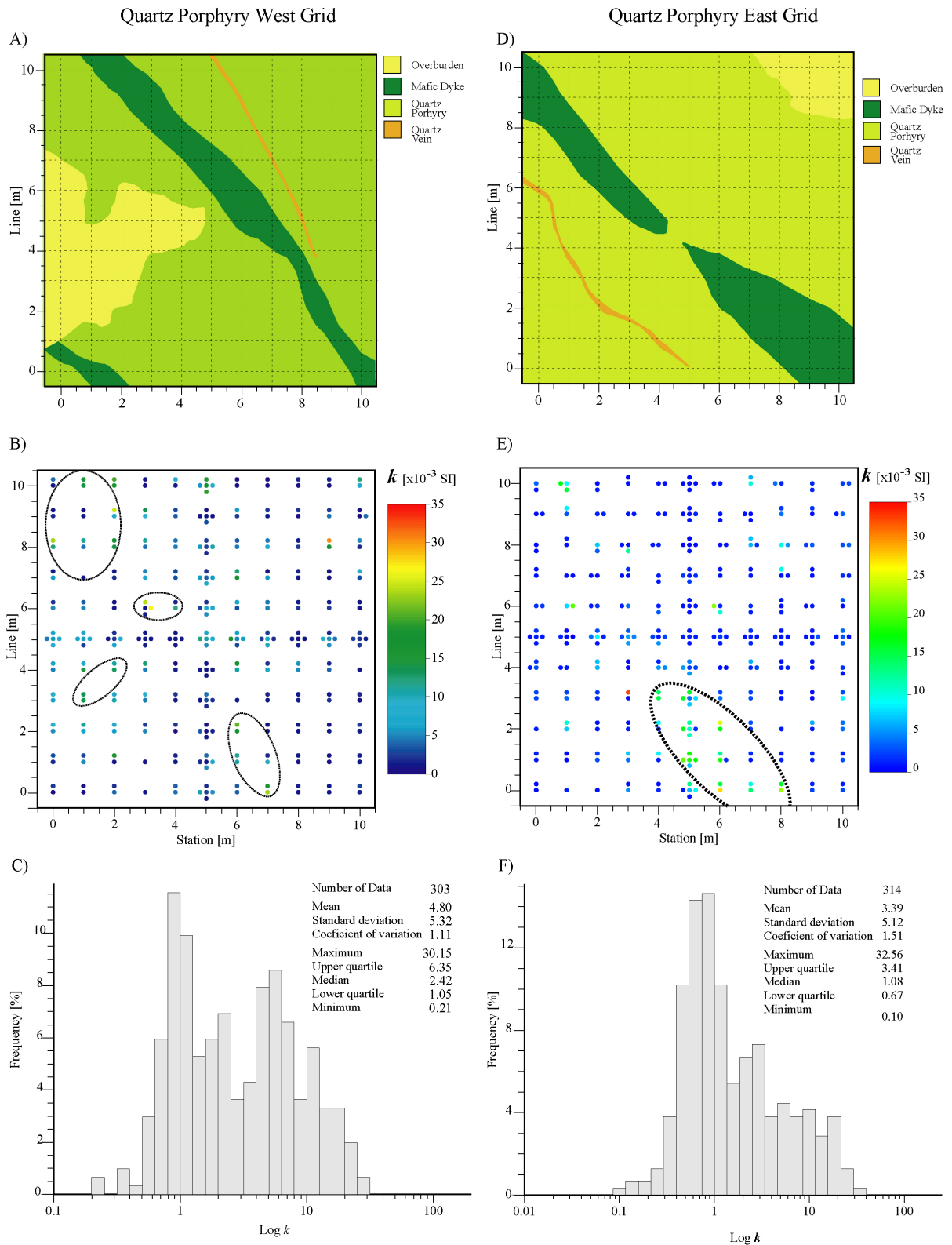
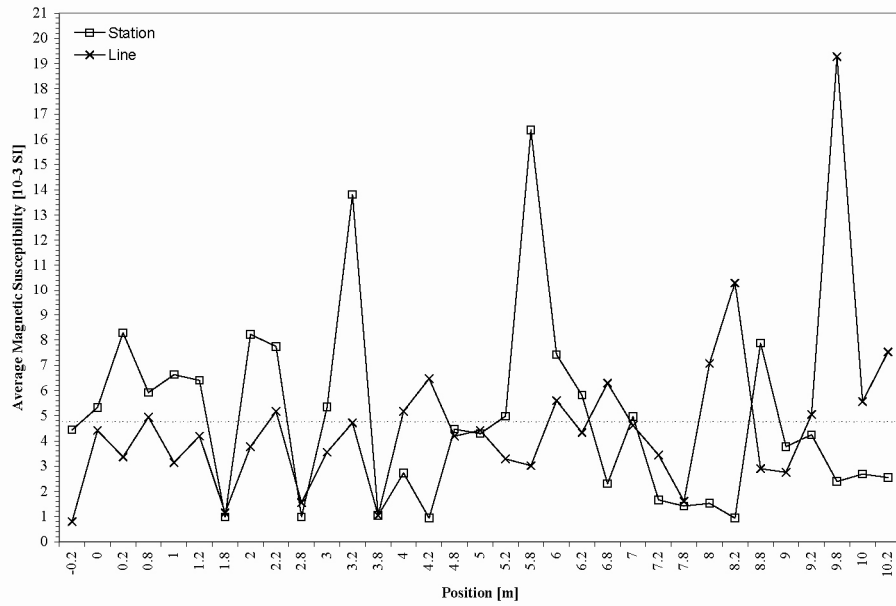


Figure 4.11. Quartz Porphyry 10 m grids, QP-West (left) and QP-East (right). A), D) Geologic sketch. B), E) Point scale magnetic susceptibility measurements spatial distribution and C), F) Frequency histogram and statistical distribution of the collected measurements.

A) Quartz Porphyry West



B) Quartz Porphyry East

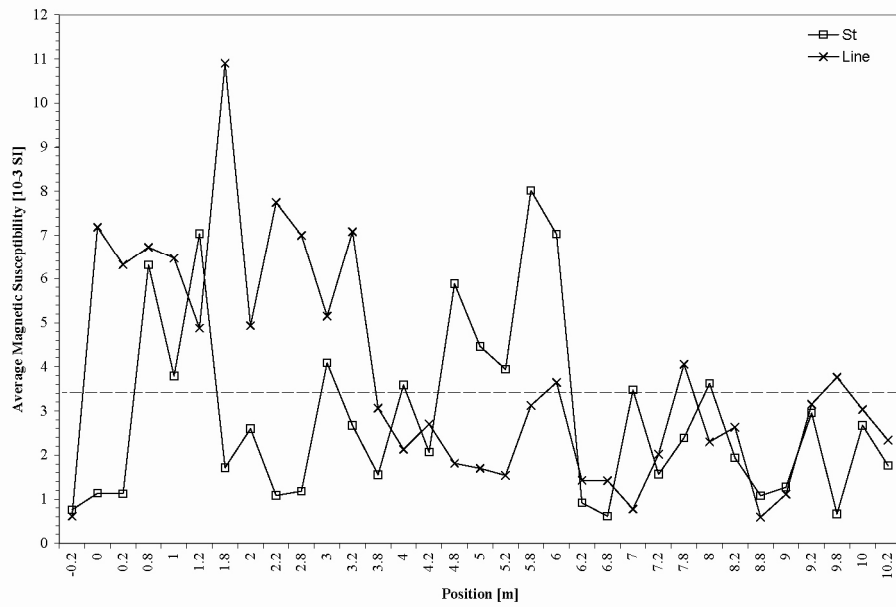


Figure 4.12. Local average of magnetic susceptibility as a function of position along the station and line axis. A) Quartz Porphyry West grid and B) Quartz Porphyry West grid. Dashed horizontal line plot the global magnetic susceptibility average for each grid.

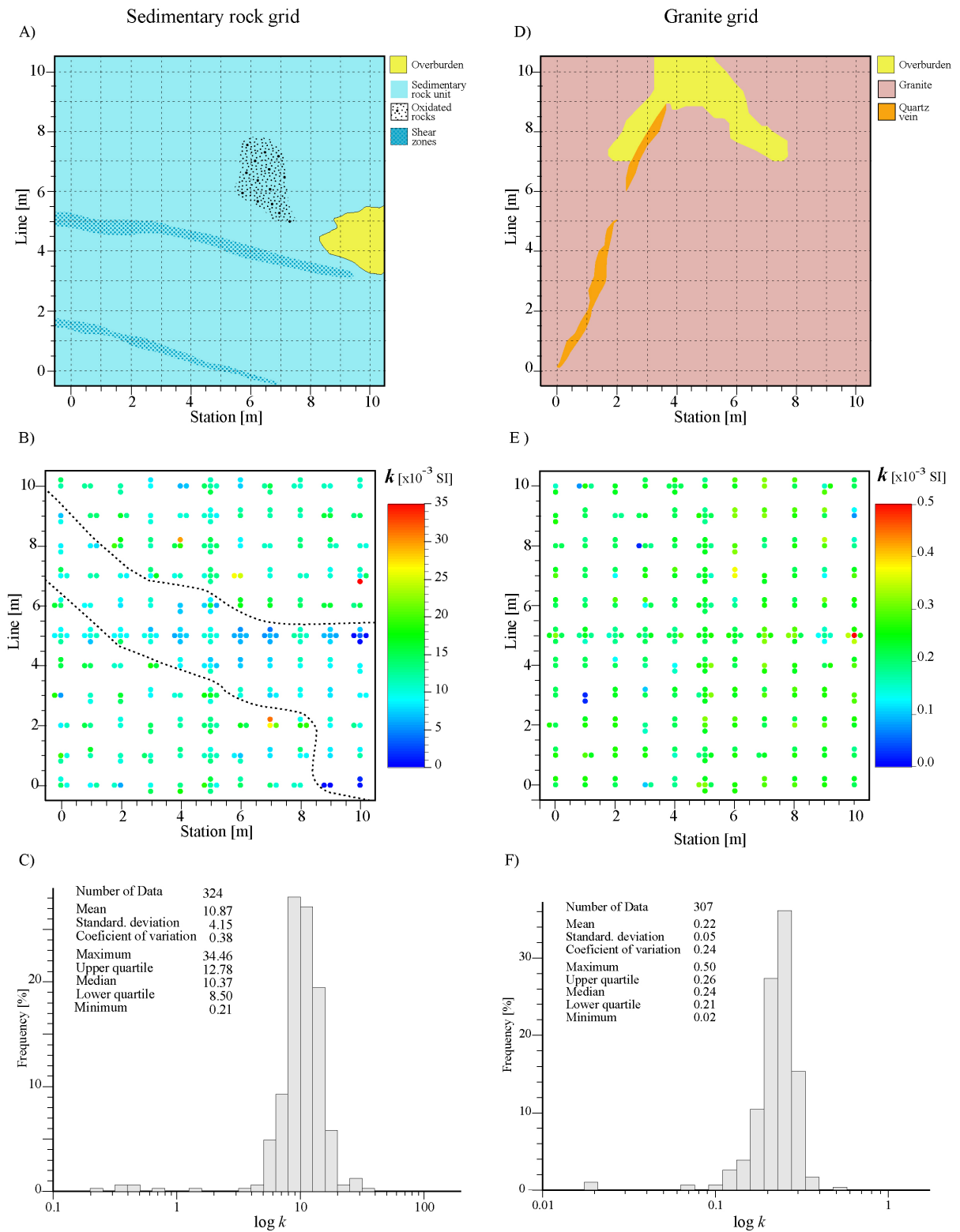
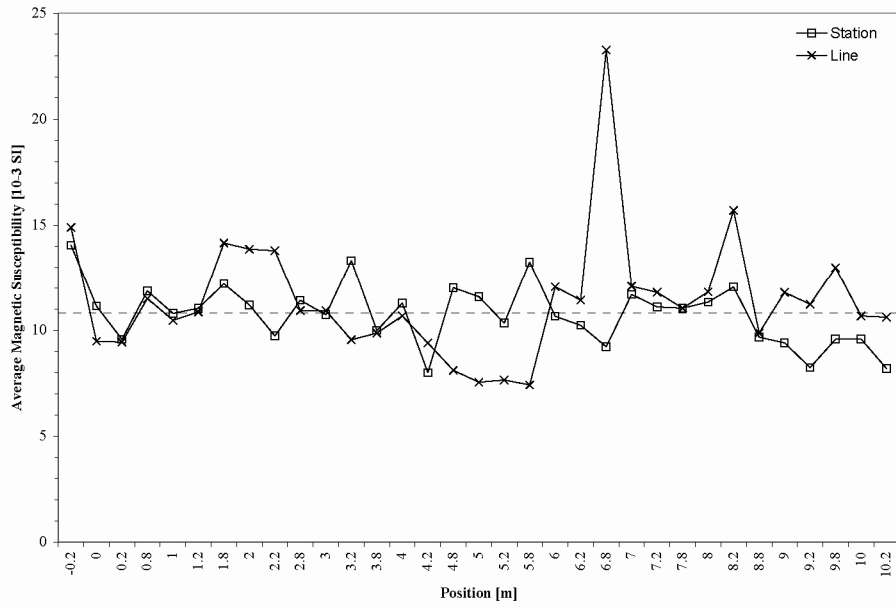


Figure 4.13. Sedimentary Rocks (left) and Granite (right) 10 m grids. A), D) Geologic sketch. B), E) Point scale magnetic susceptibility measurements spatial distribution and C), F) Frequency histogram and statistical distribution of the point scale collected measurements.

A) Sedimentary Rocks



B) Granite

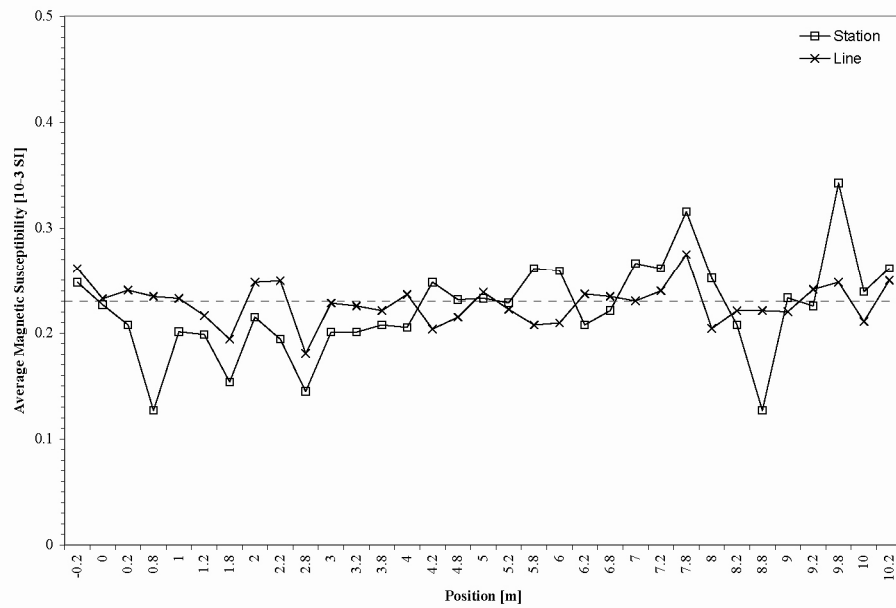


Figure 4.14. Average magnetic susceptibility as a function of position in station and line for A) Sedimentary Rock grid and B) Granite grid. Dashed horizontal line plot the global magnetic susceptibility average.

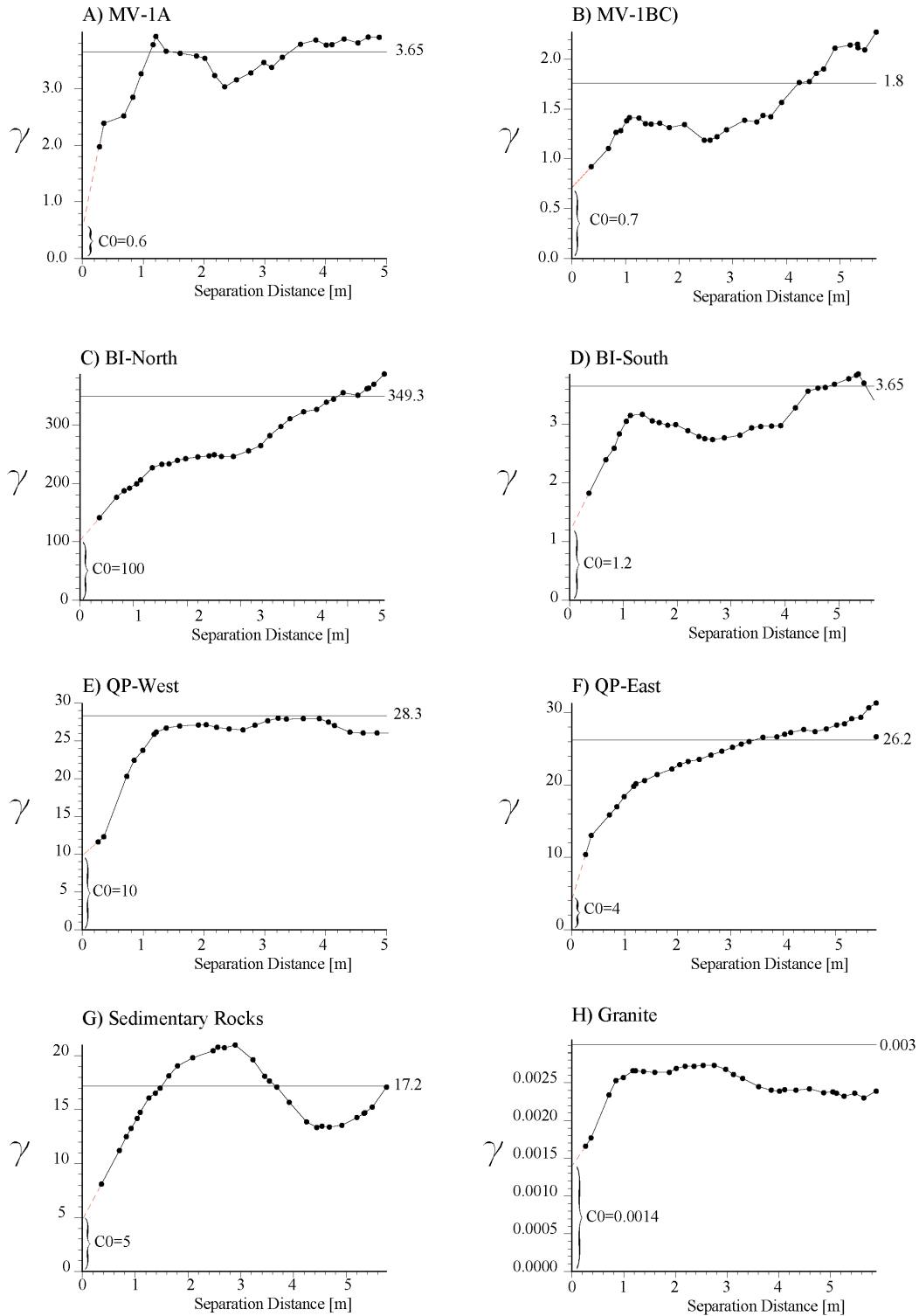


Figure 4.15. Isotropic Magnetic Susceptibility Experimental Variograms calculated using the point scale measurements collected at 10 m grids. A) Mafic Volcanics 1A, B) Mafic Volcanics 1B, C) Mafic Boundary Intrusive North, D) Mafic Boundary Intrusive South, E) Quartz Porphyry West, F) Quartz Porphyry East, G) Sedimentary Rocks and H) Granite. The sill/variance values are obtained from the statistical summary (Table 4.1), nugget effect (C_0) are displayed along with range distances.

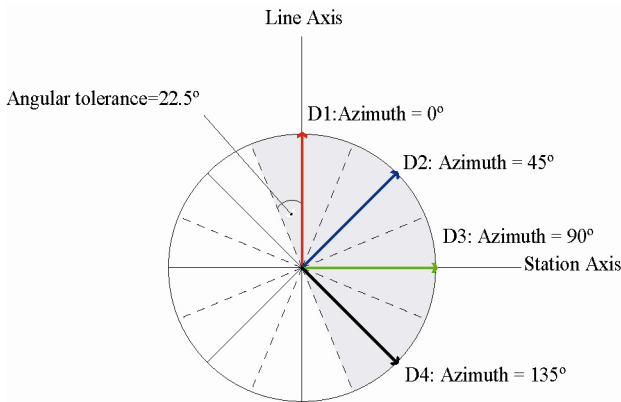
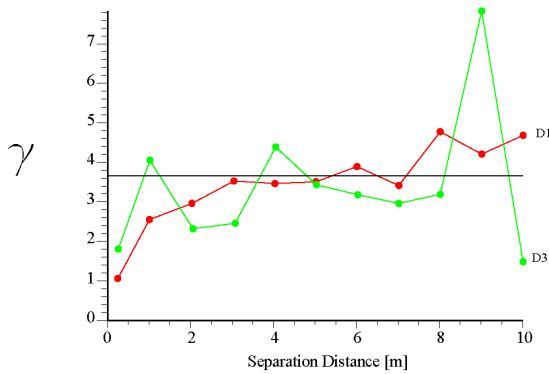
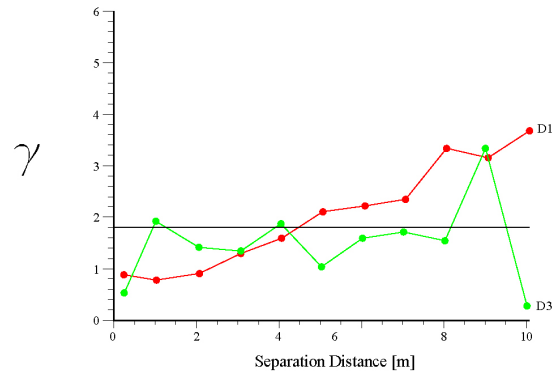


Figure 4.16. Cartoon illustrating the relation between the directional experimental variograms and the grid coordinate system. Also is shown the angular tolerance used and the shaded area covered by D1 to D4 along with the angular tolerances.

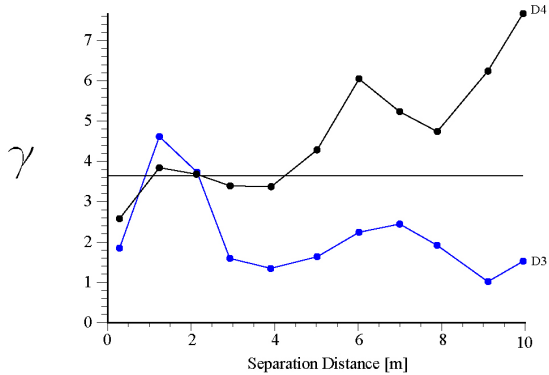
A) MV-1A



C) MV-1B



B) MV-1A



D) MV-1B

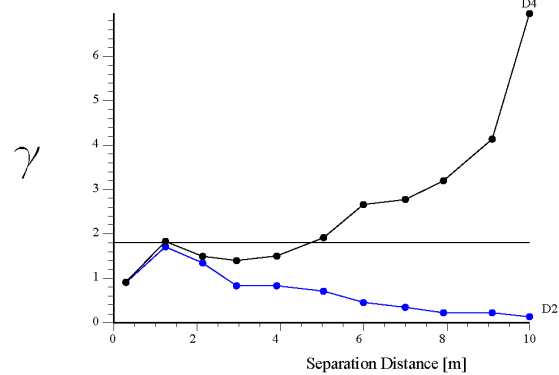


Figure 4.17. Directional point scale magnetic susceptibility experimental variograms for A) MV-1A at D1 and D3, B) MV-1A at D2 and D4, C) MV-1B at D1 and D3 and D) MV-1B at D2 and D4. Spatial orientations as indicated in Fig 4.16, solid horizontal line at the variance value for each grid (Table 4.1).

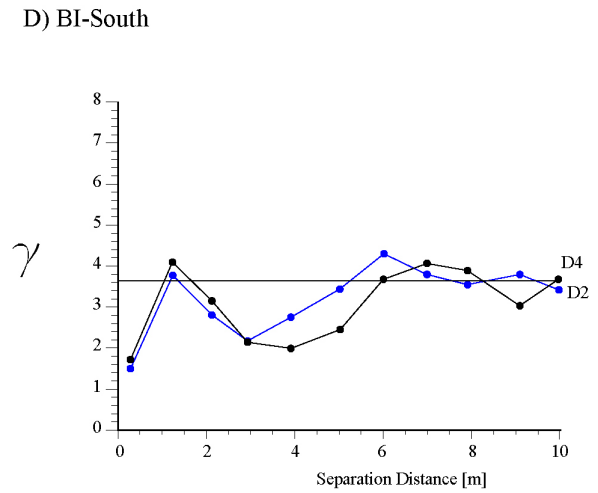
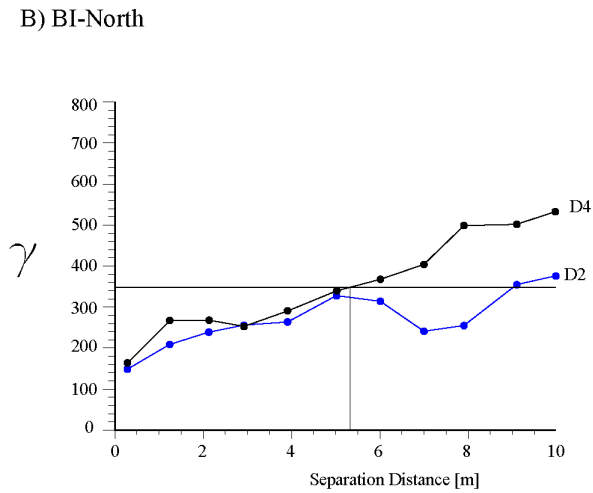
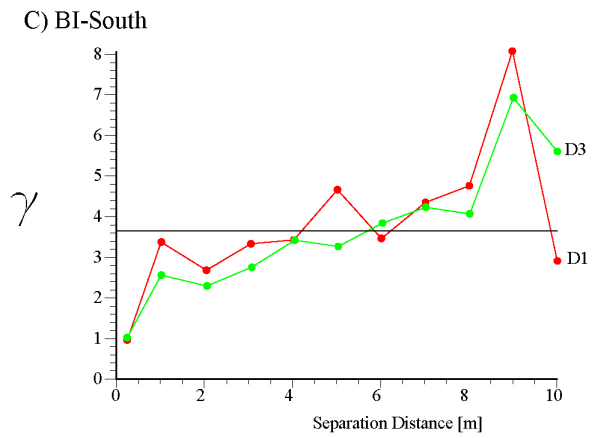
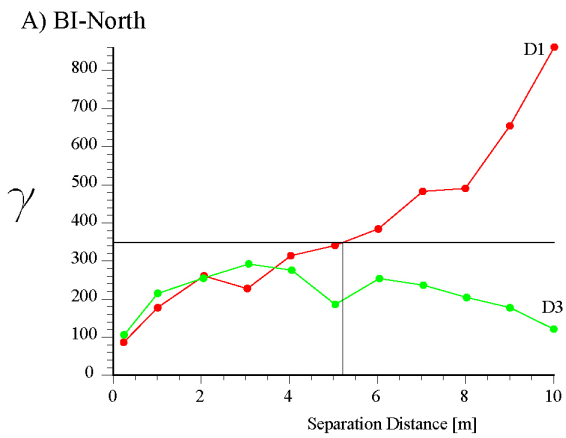
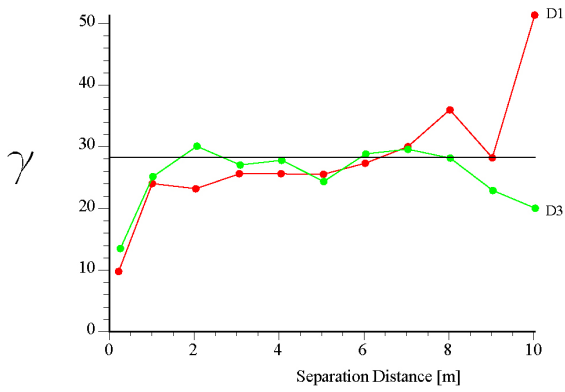
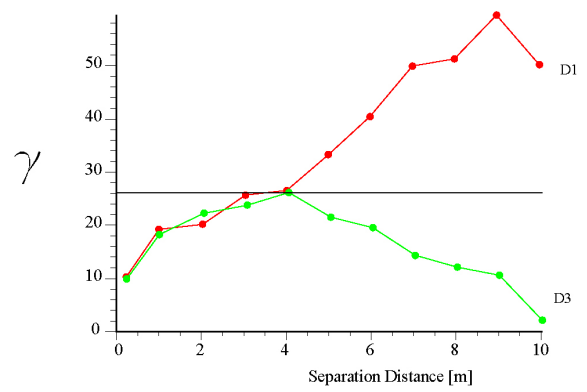


Figure 4.18. Directional point scale magnetic susceptibility experimental variograms for A) BI-North at D1 and D3, B) BI-North at D2 and D4, C) BI-South at D1 and D3 and D) BI-South at D2 and D4. Spatial orientations as indicated in Fig 4.16.

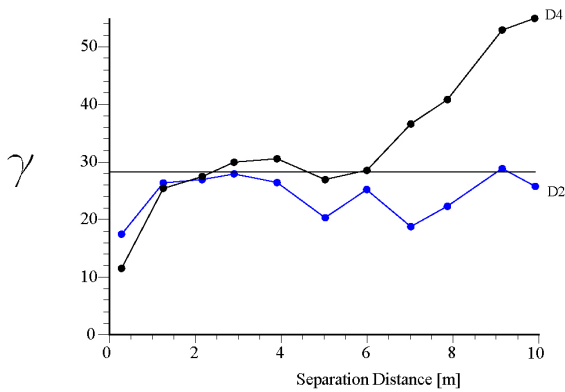
A) QP-West



C) QP-East



B) QP-West



D) QP-East

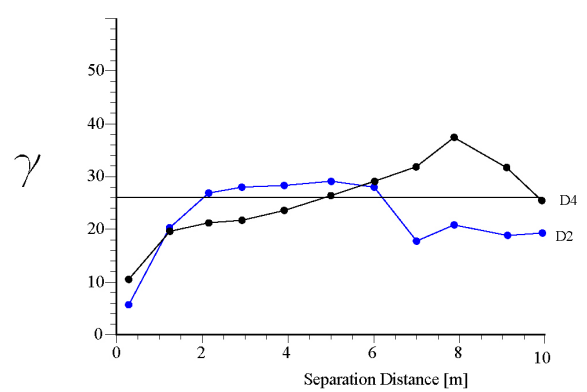
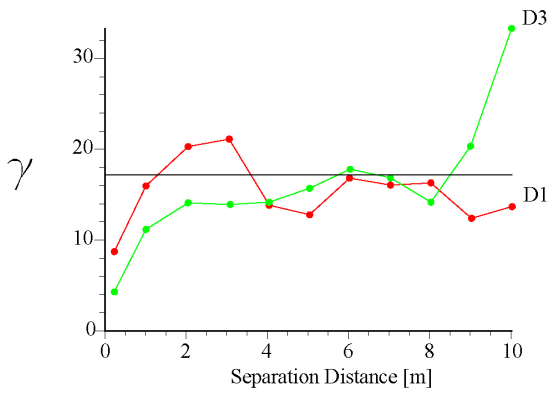
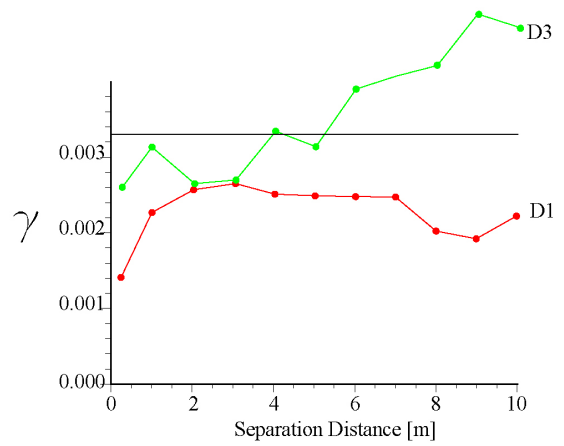


Figure 4.19. Directional point scale magnetic susceptibility experimental variograms for A) QP-West at D1 and D3, B) QP-West at D2 and D4, C) QP-East at D1 and D3 and D) QP-East at D2 and D4. Variogram spatial orientations as indicated in Fig 4.16.

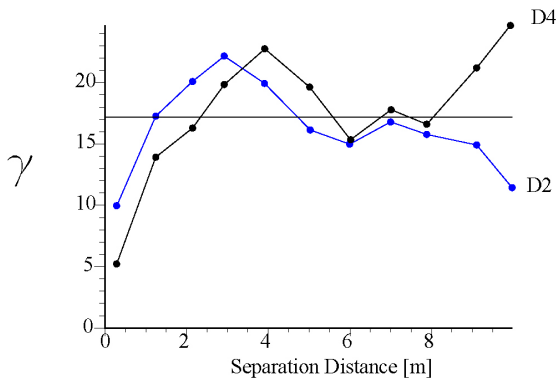
A) Sedimentary Rocks



C) Granite



B) Sedimentary rocks



D) Granite

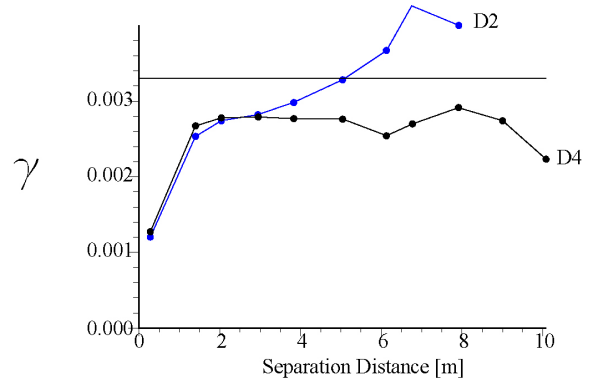


Figure 4.20. Directional point scale magnetic susceptibility experimental variograms for A) Sedimentary Rocks at D1 and D3, B) Sedimentary Rocks at D2 and D4, C) Granite at D1 and D3 and D) Granite at D2 and D4. Variogram spatial orientations as indicated in Fig 4.16.

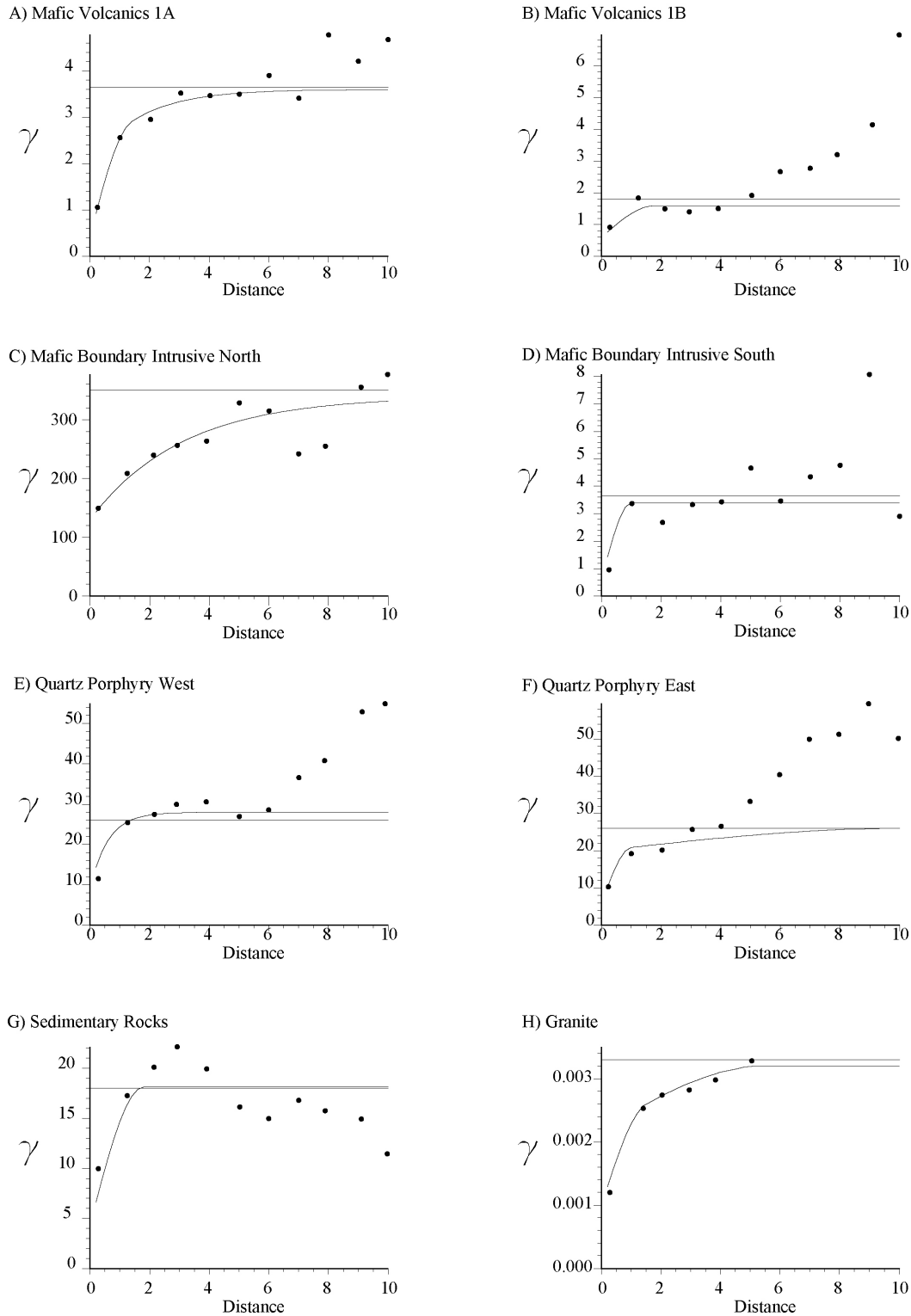


Figure 4.21. Isotropic variogram models (solid lines) fitted to the experimental variograms (dots) calculated for the magnetic susceptibility measurements at the point scale. A) Mafic Volcanic 1A, B) Mafic Volcanics 1B, C) Mafic Boundary Intrusive North, D) Mafic Boundary Intrusive South, E) Quartz Porphyry West, F) Quartz Porphyry East, G) Sedimentary Rocks and H) Granite. Horizontal line at the variance value of each grid (Table 4.1).

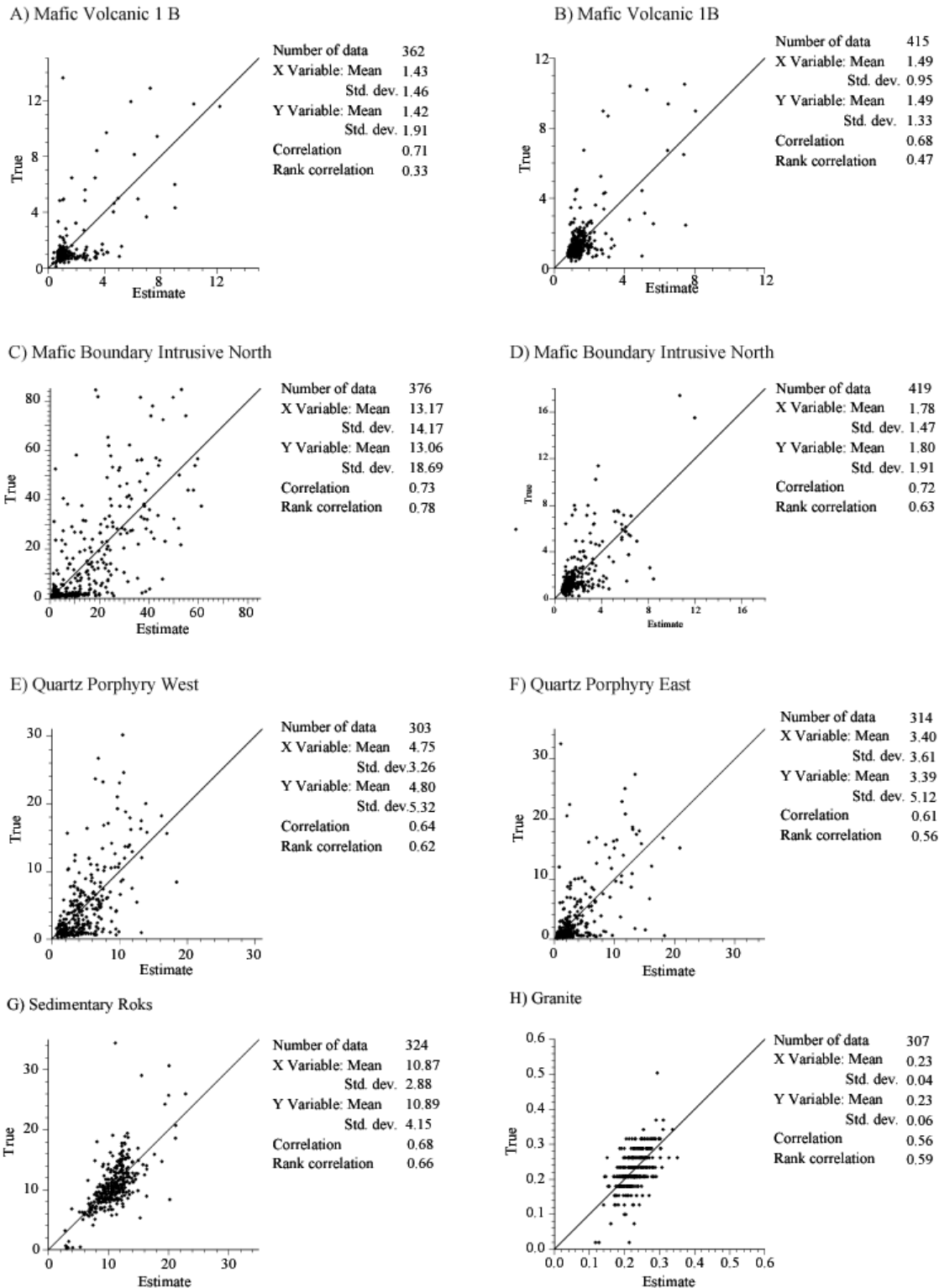
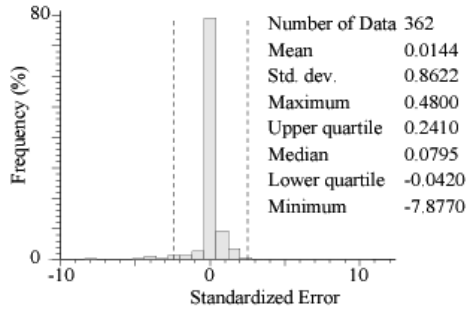
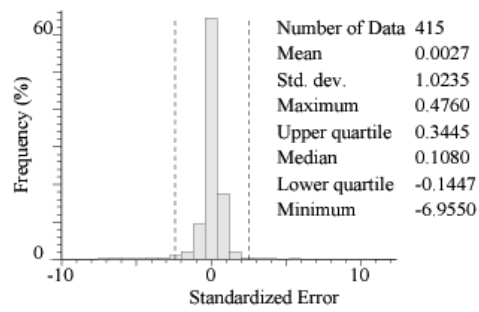


Figure 4.22. Variogram modeling cross validation results, presented as True versus Estimated magnetic susceptibility scatter plots. The quality of the fitted model is quantified by the correlation factor, which ideally should be close to 1. A) Mafic Volcanic 1A, B) Mafic Volcanics 1B, C) Mafic Boundary Intrusive North, D) Mafic Boundary Intrusive South, E) Quartz Porphyry West, F) Quartz Porphyry East, G) Sedimentary Rocks and H) Granite.

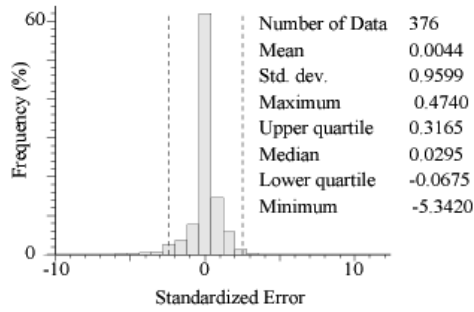
A) Mafic volcanics IA



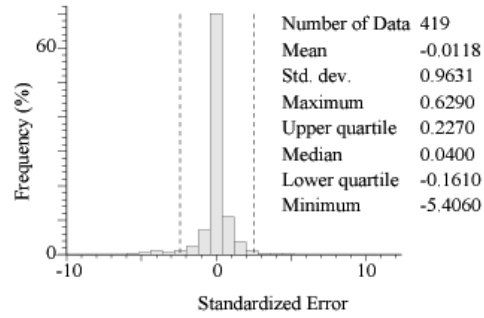
B) Mafic volcanics IB



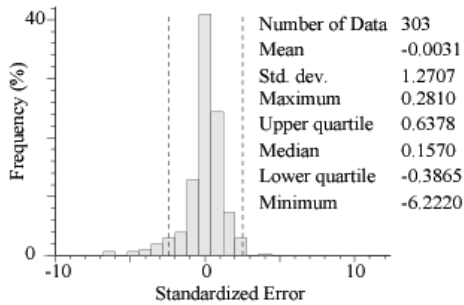
C) Mafic Boundary Intrusive North



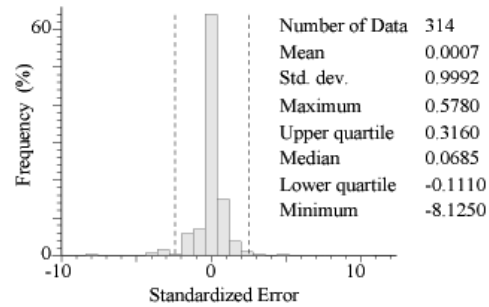
D) Mafic Boundary Intrusive South



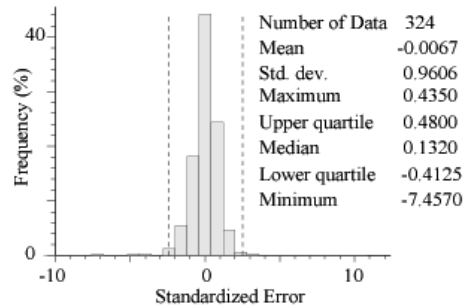
E) Quartz Porphyry West



F) Quartz Porphyry East



G) Sedimentary Rocks



H) Granite

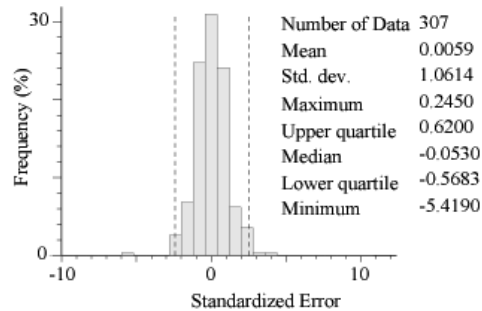
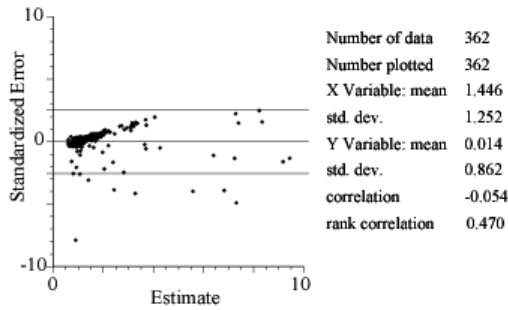
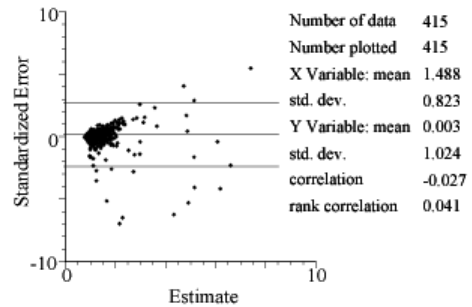


Figure 4.23. Histograms of the standardized estimation errors plotted for the analyzed grids. Vertical dotted lines located at -2.5 and 2.5 errors. In all cases the error are centered on a zero error valued consistent with unbiased estimations.

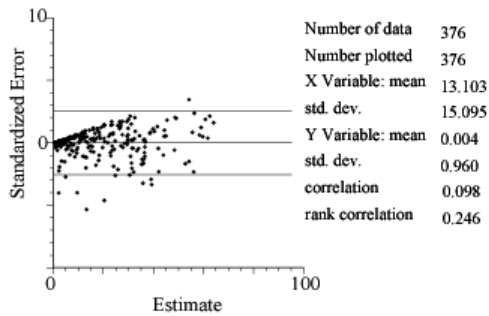
A) Mafic volcanics 1A



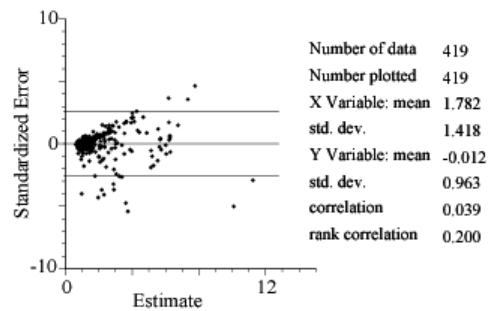
B) Mafic volcanics 1B



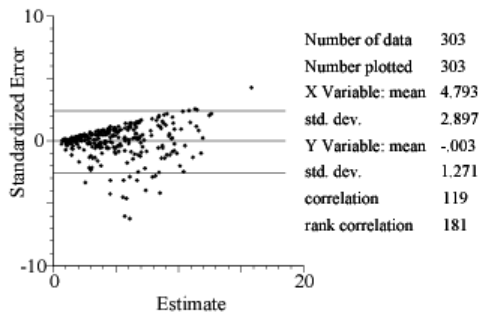
C) Mafic Boundary Intrusive North



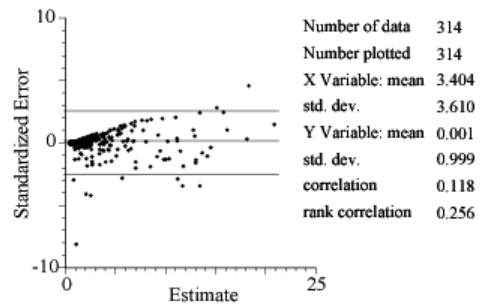
D) Mafic Boundary Intrusive South



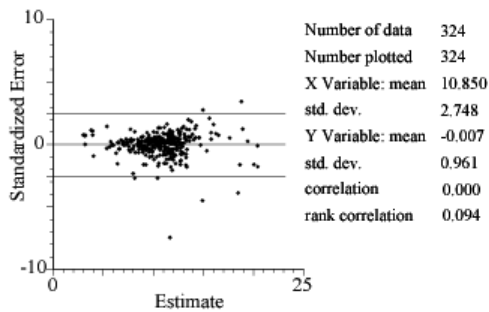
E) Quartz Porphyry West



F) Quartz Porphyry East



G) Sedimentary Rocks



H) Granite

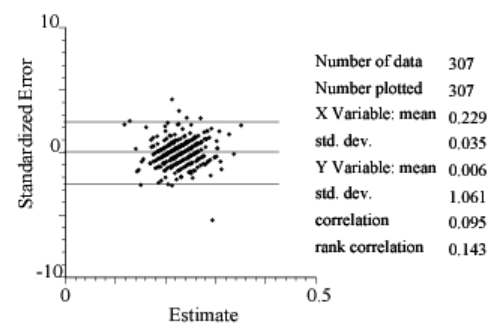


Figure 4.24. Standardized estimation error vs. estimated value. Triangular shapes of the cloud point are observed in most of the grid suggesting a proportional effect, except for the Sedimentary and Granite grids. Horizontal lines located at thresholds of -2.5 and 2.5.

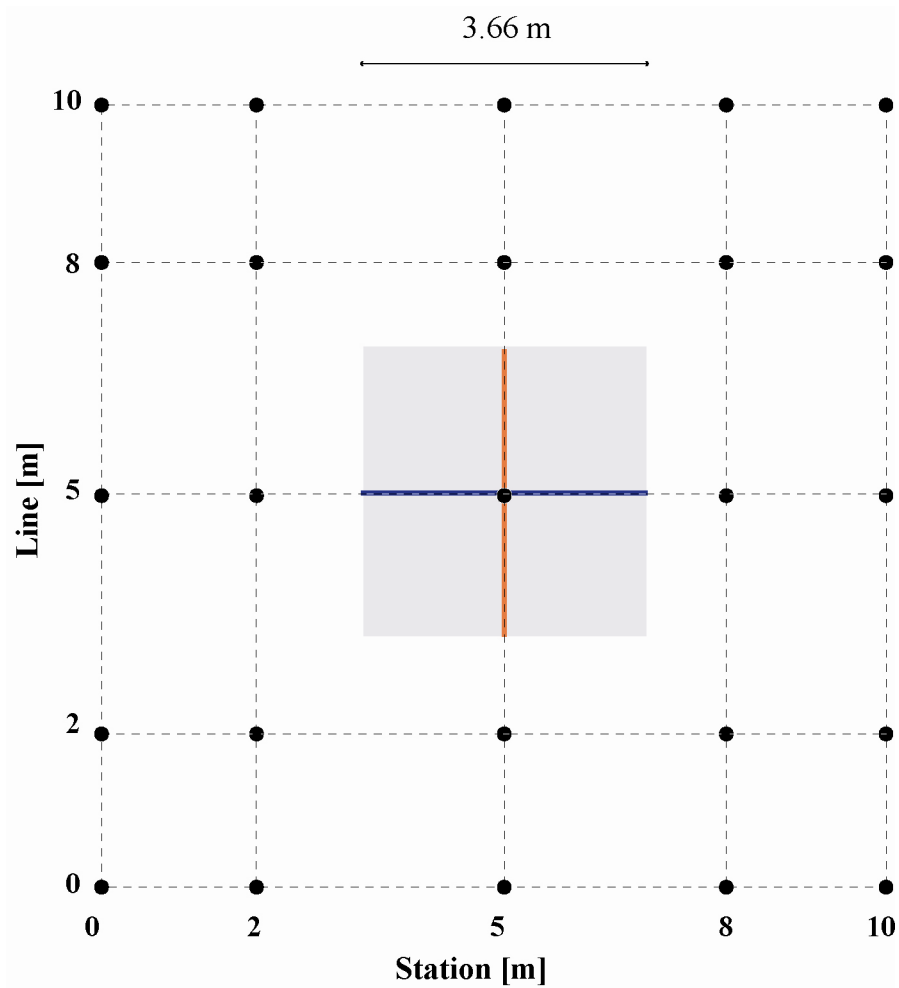


Figure 4.25. Geometric sample array for the EM-31 survey. Survey lines are located at 0, 2, 5, 8 and 10 coordinates in the Station-Line system. At each node (black bullets) EM-31 instrument is oriented parallel to both main axes as is showed by blue and red lines. Gray square represents the area ‘footprint’ (3.66 x 3.66 m) obtained with the pair of measurements.

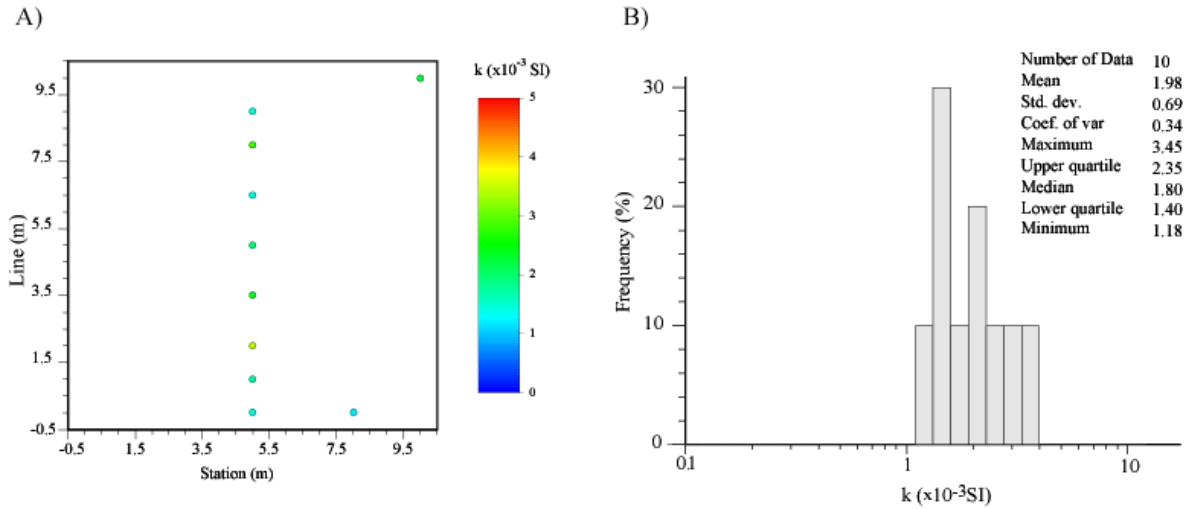


Figure 4.26. Magnetic susceptibility distribution recovered from inversion of EM-31 data at the Mafic Volcanic 1B grid. A) Spatial distribution. B) Statistical distribution.

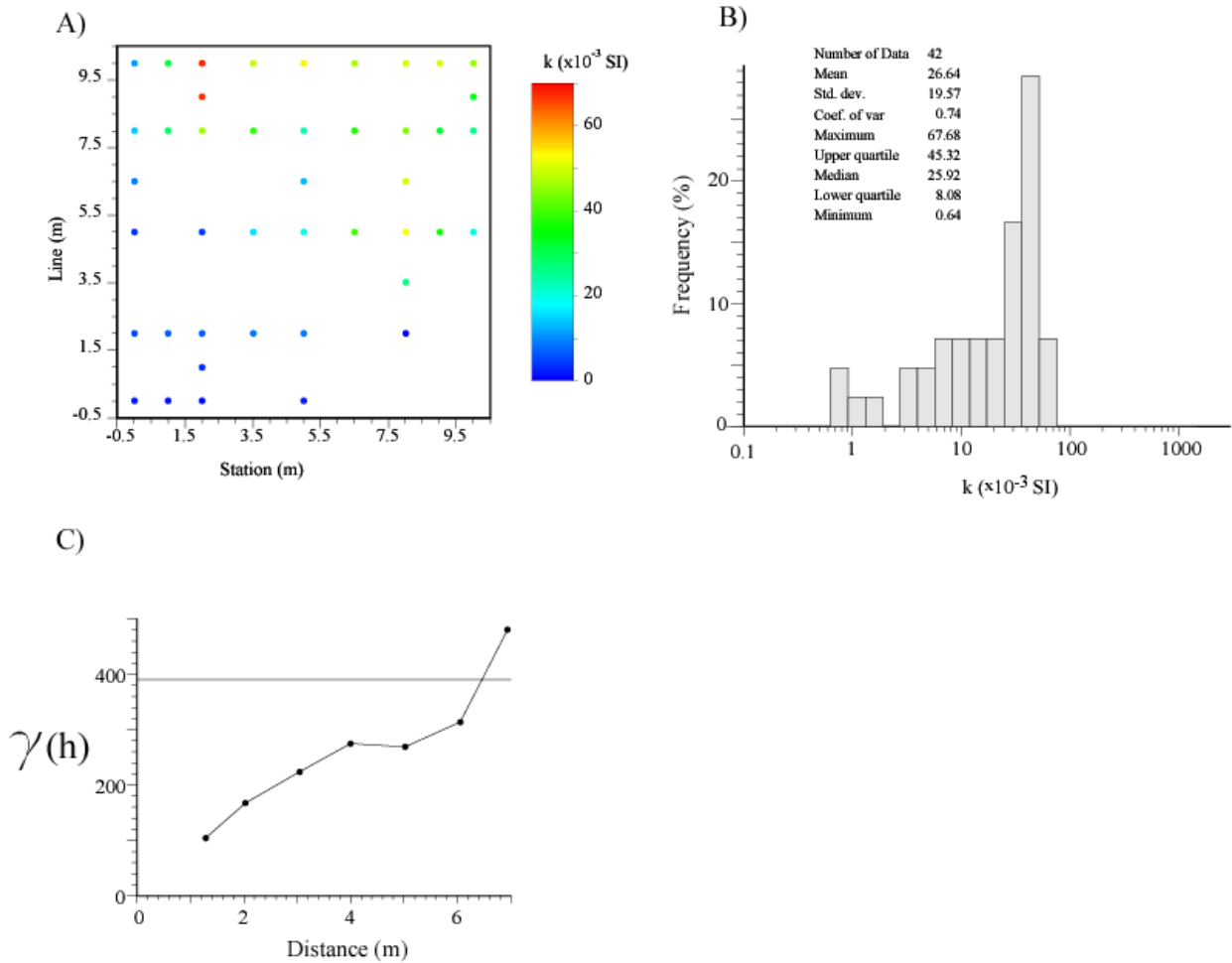


Figure 4.27. Magnetic susceptibility distribution recovered from the geophysical inversion of EM-31 data at the Mafic Boundary Intrusive North Grid. A) Spatial distribution. B) Statistical distribution. C) Experimental isotropic variogram.

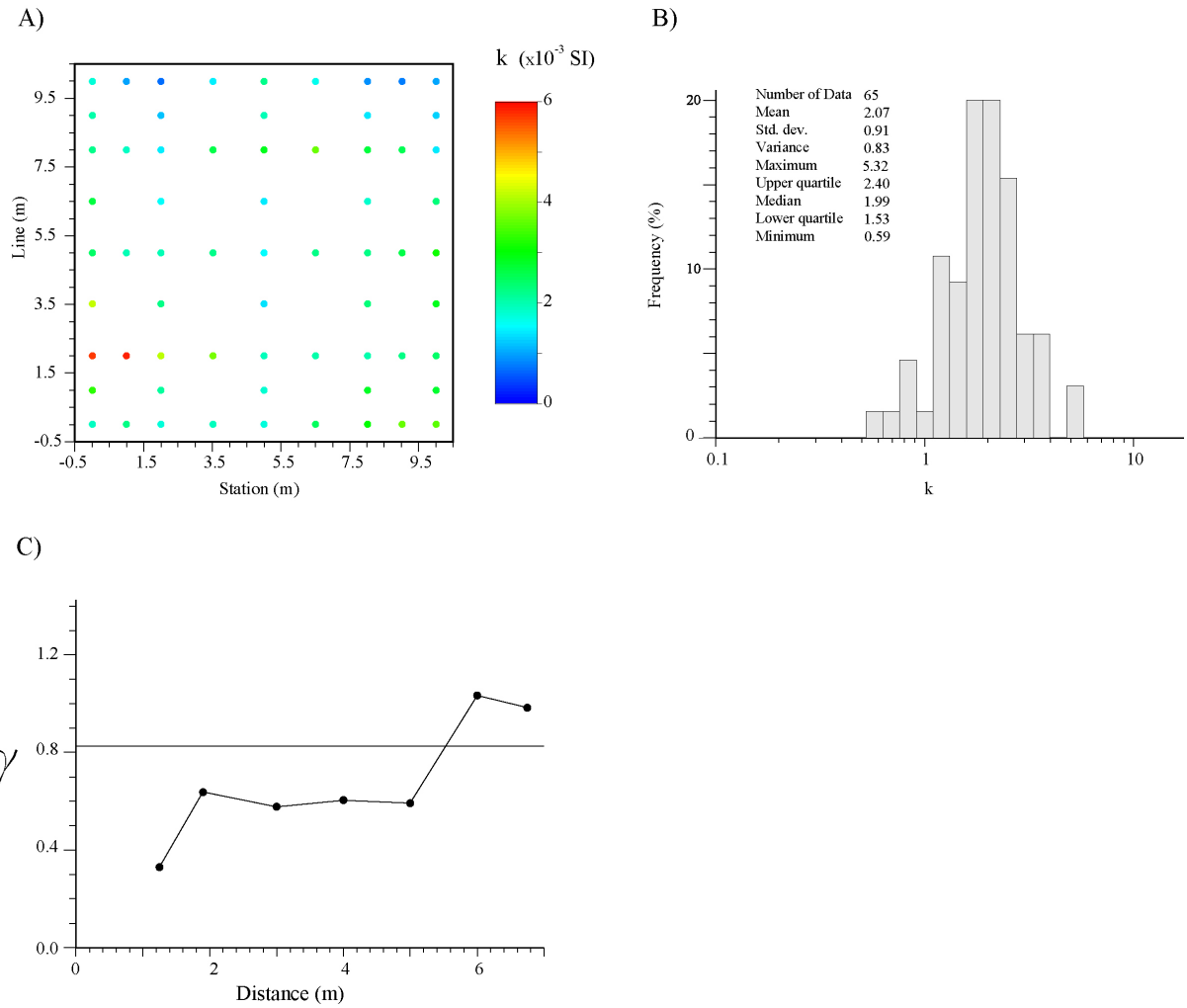


Figure 4.28. Magnetic susceptibility distribution recovered from the geophysical inversion of EM-31 data at the Mafic Boundary Intrusive South Grid. A) Spatial distribution. B) Statistical distribution. C) Experimental isotropic variogram.

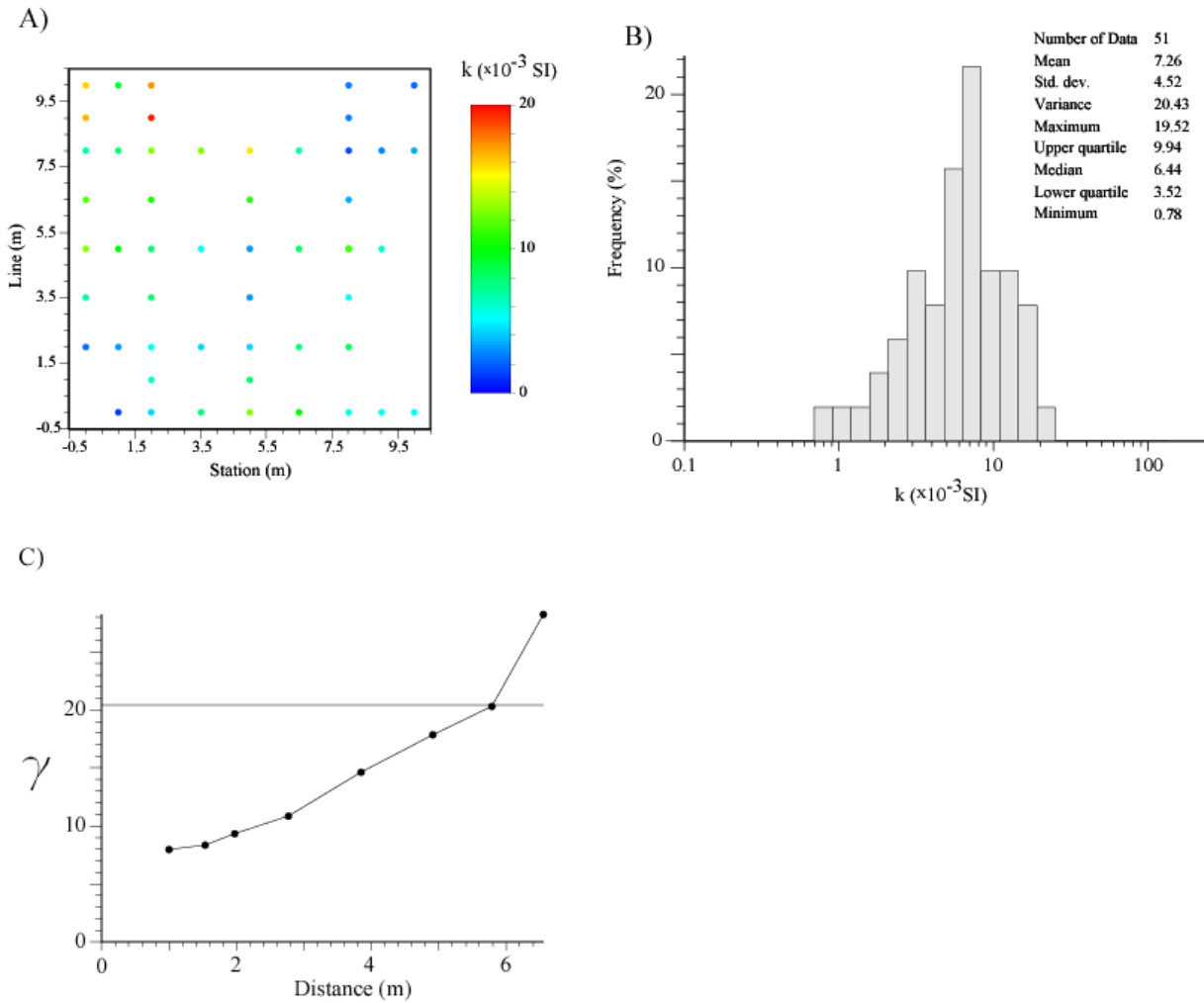


Figure 4.29. Magnetic susceptibility distribution recovered from the geophysical inversion of EM-31 data at the Quartz Porphyry West Grid. A) Spatial distribution. B) Statistical distribution. C) Experimental isotropic variogram.

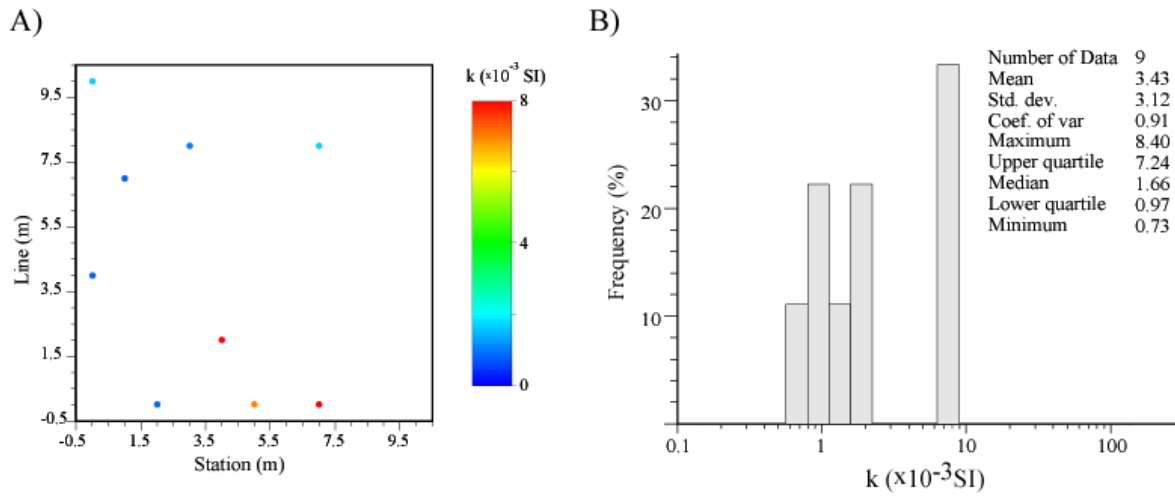


Figure 4.30. Magnetic susceptibility distribution recovered from geophysical inversion of EM-31 data at the Quartz Porphyry East Grid. A) Spatial distribution. B) Statistical distribution.

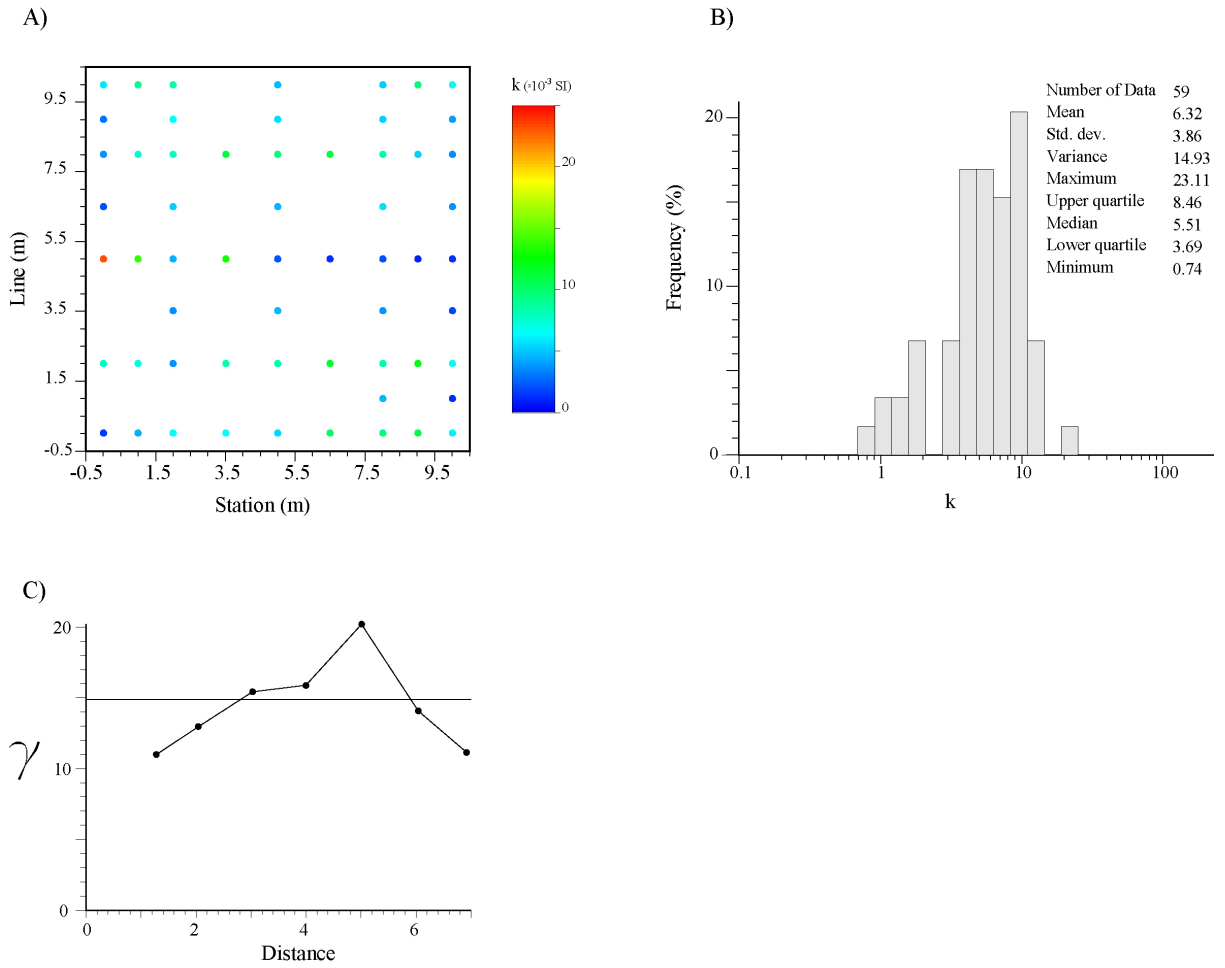
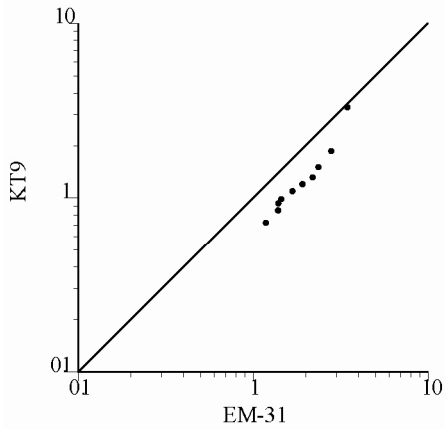
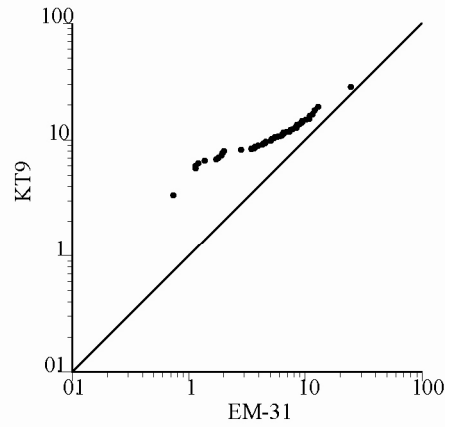


Figure 4.31. Magnetic susceptibility distribution recovered from the geophysical inversion of EM-31 data at the Sedimentary Rock site. A) Spatial distribution. B) Statistical distribution. C) Experimental isotropic variogram.

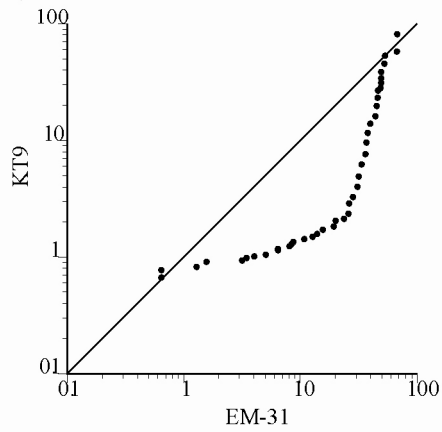
A) MV-1B



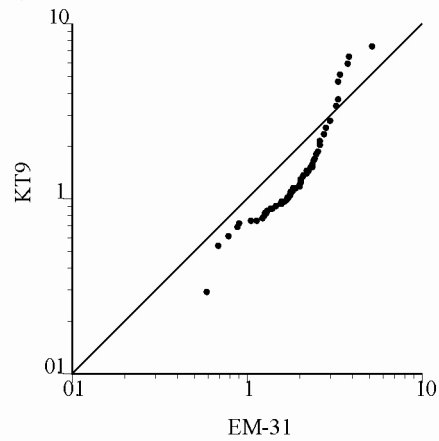
B) Sedimentary Rocks



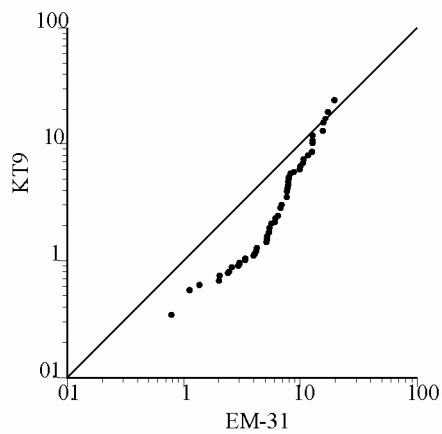
C) BI-North



D) BI-South



E) QP-West



F) QP-East

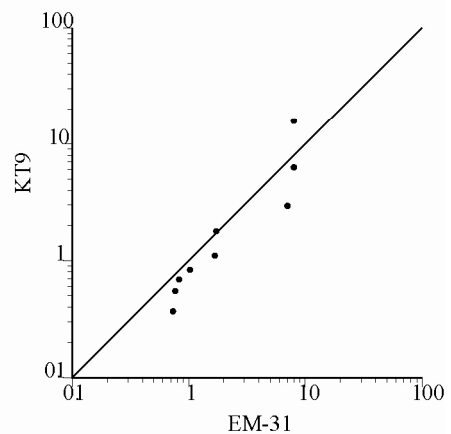


Figure 4.32. Quartile-quartile scatter plots in log-scale of magnetic susceptibility at the point scale (KT-9) versus magnetic susceptibility recovered from the geophysical inversions of the EM-31 data at A) Mafic Volcanics 1B, B) Sedimentary Rocks, C) Mafic Boundary Intrusive North, D) Mafic Boundary Intrusive South, E) Quartz Porphyry West and F) Quartz Porphyry East grids.

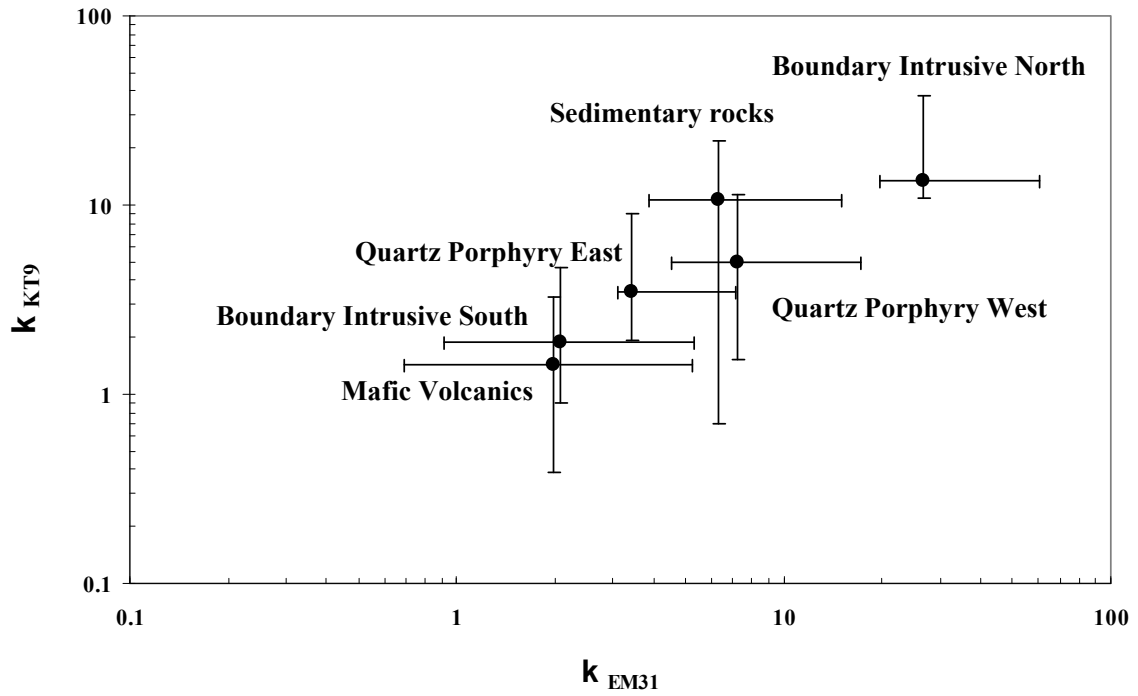


Figure 4.33. Average magnetic susceptibility at the hand sample scale (k_{KT9}) versus average magnetic susceptibility at the scale of the EM-31 (k_{EM31}) data, plotted in a logarithmic scale for the different sampled grids. A linear relation of the logarithm between both variables is observed, consistent with a power law relation. Error bars plotted at an uncertainty level of one standard deviation.

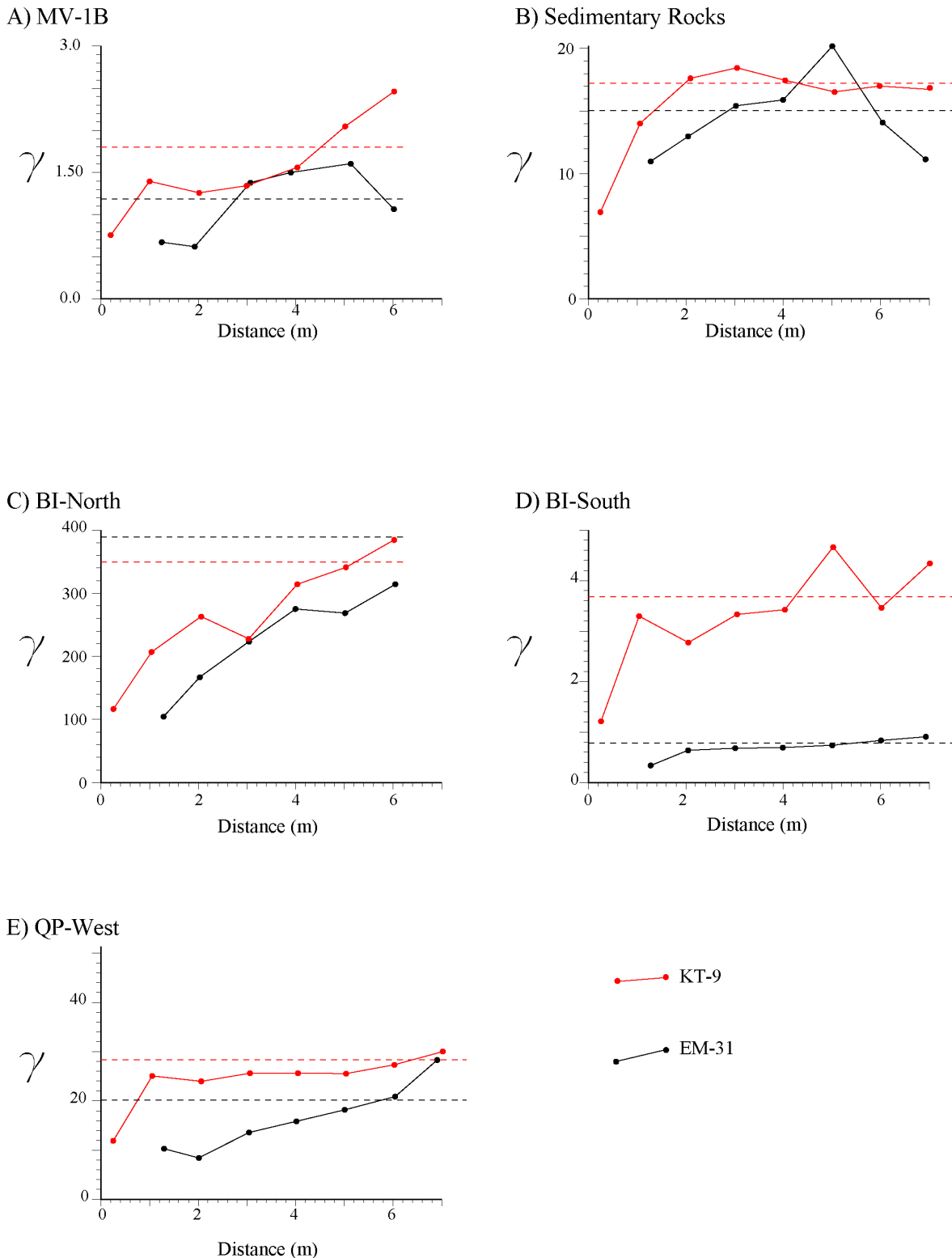


Figure 4.34. Isotropic experimental variogram of magnetic susceptibility at the point scale KT-9 (red) and EM-31 scale (black) for A) Mafic Volcanic 1B, B) Sedimentary rocks, C) Boundary Intrusive North, D) Boundary Intrusive South and E) Quartz Porphyry West. Dashed line plotted at the variance calculated for each scale and grid (as in Table 4.4).

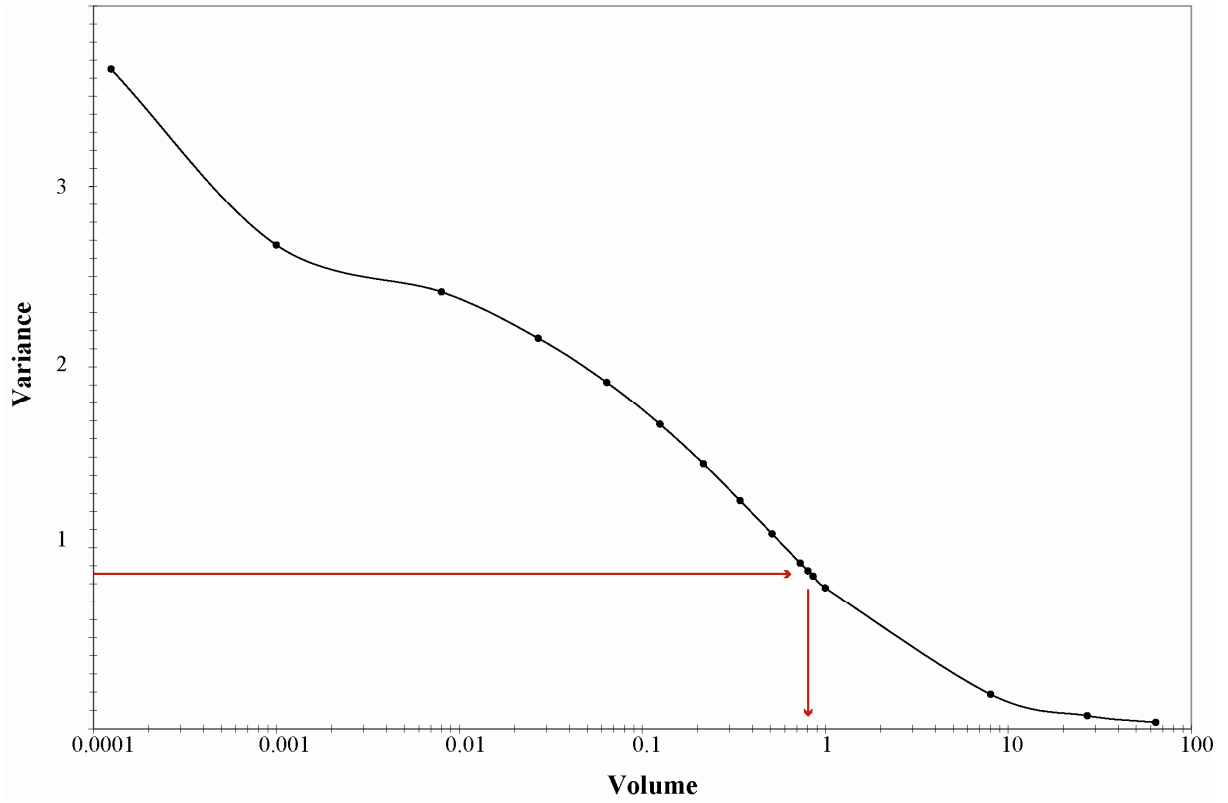


Figure 4.35. Modeled curve of magnetic susceptibility variance, as a function of the sampled volume at the Boundary Intrusive South grid. Curve points calculated using the geostatistics scaling relation. For a magnetic susceptibility variance of 0.83, the associated sampled volume is 0.8 m³ approximately.

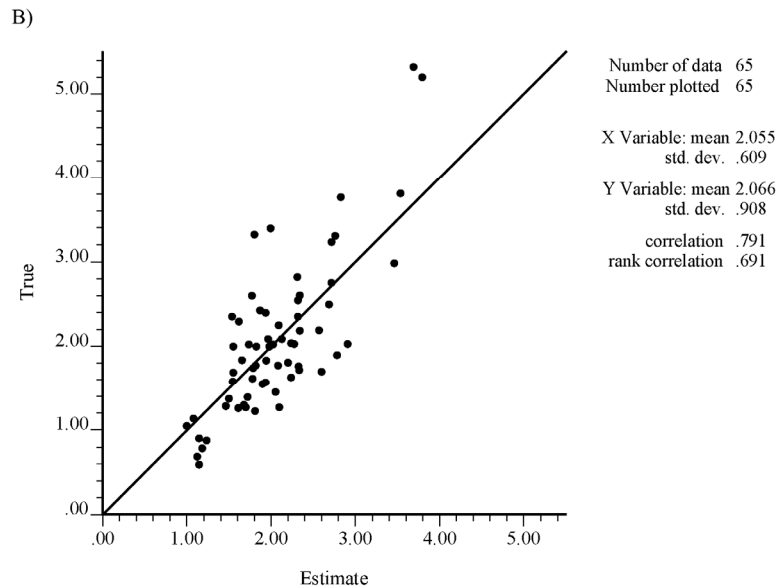
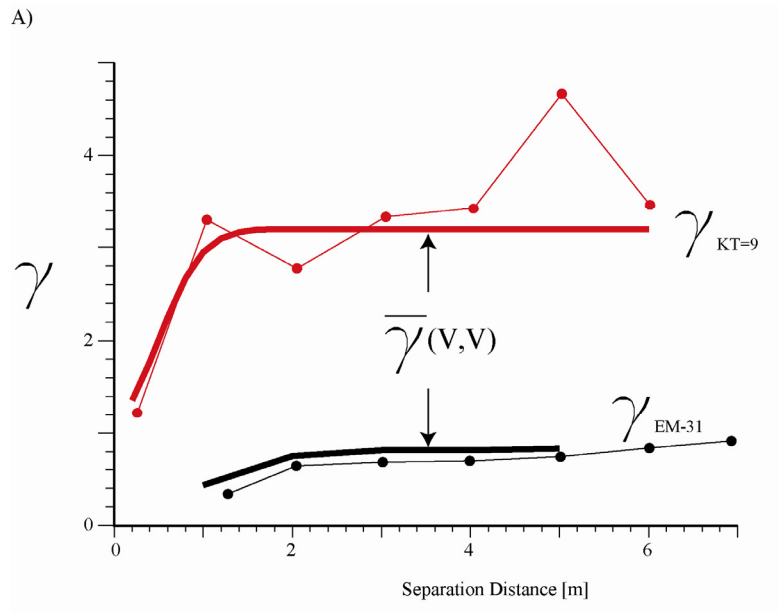


Figure 4.36. A) Scaling of experimental and modeled isotropic variograms of magnetic susceptibility for the Mafic Boundary Intrusive South grid. Red curves are point scale experimental (red line and dots) and model (coarse red solid line) variograms and black curves the experimental red line and dots and model (coarse black solid line) variograms at the larger scale. B) Cross validation results for the scaled variogram model. A correlation factor of 0.79 between the 'True' versus estimated magnetic susceptibility accounts for an acceptable level of matching between the model and the recovered magnetic susceptibility distribution supporting the scaling relation of the physical property.

Table 4.1. Point scale magnetic susceptibility statistics summary for the 10 m grids. Minimum, maximum and mean values in SI units scaled by a factor of 10^{-3}

Grid	Number of Data	Minimum-Maximum	Mean	Variance
Mafic Volcanic-1A	362	0.13-15.42	1.42	3.65
Mafic Volcanic-1B	415	0.4-10.52	1.49	1.77
Quartz Porphyry West	303	0.21-30.15	4.8	28.30
Quartz Porphyry East	314	0.1-32.56	3.39	26.21
Mafic Boundary Intrusive North	376	0.56-84.82	13.06	349.32
Mafic Boundary Intrusive South	419	0.21-17.41	1.8	3.65
Sedimentary Rocks	324	0.21-34.46	10.87	17.22
Granite	307	0.02-0.5	0.22	0.0025

Table 4.2 Nugget effect, relative nugget effect calculated as a variance percent, and range distance in meters from isotropic experimental variograms at each grid. nc=no calculated.

Grid	Nugget Effect (C_0)	Variance	Relative nugget effect	Range
Mafic Volcanic-1A	1.2	3.65	33	3
Mafic Volcanic-1B	0.6	1.77	34	nc
Quartz Porphyry West	8	28.30	28	1
Quartz Porphyry East	7	26.21	27	4.2
Mafic Boundary Intrusive North	85	349.32	24	nc
Mafic Boundary Intrusive South	0.6	3.65	16	4.2
Sedimentary Rocks	5	17.22	29	nc
Granite	0.0013	0.0025	52	1

Table 4.3. Variogram parameters calculated from directional variograms of magnetic susceptibility.

Grid	Directional C_0 values				Range Distance (m)				C_0 (average)
	D1	D2	D3	D4	D1	D2	D3	D4	
MV-1A	0.6	1	1	2.2	3	0.9	0.9	1	1.2
MV-1B	1	0.6	0	0.6	4.5	1.2	1	1.2	0.6
BI-North	60	80	130	130	5.1	-	-	5.2	100.0
BI-South	0	0.4	0.8	1	4.3	1.2	5.6	1	0.6
QP-West	6	16	10	6	6.2	3	1.8	2.5	9.5
QP-East	8	2	8	8	3	2	4	8	6.5
Sedimentary Rocks	6	8	2	3	1.4	1.2	5.8	2.4	4.8
Granite	0.0012	0.0008	0.0024	0.0008	-	5	4	-	0.0013

Table 4.4. Parameters for quantitative assessment of variogram cross validations.

Grid	Points estimated	Points estimated within (-2.5, 2.5) standardized error interval	Percent of estimated values out of (-2.5, 2.5) standardized error interval	Average quadratic standardized error
Mafic Volcanic 1A	362	353	2	0.74
Mafic Volcanic 1B	415	400	4	1.05
Mafic Boundary Intrusive North	376	365	3	0.92
Mafic Boundary Intrusive South	419	402	4	0.93
Quartz Porphyry West	303	286	6	1.61
Quartz Porphyry East	314	304	3	1.00
Sedimentary Rock	324	317	2	0.92
Granite	307	298	3	1.13

Table 4.5. Statistics summary of magnetic susceptibility distribution recovered from geophysical inversion of EM-31 data. Minimum, maximum and mean values in SI units scaled by a factor of 10^{-3} .

Grid	Number of Data	Minimum-Maximum	Mean	Variance
Mafic Volcanic - 1B	9	1.18-3.45	1.98	0.48
Quartz Porphyry West	51	0.001-19.52	7.26	20.43
Quartz Porphyry East	9	0.73-8.40	3.43	9.73
Boundary Intrusive North	42	0.64-67.68	26.64	382.99
Boundary Intrusive South	65	0.59-5.32	2.07	0.83
Sedimentary rocks	59	0.74-24.39	6.14	15.08

Chapter 5. Magnetic modeling at Rio Blanco

5.1 Introduction

Integrating magnetic susceptibility measurements collected at drill-hole scale with models of the physical property calculated from larger scale magnetic surveys is important to enhance numerical modeling of geophysical data. In order to integrate the magnetic data, experimental variograms of the magnetic susceptibility from the core measurements allows describing and modeling the spatial variability of the physical property at the point scale. Using the variogram model, interpolation with kriging permits the construction of a physical property model that first honors the spatial variability features at the drill-hole core scale and secondly is suitable to be scaled up to that of the magnetic regional data. The resulting geostatistical susceptibility model can be then compared to the magnetic susceptibility model recovered from the geophysical inversion of the airborne magnetic field in order to evaluate the solution of the inversion. A second use of the geostatistical model of susceptibility is as reference model used to constrain the inversion. Both alternatives are suitable ways to integrate magnetic data available from different sources and scales.

The goal of this chapter is to integrate magnetic information available at two different scales from the Rio Blanco-Los Bronces porphyry copper deposit, located in the Andes of central Chile (Fig 5.1). Magnetic data used herein is provided by CODELCO-CHILE, the Chilean copper mining company that owns and operates this copper-molybdenum mine. The geophysical information includes a regional scale grid of airborne magnetic data and a drill-hole database with magnetic susceptibility measurements. Drill core mapping record down the hole provided the geologic constraints.

5.2 Available information.

The airborne magnetic data is obtained from two magnetic flights provided by CODELCO embracing a surface of 10x10 km² where the Rio Blanco-Los Bronces deposit is located (Fig. 5.2A and Fig. 5.2B).

The drill-holes are irregularly distributed within the deposit (Fig. 5.2C) and cover a vertical column of 2 km. The drill-holes are distributed across an area of 2 km in the east-west direction and 3 km in the north-south direction (Fig 5.2B). Magnetic susceptibility measurements at the core scale are systematically collected down the drill holes with hand portable magnetic susceptibility meter (SM-30). The dataset consists in 47,850 meters corresponding to 82 drill-holes with a total of 24,000 measurements of magnetic susceptibility.

5.3 Geology.

5.3.1 Regional and district context.

The Rio Blanco-Los Bronces copper deposit is part of one of the largest metallogenic belts of Chile. This late Miocene-Pliocene metallogenic province, extending through 200 km of the Andes of central Chile contains three giant breccia-porphyry related systems, Los Pelambres, Rio Blanco-Los Bronces and El Teniente copper deposits (Fig. 5.2). Rio Blanco-Los Bronces deposit has been widely studied in the past (Serrano *et al.*, 1996, Vargas *et al.*, 1999), but recently Frikken *et al* (2005) provided an ore deposit model and Deckart *et al.* (2005) established the temporal framework of most of the rock units within the deposit.

Outcropping and sub-surface rock units at Rio Blanco are grouped into more than 15 rock types by the mine and exploration geologists (Serrano *et al.*, 1996, Vargas *et al.*, 1999, Frikken *et al.*, 2005). For the purposes of this study the rocks are grouped in four main units:

plutonic, porphyry, volcanic and breccias. Within each of the main rock units, 2 or 3 subunits are separated, resulting in ten rock types used to construct a simple rock model (Table 5.1). The rocks units outcrop over a surface of 4 km by 3 km in the north-south and east-west directions, respectively and have been recognized through 1.5 to 2.5 km of vertical extension in both mine tunnels and drill-hole intersections. The spatial distribution of the rock units is displayed in the geologic map and in the vertical cross section (Figs 5.3 and 5.4) where the north-south and north-west trend of the porphyry and breccias system can be observed as well as the vertical and sharp geological contacts between most of the units. The contact between the mafic volcanic unit (MV) and the Rio Blanco Granodiorite-GDRB (Fig 5.4-A) is horizontal.

5.3.2 Rock types.

Plutonic rocks include the Rio Blanco Granodiorite (GDRB), the Cascada Granodiorite (GDCC) and the Diorite (DIOR). Granodioritic rocks are differentiated by grain size and by location (Fig 5.3). The GDRB unit has larger crystal size and is spatially located in the northern half of the district whereas GDCC is restricted to the southern sector (Fig 5.3). The third plutonic rock type is a fine grained diorite (DIOR), which appears in the southeast sector of the deposit and is characterized by acicular plagioclase as well as a higher magnetic signature (see below).

The porphyry group includes the dacitic porphyry (PDL) and the quartz-monzonitic porphyry (PQM). The PDL is the largest porphyry body occupying the central part of the deposit (Fig 5.3), with horizontal lengths of 1,500 by 900 m in the north-south and east-west directions, respectively. The eastern margin of the PDL is formed by large breccia bodies. The PQM unit is located in the north and western sector of the deposit. The 500 m long intrusion is oriented N30W, and 200 at the widest point.

Volcanic rocks are subdivided into the mafic volcanic unit (MV) and a felsic volcanic unit (FV). MV unit consists of andesitic lava flows (Frikken 2003) which are generally flat lying

and located in the west and southern parts of the district. Rocks assigned to this unit can be found up to 150 m below the subsurface, usually in horizontal contact with GDRB (Fig 5.4-A). The felsic volcanic rocks (FV) are rhyolitic to dacitic flows that outcrop in the northern part of the deposit. They are related to caldera type volcanism interpreted to be largely post- and potentially contemporaneous with porphyry emplacement (Deckart et al, 2005).

The breccia rock group is divided in two sub-groups, a hydrothermal and a late-magmatic breccia. Two types of hydrothermal breccias are recognized, the Tourmaline Breccia (BXT) and the Monolito Breccia (BXMN). Both hydrothermal breccia types are located in the southern part of the district and along north trending geologic contact between is traced for almost 1,500 m (Fig 5.3). The BXT consists of variable sized granodiorite and diorite fragments, supported by cement composed of tourmaline, sulfides, magnetite/specularite and quartz. The BXMN is a rock flour supported matrix breccia with fragments of the GDCC, PDL, MV and BXT rock types. Both the matrix and the fragments of this breccia are pervasively altered to a chlorite assemblage. It outcrops as a northerly elongated body at the western margin of the BXT unit.

The late-magmatic breccia (BXTM) contains fragments of GDRB in fine crystalline igneous cement, containing mainly biotite (Frikken et al, 2005). The matrix of the breccia is made up of rock flour (broken minerals and rock fragments), magnetite, sulfides, anhydrite and quartz. . The rock unit is confined to the northernmost part of the district, and is spatially associated to the PQM rock unit.

5.3.3 Tridimensional model of rock types.

Using the geological information from the surface geology, the vertical cross sections, and the insight about subsurface rock distribution provided by the drill-hole cores, a 3-D model of the spatial distribution of the rock type is built within a region of 3,000 m in the X (East) direction, 4,000 m in the Y (North) direction and 3,300 in the Z (elevation). This region is divided into a grid of cells, each having a unique numeric code as a proxy of the rock type

(Table 5.1), according to the geological constraints. The width of each cell is 100 m in the horizontal directions, whereas the cell size in the Z direction is varied from 50 m within the first 1,300 m, 100 m for the next 1,500 m and 250 for the deepest 500 m. This allows a 3-D representation of the geologic features observed, such as the north-south trend of the geologic contact between the breccia units and the plutonic rocks and the sharp and vertical contact among the porphyry units (Fig 5.5).

5.4 Magnetic susceptibility distribution within the rock units.

Statistical distributions are calculated from the core measurements of magnetic susceptibility for each of the ten rock types, after they regularized, by calculating 2 m length weighted averages. The resulting distributions permit determination of the minimum, maximum, average and standard deviation of the physical property. In all of the rock types, the range of magnetic susceptibility for the rocks covers more than one magnitude order, requiring that the histograms be plotted using a logarithmic scale (Fig. 5.7).

Within the plutonic rock group, DIOR and GDCC have average magnetic susceptibility of 29.1 and 13.2, respectively, one order of magnitude greater than GDRB whose physical property average is of 1.95. The breccia rock group is characterized by one unit of high magnetic susceptibility, the BXT with an average value 27.1 and two units of low physical property, 2.8 for BXTM and 3.9 for BXMN. For the porphyry group, both PDL and PQM have low average magnetic susceptibility with values of 0.48 and 0.46, respectively. And finally, within the volcanic rock group, a high magnetic susceptibility average is found for MV with a value of 12.8 and a remarkably lower physical property average of 0.3 for the FV is observed.

The magnetic susceptibility ranges observed for the different rock units of the deposit are large, involving 4 magnitude orders, from 10^{-5} to 10^{-1} SI units for most of them (Fig 5.7A). Compared with the susceptibility ranges commonly observed for various rocks (Fig 5.7B), the deposit rocks have greater susceptibility ranges than common rocks, as a result of alteration

and deposition of magnetic minerals resulting from hydrothermal activity. The plutonic, breccias and the MV unit reach their maximum magnetic susceptibility within the zone where the magnetite volume percent is between 1 and 5 %, indicating that magnetic mineral deposition is widely developed within these rocks. The two porphyries, PQM and PDL, and the FV reach maximum values where the magnetite content is below 0.5%, consistent with the intermediate to felsic composition of these rocks.

5.5 Magnetic susceptibility variograms.

The available data from the drill-hole cores include the spatial location of each magnetic susceptibility measurement. Magnetic susceptibility measurements for each rock type allow computation of physical property experimental variogram, used to explain the physical property variability within rock units at the core scale (Fig.5.8).

For the plutonic rocks, the variograms increase gradually with the distance, indicating a certain degree of physical property spatial correlation. The range of correlation is achieved for sampled locations separated less than 20 m for GDRB and less than 40 m for GDCC and DIOR, although in the three cases, the variogram reaches a sill below the calculated magnetic susceptibility variance, indicating that zones of different magnetic susceptibility distribution might be encountered within the rock units. This reflects zonal anisotropy. The variogram behavior near the origin suggests nugget effect values of 2, 10 and 0 for GDRB, GDCC and DIOR, respectively.

The magnetic susceptibility variograms for the breccias (Fig 5.8) present a similar pattern compared to the plutonic rocks. The three variograms increase their values with the distance and level off at a range distance value of 6, 14 and 40 m for BXTM, BXMN and BXT, respectively. However BXT and BXMN reach the sill at the sample variance (Fig 5.8) whereas the sill for BXTM is smaller than the magnetic susceptibility variance within this rock unit. Regarding the nugget effects, the observed values are 200, 0 and 5 for BXT, BXTM and BXMN, respectively.

Within the porphyry rocks, the magnetic susceptibility variogram for PDL shows that the sample variance is reached around 14, but instead of leveling off around the variance, the variogram drops and behaves erratically with large variogram oscillations for larger distances. The large oscillations of the variogram values are associated with the large coefficient of variation (3.05) calculated from the available measurements of susceptibility. This might be related to different magnetic susceptibility populations within PDL that were not discriminated by the rock code. The nugget effect is considered 0 as the experimental variogram is close to the origin over the short distances. For the PQM unit the variogram does not reach the sample variance and displays an erratic behavior through the considered distance spectrum, thereby hampering interpretation.

For the volcanic rocks type, the calculated variograms permit the recognition of spatial correlation within the FV unit. The observed variogram is characterized by a correlation distance near 40 m where the variance is reached after a steadily increasing variogram. In the case of the MV unit, the interpretation is complicated because after the sill is reached the variogram behaves erratically with large oscillations around the variance. Before the variance is reached near 20 m, the variogram increases value revealing that a certain degree of spatial correlation is achieved, but no sills are encountered.

5.5.1 Variogram modeling.

In order to calculate 3-D distributions of magnetic susceptibility using the core measurements, the calculated experimental variograms are modeled using the available functions implemented within GSLIB software package. The parameters involved in the variogram models include the nugget effects, the ranges and the variance contribution values obtained from the previous section (Table 5.2). The resulting geostatistical models are then cross validated to obtain a quantification of the quality of the fitted variogram models (Figs 5.9, 5.10 and 5.11). The results of the cross validation indicate that the modeled spatial variability of the magnetic susceptibility is reproduced by the fitted models achieving correlation coefficients ranging from 0.76 to 0.9.

5.6 Magnetic susceptibility model.

The variogram models obtained for each rock type are used to calculate ‘local’ magnetic susceptibility models using the core physical property measurements. The interpolation method used is kriging which accounts for the physical property spatial variability quantified with the variogram models. The interpolation nodes are located at the center of the cells of the rock type model defined previously. That is, each node is separated 100 m in the horizontal directions and 50, 100 or 125 m in the vertical direction. As a result, local models of the physical property are for each rock type, grouping all results in a magnetic susceptibility model for the entire deposit. To observe the physical property features within the model, a cutoff magnetic susceptibility value of 0.0228 (SI) is applied. Two zones appear to have values larger than this threshold; there is a small zone located in the north-west area composed by a single body of susceptibility 0.0238 which is spatially associated with BXTM (Fig 5.12). The south-east sector is composed by tabular bodies with susceptibility between 0.034 and 0.069 SI. The larger zone corresponds to BXT whereas the smaller, located 300-500 m east of BXT is related with the DIOR unit (Fig 5.12).

In terms of the statistical distributions, the resulting magnetic susceptibility models are characterized by smaller variability compared to the original physical property distributions calculated from core measurement as a result of the smoothing effect of kriging. This is verified by a reduction in both the variance and the range of the estimated physical property (Fig. 5.13).

5.7 Integrating magnetic data and models.

Airborne magnetic data are available from 2 data sets, one regional survey involving 20x20 km² approximately and a second at a district scale embracing a surface of 5x5 km². The data in both cases are gridded, corresponding to total magnetic anomaly in the first case and total magnetic intensity in the latter. The survey lines are oriented north south and east west in both

cases, but with separations of 150 m for the larger scale data set and 50 m for the district scale. The regional scale is performed by airplane at an average height of 390 above the terrain surface whereas the detailed survey, performed by helicopter, had an elevation on average of 122 m over the topography. Finally both surveys were performed during two campaigns, the regional scale is performed on 1994 and the district scale in 2005.

The magnetic survey at the district scale and the magnetic data forward modeled using the physical property model calculated from the geostatistical analysis are compared as a means of integrating the magnetic data at the different scales (Fig 5.14). Both maps differ in the magnitude of the values for the anomalies. In the case of the forward modeled data, the values of the anomaly are in the range of tens of nT. In the case of the measured data the anomalies are in the order of hundreds of nT, suggesting that shallow magnetic material (not sampled by the deep drill-holes) might be strongly controlling the magnetic response. In the case of forward modeled magnetic maps, a zone of magnetic response associated with the Rio Blanco Breccia complex is observed. The Sur-Sur area is characterized by a zone of large and positive magnetic response just east of the breccias. This anomaly is associated with the susceptibilities measured in the drill-hole cores that intercept the DIOR rock type. The same area in the case of the measured data is characterized by lower magnetic response. The large zone of low magnetic response observed in the forward map at the south west corner is due to scarce or lack of sampling as no drilling is available in that area.

5.8 Conclusions

Integrating magnetic data from different survey methods at different scales can be facilitated by applying the geostatistical analysis. From the core scale measurement, it is possible to obtain a variogram model of the spatial variability of magnetic susceptibility. The variogram model can be used by kriging in order to calculate a physical property model at a larger scale. The resulting model can be used, as was in here, to calculate magnetic data forward modeling the magnetic susceptibility model and then compare with the actual measured data. If the results of geophysical inversions are available then two physical property models can be

contrasted. The third use of this model is used as a reference model to run constrained geophysical inversions. Finally, the comparison between forward modeled magnetic data and the district scale magnetic map presented here probe to be a suitable approach to integrate both data sets, but largely constrained to the quantity and geometric configuration of the data.

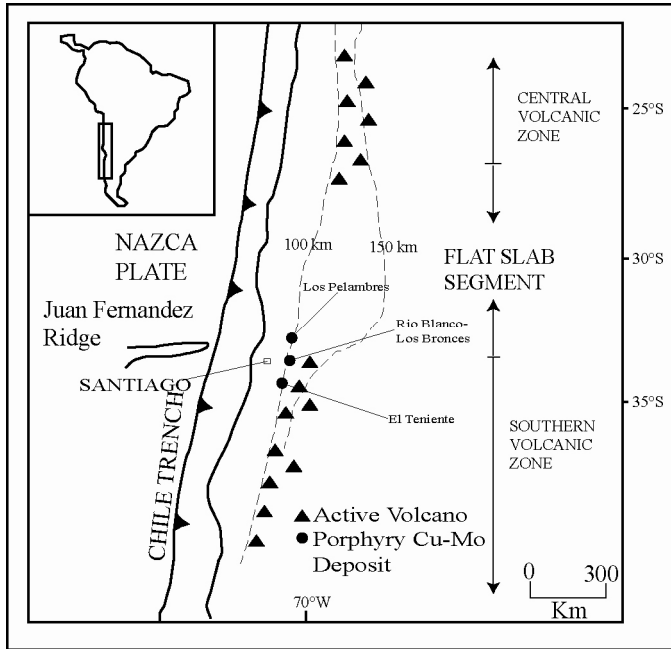


Figure 5.1. Tectonic setting of the Miocene-Pliocene porphyry copper deposits located in central Chile (modified from Skewes et al. 2003).

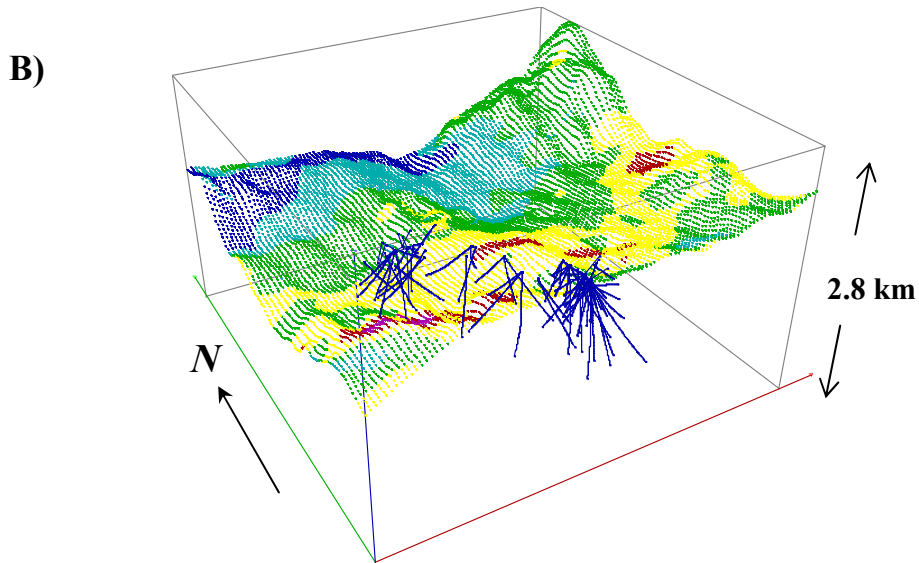
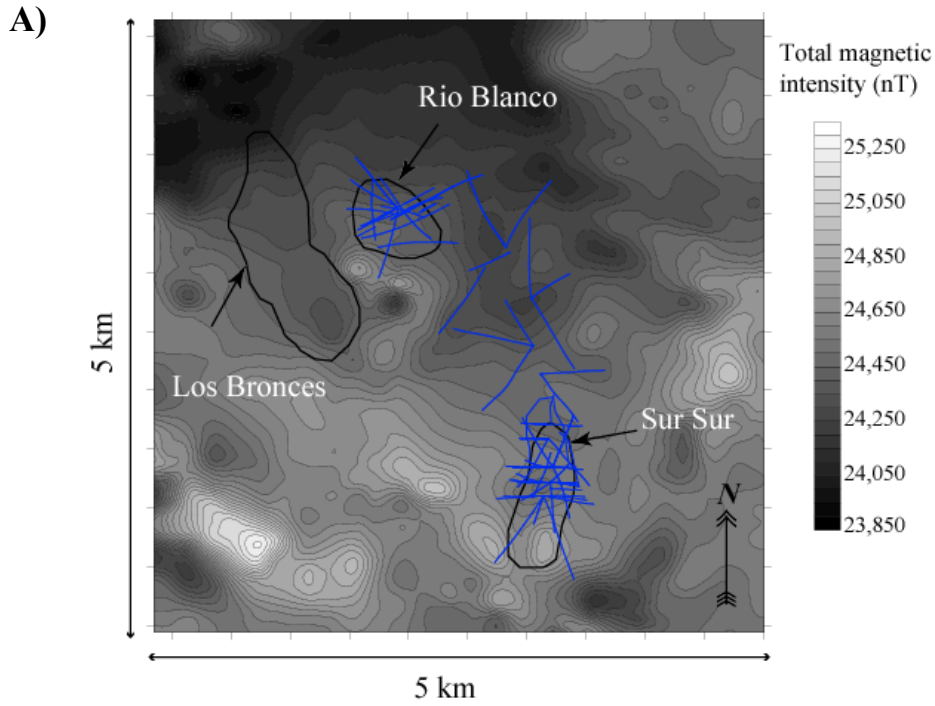


Figure 5.2. A) Total magnetic anomaly map at over the Rio Blanco District. Location of breccia complexes is outlined, horizontal projection of drill-holes plotted in solid blue line. B) Perspective view looking NE of the aeromagnetic data and the drill-hole distribution within the deposit. Drill-holes recognized 2 km vertically.

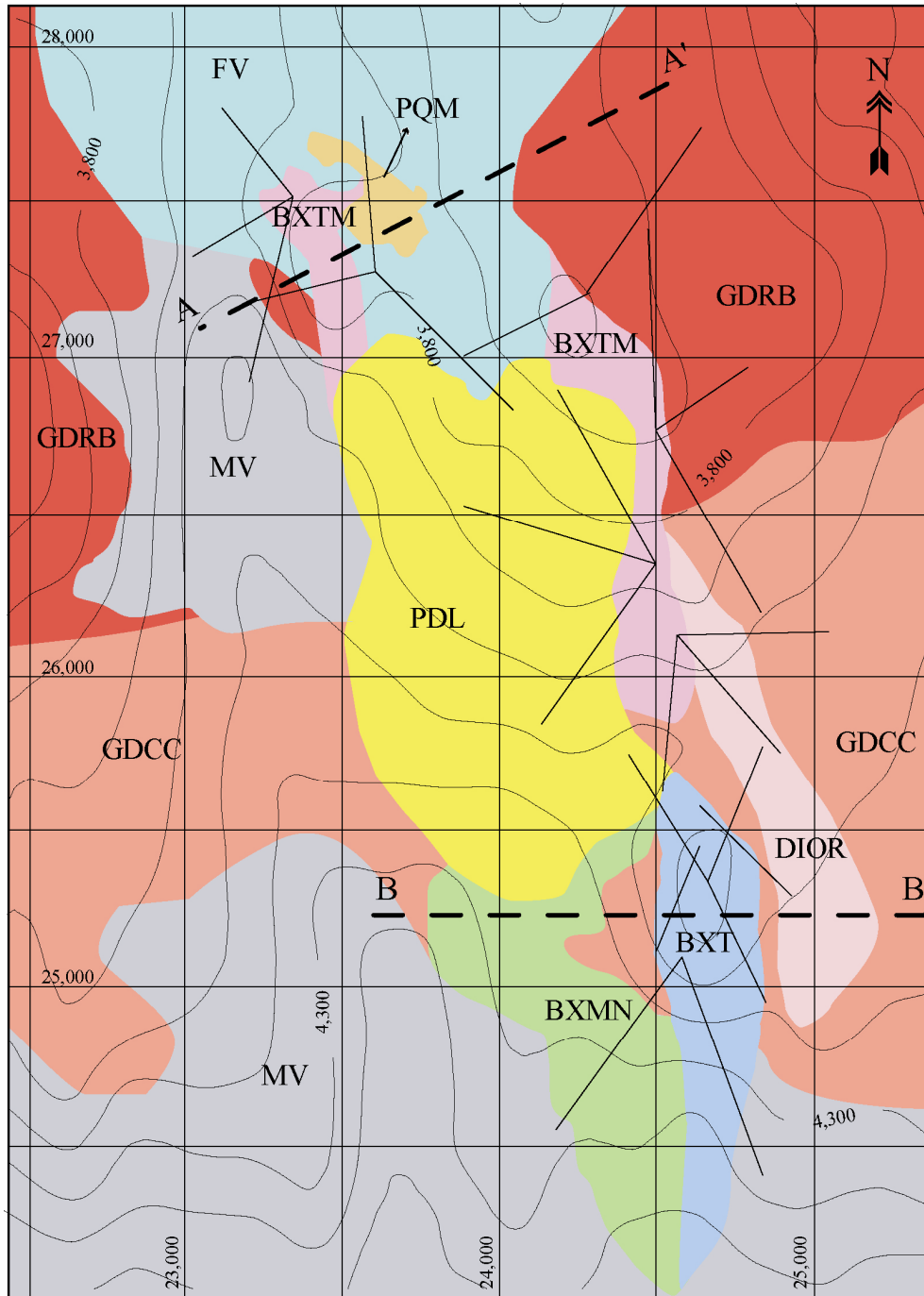


Figure 5.3. Geologic Map of the Rio Blanco District (modified after Vargas et al. 1999 and Frikken et al. 2005). GDRB-Rio Blanco Granodiorite, GDCC-Cascada Granodiorite, DIOR-Diorite, PDL: Dacitic porphyry, PQM-Quartz monzonite porphyry, MV-Mafic volcanics, FV-Felsic Volcanics, BXTM-Late-magmatic breccia, BXT-Tourmaline breccia, BXMN-Monolito Breccia. Solid and dashes lines indicating location of drill-holes and cross sections (AA' and BB'), respectively. Topographic contours separated 100 m.

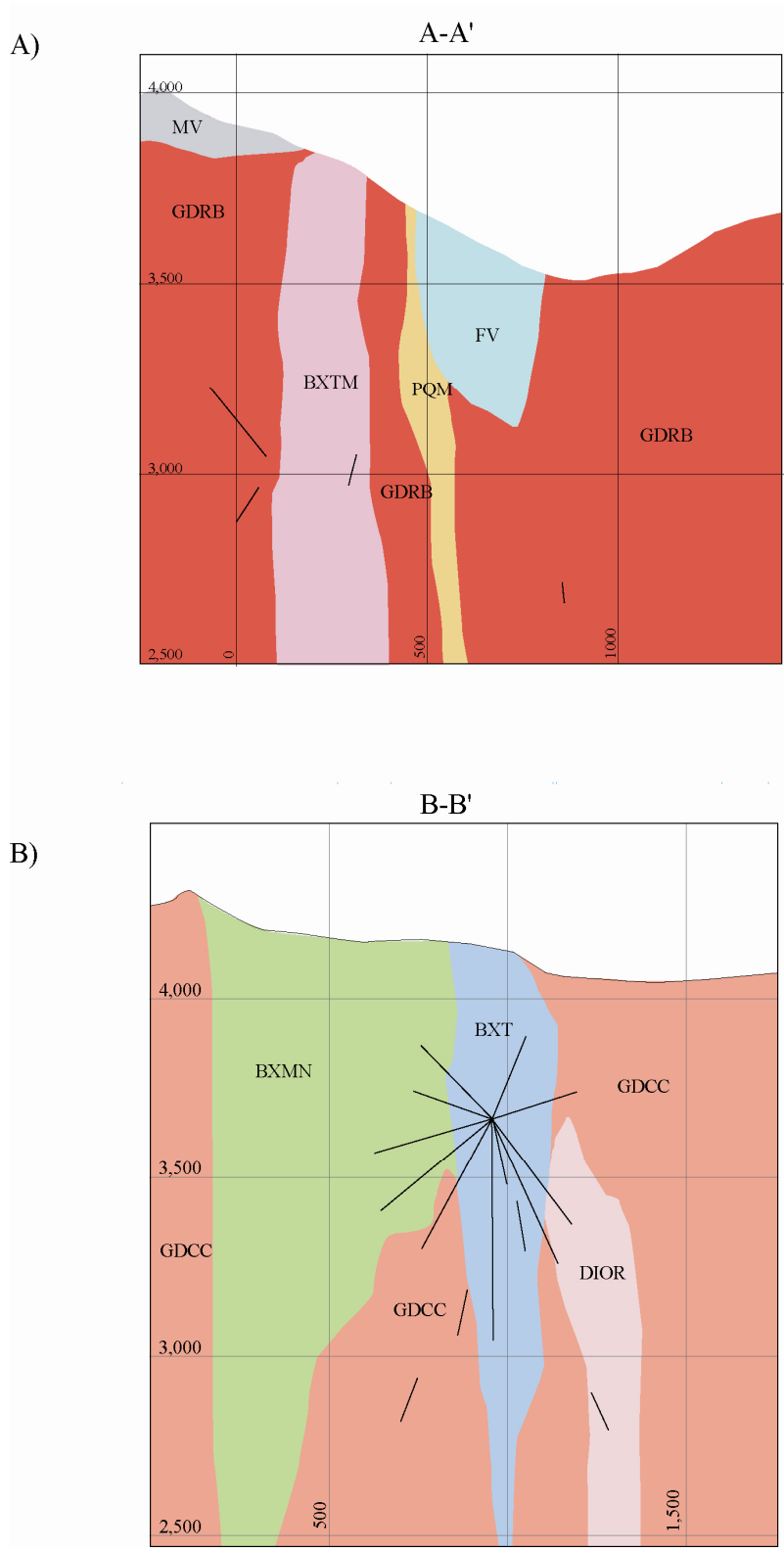


Figure 5.4. Vertical cross sections through the Rio Blanco porphyry copper deposit. A) Section across the Rio Blanco sector. B) Section across the Sur-Sur sector. Vertical and sharp geological contacts among units are observed through a rock column of 2 km.

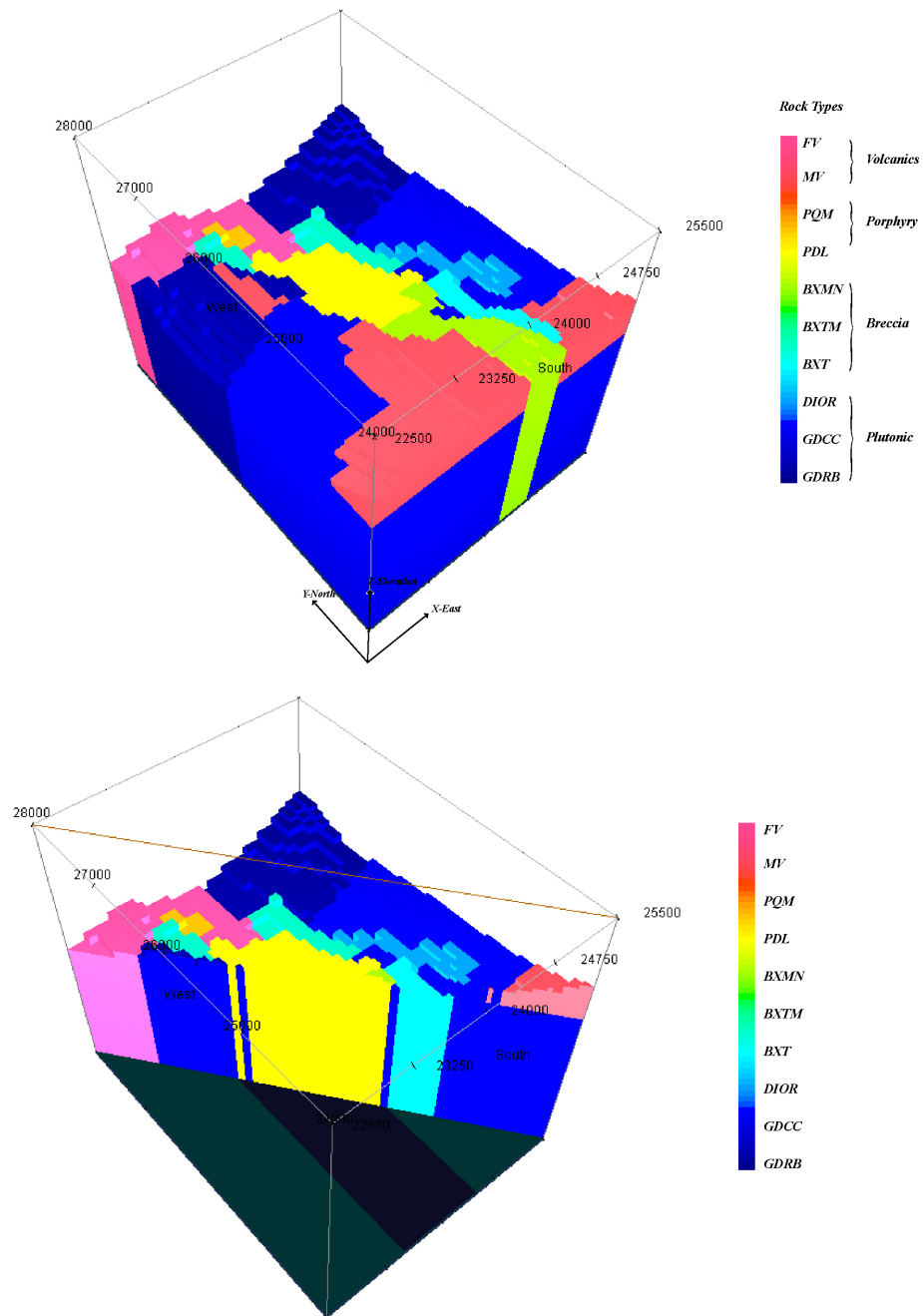


Figure 5.5. Three dimension rock model of the Rio Blanco deposit. Top panel shows the entire model region in a NE view. Bottom panel is a NW-SE cross cut through the model displaying the sharp and vertical contacts between the rock types. FV-Felsic Volcanics, MV-Mafic Volcanics, PQM-Quartz Monzonitic Porphyry , PDL-Dacitic Porphyry, BXMN- Monolito Breccia, BXTM- Late-magmatic Breccia, BXT Hydrothermal Breccia, DIOR-Diorite, GDCC-Cascada Granodiorite, GDRB Rio Blanco Granodiorite.

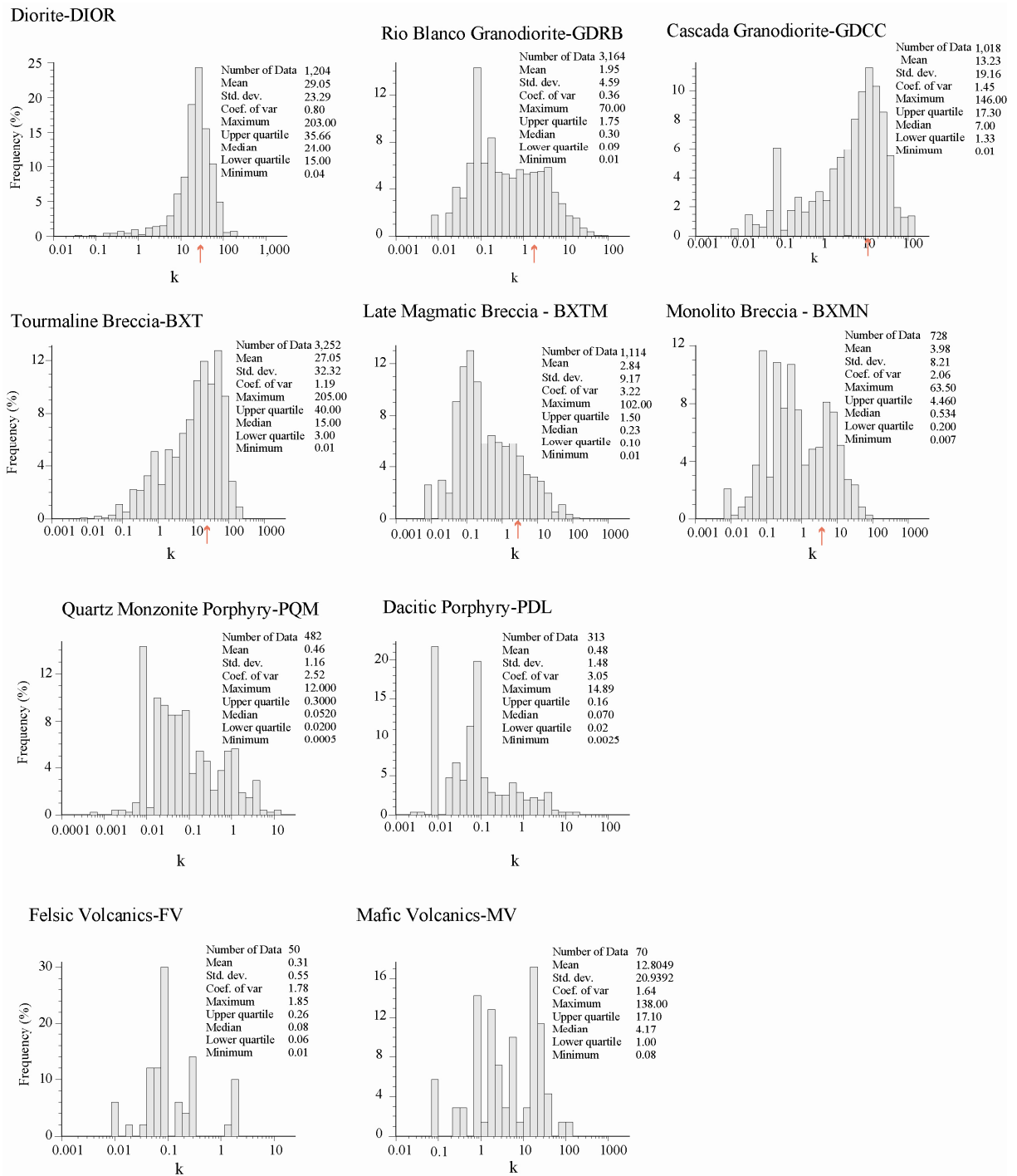


Figure 5.6. Magnetic Susceptibility histograms for the 10 rock types studied from Rio Blanco Deposit. Several orders of magnitudes are observed for the physical property within the different rock types.

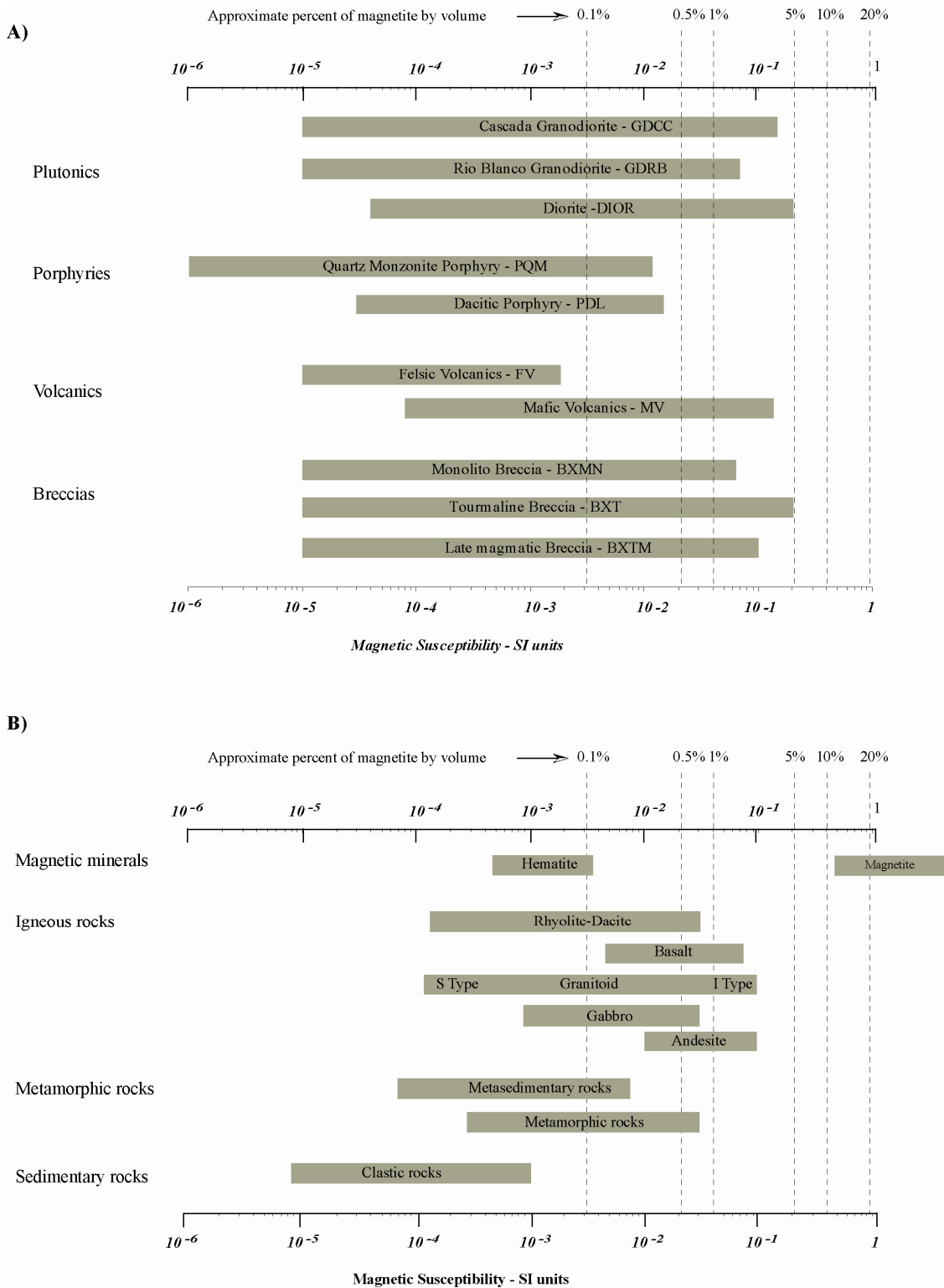


Figure 5.7. Magnetic susceptibility ranges for A) core measurements from rock units within Rio Blanco Deposit, B) Various rock types, modified from Clark, 1997.

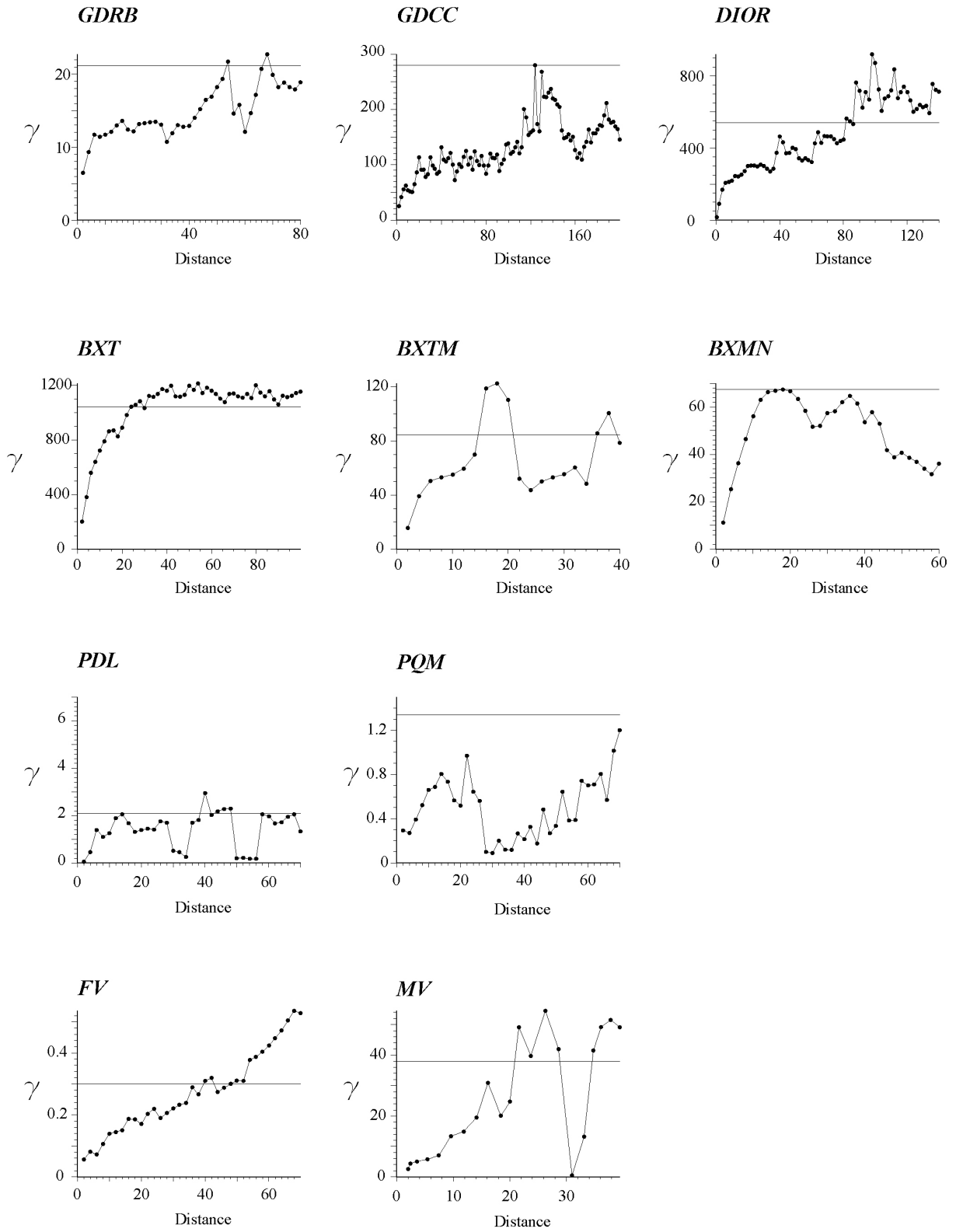


Figure 5.8. Magnetic susceptibility experimental variograms for each of rock types from Rio Blanco deposit.

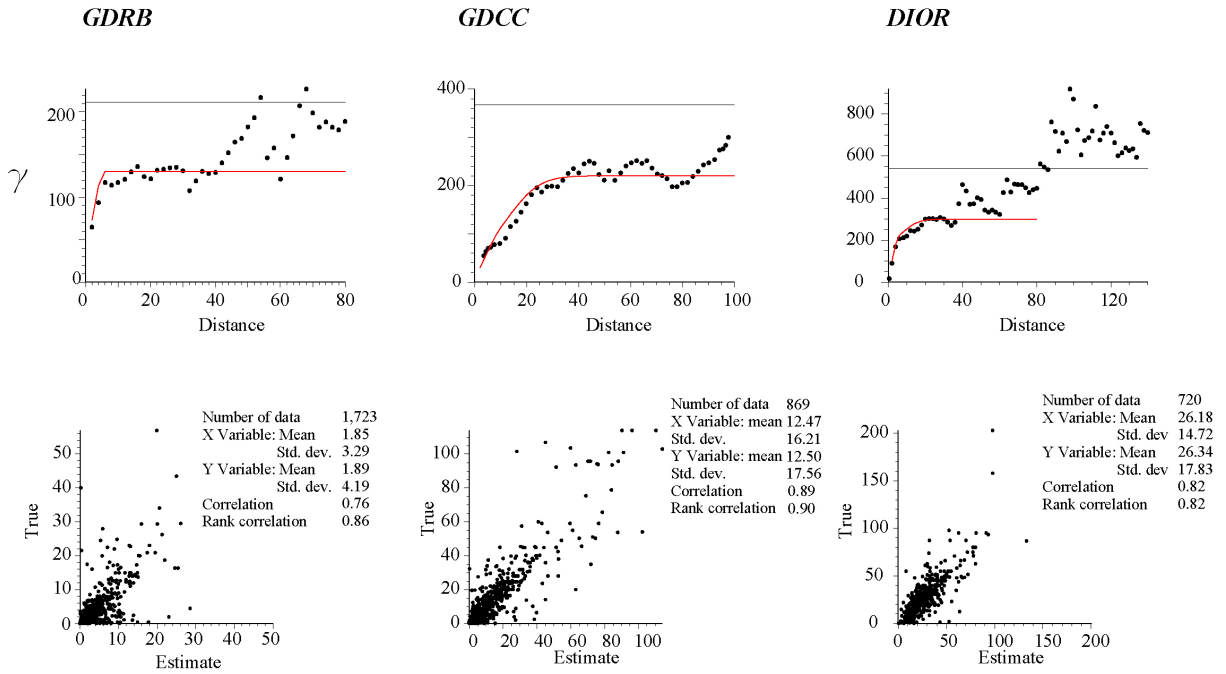


Figure 5.9. Variogram models (red line in top panel) for the plutonic rocks. Scatter plots of true versus estimate magnetic susceptibility resulting from cross validations.

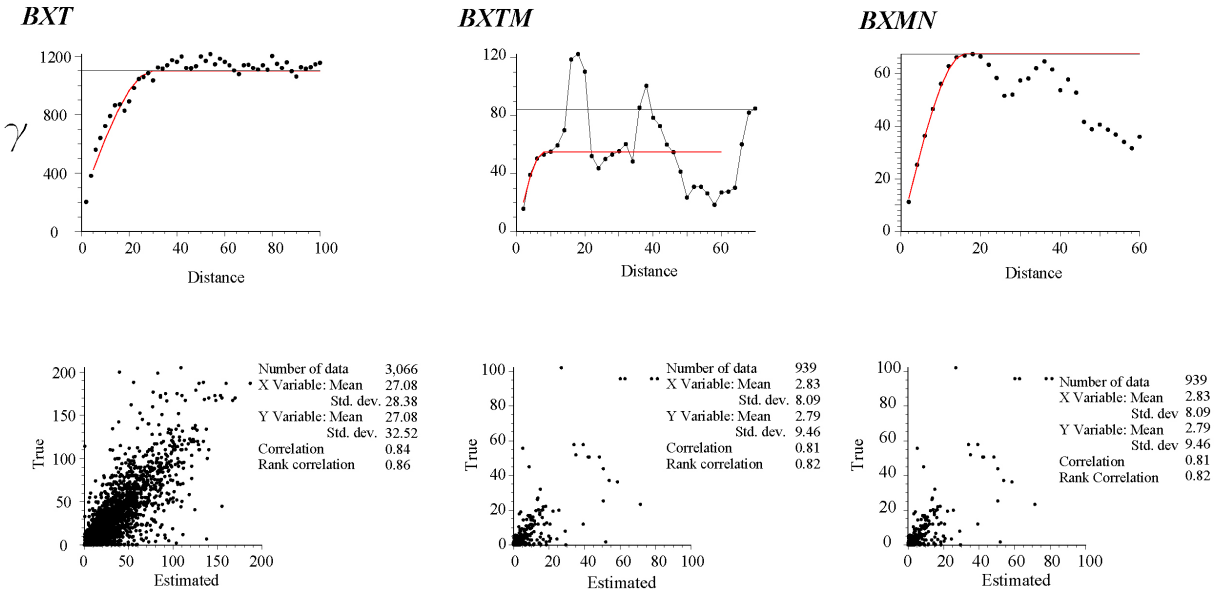


Figure 5.10. Variogram models (red line in top panel) for the breccia rock types. Scatter plots of true versus estimated magnetic susceptibility resulting from cross validations (bottom).

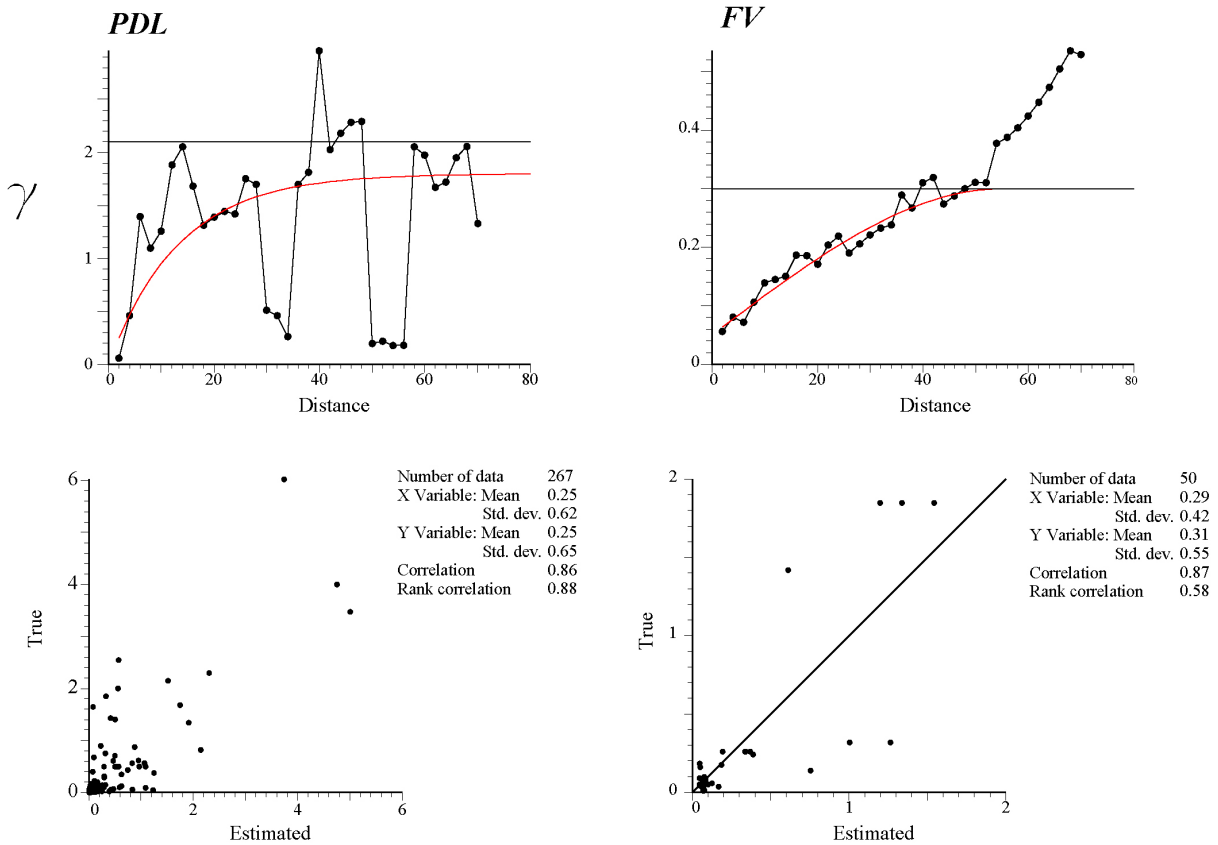


Figure 5.11. Variogram models (red line in top panel) for the Dacitic Porphyry (PDL) and Felsic Volcanics (FV) rock types. Scatter plots of true versus estimate magnetic susceptibility resulting from cross validations (bottom).

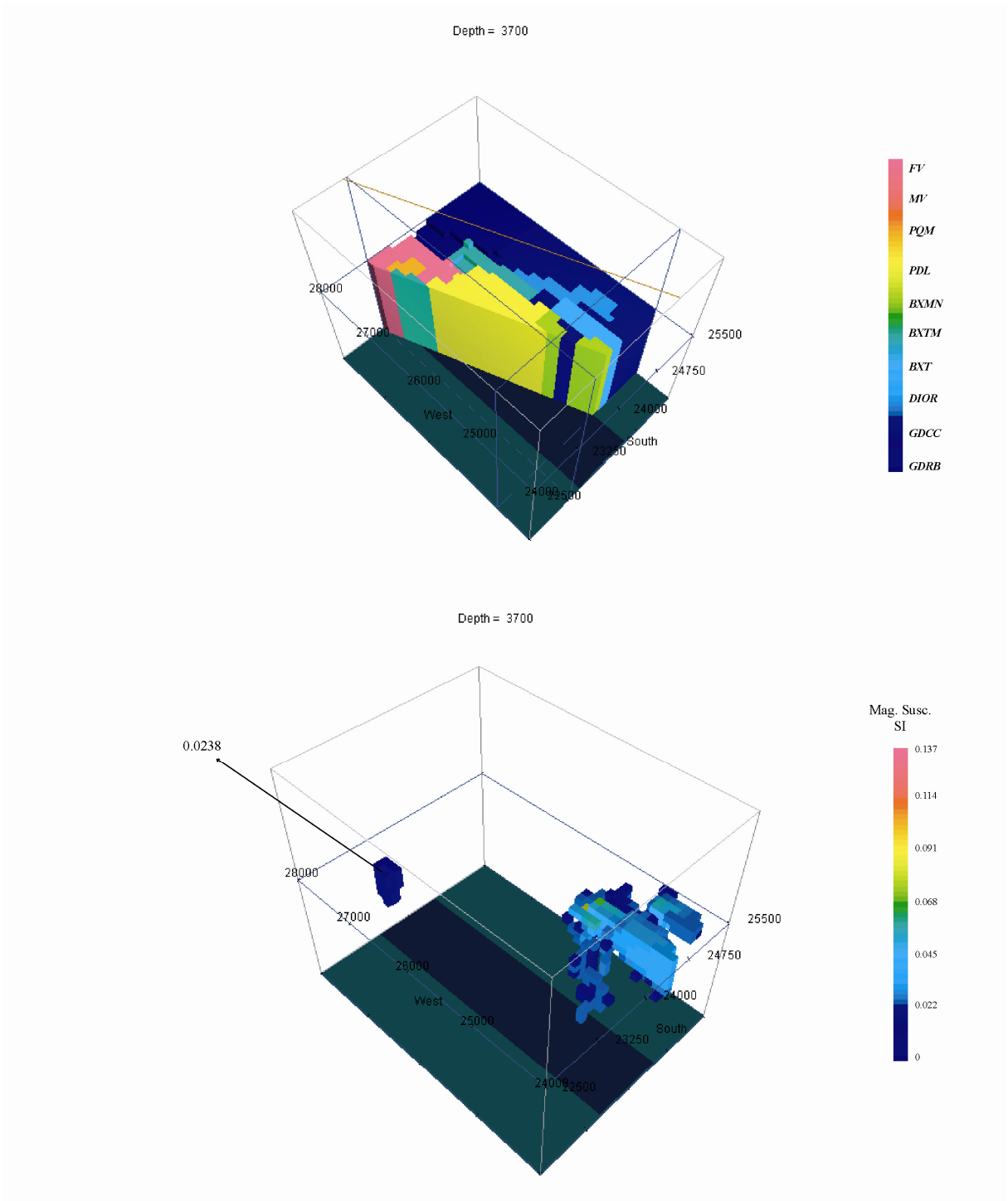


Figure 5.12. Rock type model (top) and magnetic susceptibility model (bottom). Two zones of magnetic susceptibility values above 0.0228 are observed. The northern one is associated to Late Magmatic Breccia and the south-east one are associated with Tourmaline breccia and Diorite rock types.

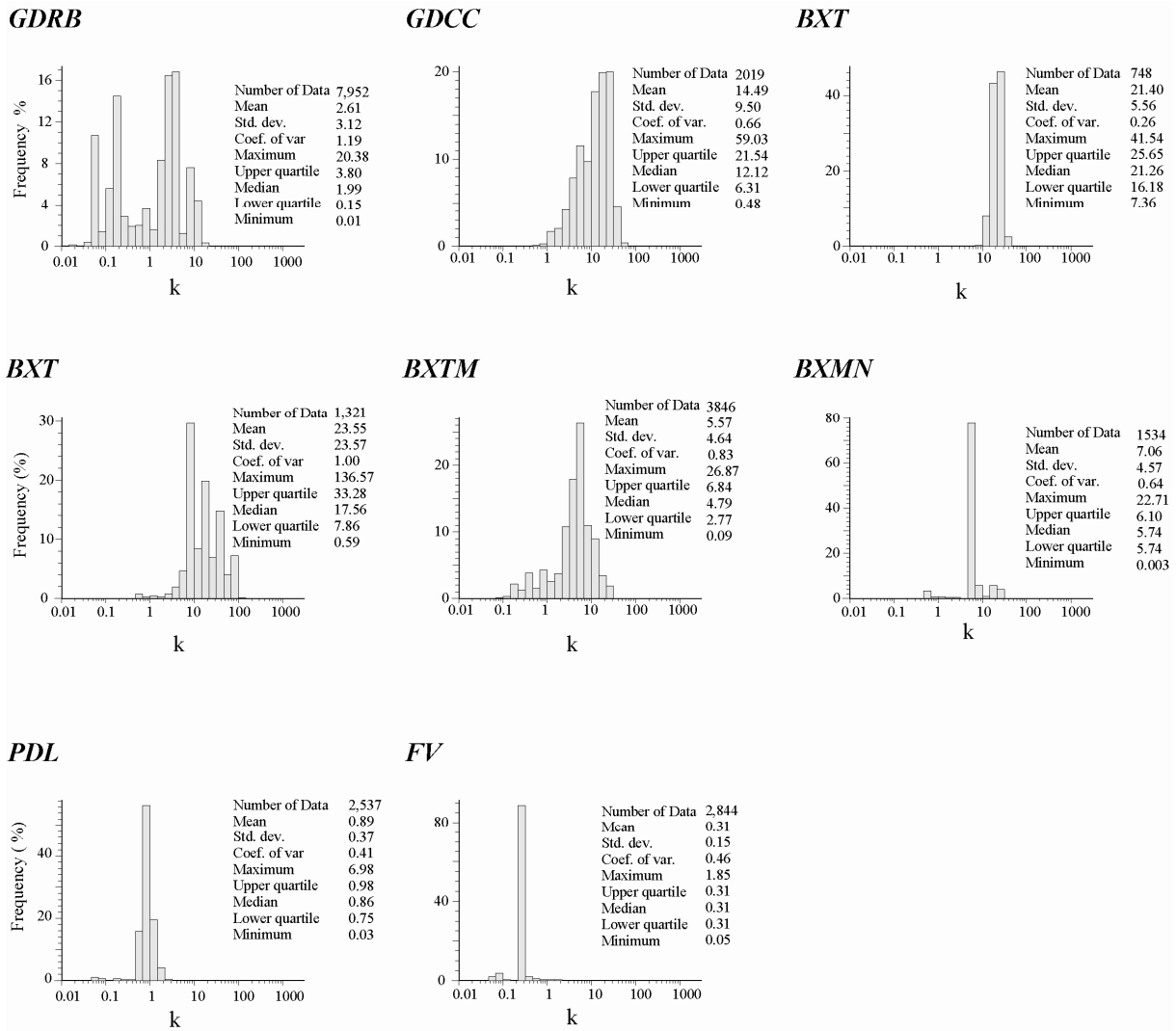


Figure 5.13. Histograms for the magnetic susceptibility distribution for each of the rock types modeled using the geostatistical analysis. A reduction of the variance population and in the range of the distribution because of the kriging smoothing effect (compared to the histograms of figure 5.6).

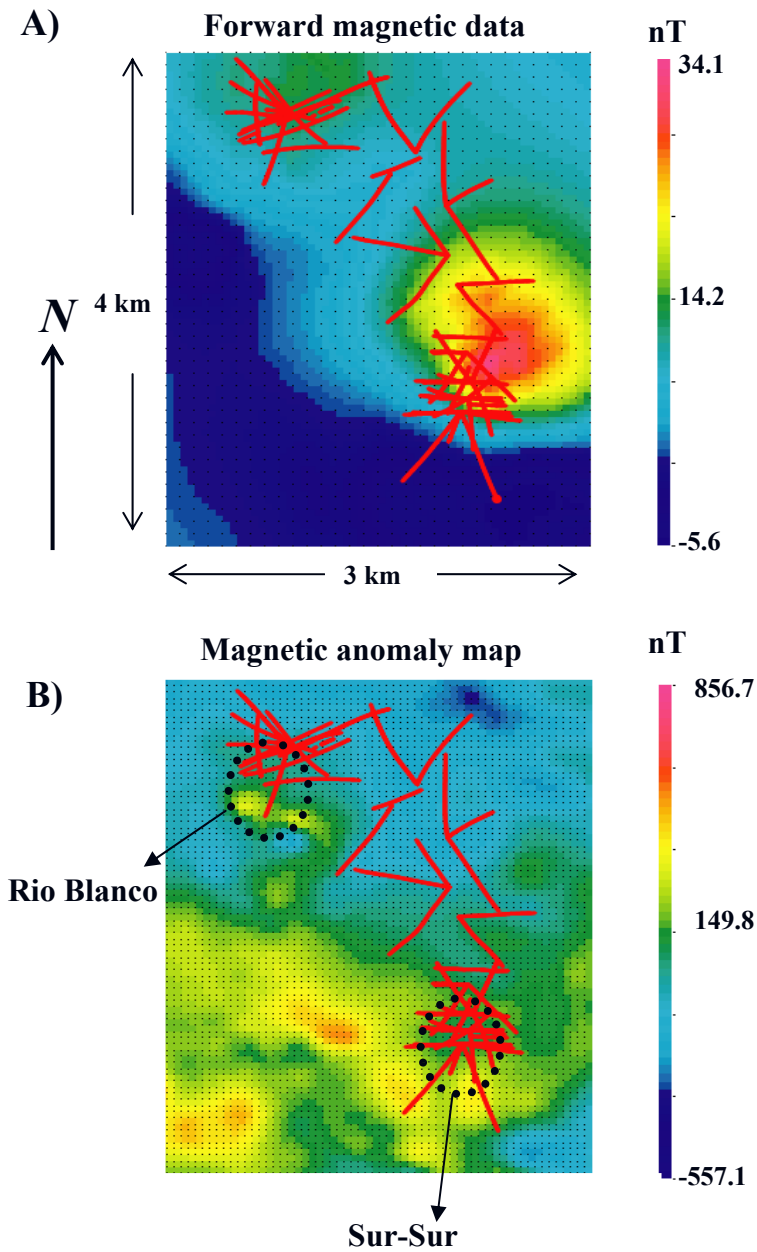


Figure 5.14. A) Magnetic data forward modeled from the magnetic susceptibility model calculated after the geostatistical analysis. Parameter used are Inclination= -32° , Declination = 4.9 , Magnetic Field Strength = $24,402$ nT, line separation 100 m and 100 m above topographic surface. B) Gridded helicopter-borne magnetic anomaly over the district. In both maps the horizontal projection of drill-hole are plotted in red solid lines to locate the breccia complexes.

Table 5.1. Rock codes, average and standard deviation of magnetic susceptibility measurements available from drill-hole cores from Rio Blanco Deposit.

Rock Unit	Rock code	Numerical code	Mag. susc. (x10 ⁻³ SI) Average	Mag. susc. (x10 ⁻³ SI) Standard deviation
Plutonics				
Rio Blanco Granodiorite	<i>GDRB</i>	1	2.05	4.58
Cascade Granodiorite	<i>GDCC</i>	2	7.60	13.33
Diorite	<i>DIOR</i>	3	21.29	21.24
Breccias				
Hydrothermal Breccia	<i>BXT</i>	4	26.73	32.15
Late magmatic breccia	<i>BXTM</i>	5	4.82	11.40
Monolito Breccia	<i>BXMN</i>	6	3.98	8.22
Porphyritic rocks				
Don Luis Dacitic Porphyry	<i>PDL</i>	7	0.49	1.48
Quartz monzonitic porphyry	<i>PQM</i>	8	0.69	2.03
Volcanics				
Mafic Volcanic	<i>MV</i>	9	12.81	
Felsic Volcanic	<i>FV</i>	10	0.31	0.56

Table 5.2. Variogram model parameters.

Rock Type	Nugget effect	Model Type	Variance contribution	Range (m)
<i>GDRB</i>	2	Spherical	11	6
<i>GDCC</i>	10	Spherical	60	10
	10	Gaussian	150	30
<i>DIOR</i>	0	Spherical	200	6
	0	Gaussian	100	20
<i>BXT</i>	200	Spherical	900	30
<i>BXTM</i>	0	Spherical	55	8
<i>BXMN</i>	5	Spherical	62.5	16
<i>PDL</i>	0	Exponential	1.8	40
<i>FV</i>	0.05	Exponential	0.25	38

Chapter 6. Conclusions

6.1 Summary of work completed.

The work completed in this thesis has demonstrated how the scaling property of magnetic susceptibility can be used to integrate models of the physical property. In the synthetic example, physical property models have been used to test how the statistical distribution and the spatial variability pattern of magnetic susceptibility models change when the cell size of the models is increased. This approach provides a methodology to integrate physical property measurements available at different sample volumetric scales. Testing of the scaling relations of magnetic susceptibility models indicate that if a model is randomly populated, the physical property models can be scaled up by arithmetically averaging. In this case, the variance of the magnetic susceptibility for scaled models and the volume/cell size of the models follow a linear inverse relation. How the variance is reduced depends on the rate of volume change. Similarly, for the smoothed physical property models, the scaling relation between the variance of the magnetic susceptibility and the cell volume follows an inverse relation. However, the relation is not linear, but depends on the degree of spatial correlation.

In the case of the field data from Flin-Flon, the point scale magnetic susceptibility measurements for the analyzed sites display a wide range of values, spanning the complete spectrum for diamagnetic, paramagnetic and ferromagnetic materials. The statistical distributions of the physical property are skewed to the low values classes, which is compatible with a log-normal distribution. At each grid the variability, is a function of the quantity of magnetic susceptibility populations present within each grid. Spatial variability of magnetic susceptibility is described by the physical property experimental variograms, although the random or noisy characteristics of the available physical property data hindered their interpretation and modeling. Comparison between physical property datasets available at two volumetric scales proved a dependency of magnetic susceptibility with the size and hence with the scale of the sampling support. The relation between point scale magnetic susceptibility measurements and the recovered distribution of the physical property at larger

volumetric scales seem to follow a power law, with an exponent (scaling factor) less than 1. Variogram scaling of magnetic susceptibility results in a suitable methodology to integrate different scale physical property distributions, when a reliable model is fitted to the experimental variogram.

The field data from Rio Blanco deposit provide the chance to integrate magnetic data collected using different survey methods at different sampling scales, applying the geostatistical analysis. Using the core magnetic susceptibility measurements, it is possible to fit a variogram model of the magnetic susceptibility spatial variability. This model is suitable to be used by kriging to calculate a physical property model at the scale of geophysical inversions of regional or district magnetic data. A comparison between forward modeled magnetic data and district scale magnetic map probe to be a suitable approach to integrate both data sets, but largely constrained to the quantity and geometric configuration of the data.

Limitation of the methodology is related to the variable behavior in terms of the stationarity hypothesis. If stationarity is not satisfied, then the variogram fails to characterize properly the spatial variability of the physical property and moreover the relation between the variograms at different scales is not applicable. Along with stationarity, no volumetric overlapping between the sampled volumes at the different scales can take place. This additional constraint is hard to be evaluated in the field during a geophysical survey. Both issues can be invoked to explain why in only one of the grids at Flin-Flon, the methodology yields reasonable results.

6.2 Recommendation for further work

There are several applications of the scaling relation of magnetic susceptibility potentially useful to enhance geophysical and geologic models that might be investigated. Physical property simulation algorithms can use the physical property variogram model obtained from small scale measurements to calculate multiple realizations of the physical property at larger scales allowing assessment of the uncertainty associated to the models.

The scaling relation of magnetic susceptibility at smaller scales than drill-hole cores or hand samples is one of the open research lines that can be followed. For example what is the relation of the physical property with the size of the magnetic domains and the physical property should be studied.

One further application of the methodology proposed here is the estimation of the sampling volume associated to geophysical surveys of other physical properties such as density or electrical conductivity. Having reliable models of spatial variability at particular volumetric scales allows estimating the sampling volume associated to larger scale surveys.

References

- Beard, L.P., Nyquist, J.L., 1998. Simultaneous inversion of airborne electromagnetic data for resistivity and magnetic permeability, *Geophysics*, vol. 63, No. 5, p. 1556-1564.
- Berger, B. R., King, T. V., Morath, L. C. and Phillips, J.D. 2003. Utility of High-Altitude Infrared Spectral Data in Mineral Exploration: Application to Northern Patagonia Mountains, Arizona. *Economic Geology*, vol.98, p.1003-1018.
- Blakely, R. J. 1995. *Potential Theory in Gravity and Magnetic Applications*. Cambridge University Press. 441 p.
- Camus, F. 2003. *Geología de los Sistemas Porfíricos en los Andes de Chile*. Servicio Nacional de Geología y Minería, 267 p. Santiago, Chile.
- Clark, D.K. 1997. Magnetic petrophysics and magnetic petrology: aids to geological interpretation of magnetic surveys. *Journal of Australian Geology & Geophysics*. Vol 17(2), p. 83-103
- Cooke, D.R., Hollings, P and Walshe, J.L. 2005. Giant Porphyry Deposits: characteristics, Distribution and Tectonic Controls. *Economic Geology*. Vol 100. N0 5. p. 801-818.
- Corn, R. M. 1975, Alteration-mineralization zoning, Red Mountain, Arizona. *Economic Geology and the Bulletin of the Society of Economic Geologists*, vol.70, no.8, pp.1437-1447.
- Cox, D.P. 1986 Descriptive model of porphyry copper: U.S. Geological survey 1693,
- Deckart, K. Clark, A.H., Aguilar A., C., Vargas R., R. Bertens A., N., Mortensen, J.K, and Fanning, M. 2005. Magmatic and Hydrothermal Chronology of the Giant Río Blanco Porphyry Copper Deposit: Implications of an Integrated U-Pb and $^{40}\text{Ar}/^{39}\text{Ar}$ Database. *Economic Geology*, vol. 100, No. 5. pp905-934.
- Deutsch, C.V. and Journel, A.G. 1998. *GSLIB. Geostatistical Software Library and User's Guide*. Applied Geostatistics Series. Oxford University Press. New York.
- Dilles, J.H. and Einadi, M. T. 1992. Wall-Rock Alteration and Hydrothermal Flow Paths about the Ann-Mason Porphyry Copper Deposit, Nevada—A 6-Km Vertical Reconstruction. *Economic Geology*, Vol 67. p. 1963-2001.
- Emery, X., 2000. *Geostadística Lineal*. Departamento de Ingeniería de Minas. Facultad de Ciencias Físicas y Matemáticas. Universidad de Chile. P. 411.

- Farquharson, C.G., Oldenburg, D.W. and Partha, S.R. 2003. Simultaneous 1D inversion of loop-loop electromagnetic data for magnetic susceptibility and electrical conductivity. *Geophysics*, vol. 68. No. 6 p. 1857-1869.
- Franklin, J.M., Gibson, H.L., Jonasson, I.R. and Galley A.G. 2005. Volcanic Massive Sulfide Deposits. *Economic Geology 100th Anniversary Volume*. P523-560.
- Frikken, P. H., Cooke, D. R., Walshe, J. L., Archibald, D., Skarmeta, J., Serrano, L., Vargas, R. 2005. Mineralogical and Isotopic Zonation in the Sur-Sur Tourmaline Breccia, Río Blanco-Los Bronces Cu-Mo Deposit, Chile: Implication for Ore Genesis. *Economic Geology*, vol. 100, No. 5, pp. 935-961.
- Frykman and Deutsch, C , 2002. Practical application of geostatistical scaling laws for data integration. *Petrophysics*, vol.43, No. 3, pp. 153-171.
- Gattacceca, J., Eisenlohr, P., Rochete, P., 2004. Calibration of *in situ* magnetic susceptibility measurements. *Geophysical Journal International*,158, 42-49.
- Gettings, M.E., 2005. Multifractal magnetic susceptibility distribution models of hydrothermal altered rocks in the Needle Creek Igneous Center of the Absaroka Mountains, Wyoming. *Nonlinear Processes in Geophysics*, vol 12, 587-601.
- Gow, P.A. and Walshe J. L., 2005. The role of Preexisting Geologic Architecture in the Formation of Giant Porphyry related Cu \pm Au Deposits: Examples from New Guinea and Chile. *Economic Geology*, vol 100, p. 819-833.
- Gubbins, D., Herrero-Bervera. 2007. *Encyclopedia of Geomagnetism and Paleomagnetism* 1054 p. *Encyclopedia of Earth Sciences Series*.
- Gringarten, E. and Deutsch, C. 2001. Teacher's Aid Variogram interpretation and Modeling. *Mathematical Geology*, vol 33, No. 4. p 507-534.
- Hedenquist, J.W. & Lowenstern, J.B., 1994, The role of magmas in the formation of hydrothermal ore deposits: *Nature*, vol 370, p. 519-527.
- Herzig, P.M. and Hannington M.D. 1995. Polimetallic massive sulphides at the modern sea-floor A review. *Ore Geology Reviews*, vol. 10, p. 95-115.
- Huang, H. and Fraser, D.C., 2001. Mapping of the resistivity, susceptibility, and permittivity of the earth using a helicopter-borne electromagnetic system. *Geophysics*, Vol. 66. No.1, p. 148-157.
- Hunt, C.P., Moskowitz, B. M., Banerjee, S. K. 1995. *Magnetic Properties of Rocks and Minerals. Rock Physics and Phase Relations. A Handbook of Physical Constants.* American Geophysical Union. Reference Shelf 3.

- Isaaks, H.I and Srivastava, R.M. 1989. An Introduction to Applied Geostatistics. Oxford University Press. 561 p.
- Journel, A.G and Huijbregts, Ch. J, 1978. Mining Geostatistics. Academic Press. p.600.
- Krige, D.G. 1966. A study of gold and uranium distribution patterns in the Klerksdorp gold field. *Geoexploration*. Vol 4, Issue 1. pp. 43-53.
- Lange, G. and Seidel, K. 2007. Electromagnetic Methods. *In Environmental Geology: Handbook of Field Methods and Case Studies*. Knödel, Klaus, Lange, Gerhard, Voigt, Hans-Jürgen. Springer. pp.1358.
- Leonardi, H. Kumpbel, J. 1996. Scaling behavior of vertical magnetic susceptibility and its fractal characterization an example from the German continental Deep Drilling Project (KTB) *Geol Rundsch* (1996) 85:50-57.
- Limpert, E., Stahel, W.A., Abbt, M. 2001. Log-normal distributions across the sciences: Keys and Clues. *Biosciences*, vol. 51. No. 5. pp 341-352.
- Lydon, J.W, 1988. Volcanogenic Massive Sulphide Deposits Part 1: A descriptive Model. *In: Ore Deposit Models*. Volume I. Edited by R.G. Roberts and P.A. Sheahan, Geosciences Canada. Reprint Series 3. 194 p.
- Matheron, G., 1971. The theory of regionalized variables and its applications. *Les cahiers du Centre de morphologie mathématique de Fontainebleau*. Fascicule 5. p. 211.
- Maus, S and Dimri, V.P. 1994. Scaling properties of potential fields due to scaling sources. *Geophysical Research Letters*, Vol 21, No 10. pp 891-894.
- Meju, M.A. 2002. Geomagnetic Exploration for natural resources: Models, Case studies and Challenges. *Surveys in Geophysics*, vol. 23, p.133-205.
- Oldenburg, D. and Li, Y, 2005. Geophysical Inversion: A Tutorial. *Near-Surface Geophysics*. SEG. Investigations in Geophysics Series No 13 edited by D.K. Butler, pp 89-150, 2005
- Oz, B. Deutsch, C.V, Frykman, P., 2002. A visual basic program for histogram and variogram scaling. *Computers & Geosciences*. Vol.28, Issue 1. pp 21-31.
- Parker, R.L. 1994. Geophysical Inverse Theory. Princeton University Press. 386 p.
- Phillips, Nigel. 1996. Geophysical Inversion in an Integrated Exploration Program: Examples of the San Nicolas Deposits. Unpublished Msc Thesis, Canada, University of British Columbia. 236 p.
- Phillips, N., Oldenburg, D., Chen, J., 2001, Cost effectiveness of geophysical inversions in mineral exploration: Applications at San Nicolas. *The Leading Edge*, Vol. 20, Issue 12, p. 1351-1360.

- Pilkington, M. Gregotski, M.E. and Todoeschuck. 1994. Using fractal crustal magnetization models in magnetic interpretation. *Geophysical Prospecting*, Vol. 42, p. 677-692.
- Pilkington and Todoeschuck, 1995. Scaling nature of crustal susceptibilities. *Geophysical Research Letters*, Vol. 22, No. 7, p.779-782.
- Quinland, J.L., 1986. Geology and silicate-alteration zoning at the Red Mountain porphyry copper deposit, Santa Cruz County, Arizona. *Arizona Geological Society Digest*, vol.16, p.294-305.
- Richards, J.P. 2003. Tectono-Magmatic Precursors for Porphyry Cu-(Mo-Au) Deposit Formation. *Economic Geology*, vol.98, p. 1515-1533.
- Syme E.C and Bailes A.H. 1993 Stratigraphic and Tectonic Setting of Early Proterozoic Massive Sulfide Deposits, Flin Flon, Manitoba. *Economic Geology* Vol 88, p. 566-589.
- Serrano, L., Vargas, R., Stambuk, V., Aguilar, C., Galeb M., Holmgren, C., Contreras, A., Godoy, S., Vela, I., Skewes, M. A., and Stern, C.R. 1996, The late Miocene to early Pliocene Río Blanco-Los Bronces copper deposit, central Chilean Andes: society of Economic Geologist Special Publication 5, p. 119-130.
- Skewes, M.A., Holmgren, C. and Stern C.R. 2003. The Donoso copper-rich, tourmaline-bearing breccia pipe in central Chile: petrologic, fluid inclusion and stable isotope evidence for an origin from magmatic fluids. *Mineralium Deposita*. Vol.38, p. 2-21.
- Telford, W.M., Geldart, L. P., Sheriff, R.E. and Keys, D.A. 1976. *Applied Geophysics*. Cambridge University Press. p. 860
- Vargas, R., Gustafson, L.B., Vukasovic, M., Tidy, E. and Skewes, A., 1999, Ore breccias in the Río Blanco-Los Bronces porphyry copper deposit, Chile. *Society of Economic Geologists Special Publication* 7, p.281-297.
- Wen, R., Sinding-Larsen R., 1997. Uncertainty in Fractal Dimension Estimated from Power spectra and Variograms. *Mathematical Geology*. Vol 29, No. 6. p.727-753.
- Zhou, S. and Thybo, H. 1998, Power Spectra Analysis of Aeromagnetic Data and KTB Susceptibility Logs, and their Implication for Fractal Behavior of Crustal Magnetization. *Pure and Applied Geophysics*. Vol. 151., p. 147-159.

Appendix

This appendix contains the description of the data included in a DVD attached to the thesis.

A.1 Petrography study at Flin-Flon.

In this appendix descriptions of 25 samples are provided as tables in excel spreadsheets. A list of the sampled included is presented following list:

- 1.- petrography_4a.xls
- 2.- petrography_4b.xls
- 3.- petrography_4c.xls
- 4.- petrography_BI-2-34.xls
- 5.- petrography_BI-2-92.xls
- 6.- petrography_BI-A.xls
- 7.- petrography_BI-C.xls
- 8.- petrography_BI-N-13.xls
- 9.- petrography_BI-N-23.xls
- 10.- petrography_BI-N-23.xls
- 11.- petrography_BI-N-102.xls
- 12.- petrography_granite_A.xls
- 13.- petrography_mv_B.xls
- 14.- petrography_mv_D.xls
- 15.- petrography_mv_F.xls
- 16.- petrography_mv_G.xls
- 17.- petrography_mvn_33.xls
- 18.- petrography_mvn_37.xls
- 19.- petrography_mvn_39.xls
- 20.- petrography_mvs_24.xls
- 21.- petrography_mvs_27.xls
- 22.- petrography_mvs_29.xls
- 23.- petrography_qpe_24.xls
- 24.- petrography_qpe_34.xls
- 25.- petrography_qpe_74.xls

A.2 Geophysical and magnetic susceptibility data from Flin-Flon.

In this appendix the magnetic susceptibility measurements collected with the KT-9 hand susceptibility meter and the electromagnetic measurement with the EM31 instrument are provided in two excel spreadsheet files:

1. FF_KT9.xls

This file contains 8 sheets named:

1. mafic_volc_1a
2. mafic_volc_1b
3. granite
4. sedimentary_rocks
5. boundary_intrusive_north
6. boundary_intrusive_south
7. quartz_porphyry_east
8. quartz_porphyry_west

The columns of each sheet correspond to:

Column A, labeled as St: corresponds to the coordinate in the station axe in meters

Column B, labeled as Ln corresponds to the coordinate in the line axe in meters.

Column C, labeled as k, correspond to the magnetic susceptibility measurement in unit of the SI system scaled by a factor of 10^{-3} .

2.-FF_EM31.xls

Contains one sheet named grids where each column corresponds to:

Column A Site: name of the grid according to the site.

Column B Date: day/month/year

Column C User: name of the operator performing the survey.

Column D Stn (X): location of the middle point of the instrument, measured in meters in the station axe of the grid

Column E Line (Y): location of the middle point of the instrument, measured in meters in the station axe of the grid

Column F Z: Elevation of the instrument measured in meters above the terrain surface

Column G Dipole: operation mode of the instrument, in this survey the mode is set to vertical.

Column H Tx Location (orientation): spatial orientation of the instrument respect to the axe of surveyed grid.

Column I In-phase: Real component of the secondary electromagnetic field in parts per million.

Column J Quadrature: Imaginary component of the secondary electromagnetic field in parts per million.

Column K IP err: error value associated to the in phase component in parts per million.

Column L Quad err: error value associated to the quadrature component in parts parts per million.